


1-1-2010

# Supercritical Carbon Dioxide Processing Of Nano - Clays And Polymer/clay Nanocomposites

Mihai Manitiu  
*Wayne State University*

Follow this and additional works at: [http://digitalcommons.wayne.edu/oa\\_dissertations](http://digitalcommons.wayne.edu/oa_dissertations)

 Part of the [Chemical Engineering Commons](#), and the [Nanoscience and Nanotechnology Commons](#)

---

## Recommended Citation

Manitiu, Mihai, "Supercritical Carbon Dioxide Processing Of Nano - Clays And Polymer/clay Nanocomposites" (2010). *Wayne State University Dissertations*. Paper 129.

This Open Access Dissertation is brought to you for free and open access by DigitalCommons@WayneState. It has been accepted for inclusion in Wayne State University Dissertations by an authorized administrator of DigitalCommons@WayneState.

**SUPERCRITICAL CARBON DIOXIDE PROCESSING OF NANO-CLAYS AND  
POLYMER/CLAY NANOCOMPOSITES**

by

**MIHAI MANITIU**

**DISSERTATION**

Submitted to the Graduate School

of Wayne State University,

Detroit, Michigan

in partial fulfillment of the requirements

for the degree of

**DOCTOR OF PHILOSOPHY**

2010

MAJOR: CHEMICAL ENGINEERING

---

Advisor

Date

---

Co-Advisor

Date

---

---

---

## ACKNOWLEDGMENTS

I owe a great deal of gratitude to both Dr. Rangaramanujam M. Kannan and Dr. Esin Gulari for believing and giving me the opportunity to perform research. Their tremendous patience, knowledge, and leadership have proved to be invaluable. I would like to thank Dr. Steven Horsch for his guidance and assistance especially at the beginning of my thesis work. Also, my thanks to the committee members (Dr. Kannan, Dr. Gulari, Dr. Manke, Dr. Potoff and Dr. Newaz,) who have kindly taken time out of their busy schedules to participate in this dissertation. I would like to thank Dr. Robert Bellair who has worked with me on some of the projects. I would also like to thank Dr. Liu of the Wayne State University's' Central Instrument Facility for his assistance in acquiring the TEM images. I also want to thank the group members who gave me some helpful insight and made the lab a fun place to be. Finally, I would like to thank my parents, Zachei and Maria Manitiu for their tremendous support and for the many sacrifices they made so that I might further my education and my knowledge.

## TABLE OF CONTENTS

|   |           |
|---|-----------|
| Acknowledgements .....  | ii        |
| List of Tables .....  | viii      |
| List of Figures .....   | x         |
| <b>CHAPTER 1: Introduction .....</b>  | <b>1</b>  |
| <b>1.1 Overview.....</b>  | <b>1</b>  |
| <b>1.2 Polymer/clay nanocomposites.....</b>                                     | <b>3</b>  |
| 1.2.1 Structure and morphology of nano-clays.....                               | 5         |
| 1.2.2 Types of nanocomposites.....  | 8         |
| 1.2.3 Polymer/clay nanocomposites preparation methods.....                      | 10        |
| <b>1.3 Supercritical carbon dioxide (scCO<sub>2</sub>) process.....</b>         | <b>20</b> |
| <b>1.4 Significance of research.....</b>  | <b>23</b> |
| <b>CHAPTER 2: Supercritical CO<sub>2</sub> processing of Cloisite 10A .....</b> | <b>25</b> |
| <b>2.1 Materials .....</b>  | <b>25</b> |
| <b>2.2 Methods of characterization.....</b>                                     | <b>26</b> |
| 2.2.1 Wide angle X-ray diffraction (WAXD).....                                  | 26        |
| 2.2.2 Scanning electron microscopy (SEM).....                                   | 27        |
| 2.2.3 Thermogravimetric analysis (TGA).....                                     | 27        |
| 2.2.4 Volume/density change determination.....                                  | 28        |
| <b>2.3 Nano-clay preparation.....</b>   | <b>28</b> |
| <b>2.4 Nano-clay characterization.....</b>                                      | <b>28</b> |
| 2.4.1 Thermogravimetric analysis.....   | 28        |
| 2.4.2 Wide angle X-ray diffraction.....   | 30        |

|   |           |
|---|-----------|
| 2.4.3 Scanning electron microscopy.....                                       | 31        |
| 2.4.4 Volume change measurements.....   | 37        |
| 2.5 Conclusions.....  | 39        |
| <b>CHAPTER 3: Supercritical Carbon Dioxide - Processed Dispersed</b>          |           |
| <b>Polystyrene – Clay Nanocomposites: Investigation of Processing</b>         |           |
| <b>Parameters Effects on the Nanocomposites Morphology</b>                    |           |
| <b>and Properties.....</b>  |           |
| <b>3.1 Materials .....</b>  | <b>42</b> |
| 3.1.1 Nano-clays.....   | 42        |
| 3.1.2 Polymers, solvent and gas.....  | 42        |
| <b>3.2 Methods of characterization.....</b>                                   | <b>44</b> |
| 3.2.1 Wide angle X-ray diffraction.....                                       | 44        |
| 3.2.2 Transmission electron microscopy (TEM).....                             | 44        |
| 3.2.3 Thermogravimetric analysis.....   | 44        |
| 3.2.4 Permeability measurements .....   | 45        |
| 3.2.5 Rheology.....   | 45        |
| <b>3.3 Nanocomposites preparation.....</b>                                    | <b>47</b> |
| <b>3.4 Low molecular weight 5k PS/clay nanocomposites characterization</b>    |           |
| <b>(WAXD and rheology).....</b>   | <b>54</b> |
| 3.4.1 Wide angle X-ray diffraction.....                                       | 54        |
| 3.4.2 Rheological measurements.....   | 56        |
| <b>3.5 High molecular weight 280k PS/clay nanocomposites characterization</b> |           |
| <b>(WAXD, TEM, rheology, permeability and TGA).....</b>                       | <b>60</b> |

|   |     |
|---|-----|
| 3.5.1 <i>Effect of organic clay modifier on nanocomposite morphology</i>                  |     |
| <i>and properties</i> .....   | 60  |
| 3.5.1a <i>Wide angle x-ray diffraction</i> .....  | 64  |
| 3.5.1b <i>Transmission electron microscopy</i> .....                                      | 68  |
| 3.5.1c <i>Rheology</i> .....  | 73  |
| 3.5.1d <i>Thermogravimetric analysis</i> .....  | 80  |
| 3.5.1e <i>Permeability</i> .....  | 87  |
| 3.5.2 <i>Effect of scCO<sub>2</sub> processing parameters on nanocomposite morphology</i> |     |
| <i>and properties</i> .....   | 101 |
| 3.5.2a <i>Effect of depressurization rate on nanocomposite morphology</i>                 |     |
| <i>and properties</i> .....   | 103 |
| 3.5.2b <i>Effect of nano - clay scCO<sub>2</sub> pre - dispersion on nanocomposite</i>    |     |
| <i>morphology and properties</i> .....  | 106 |
| 3.5.2c <i>Effect of nano - clay weight fraction on nanocomposite</i>                      |     |
| <i>morphology and properties</i> .....  | 109 |
| 3.5.2d <i>Effect of scCO<sub>2</sub> processing pressure and processing time on the</i>   |     |
| <i>morphology and properties of the resulting nanocomposites</i> .....                    | 117 |
| <b>3.6 Conclusions</b> .....  | 121 |

## **CHAPTER 4: Role of Polymer-Clay Interactions and Nano-clay Dispersion on the**

### **Viscoelastic Response of Supercritical CO<sub>2</sub> Dispersed**

#### **Polyvinylmethylether (PVME)-Clay Nanocomposites**.....124

#### **4.1 Materials** .....127

#### **4.2 Methods of characterization**.....128

|   |            |
|---|------------|
| 4.2.1 Wide angle X-ray diffraction.....   | 128        |
| 4.2.2 Rheology.....   | 129        |
| 4.2.3 Thermogravimetric analysis.....   | 129        |
| <b>4.3 Nanocomposites preparation.....</b>  | <b>129</b> |
| 4.3.1 Nanocomposite formation using the scCO <sub>2</sub> processing technique.....           | 130        |
| 4.3.2 Nanocomposite Formation using the solution cast freeze drying<br>method.....            | 130        |
| <b>4.4 Nanocomposites characterization .....</b>  | <b>131</b> |
| 4.4.1 Determination of clay mass fraction in organophilic<br>Nano - clays.....                | 131        |
| 4.4.2 Role of substantial nano-clay dispersion with ‘weak’ polymer-<br>clay interactions..... | 132        |
| 4.4.3 Role of polymer - clay interactions with comparable levels of<br>intercalation.....     | 144        |
| <b>4.5 Conclusions.....</b>   | <b>156</b> |
| <b>CHAPTER 5: Future Work.....</b>  | <b>158</b> |
| <b>5.1 Surface modification of “as received” Cloisite Na<sup>+</sup>.....</b>                 | <b>158</b> |
| <b>5.1.1 Preliminary results.....</b>   | <b>159</b> |
| <b>5.2 Styrene-butadiene-styrene (SBS)/clay nanocomposites.....</b>                           | <b>164</b> |
| <b>5.2.1 Preliminary results.....</b>   | <b>165</b> |
| <b>5.3 High density polyethylene (HDPE)/clay nanocomposites.....</b>                          | <b>172</b> |

|  |     |
|--|-----|
| <i>5.3.1 Preliminary results</i> ..... | 172 |
| Appendix A.....                        | 176 |
| References.....                        | 177 |
| Abstract.....                          | 187 |
| Autobiographical Statement.....        | 190 |



## LIST OF TABLES

|   |     |
|---|-----|
| <b>Table 1.</b> Physical data of Cloisite 10A. HT = hydrogenated tallow (~ 65% C18; ~ 30% C16; ~5% C14. (Data provided by Southern Clay Inc.).....  | 26  |
| <b>Table 2.</b> Physical data of Cloisite 93A, 15A, 10A and Nanocor I.30P. HT = hydrogenated Tallow ~ 65% C18; ~ 30% C16; ~ 5% C14. (Data provided by Southern Clay Inc).....   | 43  |
| <b>Table 3.</b> Polymer properties.....   | 43  |
| <b>Table 4.</b> 5k Polystyrene/Cloisite 10A nanocomposites samples composition and nomenclature.....  | 50  |
| <b>Table 5.</b> Polystyrene/Cloisite 93A, 15A, Nanocor I.30P nanocomposites sample composition and nomenclature.....  | 50  |
| <b>Table 6.</b> Polystyrene/Cloisite 10A nanocomposites sample compositions and nomenclature.....   | 51  |
| <b>Table 7.</b> Polystyrene/Cloisite 10A nanocomposites sample composition and nomenclature.....  | 52  |
| <b>Table 8.</b> Summary of TGA and WAXD for “as received” and dried clay at 160°C for 6 hrs. TGA data was taken as weight percent that remained as char at 650°C.....   | 53  |
| <b>Table 9.</b> X-ray diffraction data summary. The initial and final 2 theta and d001 spacing are shown for all the “as received” nano-clays and PS/clay nanocomposites.....   | 67  |
| <b>Table 10.</b> Average tactoid sizes measured from TEM and the number of platelets per tactoid was calculated from the d001 spacing found with WAXD (Appendix A).....   | 70  |
| <b>Table 11.</b> Theoretical percolation threshold for all the solution blended and scCO <sub>2</sub> processed PS/5wt% 10A, 15A, 93A and I.30P nanocomposites.....   | 77  |
| <b>Table 12.</b> Residual mass (char %) for “as received” clays and separated clays from solution blended and scCO <sub>2</sub> processed nanocomposites.....   | 82  |
| <b>Table 13.</b> TGA Summary: Temperature at 10 and 50 wt % Weight Loss, Maximum Rate of Decompositions (MRD), Change in MRD Compared to PS (°C) and Percent Char (residual mass fraction at 650°C).....  | 85  |
| <b>Table 14.</b> Average and standard deviation data for oxygen permeability of 280k PS, solution blended and scCO <sub>2</sub> processed Cloisite 10A, 93A, 15A and Nanocor I.30P nanocomposites. The table includes percent reduction in O <sub>2</sub> permeability relative to neat 280k PS and to corresponding benchmarks of solution blended nanocomposites..... | 100 |

**Table 15.** Water vapor permeability of 280k PS, solution blended and scCO<sub>2</sub> processed Cloisite 10A, 93A, 15A and Nanocor I.30P nanocomposites. The table includes percent reduction in water vapor permeability relative to neat 280k PS and to corresponding benchmark solution blended nanocomposite.....100

**Table 16.** TGA Summary: Temperature at 10%, 50% Weight Loss, Maximum Rate of Decompositions, and the percent residual mass at 600°C (amount of char left in the nanocomposite).....115

**Table 17.** Nano-clay surfactant composition, basal spacing, and platelet density, as reported by supplier. T is Tallow (~65% C18; ~30% C16; ~5% C14) and HT-Hydrogenated Tallow (~65wt% C18; ~30wt% C16; ~5wt% C14).....128

**Table 18.** The first entry in each column refers to the nanocomposite and the second, in parenthesis, refers to the as-received nano-clay corresponding to a particular nanocomposite. n/a appears where no diffraction pattern was observed or the pattern did not resemble a Gaussian distribution.....147

**Table 19.** Oxygen permeability of HDPE and HDPE/5 wt% 15A nanocomposites.....176

## LIST OF FIGURES

|   |    |
|---|----|
| <b>Figure 1.</b> Crystal morphology of natural sodium montmorillonite.....  | 7  |
| <b>Figure 2.</b> Schematic of nano-clay ion-exchange reaction where the sodium ions are replaced by the ammonium ions rendering the clay more organophilic and increasing the gallery spacing.....  | 8  |
| <b>Figure 3.</b> Nano-clay morphology in a polymer matrix. A. Immiscible (Microcomposite) B. Intercalated (Nanocomposite) and C. Exfoliated (Nanocomposite).....  | 9  |
| <b>Figure 4.</b> scCO <sub>2</sub> processing reactor, controller and high pressure pump.....   | 23 |
| <b>Figure 5.</b> Supercritical fluid processing.....  | 23 |
| <b>Figure 6.</b> TGA analysis of “as received” Cloisite 10A and scCO <sub>2</sub> processed “as received” 10A. The final weight present does not change significantly following scCO <sub>2</sub> processing and/or during depressurization indicating that the scCO <sub>2</sub> processing technique does not remove of the nano-clay organic modifier..... | 29 |
| <b>Figure 7.</b> Derivative TGA curves for “as received” Cloisite 10A and scCO <sub>2</sub> processed Cloisite 10A. There is no change in the maximum degradation rate (MRD) between the two providing further evidence that scCO <sub>2</sub> does not the removal of the organic modifier..   | 30 |
| <b>Figure 8.</b> WAXD of as received Cloisite 10A and scCO <sub>2</sub> processed 10A. The disappearance of the d <sub>001</sub> peak following scCO <sub>2</sub> processing is a good indication that the clay has been dispersed and/or disordered.....   | 31 |
| <b>Figure 9.</b> SEM image of “as received” Cloisite 10A particles.....   | 33 |
| <b>Figure 10.</b> SEM images of an “as received” Cloisite 10A particle.....   | 34 |
| <b>Figure 11.</b> Illustration of “as received” Cloisite 10A particle.....  | 34 |
| <b>Figure 12.</b> SEM image of scCO <sub>2</sub> Cloisite 10A particles processed 1 time for 24 hours.....  | 35 |
| <b>Figure 13.</b> SEM image of a scCO <sub>2</sub> processed Cloisite 10A particle processed 1 time for 24 hours.....   | 35 |
| <b>Figure 14.</b> SEM images of a scCO <sub>2</sub> Cloisite 10A particle processed 1 time for 24 hours.....  | 36 |
| <b>Figure 15.</b> Illustration of scCO <sub>2</sub> processed Cloisite 10A particle.....  | 36 |
| <b>Figure 16.</b> Percent volume change of Cloisite 10A after multiple scCO <sub>2</sub> processings.....   | 38 |

|   |    |
|---|----|
| <b>Figure 17.</b> Percent volume change of Cloisite 10A after scCO <sub>2</sub> processing.....   | 39 |
| <b>Figure 18.</b> TGA (left) and WAXD (right) of “as received” Cloisite 10A and 10A after drying in the vacuum oven at 160°C for 6 hours.....   | 53 |
| <b>Figure 19.</b> X-ray diffractogram of “as received” Cloisite 10A and 5k PS/10A nanocomposite prepared using the melt blending technique. The nanocomposite shows a shift to higher d <sub>001</sub> spacing (1.9 to 4.32 nm) due to polymer confinement into the inner gallery spacing of the nano clay.....   | 56 |
| <b>Figure 20.</b> Storage modulus of 5k PS and 5k PS/10A nanocomposite.....   | 59 |
| <b>Figure 21.</b> X-ray diffractogram of “as received” Cloisite 10A and 280k PS/10A nanocomposite prepared using the melt blending technique.....   | 62 |
| <b>Figure 22.</b> Storage modulus of 280k PS and 280k PS/10A nanocomposite prepared using the melt blending technique.....  | 62 |
| <b>Figure 23.</b> X-ray diffractograms of PS/10A, PS/15A, PS/93A and PS/L30P nanocomposites. Solution blended samples are shown as open symbols while scCO <sub>2</sub> samples are displayed as filled symbols. The change in spacing of each clay from its equilibrium “as received” spacing to the final spacing in the PS/clay nanocomposites is shown below the graph..... | 68 |
| <b>Figure 24.</b> TEM micrograph of 5 wt % 10A solution blended with polystyrene at 30K and 200K magnifications.....  | 71 |
| <b>Figure 25.</b> TEM micrograph of 5 wt % 10A scCO <sub>2</sub> processed with polystyrene at 30K and 200K magnifications.....   | 71 |
| <b>Figure 26.</b> TEM micrograph of 5 wt % 15A solution blended with polystyrene at 30K and 200K magnifications.....  | 72 |
| <b>Figure 27.</b> TEM micrograph of 5 wt % 15A scCO <sub>2</sub> processed with polystyrene at 30K and 200K magnifications.....   | 72 |
| <b>Figure 28.</b> TEM micrograph of 5 wt % 93A solution blended with polystyrene at 30K and 200K magnifications.....  | 72 |
| <b>Figure 29.</b> TEM micrograph of 5 wt % 93A scCO <sub>2</sub> processed with polystyrene at 30K and 200K magnifications.....   | 73 |
| <b>Figure 30.</b> Storage modulus for the 5wt% solution blended nanocomposites.....   | 75 |
| <b>Figure 31.</b> Storage modulus for the 5wt% scCO <sub>2</sub> nanocomposites.....  | 75 |

|  |    |
|--|----|
| <b>Figure 32.</b> Storage and loss moduli for PS-5% 10A-scCO <sub>2</sub> (A), PS-5% 10A-sol(B), PS-5% 15A-scCO <sub>2</sub> (C), PS-5% 15A-sol(D), PS-5% I.30P-scCO <sub>2</sub> (E), PS-5% I.30P-sol(F), PS-5% 93A-scCO <sub>2</sub> (G), PS-5% 93A-sol(H).....  | 76 |
| <b>Figure 33.</b> TGA curves and Derivative TGA curves for “as received” 10A and separated 10A from PS-5% 10A-sol and PS-5% 10A-scCO <sub>2</sub> .....  | 82 |
| <b>Figure 34.</b> TGA curves and Derivative TGA curves for “as received” 15A and separated 15A from PS-5% 15A-sol and PS-5% 15A-scCO <sub>2</sub> .....  | 83 |
| <b>Figure 35.</b> TGA curves and Derivative TGA curves for “as received” 10A and separated 93A from PS-5% 93A-sol and PS-5% 93A-scCO <sub>2</sub> .....  | 83 |
| <b>Figure 36.</b> TGA curves and Derivative TGA curves for “as received” I.30P and separated I.30P from PS-5% I.30P-sol and PS-5% I.30P-scCO <sub>2</sub> .....  | 83 |
| <b>Figure 37.</b> TGA curves and Derivative TGA curves for “as received” PS280 and PS-5% 10A-sol and PS-5% 10A-scCO <sub>2</sub> .....   | 86 |
| <b>Figure 38.</b> TGA curves and Derivative TGA curves for “as received” PS280 and PS-5% 15A-sol and PS-5% 15A-scCO <sub>2</sub> .....   | 86 |
| <b>Figure 39.</b> TGA curves and Derivative TGA curves for “as received” PS280 and PS-5% 93A-sol and PS-5% 93A-scCO <sub>2</sub> .....   | 87 |
| <b>Figure 40.</b> TGA curves and Derivative TGA curves for “as received” PS280 and PS-5% I.30P-sol and PS-5% I.30P-scCO <sub>2</sub> .....   | 87 |
| <b>Figure 41.</b> Tortuosity path in a polymer/clay nanocomposite. Path A displays the path a gas molecule will take to permeate through a neat polymer. Paths B-E are possible paths that a gas molecule can take in polymer filled with layered clay of different width (W), length (L) and orientation relative to the diffusion direction..... | 88 |
| <b>Figure 42.</b> Values of the order parameter for three orientations of the platelets (top). Influence of the degree of delamination on the tortuosity factor and the aspect ratio of nano-clay tactoids. W is the width of the nano-clay tactoid (bottom).....  | 91 |
| <b>Figure 43.</b> Dependence of the relative permeability on the order parameter at different sheet lengths (left). Dependency of the relative permeability on the average tactoid size (W) at several different plate lengths (right) .....   | 91 |
| <b>Figure 44.</b> Oxygen permeability of 280k PS, solution blended and scCO <sub>2</sub> processed Cloisite 10A nanocomposites.....  | 96 |

|  |     |
|--|-----|
| <b>Figure 45.</b> Water vapor permeability of 280k PS, solution blended and scCO <sub>2</sub> processed Cloisite 10A nanocomposites.....   | 97  |
| <b>Figure 46.</b> Oxygen permeability of 280k PS, solution blended and scCO <sub>2</sub> processed Cloisite 15A nanocomposites.....  | 97  |
| <b>Figure 47.</b> Water vapor permeability of 280k PS, solution blended and scCO <sub>2</sub> processed Cloisite 15A nanocomposites.....   | 98  |
| <b>Figure 48.</b> Oxygen permeability of 280k PS, solution blended and scCO <sub>2</sub> processed Cloisite 93A nanocomposites.....  | 98  |
| <b>Figure 49.</b> Water vapor permeability of 280k PS, solution blended and scCO <sub>2</sub> processed Cloisite 93A nanocomposites.....   | 99  |
| <b>Figure 50.</b> Water vapor permeability of 280k PS, solution blended and scCO <sub>2</sub> processed Nanocor I.30P nanocomposites.....  | 99  |
| <b>Figure 51.</b> X-ray diffractograms of “as received” Cloisite 10A and solution blended, and scCO <sub>2</sub> PS/10A nanocomposites processed and depressurized at various rates prepared.....  | 104 |
| <b>Figure 52.</b> Storage modulus of 280k PS and solution blended, and scCO <sub>2</sub> PS/10A nanocomposites processed and depressurized at various rates prepared.....  | 106 |
| <b>Figure 53.</b> X-ray diffractograms of “as received” Cloisite 10A and PS/10A nanocomposites prepared with “as received” and pre-dispersed 10A to determine the effect of nano-clay pre-dispersion of the final nanocomposite morphology and rheological properties..... | 107 |
| <b>Figure 54.</b> Storage moduli of 280k PS and PS/10A nanocomposites prepared with “as received” and pre-dispersed 10A. SEM pictures of “as received” 10A (bottom) and pre-dispersed 10A (top).....   | 109 |
| <b>Figure 55.</b> X-ray diffractograms of “as received” Cloisite 10A and 93A and PS/10A and PS/93A nanocomposites with varying nano-clay weight fractions.....   | 110 |
| <b>Figure 56.</b> Storage modulus of 280k PS, PS/10A scCO <sub>2</sub> and solution blended processed nanocomposites.....  | 113 |
| <b>Figure 57.</b> Storage modulus of 280k PS and PS/93A scCO <sub>2</sub> processed nanocomposites.....  | 114 |
| <b>Figure 58.</b> TGA of 10wt% PS/Cloisite 10A and 93A nanocomposites.....   | 116 |

|  |     |
|--|-----|
| <b>Figure 59.</b> TGA derivative curves for 10wt% PS/Cloisite 10A and 93A nanocomposites detailing the improvement in the maximum rate of decomposition of polymer due to nano-clay addition.....  | 116 |
| <b>Figure 60.</b> Storage modulus of 280k PS and PS/10A scCO <sub>2</sub> nanocomposites processed at various 0.5, 4, 12 and 24 hours.....   | 118 |
| <b>Figure 61.</b> Carbon dioxide density as a function of temperature at various pressures.....  | 120 |
| <b>Figure 62.</b> Storage modulus of 280k PS and PS/10A scCO <sub>2</sub> nanocomposites processed for 24 hours at 80°C and 10.34, 13.79 and 27.58 MPa.....  | 120 |
| <b>Figure 63.</b> TGA analysis of pure nano-clays, Cloisite Na <sup>+</sup> , Cloisite 30B and Nanocor I.30P, the 6% reduction in weight of Cloisite Na <sup>+</sup> is attributed to the evaporation of water.....  | 132 |
| <b>Figure 64.</b> WAXD of PVME/Na <sup>+</sup> samples 15-NA, 15NA-S, and as received Cloisite Na <sup>+</sup> .....   | 135 |
| <b>Figure 65.</b> WAXD of sample Cloisite Na <sup>+</sup> /PEO reveals the sample is intercalated as evident by the significant shifting of the d <sub>001</sub> diffraction peak and the presence of higher order peaks (d <sub>002</sub> ).....  | 135 |
| <b>Figure 66.</b> Storage and loss moduli for PEO and PEO/15wt% Cloisite Na <sup>+</sup> nanocomposite with a reference temperature of 80°C.....   | 137 |
| <b>Figure 67.</b> Storage and loss moduli for PVME and PVME 15wt% Cloisite Na <sup>+</sup> nanocomposite with a reference temperature of 80°C for comparison with the PEO nanocomposites.....  | 138 |
| <b>Figure 68.</b> Storage and loss moduli for PVME and 15-NA nanocomposite (frequency shift factors shown as inlays).....  | 140 |
| <b>Figure 69.</b> Storage and loss moduli for PVME and 15NA-S nanocomposite (frequency shift factors shown as an inlay).....   | 140 |
| <b>Figure 70.</b> Log-linear plot of dynamic moduli vs. reduced frequency to more clearly show the cross-over frequency of the neat PVME, 15NA and 15NA-S.....   | 143 |
| <b>Figure 71.</b> Complex viscosity of the neat PVME, 15NA and 15NA-S.....   | 144 |
| <b>Figure 72.</b> (a) FTIR spectroscopy of Cloisite 30B shows free hydroxyl group stretch (peak 3650 cm <sup>-1</sup> ). (b) FTIR spectroscopy of PVME shows the absence of an intermolecular hydrogen bond peak (3350 cm <sup>-1</sup> ). (c) FTIR spectroscopy of sample 15-30B has an intermolecular hydrogen bond peak (3350 cm <sup>-1</sup> ). (d) Proposed hydrogen bond between surfactant and PVME..... | 146 |

|  |     |
|--|-----|
| <b>Figure 73.</b> WAXD of “as received” 30B and sample 15-30B.....   | 149 |
| <b>Figure 74.</b> WAXD of “as received” I.30P and sample 15-I.30P.....   | 149 |
| <b>Figure 75.</b> Log Storage and loss moduli for PVME and 15-30Bnanocomposite (frequency shift factors shown as an inlay).....  | 151 |
| <b>Figure 76.</b> Complex viscosity vs. reduced frequency for sample 15-30B diverges at low frequencies. ....  | 151 |
| <b>Figure 77.</b> Storage and loss moduli for PVME and 15-I30P nanocomposite (frequency shift factors shown as an inlay).....  | 155 |
| <b>Figure 78.</b> Complex viscosity vs. reduced frequency for sample 15-I.30P displays a diverging viscosity at low frequencies.....   | 156 |
| <b>Figure 79.</b> 1-hexadecyl amine (left) and N-[4-(40-aminophenoxy)] phenyl phthalimide (right).....   | 160 |
| <b>Figure 80.</b> FTIR of Na <sup>+</sup> (A), the organic modifiers 1-hexadecyl amine (B) and N-[4-(40-aminophenoxy)] phenyl phthalimide (D) and of the organically modified Na <sup>+</sup> , MMT-1-hexadecyl amine (MMT-A) (C) and (and N-[4-(40-aminophenoxy)] phenyl phthalimide (MMT-B) (E)..... | 161 |
| <b>Figure 81.</b> WAXD of MMT – Na <sup>+</sup> , MMT- A and MMT- B.....   | 163 |
| <b>Figure 82.</b> TGA at 200°C for 24 hours for MMT-A, MMT-B, Cloisite 93A and 30B.....  | 163 |
| <b>Figure 83.</b> WAXD of 10A and SBS/10A nanocomposites prepared using solution blended and scCO <sub>2</sub> processing methods.....   | 167 |
| <b>Figure 84.</b> Storage modulus of SBS and 5 wt% 10A and 20A/SBS nanocomposites prepared using solution blended and scCO <sub>2</sub> processing methods. At the right are TEM images of 5 wt% 10A nanocomposites 30,000 magnification (scCO <sub>2</sub> – top and solution blended – bottom).....  | 169 |
| <b>Figure 85.</b> TEM images of SBS/5wt%10A scCO <sub>2</sub> processed nanocomposite (30k magnification (A), 100k magnification (B)) and images of SBS/5wt%10A solution blended sample (30k magnification (C), 100k magnification (D)).....   | 170 |
| <b>Figure 86.</b> Tensile modulus, tensile strengths and stain at break for the SBS and SBS/10A scCO <sub>2</sub> and solution blended nanocomposites.....   | 171 |
| <b>Figure 87.</b> WAXD of “as received” 15A and HDPE/5 wt% 15A nanocomposites.....   | 173 |



**Figure 88.** Storage modulus of HDPE and HDPE/5 wt% 15A nanocomposites.....174

**Figure 89.** Tactoid thickness calculation diagram.....176

# CHAPTER 1

## INTRODUCTION

### 1.1 Overview

It was not until 1920 when Staudinger proposed the macromolecular hypothesis that scientists started to have a better understanding about polymers. The hypothesis states that polymers are molecules made of covalently bonded elementary units, called monomers. Before Staudinger's macromolecular hypothesis, chemists were synthesizing macromolecules in the middle of the nineteenth century, but they did not believe that what they were creating very large molecules.<sup>1</sup> Their standard point of view was that these materials were colloids-physically associated clusters of small molecules, with "mysterious non-covalent bonding" holding the clusters together. Although its hypothesis was met with strong resistance at the beginning, it laid the background to further research in the era of polymers. In the subsequent years, Carothers had synthesized several polymers with well – defined structures and the "Polymer Age" was born. In the following 30 years (1930 – 1960) many scientists including Kuhn, Flory, Huggins, Guth, Stockmayer, Rouse, and Zimm laid much of the ground work for modern polymer theory. Between 1960 and 1980 Edwards, des Cloizeaux, de Gennes, Doi and Edwards have further made progress in the field of polymer science.<sup>1</sup> Furthermore, following these early times, organic based macromolecules have become omnipresent in our society. Polymers are found in the packing, transportation, communications, space, recreational, medical and construction industry. The need to produce polymers with better physical properties in order to expand their utility has gone in many directions. Manipulating the molecular architecture of polymers, cross-linking the molecules, blending different polymers together, and adding organic and non-organic based fillers to make composites are some of the ways mechanical, transport and thermal properties of

many of the early materials have been significantly improved.

A composite material is a combined material created from two or more components, selected filler or reinforcing agent and a compatible matrix, binder (i.e. resin) in order to obtain some specific characteristics and properties. The matrix is the continuous phase, and the reinforcement constitutes the dispersed phase. The combination of dissimilar materials can have unique and very advantageous properties if the materials have appropriate characteristics, and result in a material that is better in certain key properties than either of the materials alone. The reinforcements and the matrix are usually very distinct types of materials with widely different properties. The properties of the composite are generally controlled by the behavior and properties of the interface and the level of dispersion of the reinforced material.

Improving material properties by making composites is not a new idea. The first man made composites based upon polymers appeared in about 5000 B.C. in the Middle East where pitch was used as a binder for reeds in boat-building.<sup>2</sup> Later in 3000 B.C. in ancient Egypt, the addition of straw in wet clay improved heat resistance and stress induced failure of clay bricks that were used as the man building material.<sup>3</sup> During the 1950's the demand for low weight high rigidity materials was a major driving force behind composite material research and fabrication. Corporations like U.S. Steel, AT&T, General Electric and IBM invested in vast laboratories, forming research centers built around solid-state physics. Copper-clad 316 stainless steel was one of the early metal composites. It was used for rockets and re-entry vehicle design. However, due to the re-entry speed requirements which generated a lot of heat the metal composites would vaporize like a meteor. Due to the need for a more heat resistant composite, ceramic/metal composites were developed. By the 1960s advanced composites were coming of age with the development of high-modulus whiskers and filaments. While whiskers were easily made, their

composites were of poor quality; but the 60 million modulus boron filaments reinforcing epoxy were very successful and were used in fighter aircraft. However, large modulus differences between the fiber and matrix material were accompanied by large thermal expansion coefficients and consequent residual thermal stresses. As research progressed, graphite fibers were successfully used in golf clubs, tennis rackets, and fishing rods. The success of graphite-epoxy for golf clubs, tennis rackets, and fishing rods encouraged the next wave of development—high-modulus organic filaments. All of the chemical laboratories had processes and patents for high molecular weight/high modulus organic fibers, but it was DuPont that made the plunge due the development of Kevlar. The development of Kevlar, a high modulus organic filament paved the road to many other composites.<sup>4</sup>

## **1.2 Polymer/clay nanocomposites**

Today engineers and scientists are still trying to develop new materials or enhance the properties of existing materials to extend their utility beyond the current limits. From the viewpoint of today's industrial and economical activities, it can be easily assumed that the technology has opened new windows for opportunity which determines the standards of our lives. These requirements result in continuous efforts for new, high performance besides low cost materials to meet increasing demands. Polymers, due to their elastic and viscous like properties, have been the objects of intense study.

Polymer nanocomposites containing nanoscale particles continue to be an area of great interest both in industry and in academia due to significant improvements in mechanical, thermal and barrier properties that can be achieved over conventional macro- or micro-composites.<sup>5, 6</sup> Nanoscale fillers with much different geometry have been used for preparing nanocomposites ranging from large aspect ratio layered thin nanosheets to long narrow nanofibers to tiny

nanospheres.<sup>7</sup> Reducing the size scale of the filling material to the nano-level will allow the use of a much smaller weight fraction of reinforcement phase. The surface area available for interaction with polymer per mass is increased, which is a key factor in composite property enhancement. Polymer layered silicate (PLS) nanocomposites are a new class of materials which consist of polymer matrices filled with low amounts (usually less than 5%) of layered silicates dispersed at nanoscale level. The essential raw material for a nano-clay (nano-sized layered silicate) is montmorillonite, a 2-to-1 layered smectite clay with a parallel platelet structure. Benefits from this clay technology result in part from the high-surface area of montmorillonite (approx 760 m<sup>2</sup>/g) and high-aspect ratio (about 100 - 1000). Polymer nanocomposites (PNC) based on highly anisotropic layered mica-type silicate fillers have attracted great interest because they often exhibit remarkable improvement in materials properties when compared with virgin polymer or conventional micro and macro-composites without significant drawbacks to the resulting materials such as weight increase, opacity, brittleness and many others.<sup>8</sup> The improvements can include high moduli, increased strength and heat resistance, decreased permeability, decreases flammability and increase fire retardancy.<sup>9-12</sup> These improvements depend on many factors including the extent of platelet dispersion, tactoid/platelet orientation, clay network formation, and the strength of physical/chemical interactions between the polymer-clay and polymer-clay modifier. Furthermore, there has been considerable interest in theory and simulations addressing the preparation and properties of these materials and they are also considered to be unique model systems to study the structure and dynamics of polymers in confined environments.<sup>13-16</sup>

Well-defined polymer/layer-silicate (like Montmorillonite-MMT) composites were first reported by Blumstein in the 1960's, who polymerized methyl methacrylate in the presence of

clay and found that the resulting polymer had unusual properties. At the time it was not known that these were nanocomposites and, indeed, the term did not yet exist.<sup>17, 18</sup> Moreover, polymer/clay nanocomposites intercalation chemistry has been developed and known for a long time.<sup>19</sup> The field however was not widespread until it gained momentum in the 90s' due to two major findings. First the Toyota research group prepared a polyamide-6 material by polymerization of caprolactam in the presence of montmorillonite clay. They found that very small amounts of layered silicate loadings (typically less than 5wt.%) resulted in substantial improvements of thermal and mechanical properties of Nylon 6.<sup>20</sup> Second, Vaia and co-workers showed that it was possible to melt-mix polymer and layered silicates without the use of organic solvents.<sup>21</sup> The above work was the genesis of the vivid research which now occurs throughout the world on polymer nanocomposites and it has sparked numerous publications, several reviews, and books on this subject.

### **1.2.1 Structure and morphology of nano-clays**

The layered - clay materials used to prepare nanocomposites, are popular due to the very large amount of potential interfacial surface area that could be available to interact with the host polymer (760 m<sup>2</sup>/g if totally delaminated). The crystallographic structure of natural montmorillonite, which is a very soft phyllosilicate (sheet silicate) mineral, is shown in Figure 1. The structure is based on that of pyrophyllite and it is idealized since in reality the lattice is distorted.<sup>22</sup> It is the main constituent of the volcanic ash weathering product, bentonite. MMT a member of the smectic family is a 2-to-1 nano-clay, meaning that individual clay sheets consist of an alumina octahedral layer fused between two silicate tetrahedral layers and has the following general chemical formula  $(\text{Na,Ca})_x(\text{Al,Mg})_2(\text{Si}_4\text{O}_{10})(\text{OH})_2\text{-}(n\text{H}_2\text{O})$ . Natural montmorillonite undergoes an isomorphous substitution in the octahedral site where  $\text{Al}^{3+}$  is

replaced by  $Mg^{2+}$  or  $Fe^{2+}$  and in the tetrahedral lattice where is  $Si^{4+}$  replaced by  $Al^{3+}$  leading to a permanent excess of negative charge. This negative charge is counterbalanced by the sorption of alkali cations such as  $Ca^{2+}$  and  $Na^+$  between the silicate layers.<sup>23</sup> Staking of the individual clay layers leads to a regular van der Waals gap (interlayer, basal spacing or d-spacing) resulting in a layered structure (also called tactoid). The individual sheets are about 0.96 nm thin which is calculated from the (001) harmonics obtained from wide angle x-ray diffraction (WAXD) and have a diameter between 10 – 1000 nm. Due to the width to length ratio MMT has high-aspect ratio (about 100 to 1000) which along with the very high surface area are responsible for many enhancements in the properties of polymer/nano - clay nanocomposites.

A unique trait of smectic clays like MMT is the ability to sorb certain cations and retained them in an exchangeable state. The layered silicate is characterized by a certain cation exchange capacity (CEC) which is typically measured in milliequivalents per 100 g. This represents the maximum amount of cations that can be taken up by given clay. The nano - clays go through ion - exchange reactions where the  $Na^+$  and  $Ca^{2+}$  are replaced with primary, secondary, ternary and quaternary alkylammonium or alkylphosphonium salts (Figure 2). The small equilibrium spacing of natural clay (~1 nm) as well as its inherent hydrophilicity makes most polymer penetration unfavorable and therefore limits polymer access to the large potential surface area. The purpose of exchanging alkali cations with alkylammonium cations is to overcome the above mentioned barriers in making polymer/clay nanocomposite. The alkylammonium cations make the original hydrophilic clay more organo - philic extending its utility to a wider range of polymers. Also, the alkyl groups of the ammonium salt help in expanding the d-spacing, which in turn helps in lowering the entropic penalty of polymer penetrating the inter-gallery spacing of the clay.<sup>24</sup>

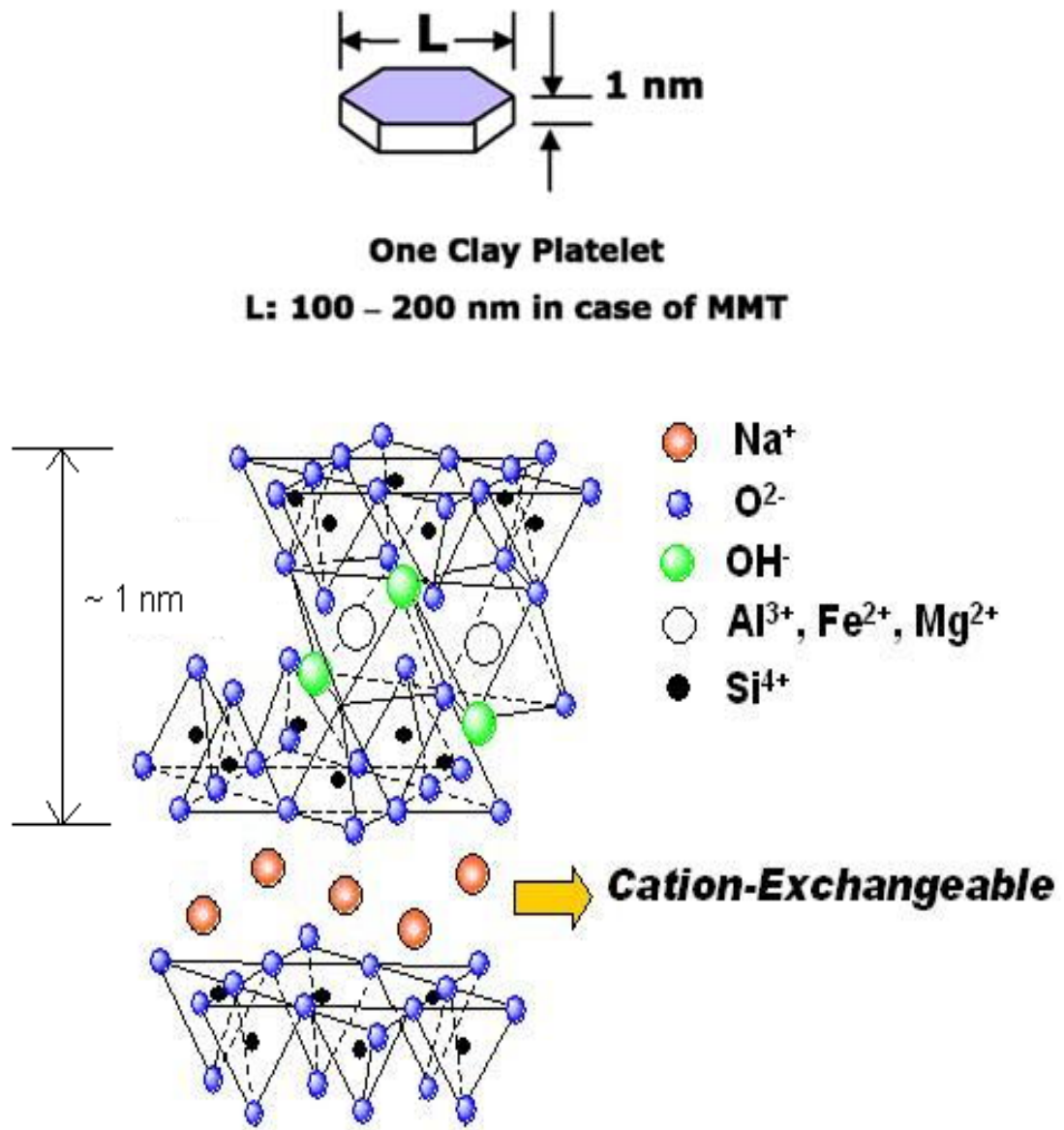
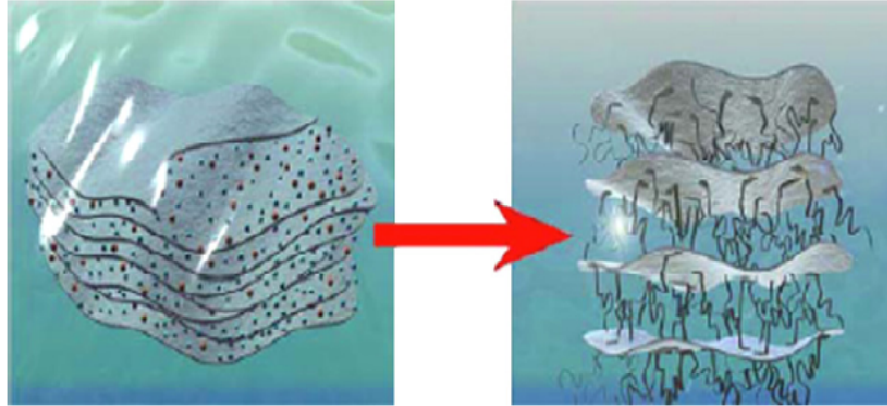


Figure 1. Crystal morphology of natural sodium montmorillonite.<sup>25</sup>





**Figure 2.** Schematic of nano-clay ion-exchange reaction where the sodium ions are replaced by the ammonium ions rendering the clay more organophilic and increasing the inner - gallery spacing.<sup>26</sup>

### 1.2.2 Types of nanocomposites

Polymer/nano - clay nanocomposites can result in a range of clay morphologies depending on the strength of interfacial interactions between the polymer matrix and layered silicate (modified or not) and the dispersion state of the nano - clay. They are divided into three general types that are thermodynamically achievable, namely conventional, intercalated, and delaminated or exfoliated (Figure 3). An immiscible system shown in Figure 3A occurs when there is no polymer present in-between the clay and large tactoids structure remain unchanged. In these composites the miscibility between the polymer matrix and the filler does not support favorable interactions to overcome the thermodynamic considerations and the silicate layers do not separate at all. These systems are generally not considered to be nanocomposites, but regular composites. In intercalated nanocomposites, the insertion of a polymer matrix into the layered silicate structure occurs in a crystallographically regular fashion which results in clay basal spacing increase, regardless of the clay to polymer ratio. A few molecular layers of polymer are present in between the clay interlayer spacing in an intercalated nanocomposite (Figure 3B).

Exfoliated systems (Figure 3C), although less common, arise when the polymer penetration is so extensive that the clay platelets are too far apart to see each other ( $\sim 6 - 8$  nm). In this case the van der Waals interactions are too weak to impact the overall structure and the clay platelets remain separated. The last two are more desirable nano-clay morphologies since they result in the highest improvements in nanocomposites properties with the later being the most desirable since the utilization of the nano-clay surface area is maximize. Generally, most nanocomposites fall somewhere in between the two categories with the final morphology containing an expanded structure with several individual clay platelets present. However, if the layers can be fully exfoliated the property improvement can be maximized.

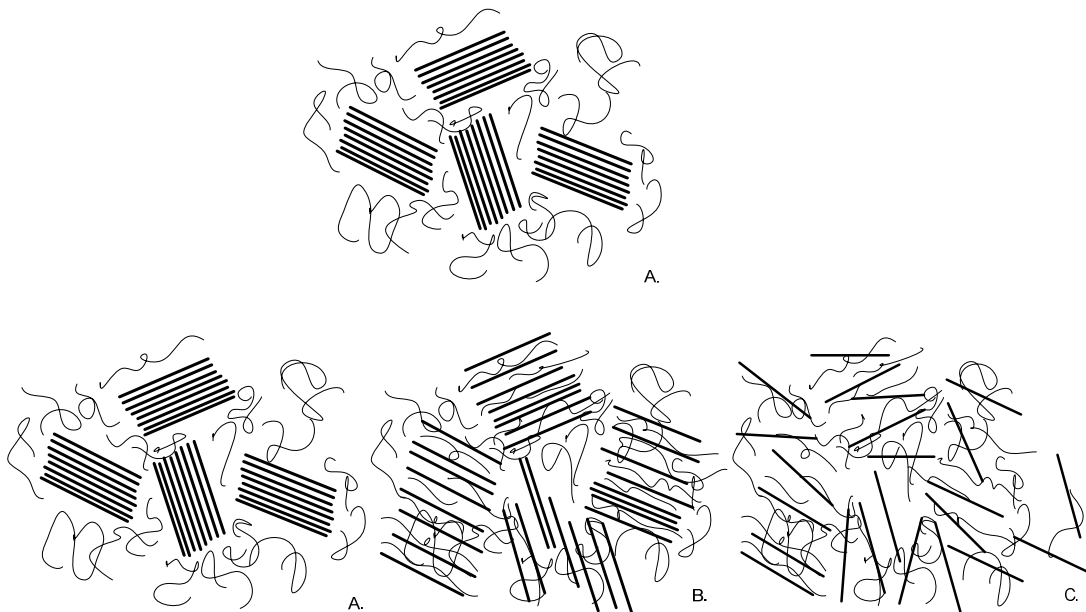


**Figure 3.** Nano - clay morphology in a polymer matrix. A. Immiscible (Microcomposite) B. Intercalated (Nanocomposite) and C. Exfoliated (Nanocomposite)

### 1.2.3 Polymer/clay nanocomposites preparation methods

Polymer layered silicate nanocomposites have been studied in industrial, academic, and government laboratories for nearly 50 years. The role of processing becomes more important in nanocomposite production affecting the resulting structure. Enhancement in material properties are directly related to the extent of dispersion of the clay platelets in the polymer matrix and extent of interactions between clay and polymer. Much of the present research in clay nanocomposites is focused on overcoming the difficulties in separating and evenly dispersing the clay layers in the polymer matrix through different processing methods while still maintaining the high aspect ratio of the clay layers. Separating the clay layers will allow for a higher surface area to be available for better polymer – clay interactions which in turn contribute to enhancements in polymer/clay nanocomposite properties.

Although nano - clays have been successfully intercalated or exfoliated in many different industrially important polar polymers such as polyamides<sup>27, 28</sup> and epoxides<sup>29, 30</sup>, dispersing clay in systems with non - polar polymers such as polystyrene, polypropylene and polyethylene has proven to be much more challenging.<sup>31-35</sup> The most common strategies for processing nanocomposites fall into one of three categories: *in-situ* polymerization, mechanical compounding/melt mixing and solution blending.

*In-situ* polymerization was the first used to prepare polymer/clay nanocomposites by Kojima et al. in a polyamide 6/MMT system.<sup>36</sup> In this method the nano - clay is swollen in monomer and the reaction is initiated by increasing the temperature, by the addition of a curing agent or peroxide. *In-situ* polymerization has been shown to give a wide range of dispersion levels with a variety of different property enhancements depending on the polymerization scheme used. The best property improvements were obtained from chain tethering to the surface

of the clay or to the modifier during the polymerization process and form a bridge connecting the confined polymer to the rest of the polymer matrix. For instance, Krishnamoorti and co-workers have recently used nitrox oxide mediated *in-situ* polymerization to prepare exfoliated polystyrene/clay nanocomposites resulting from polymer chain (6 – 9 wt%) tethering to the clay modifier which showed substantial improvements in properties over pure polymer.<sup>35</sup> Although exfoliation may be attainable, *in-situ* polymerization is complex, expensive, system specific, and can only be utilized at the time of polymer polymerization which limits its applicability in industrial applications.<sup>37</sup>

The melt intercalation process was first reported by Vaia and co-workers in 1993 when they prepared polystyrene/clay nanocomposites.<sup>21</sup> In this technique a molten thermoplastic is annealed along with an organo - clay at a temperature above the glass transition temperature of the polymer. In this method the polymer chains undergo center of mass transport in between the clay layers even though the unperturbed radius of gyration of the polymer is roughly an order of magnitude greater than the inter - gallery spacing of the clay. The polymer loses its conformational entropy during the intercalation and the proposed driving force is the enthalpic contribution of the polymer/clay interactions during annealing.<sup>38</sup> Mechanical compounding is advantageous due to the short processing times, the absence of solvents, and the ease of incorporation into industrial applications, although it has been met with limited success when additives are not used.<sup>32, 39, 40</sup> Although this method can be successful in several systems, in most industrially important polymers, high temperatures must be used to promote chain diffusion into galleries in order to minimize processing time. However, these temperatures can also have a detrimental effect on clay spacing by degrading the organic modifier and causing platelet collapse.<sup>41</sup> The collapse leads to a negative effect on nanocomposite properties since the inter-

gallery spacing is reduced and fewer polymer chains can penetrate it. This issue is most prevalent for high molecular weight polymers, which have the most demanding processing temperature requirements. Increasing shear rate can help to introduce enough energy to assist in clay delamination, yet it also causes a decrease in platelet aspect ratio.<sup>42</sup> To overcome these dispersion limitations, researches have employed polar compatibilizers and co-polymers to increase the inter - gallery spacing and make the local environment more organophilic enabling dispersion upon application of shear.<sup>40, 43</sup> Scaling theory has recently been used to show that functionalized polymers are necessary to obtain exfoliated systems from melt compounding.<sup>44</sup> Recently, Kawasumi et al. demonstrated the utility of polypropylene maleic anhydride as a polar compatibilizers to create well dispersed polypropylene nanocomposites.<sup>45</sup> Functionalized polymers however are a relatively expensive solution to dispersion and need to be tailored to maximize polymer - compatibilizers and compatibilizers - clay interactions. Furthermore, compatibilizers generally have low molecular weight and this can have a negative effect on the nanocomposite properties.

In the solution blending technique first the nano - clay is swollen in an organic solvent. The polymer which is also pre-dissolved in a solvent is added to the clay/solvent solution and intercalation of polymer between the clay layers occurs. The technique requires copious amount of organic solvents which later needs to be removed, making this an environmental unfriendly method. Although it is simple in its approach, has generally proven to be relatively ineffective at producing good clay dispersion.<sup>12, 31, 46</sup> Wide spread exfoliation is not seen in these systems due to thermodynamic barriers present. Clay intercalation increases polymer confinement, which is entropically unfavorable. To overcome such a barrier requires good interactions between the polymer and clay which may not occur due to competition between the polymer and solvent for

clay modifier interaction.<sup>4, 15</sup> However, Zhao et al. have demonstrated that sonication assisted solution blending may introduce enough energy to disperse the clay layers in a polystyrene matrix.<sup>47</sup>

There is a high demand for alternative methods for producing well dispersed nanocomposites that can easily be applied to the industrial scale; however such methods are in short supply. In general, supercritical fluids, SCFs, are more environmentally friendly and offer mass transfer advantages over conventional organic solvents. They have “gas-like” diffusivity and surface tension, and liquid-like density and low viscosity.<sup>48-50</sup> Supercritical CO<sub>2</sub> (scCO<sub>2</sub>) has recently been gaining more popularity in research and industry as an environmentally friendly solvent and blowing agent in a wide range of applications including polymerization, polymer purification and fractionation, coating applications, and powder formation.<sup>24, 51-53</sup> Moreover, scCO<sub>2</sub> has many desirable attributes such as low cost, abundance, low toxicity, and readily accessible supercritical conditions (critical temperature,  $T_c = 31.1^\circ\text{C}$ , critical pressure,  $P_c = 7.38$  MPa, critical density,  $\rho_c = 0.472$  g/mL). When CO<sub>2</sub> is raised above its critical point, its physicochemical properties can be continuously tuned between vapor-like and liquid-like limits by varying the system pressure and/or temperature. Moreover, it has been shown that a variety of polymers exhibit solubility in SCFs and that the extent of solubility depends on the molecular weight of the polymers and the processing conditions.<sup>54</sup> For example, silicones and fluorinated hydrocarbons exhibit miscibility at pressures well below alkanes of comparable chain length in CO<sub>2</sub>.<sup>55, 56</sup> In addition, scCO<sub>2</sub> has been successfully used by Zhao *et. al* along with an extruder to produce an intercalated natural sodium montmorillonite/poly-ethylene oxide (PEO) nanocomposites.<sup>57</sup> Manke, Gulari, Kannan and Ford researchers have developed a novel process for dispersion of organically modified montmorillonite with or without the organic phase present

and utilizing scCO<sub>2</sub> for the production of polymer/clay nanocomposites.<sup>24, 58</sup> In this method the nano - clay or clay/polymer system is contacted with CO<sub>2</sub> and pressurized above its critical point and mixed to allow efficient diffusion of CO<sub>2</sub> into the space between platelets. After certain processing time the system is depressurized nearly instantaneously to atmospheric pressure, causing the CO<sub>2</sub> to escape from the nano - clay inner - gallery spacing. This method relies on the drastic volumetric expansion of scCO<sub>2</sub> between aggregated particles upon depressurization that pushes the sheets/platelets apart, effectively disordering and/or dispersing them. When the CO<sub>2</sub> is completely removed a good portion of the nano - clay platelets remain separated or in the case where polymer is present the organic material remains between the layers, coating the surfaces of the layers, thus preventing most of the reformation of the layered structure. The average particle size is also reduced after sudden depressurization, although the aspect ratio is still maintained unlike other methods where the aspect ratio may be reduced after processing. Although, a large number of tactoids are still found in particle form, the number of tactoids per particle and the tightness of packing are reduced following scCO<sub>2</sub> processing. The individual tactoids are delaminated from each other and lose their parallel registry leaving large spaces for polymer to penetrate. Furthermore, the average tactoid size is reduced containing of only a few platelets. This expended flexible structure of the scCO<sub>2</sub> process particle exposes a larger surface area and this should be easier to disperse into a polymer matrix than the “as received” particle. Recently, this method has demonstrated the ability to disperse commercially available nano - clays in a polydimethylsiloxane (PDMS) matrix, with the resultant nanocomposites exhibiting marked rheological improvement over the neat polymer.<sup>59</sup> Moreover, it was also shown that some clay (modifier dependent) can be dispersed and/or disordered without any polymer present by soaking in scCO<sub>2</sub> followed by catastrophic depressurization.<sup>59, 60</sup> The unique ability of this novel

technique to disperse clay by itself is the only currently published method demonstrating this property. The pre-dispersed/disordered clay can then be co-extruded with the polymer of interest or it can be processed again with the polymer in the presence of scCO<sub>2</sub> at the manufacturing facilities to improve the properties of the resulting products.

However, there is a need for gaining a better understanding on what the morphology of the nano - clay is after scCO<sub>2</sub> processing. Furthermore, a better understanding on the effects that different factors such as processing conditions (temperature, pressure, depressurization rate, processing time, co-solvent), clay modifiers and different polymers, have on the resulting nano-clay morphology and nanocomposite properties in order to optimize the supercritical carbon dioxide processing technique for the desired results. Researchers are using several methods for characterizing nano - clay and polymer/nano - clay nanocomposite including wide and small angle X-ray diffraction (WAXD and SAXD), scanning and transmission electron microscopy (SEM and TEM), thermogravimetric analysis (TGA), differential scanning calorimetry (DSC), permeability and mechanical testing, rheology and many others. However, each of the above mentioned characterization techniques have their own advantages and limitations. Therefore, a combination of several techniques need to be used in order to obtain a more complete picture on the effects of above mention factors on the nano - clay morphology and nanocomposite structure and properties. WAXD is one of the most widely used tools by researchers for structural characterization of nano -c lays in nanocomposites. However, the whole picture cannot be obtained if WAXD is used by itself since it has a few drawbacks. Although, it can give information about the intercalation state of the nanocomposite, it is not sensitive to an inter-gallery spacing larger than 5 nm, therefore it is relatively insensitive to exfoliated platelets and to disordered platelets. Hence, X-ray diffraction cannot provide a whole picture of the nano - clay



morphology if used as a standalone tool. Electron microscopy is used as a technique to complement X-ray diffraction data in order to better visualize the spatial dispersion state of the nano - clay in the nanocomposites. With the sub-nanometer resolution limit of the TEM, individual platelets and platelet stacks can be directly visualized and a better understating of the nano - clay morphology can be obtained when both TEM and X - ray diffraction are used together. However, TEM only gives information on the local level since only a small part of the sample is used. Rheology is a more sensitive tool to the degree of dispersion and it can also give information about polymer - clay interactions. Testing the nanocomposite permeability can also give an insight on the degree of clay dispersion since increase dispersion leads to a reduction in permeability. TGA and tensile testing are also used to complement the other characterization tools to have a more complete picture about the nano - clay dispersion status in the nanocomposites. Therefore, to really gain a more complete understanding on how different processing methods and variables affect the nano - clay dispersion, polymer - clay interactions, processability, transport properties and reinforcement of a polymer matrix, a verity of characterization techniques are used. As a result, a better understating of the scCO<sub>2</sub> processing technique can be achieved on different polymer - clay systems and a better ability of predicting the results on other systems can be acquired.

In Chapter 2 the ability of the scCO<sub>2</sub> process to dispersed and/or disorder nano - clay is investigated using “as received” Cloisite 10A from Southern Clay Products. The ability of scCO<sub>2</sub> to dispersed nano-clay was initially demonstrated by Horsch et al. (Cloisite 93A and partially Nanocor I.30P) <sup>59</sup>, however no investigation was done on understanding what is the final structure of the nano - clay following scCO<sub>2</sub> processing. Also, no analysis on how the processing parameters (processing time and multiple processing) affect the resulting nano - clay structure. In

this chapter the above mention processing parameters are explored and X-ray diffraction, scanning electron microscopy and volume change are used as characterization techniques to gain a better understating on what is going on during scCO<sub>2</sub> processing and what is the nano - clay morphology after scCO<sub>2</sub> processing. In addition, the pre-dispersed/disordered nano - clay is reprocessed using scCO<sub>2</sub> technique in the presence of polystyrene in an attempt to maximize nano - clay dispersion and evaluate its effect on the final nanocomposite properties (see Chapter 3).

Although the scCO<sub>2</sub> process has been proven to be effective on polymer melts, no research has been done on its applicability to polymer solutions. An important benefit of processing polymer in solution is that it allows for relatively low temperatures to be used in comparison to those required for melt blending. Lower processing temperature minimizes clay modifier degradation, maximizes the rate of CO<sub>2</sub> density change, and improves CO<sub>2</sub> - polymer miscibility. Additionally, the reduced temperature and viscosity in a polymer - solvent system can allow for longer processing times, giving the chains time to thoroughly penetrate the clay layers.

The research in Chapter 3 focuses on the use of a co-solvent along with scCO<sub>2</sub> to maximize nano - clay dispersion and produce dispersed low and high molecular weight PS/clay nanocomposites with enhanced properties (rheological, mass transport and thermal). The aim is to gain a better understating of the scCO<sub>2</sub> processing method which should allow optimizing it for the desired dispersion and/or properties. To achieve this goal, the role of scCO<sub>2</sub> processing parameters in promoting polymer - clay interaction, in dispersing nano - clay, in enhancing polymer thermal degradation, in enhancing viscoelastic properties, and in reducing oxygen and water vapor permeability in polystyrene nanocomposites is investigated. Furthermore, in this

work, the effects of varying clay organic modifier on the resultant nano - clay dispersion and properties of polystyrene - clay nanocomposites dispersed with scCO<sub>2</sub> method are investigated. The role of polymer - clay interactions on nano - clay dispersion and reinforcement has been the topic of many publications.<sup>7, 47, 61, 62</sup> In most of the common processing methods, the extent of dispersion is often strongly related to how favorably the particle interacts with the polymer matrix. This effect has been exhibited both experimentally and in simulation by researchers where it has been observed that the stronger the polymer - clay interactions are the higher the intercalation level is since there is sufficient enthalpic driving force to surpass the entropic penalty of polymer confinement.<sup>5, 13, 63</sup> Pandey and coworker<sup>64</sup> demonstrated through molecular simulation that if there is a repulsive polymer - clay interaction present in the nanocomposite, the clay layers prefer to disperse and if the polymer matrix is attractive, clay platelets intercalate. Ammala et al. showed in a poly(m-xylene adipamide)-montmorillonite based clays nanocomposites that the barrier properties strongly depend on the clay modifier used. The favorably interacting Cloisite 10A showed a considerable reduction in the oxygen transmission rates (66% reduction) while Cloisite 93A showed a small increase (4% increase).<sup>47</sup> In another study, Rohlmann et al.<sup>65</sup> showed that in a polypropylene/clay system prepared by melt mixing using a barbender plastograph, although Cloisite 15A and 93A nanocomposites showed similar dispersion, the nanocomposite made using 15A displayed superior rheological properties. Studying the scCO<sub>2</sub> processing parameters effects on the nano - clay morphology, rheological, transport and thermal properties in scCO<sub>2</sub> processed nanocomposites will help to better understand the parameters needed to produce nanocomposites with optimized properties. To accomplish this goals, low (5,000 g/mol) and high (280,000 g/mol) molecular weight polystyrene, styrene and “as received” Cloisite 10A, 93A, 15A and Nanocor I30P are used in this

study and processed using scCO<sub>2</sub> and solution blending processing techniques. To gain a better understanding of how processing parameters affect nano - clay morphology and the resulting polymer properties a series of samples at different processing conditions are created and characterized using viscoelastic measurements, permeability testing, TEM, WAXD and TGA. The properties of the scCO<sub>2</sub>-processed nanocomposites will be compared with those made through other techniques used in the literature.

In Chapter 4, the role of polymer - clay interactions and filler dispersion on the linear viscoelastic response of scCO<sub>2</sub> processed polymer - clay nanocomposites in the melt state is investigated. In the previous chapter emphasis is put on the use of a co-solvent to aid in improving nano - clay dispersion in the case of low and high molecular weight PS and to aid in processing high molecular weight PS. In this chapter polyvinylmethylether (PVME) is chosen as the host matrix for natural montmorillonite and two organophilic nano -clays (Cloisite 30B and Nanocor I30.P). Natural montmorillonite is chosen as a reference for the strength of the polymer - filler interactions because it has weak interactions with the host polymer. PVME is highly swellable in scCO<sub>2</sub> even at a molecular weight of 90,000 g/mol. Also, PVME is hydrophilic and may facilitate processing of even natural clay which cannot be done using PS. Poly(ethylene oxide) (PEO) is also used as the host matrix for natural montmorillonite to compare the extent of PEO - filler interactions with that of PVME - filler interactions. The rheological response of scCO<sub>2</sub> processed PEO/Cloisite Na<sup>+</sup> is compared to that of scCO<sub>2</sub> processed PVME/ Cloisite Na<sup>+</sup> to understand the role of polymer – clay interactions in the two nanocomposites and demonstrate that in the case of PVME/Na<sup>+</sup> system there are weak interactions present. Furthermore, the organophilic clays used in this study may have varying degrees of interactions with the host matrix, in addition to having different a different degree of clay dispersion upon scCO<sub>2</sub>

processing. Specifically, Cloisite 30B (methyl tallow bis-2-hydroxyethyl ammonium salt) may form a hydrogen bond between the host matrix and the surfactant, and Nanomer I.30P (trimethyl hydrogenated tallow ammonium salt) has a moderate loading of alkyl groups, thereby altering the extent of the polymer - clay interactions in each system. The scCO<sub>2</sub> processed nanocomposites are contrasted with a highly dispersed (disordered) PVME/Cloisite Na<sup>+</sup> nanocomposite produced from a solution cast/freeze drying method, with water as a solvent. As a result of the selected processing conditions, the nanocomposites produced via the scCO<sub>2</sub> method had intercalated or disordered intercalated morphologies. To understand the role of clay structure on the linear viscoelasticity of “weakly-interacting” polymer/clay nanocomposites the rheological response of the partially exfoliated PVME/Cloisite Na<sup>+</sup> nanocomposite and the intercalated PVME/Cloisite Na<sup>+</sup>/nanocomposite are compared. Furthermore, to determine the impact of specific polymer - clay interactions have on the rheological properties the two intercalated organophilic clay - PVME nanocomposites are compared to the “weakly-interacting systems” (PVME/Cloisite Na<sup>+</sup>).

### **1.3. Supercritical carbon dioxide (scCO<sub>2</sub>) process**

Three strategies are employed to produce polymer/clay nanocomposites using the scCO<sub>2</sub> processing technique. In the first approach the nano - clay is process under the appropriate conditions by itself without the presence of a polymer matrix. The resulting nano - clay can be melt-mixed, compounded with an appropriate polymer to create a nanocomposite. Alternatively, it can also be reprocessed in scCO<sub>2</sub> again in the presence of a polymer to make a nanocomposite with improved properties. To our knowledge, this is the only process currently published with the unique ability to disperse clay by itself. The second method involves blending the as received nano - clay with a CO<sub>2</sub>-philic polymer and processing the resulting mixture in scCO<sub>2</sub>. A

third method, similar to the second one involves the use of a solvent along with the polymer and nano-clay to assist in processing. This method is employed when polymers with a high glass transition temperature ( $T_g$ ) are used to increase polymer solubility. Also, due to the limited thermal stability of the clay modifiers, processing at high enough temperatures and for long enough times to make processing polymers with high  $T_g$  feasible would cause platelet gallery collapse. To address these issues, a concentrated solution of polymer in solvent is used in place of pure polymer to allow processing temperatures to be lowered. Furthermore, to optimize the clay disorder upon depressurization, it is preferential to have the most dramatic CO<sub>2</sub> density change possible. The density change decreases the farther from the critical temperature the material is processed at.

The scCO<sub>2</sub> processing method is displayed in Figure 5. It involves contacting the nano - clays, the polymer/clay mixtures and the polymer/solvent/clay mixtures with bone dry scCO<sub>2</sub>. The layered nano - clays or the polymer/clay mixtures are loaded and they are contacted with CO<sub>2</sub> in a high pressure vessel (Figure 5A). The system is then raised to the desired temperature and pressure, above the critical point of CO<sub>2</sub> ( $T_c = 31.1^\circ\text{C}$ ,  $P_c = 7.38 \text{ MPa}$ ). Following a desired processing time where the mixture is allowed to soak in scCO<sub>2</sub> (Figure 5B) the system is rapidly depressurized to atmospheric pressure (Figure 5C). In the case where a solvent is used the process is very similar. The only difference is that the polymer and solvent are loaded in the reactor and hand mixed until the mixture is homogeneous, after which the nano - clay is added to the mixture and again is hand mixed to make sure there are no clay chunks in the system. From here on the process is the same to the above steps A, B and C. The polymer viscosity can be reduced significantly depending on the polymer solubility in scCO<sub>2</sub> due to the solvation effect which helps in polymer processing. Furthermore, by carefully choosing the pressure and

temperature of the system, the density and solubility parameter of scCO<sub>2</sub> can be adjusted effectively allowing great control over these solvation and expansion effects.

The proposed hypothesis for the mechanism is that during the soaking step in the case where polymer or polymer/solvent is present, the high diffusivity and low viscosity of the CO<sub>2</sub>-philic polymer in the mixture enable clay layer penetration. In the case where only CO<sub>2</sub> and clay are present the CO<sub>2</sub> diffuses into the CO<sub>2</sub>-philic clay gallery. During depressurization, the outward force due to expansion of the scCO<sub>2</sub> between the layers pushes them apart resulting in dispersed nanocomposites or dispersed nano - clays. When the CO<sub>2</sub> is completely removed a good portion of the nano - clay platelets remain separated or in the case where polymer is present the organic material remains between the layers, coating the surfaces of the layers, thus preventing most of the reformation of the layered structure. If a solvent is used it is initially removed under high vacuum and room temperatures and then elevated temperatures and low vacuum to make sure that no residual solvent is left in the nanocomposite.

The processing vessel used is a 256 mL stainless steel THAR reactor with sapphire windows and is capable of handling pressures up to 69 MPa at 150°C without and 41 MPa with the magnetic agitator installed (Figure 4). The reactor is outfitted with a series of valves, which control the depressurization rate. The CO<sub>2</sub> is charged into the vessel via a 266 mL Teledyne Isco syringe pump capable of a pressure of 52 MPa and flow rates ranging from 0.001 – 107 mL/min.



**Figure 4.** scCO<sub>2</sub> processing reactor, controller and high pressure pump.

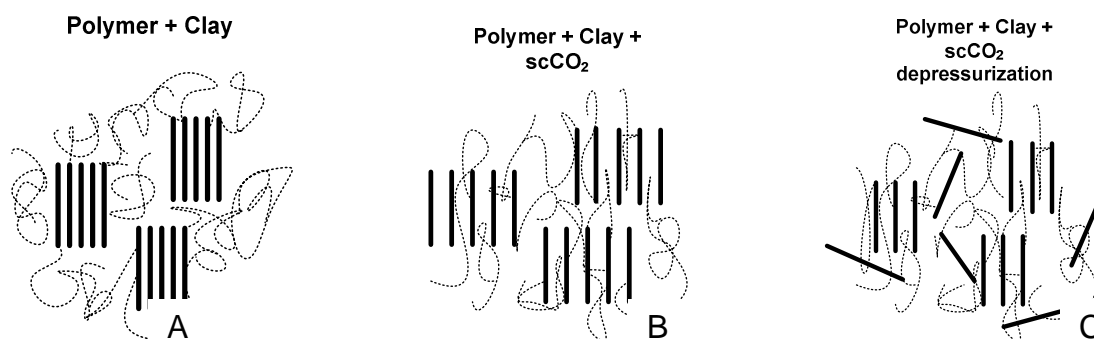


**Figure 5.** Supercritical fluid processing.

#### 1.4 Significance of research

Existing techniques for achieving significant nano - clay dispersion with or without the presence of a polymer matrix are limited. Supercritical CO<sub>2</sub> processing has the potential to create nanocomposites that display significant dispersion in a wide range of polymer matrices. Supercritical CO<sub>2</sub> offers several advantages: it can generate better exfoliated/dispersed systems (leading to enhanced properties), it eliminates the need for expensive specially modified clay, and it eliminates the use of hazardous and expensive organic solvents although it can still be used



in the presence of a co-solvent if needed. Furthermore, it has the potential for easily implementation into existing industrial process unlike solution casting and *in-situ* polymerization. Moreover, with only a small amount of dispersed nano - clay (0.5 – 5 wt %) the mass transport, mechanical and thermal properties of polymer can be significantly improved using the scCO<sub>2</sub> processing technique. The significance of this work covers both practical and fundamental aspects. There is a need for a better understanding on what is the final morphology of the nano - clay and for a method to benchmark the extent of dispersion following scCO<sub>2</sub> processing. Further research in providing a better picture of the nano - clay structure after processing may enable a better understanding on the potential property improvement that it can provide when mixed with the desired polymers. Moreover, there is a need for understanding the effects of different processing parameters on the final morphological structure of nano - clay in nanocomposites produced utilizing scCO<sub>2</sub> processing technique. Due to the wide range of morphologies that can result from the variety of specific and non specific interactions possible, understanding the role that processing variables and different materials play on the nano - clay structure and its effect on the resulting nanocomposite properties (viscoelastic, transport properties (O<sub>2</sub> and water vapor permeability) and thermal properties) is critical for process development and optimization. Further research into the structure - properties relation in these nanocomposites and how to get the most out of the process will help to make the method more effective and scientifically viable. Utilizing the results of the above mentioned studies it can be attempted to create a better picture of the physical process of nano - clay delamination (dispersion) following scCO<sub>2</sub> process with or without the presence of an organic phase and how to maximize scCO<sub>2</sub> nanocomposite properties processed produced using the scCO<sub>2</sub> technique.

## CHAPTER 2

### Supercritical CO<sub>2</sub> processing of Cloisite 10A

The ability of scCO<sub>2</sub> to dispersed nano - clay was initially demonstrated by Horsch et al. (Cloisite 93A and partially Nanocor I.30P).<sup>59</sup> It was also shown that dispersion can be controlled by tuning the pressure and temperature. The disappearance of the d<sub>001</sub> peak in X-ray diffraction was correlated to nano - clay dispersion/exfoliation.<sup>59</sup> Furthermore, no investigation was performed on how multiple processings affect the resulting nano - clay structure. In this chapter the effect of repeated scCO<sub>2</sub> processing is explored and X-ray diffraction, scanning electron microscopy and volume change are used as characterization techniques to gain a better understating on what is the nano - clay morphology subsequent to scCO<sub>2</sub> processing. Furthermore, the percent volume change can also be used to determine whether or not there is any significant change between multiple scCO<sub>2</sub> processings and may also be used as a benchmark to nano - clay dispersion. To aid in this explanation, the results from Chapter 3 will also be used where pre-dispersed nano - clay was reprocessed in scCO<sub>2</sub> in the presence of styrene and polystyrene.

#### 2.1 Materials

The nano - clay used in this investigation is Cloisite 10A. It is a dimethyl, benzyl hydrogenated tallow quaternary ammonium salt with an inter-gallery spacing of ~ 0.92 nm (Table 1). It was purchased from Southern Clay Products, Inc.

**Table 1.** Physical data of Cloisite 10A. HT = hydrogenated tallow (~ 65% C18; ~ 30% C16; ~ 5% C14. (Data provided by Southern Clay Inc.)

| Name         | Organic Modifier   | d <sub>001</sub> Spacing (nm) | CEC (meq/100g) |
|--------------|--|-------------------------------|----------------|
| Cloisite 10A | $\begin{array}{c} \text{CH}_3 \\   \\ \text{HT}-\text{N}^+-\text{CH}_2-\text{C}_6\text{H}_5 \\   \\ \text{CH}_3 \end{array}$ | 1.92                          | 125            |

## 2.2 Methods of Characterization

### 2.2.1 Wide angle X-ray diffraction (WAXD)

A Rigaku Rotaflex Powder Diffractometer with a Cu K $\alpha$  X-ray source ( $\lambda = 1.54 \text{ \AA}$ ) and an accelerating voltage of 40 kV at a current of 120 mA was used to determine the inter-gallery spacing of the “as-received” and scCO<sub>2</sub> processed clay. WAXD is widely used as a tool for characterizing the morphology of clay in nanocomposites. Due to their highly ordered platelet structure, an X-ray diffraction peak that is characteristic of the spacing between clay platelets can be obtained. Any increase or decrease in average platelet separation will result in a shift in diffraction angle, while loss of platelet parallel registry (i.e. disorder) can be detectable by reduction in peak intensity.

To perform the required scans the samples were placed in a custom made, zero-background quartz sample holder that is 0.9 mm in depth. Several scans were obtained from different locations in the sample and verified to be reproducible when diffraction patterns are superimposed on one another. The  $2\theta$  angle can be determined using the JADE software that accompanies the diffractometer and the d<sub>001</sub> spacing for the clays was calculated using Bragg's Law of diffraction:

$$n * \lambda = 2 * d * \sin \theta \quad (1)$$

where  $n$  is an integer determined by the order given,  $\lambda$  is the wavelength of X-rays,  $d$  is the spacing between the planes in the atomic lattice,  $\theta$  is the angle between the incident ray and the scattering planes). The inter-gallery spacing was then found by subtracting 0.96 nm (platelet thickness) from the  $d_{001}$  spacing. A broadening and flattening of the peaks may indicate partial exfoliation and a disappearance of the basal spacing peak may indicate the layers are either exfoliated or disordered<sup>37</sup>.

### **2.2.2 Scanning electron microscopy (SEM)**

Scanning electron microscopy was used to gain a better understanding into the morphology of nano - clay before and after scCO<sub>2</sub> processing. This method is used in conjunction with X-ray diffraction to obtain a more complete picture on the nano - clay morphology both before and after scCO<sub>2</sub> processing. Several images were collected using a Hitachi S-2400 scanning electron microscope with an electron potential of 25 kV. The samples were sputter coated with gold and several (15-20) images were collected for all samples to ensure accurate representation of the clay morphology.

### **2.2.3 Thermogravimetric analysis (TGA)**

Perkin Elmer Pyris 1 TGA was used to measure the thermal stability of the “as received” and scCO<sub>2</sub> process nano - clay to verify whether or not following scCO<sub>2</sub> processing any of the modifier is coming out with CO<sub>2</sub> during processing and/or during depressurization. Temperature ramp measurements were conducted under inert atmosphere of N<sub>2</sub> from 25 °C to 650 °C at 10 °C min<sup>-1</sup>. Before starting the test, samples were equilibrated at 25 °C for 10 minutes.

### **2.2.4 Volume/density change determination**

Centrifuge tubes (10 ml) were used to measure the volume of nano - clay following scCO<sub>2</sub> process to determine the extent of volume change that the clay undergoes after processing. The measurement was done by measuring the mass it takes to fill 5 cm<sup>3</sup> of sample. The tubes were repeatedly taped and clay was added until no further change was seen upon tapping. After the mass was obtained the density was calculated and the volume change was calculated by using 1 g of sample and the obtained density.

### **2.3 Nano-clay preparation**

The scCO<sub>2</sub> ability to dispersed “as received” Cloisite 10A without a polymer matrix present was investigated by processing it at 80°C and, 13.79 in the presence of supercritical carbon dioxide for 0.5, 1, 2, 4, 8 and 24 hours under constant stirring followed by instantaneous depressurization. Moreover, the nano – clay was processed three times consecutively to study the effect of multiple processings/depressurizations on the final clay morphology. The pre-dispersed Cloisite 10A can be used to investigate the role of clay dispersion on the resulting nanocomposite by reprocessing it in the presence of polymer (discussed in more detail in section Chapter 3).

### **2.4 Nano-clay characterization**

#### **2.4.1 Thermogravimetric analysis**

To verify whether or not following scCO<sub>2</sub> processing any of the modifier is coming out with CO<sub>2</sub> during processing or during depressurization thermogravimetric analysis on both “as received” and scCO<sub>2</sub> processed nanocomposite was obtained (Figure 6). Both clays show similar thermal behavior across the temperature range tested with the scCO<sub>2</sub> process 10A having less than 0.5% less residual mass at 650°C than unprocessed 10A which is within the analyzer error.

This suggests that the scCO<sub>2</sub> technique does not remove the organic modifier present in-between the clay layers. Furthermore, the derivative TGA curves of “as received” Cloisite 10A and scCO<sub>2</sub> processed Cloisite 10A display no change in the maximum degradation rate (MRD) between the two providing further evidence that scCO<sub>2</sub> processing and/or depressurization does not remove the organic modifier.

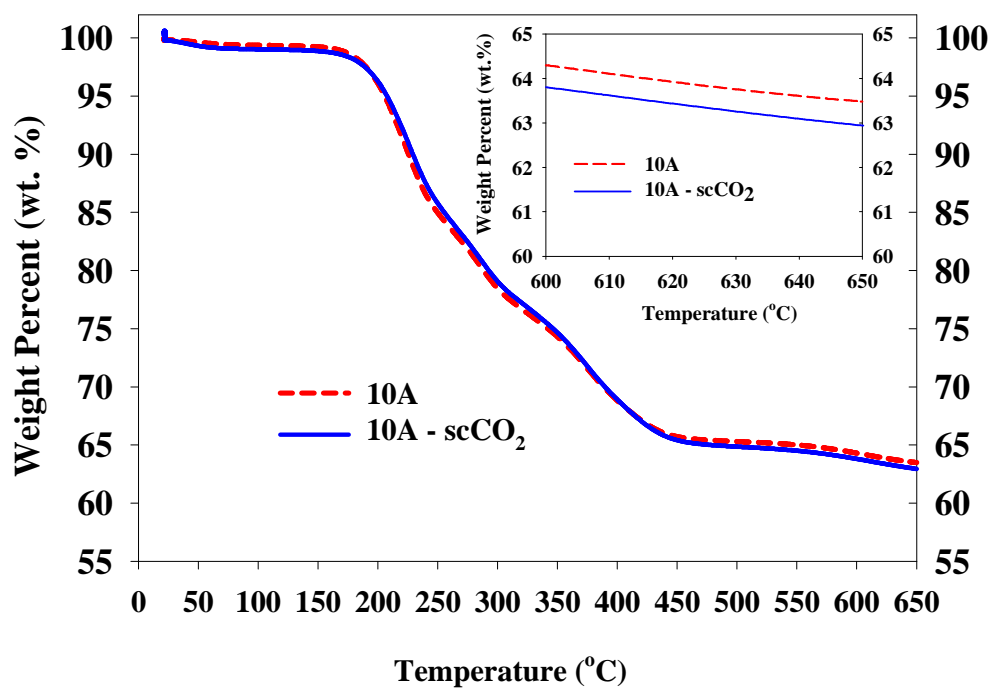


**Figure 6.** TGA analysis of “as received” Cloisite 10A and scCO<sub>2</sub> processed “as received” 10A. The final weight present does not change significantly following scCO<sub>2</sub> processing and/or during depressurization indicating that the scCO<sub>2</sub> processing technique does not remove the nano - clay organic modifier.

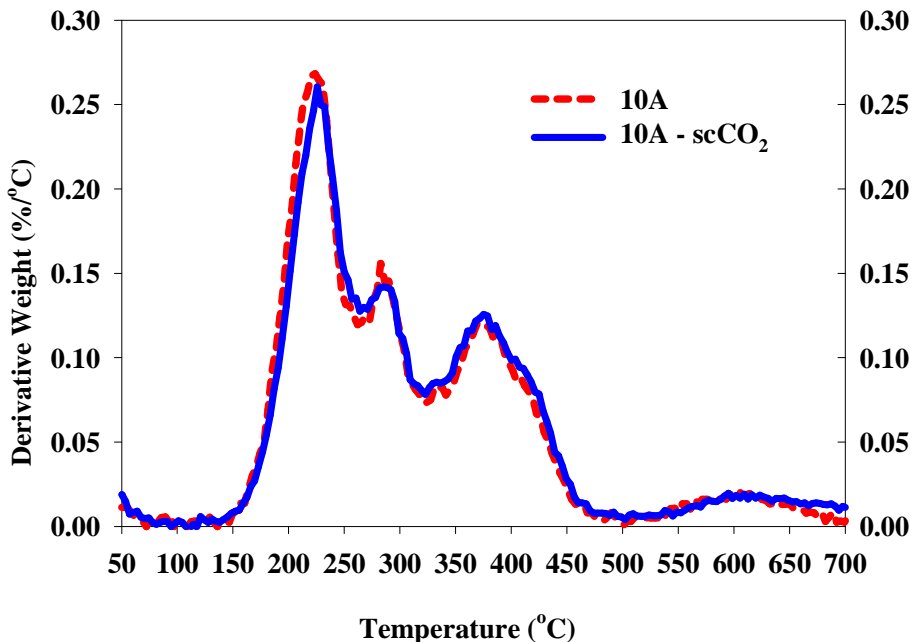


**Figure 7.** Derivative TGA curves for “as received” Cloisite 10A and scCO<sub>2</sub> processed Cloisite 10A. There is no change in the maximum degradation rate (MRD) between the two providing further evidence that scCO<sub>2</sub> does not remove the organic modifier.

#### 2.4.2 Wide angle X-ray diffraction

In order to determine if the ordered spacing of the clay platelets was disturbed upon processing, WAXD of both pure 10A and the scCO<sub>2</sub> processed 10A was collected (Figure 8). The diffraction peak of “as received” Cloisite 10A can be observed at  $2\theta = 4.7^\circ$  which corresponding to its’ equilibrium inner-gallery spacing of 0.92 nm. The lack of a peak for the scCO<sub>2</sub> processed clay was thought to indicate exfoliation. However, the scCO<sub>2</sub> pre-processed clay was reprocessed in scCO<sub>2</sub> in the presence of polystyrene/styrene and when the nanocomposite was analyzed there was a  $d_{001}$  peak in X-ray diffraction. This result was surprising at the beginning since the clay was exfoliated and there was no peak before reprocessing. It is believe that a lack of  $d_{001}$  peak rather indicates that wide spread disturbance of

the clay parallel registry has occurred and a range of morphologies from disordered intercalated to exfoliated could be present.

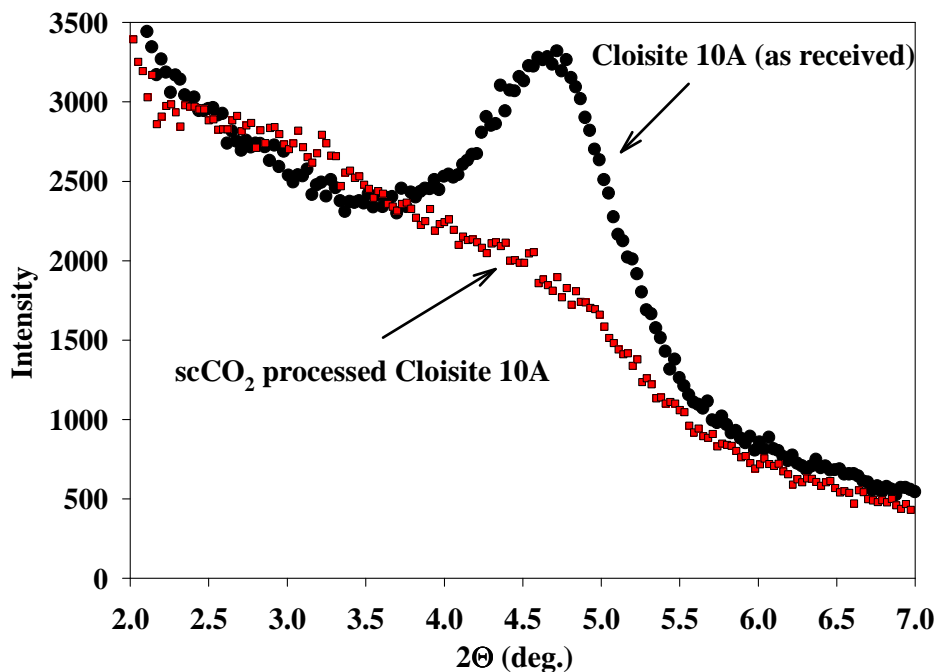


**Figure 8.** WAXD of as received Cloisite 10A and scCO<sub>2</sub> processed 10A. The disappearance of the  $d_{001}$  peak following scCO<sub>2</sub> processing is a good indication that the clay has been dispersed and/or disordered.

### 2.4.3 Scanning electron microscopy

To better visualize the effects scCO<sub>2</sub> has had on the structure of the clay particles and tactoids, SEM was employed to directly image the clay particles before and after processing. A zoomed out SEM of several “as received” particles is shown in Figure 9. Images of a typical “as received” 10A particles are shown in Figure 10. From the conceptualized image of an “as received” Cloisite 10A particle (Figure 11) it can be seen that the particle is composed of several tactoids which in turn contained many stacked platelets. The unprocessed clay is composed of particles ranging from 5-20  $\mu\text{m}$  consisting of a large number of tightly bound tactoids with an average diameter of 1.1  $\mu\text{m}$  (white circles displayed in Figure 10). The tactoids contain a number



of highly ordered stacked platelets held together by weak van der Waals forces. SEM images illustrate that tactoids are closely bound in particles and no individual platelets exist in the “as received” 10A. In contrast, the images of scCO<sub>2</sub> processed 10A display a diverse morphology (Figure 12 and Figure 13). Although a large fraction of tactoids is still found in particle form, the number of tactoids per particle and the tightness of packing are reduced. The individual tactoids have delaminated from each other and lost their parallel registry, leaving large spaces into the center of the particles for polymer to penetrate. Measuring the size of tactoids across multiple images of each material (a few of which are indicated by white circles in the figures) it was found that although the average particle size has been reduced significantly (1 - 6 μm), the tactoid aspect ratio has been preserved. Upon depressurization, it is believed that a fraction of the outer most layers is completely delaminated from the tactoids during CO<sub>2</sub> expansion while the much less mobile inner layers just lose the coherent parallel registry that is probed by X-ray diffraction. This system can be qualified as being disordered intercalated. The same clay morphology is depicted in a conceptualized image of a scCO<sub>2</sub> processed particle (Figure 15). Utilizing the SEM images alone we cannot confirm the existence of dispersed single layers due to the difficulty in differentiating individual platelets from individual tactoids in SEM images. The expanded flexible structure of the scCO<sub>2</sub> processed particles/tactoids exposes more of the available surface area and the platelets should be easier to disperse into a polymer matrix than the “as received” clay. The pre-dispersed clay could possibly produce good dispersion in extrusion compounding since the kinetic limitation of clay dispersion may no longer be an issue in the short times required for melt compounding. In Chapter 3, the pre-processed Cloisite 10A was added to polystyrene/styrene solution and reprocess the composite with scCO<sub>2</sub> in an attempt to maximize dispersion. The pre-dispersed clay will be used to study the effect that pre-

dispersing the clay has on the polystyrene/clay nanocomposites morphology compared to “as received” clay.

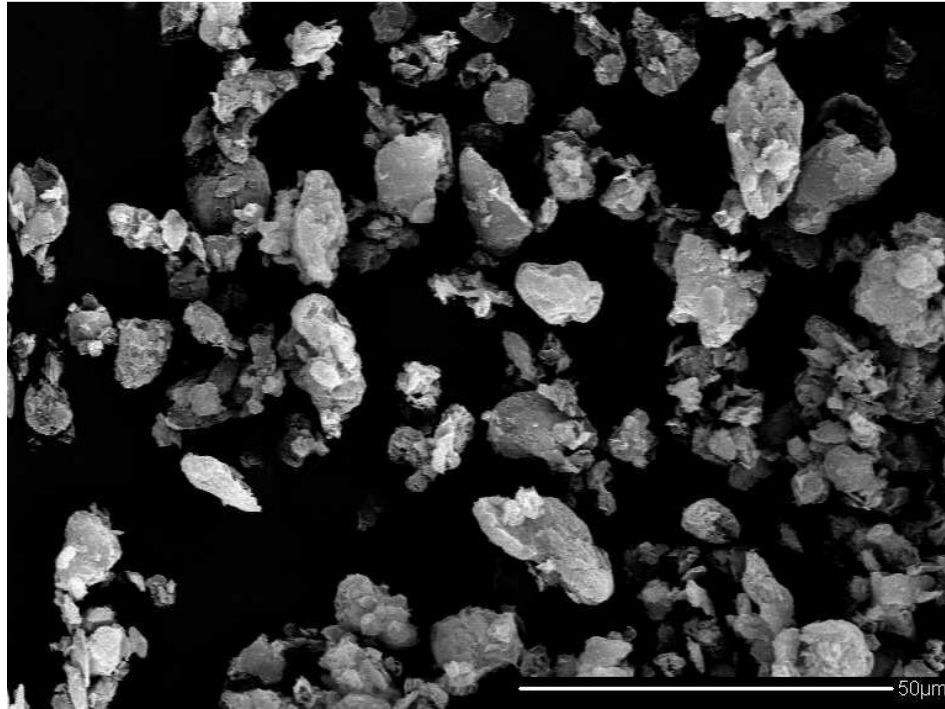


**Figure 9.** SEM image of “as received” Cloisite 10A particles.

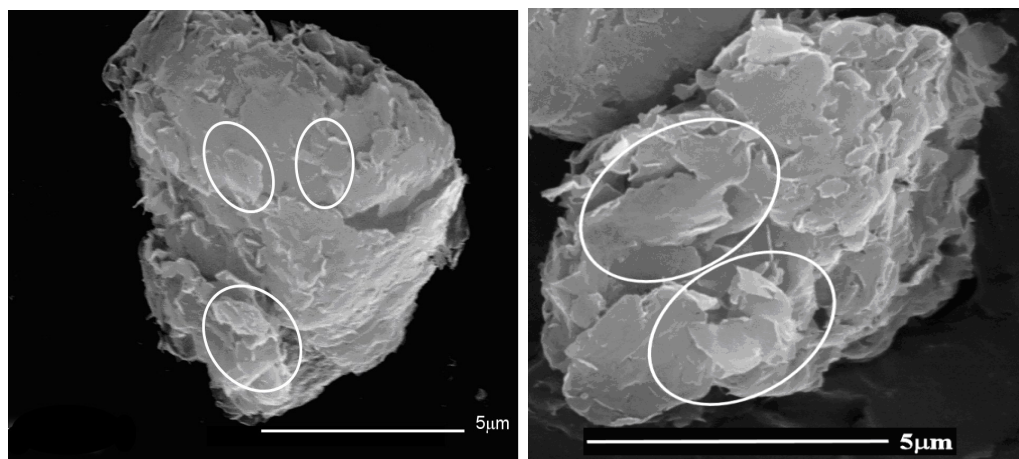


**Figure 10.** SEM images of an "as received" Cloisite 10A particle.

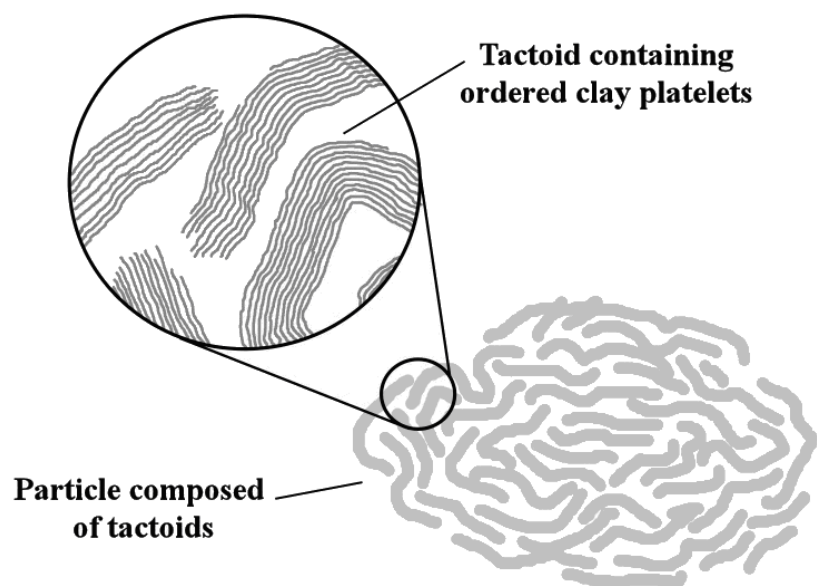


**Figure 11.** Illustration of "as received" Cloisite 10A particle

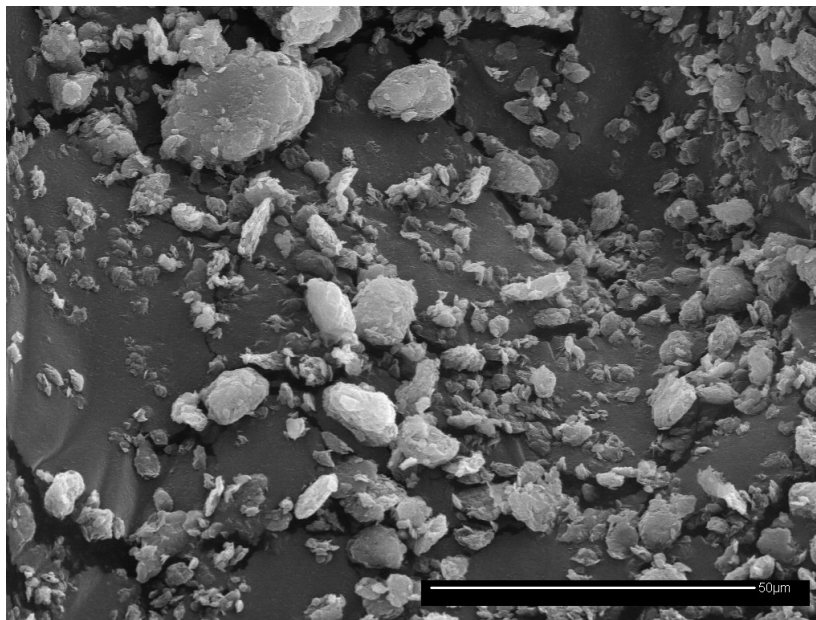


**Figure 12.** SEM image of scCO<sub>2</sub> Cloisite 10A particles processed 1 time for 24 hours.

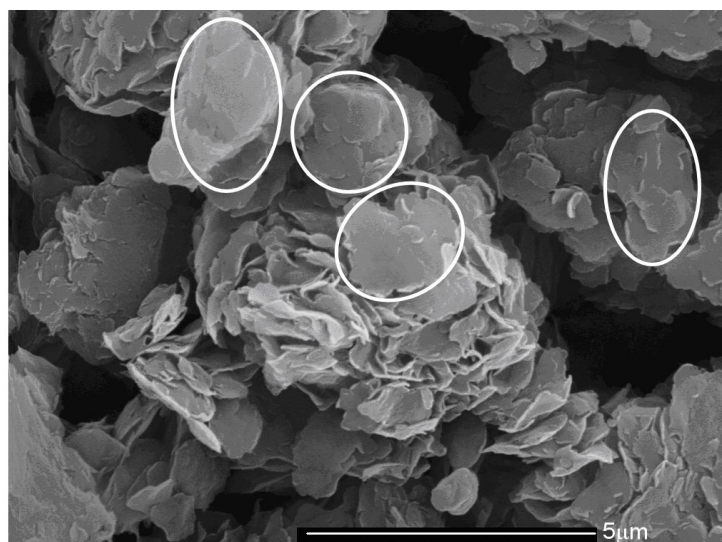


**Figure 13.** SEM image of a scCO<sub>2</sub> processed Cloisite 10A particle processed 1 time for 24 hours.

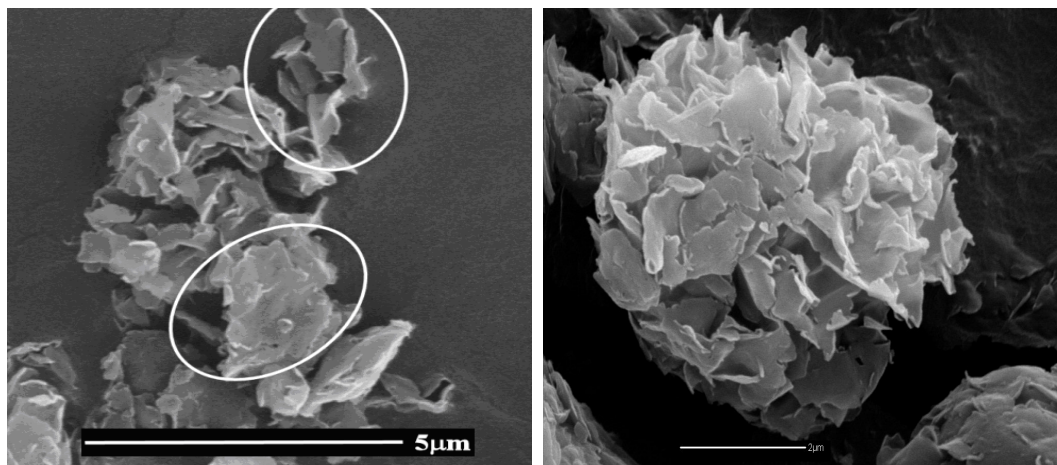


**Figure 14.** SEM images of a scCO<sub>2</sub> Cloisite 10A particle processed 1 time for 24 hours.

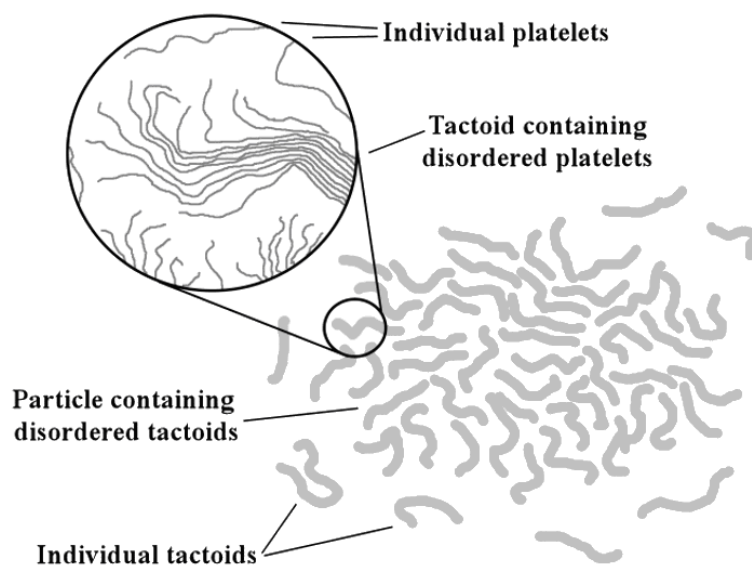


**Figure 15.** Illustration of scCO<sub>2</sub> processed Cloisite 10A particle

#### 2.4.4 Volume change measurements

To determine the effect of multiple scCO<sub>2</sub> processings on Cloisite 10A structure the clay was processed three consecutive times using the scCO<sub>2</sub> method. Since there was no discernable peak in X-ray diffraction and SEM doesn't show any further change on the particle structure, another method is needed to study the effects of multiple processings on nano - clay morphology. Volume change after each processing was measured and it was determined that after one processing there is approximately 15% increase in volume, an approximately 5% further increase after the second processing and 5% more after the third processing for a total of approximately 25 % increase in volume following 3 consecutive processings (Figure 16).

After the first processing it appears that nano - clay particles are expended from their condense "egg shape" structure to more "open cabbage" structure due to the CO<sub>2</sub> expansion during depressurization and that most of the particles have been reduced in size as seen from SEM. Further scCO<sub>2</sub> processing results in a smaller change in volume and this may be because CO<sub>2</sub> now has a pathway to escape from the clay inner-gallery during depressurization since the structure has been already expended. Although it might still cause additional expansion and delamination of more outer layers, it seems the biggest change occurs during the first processing. The result from the third processing where the additional volume change is about 5% provides further evidence of this reasoning. Furthermore, this result complements the conclusion obtained from X-ray and SEM study of the scCO<sub>2</sub> processed 10A that upon depressurization, it appears that a fraction of the outermost layers are delaminated from the tactoids during CO<sub>2</sub> expansion while the much less mobile inner layers just lose the coherent parallel registry. To determine what effect the scCO<sub>2</sub> processing time has on the final structure the percent volume change was also measured on Cloisite 10 samples that were processed for different amount of time (15 min,

0.5, 1, 2, 4, 8 and 24 hours) (Figure 17). It appears that 15 minutes is enough time to cause a big change in volume of Cloisite 10A since the volume change after 15 minutes of scCO<sub>2</sub> processing is similar to that after 2 or even 24 hours. In an industrial setting, the nano - clay can be processed repeatedly for a short time 15 minutes or 0.5 hours to maximize the structure expansion in a relatively short time.

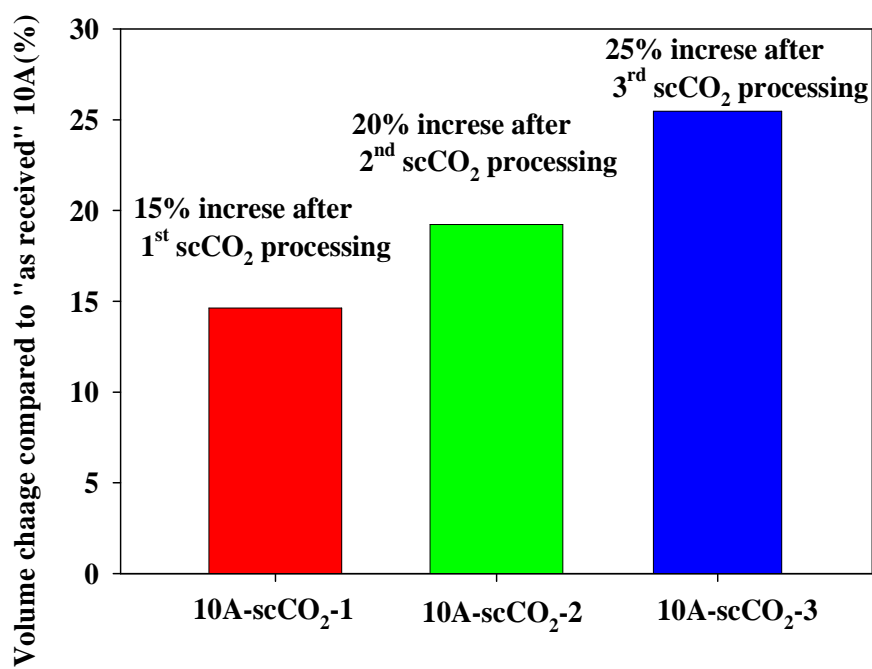


**Figure 16.** Percent volume change of Cloisite 10A after multiple scCO<sub>2</sub> processings.

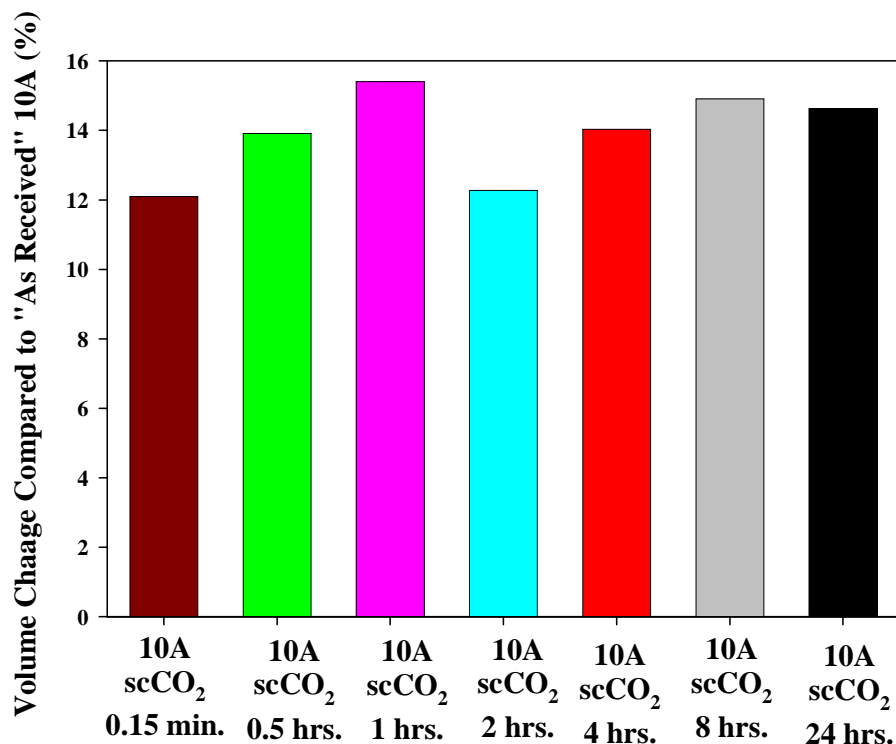


**Figure 17.** Percent volume change of Cloisite 10A after scCO<sub>2</sub> processing.

## 2.5 Conclusions

The supercritical carbon dioxide process was successfully used to disorder Cloisite 10A upon depressurization without the presence of an organic phase (polymer matrix). The lack of  $d_{001}$  peak in WAXD and disturbance of the tactoids from a tightly bound morphology to a much more loosely associated structure (SEM images) are evidence of nano - clay dispersion. Some fraction of the pre-dispersed clay regained its parallel registry after it was added to polystyrene-styrene solution as evident by the re-appearance of a defined X-ray diffraction peak. Although, several consecutive scCO<sub>2</sub> processings led to further dispersion and/or disordering of nano - clay the biggest effect was observed following the first processing when the particle size was reduced. Moreover, it is believed that a fraction of the outer most layers is completely delaminated from the tactoids during CO<sub>2</sub> expansion while the much less mobile inner layers just lose the coherent



parallel registry. Processing the clay for a 2<sup>nd</sup> and 3<sup>rd</sup> time led only to a smaller volume expansion and no further reduction in particle size, indicating that the further increase in volume change may be due to an increase in the number of individual platelets present. It was also observed that processing the clay for 15 minutes led to similar results as processing for 4, 12 or even 24 hours.

## CHAPTER 3

### **Supercritical Carbon Dioxide - Processed Dispersed Polystyrene – Clay Nanocomposites: Investigation of Processing Parameters Effects on the Nanocomposites Morphology and Properties**

The research in Chapter 2 focused on understanding and optimizing nano - clay dispersion using the supercritical carbon dioxide process without the presence of an organic phase. In this chapter the aim is to maximize nano - clay dispersion in the presence of an organic phase (polystyrene) and produce dispersed low and high molecular weight PS/clay nanocomposites with enhanced properties (rheological, transport and thermal). The aim in Chapter 3 is to gain a better understanding of the scCO<sub>2</sub> processing method which should allow optimizing it for the desired clay dispersion and/or nanocomposites properties. To achieve this goal, the role of scCO<sub>2</sub> processing parameters in promoting polymer - clay interaction, in dispersing nano - clay, in enhancing polymer thermal degradation, in enhancing viscoelastic properties, and in reducing oxygen and water vapor permeability in polystyrene nanocomposites is investigated. To accomplish this goals, low (5,000 g/mol) and high (280,000 g/mol) molecular weight polystyrene, styrene and “as received” Cloisite 10A, 93A, 15A and Nanocor I30P are used in this study and processed using scCO<sub>2</sub> and solution blending processing techniques at various conditions. To gain a better understanding of how processing parameters affect nano-clay morphology and the resulting polymer properties a series of samples at different weight fraction are created and characterized using viscoelastic and permeability testing, TEM, WAXD and TGA.

## **3.1 Materials**

### **3.1.1 Nano-clays**

The nano - clays used in this investigation were Cloisite 10A, 93A, 15A and Nanocor 1.30P. Cloisite 10A is a dimethyl, benzyl hydrogenated tallow quaternary ammonium salt with an inter-gallery spacing of  $\sim 0.92$  nm (Table 2). Cloisite 93A is a methyl dihydrogenated tallow ternary ammonium. Cloisite 15A is a dimethyl dihydrogenated tallow quaternary ammonium. Nanocor 1.30P is a trimethyl hydrogenated tallow quaternary ammonium salt. The Cloisite series was purchased from Southern Clay Products, Inc. and the 1.30P was donated by Nanocor.

### **3.1.2 Polymers, solvent and gas**

High and low molecular weight polystyrene (PS) were used in this study. Carbon dioxide in the form of compressed gas was supplied by Airgas Inc. The low molecular weight PS was obtained from Polysciences, Inc. and has a molecular weight of  $5,000 \text{ g mol}^{-1}$  and a glass transition temperature,  $T_g$ , of  $70^\circ\text{C}$ . The high molecular weight PS was purchased from Scientific Polymer Products, Inc. and has a molecular weight of  $280,000 \text{ g mol}^{-1}$ , a  $T_g$  of  $104^\circ\text{C}$  and a polydispersity of 4. The inhibited styrene and toluene used in this study was purchased from Sigma Aldrich. The physical properties of the polymers are listed in Table 3.

**Table 2.** Physical data of Cloisite 93A, 15A, 10A and Nanocor I.30P. HT = hydrogenated tallow (~ 65% C18; ~ 30% C16; ~ 5% C14. (Data provided by Southern Clay Inc.)

| Name         | Organic Modifier   | d <sub>001</sub> Spacing (nm) | CEC (meq/100g) |
|--------------|--|-------------------------------|----------------|
| Cloisite 93A | $\begin{array}{c} \text{H} \\   \\ \text{HT}-\text{N}^+-\text{CH}_3 \\   \\ \text{HT} \end{array}$                           | 2.36                          | 90             |
| Cloisite 15A | $\begin{array}{c} \text{CH}_3 \\   \\ \text{HT}-\text{N}^+-\text{CH}_3 \\   \\ \text{HT} \end{array}$                        | 3.13                          | 125            |
| Cloisite 10A | $\begin{array}{c} \text{CH}_3 \\   \\ \text{HT}-\text{N}^+-\text{CH}_2-\text{C}_6\text{H}_5 \\   \\ \text{CH}_3 \end{array}$ | 1.92                          | 125            |
| I.30P        | $\begin{array}{c} \text{CH}_3 \\   \\ \text{HT}-\text{N}^+-\text{CH}_3 \\   \\ \text{CH}_3 \end{array}$                      | 2.25                          | 145            |

**Table 3.** Polymer properties

| Polymer | Mw (g/mol) | ~ T <sub>g</sub> (°C) | ~ # of entanglements | R <sub>g</sub> (nm) |
|---------|------------|-----------------------|----------------------|---------------------|
| PS      | 5,000      | 70                    | 0                    | 1.89                |
| PS      | 280,000    | 104                   | 16                   | 14                  |

## **3.2 Methods of characterization**

### **3.2.1 Wide angle X-ray diffraction**

The intergallery spacing of the clays and clay/polymer nanocomposites was determined using a Rigaku SmartLab Diffractometer with a Cu K $\alpha$  X-ray source ( $K\alpha = 1.54 \text{ \AA}$ ) and an accelerating voltage of 40 kV at a current of 40 mA. Diffraction scans were collected from  $0.1^\circ$  to  $10^\circ$  2-theta at a scan rate of 3.0 degrees/min and a step size of  $0.3^\circ$ . The Bragg's Law of diffraction was used to calculate the  $d_{001}$  spacing for the nano-clays and their intergallery spacing was determined by subtracting the platelet thickness (1 nm) from the  $d_{001}$  spacing.

### **3.2.2 Transmission electron microscopy (TEM)**

Samples for ultramicrotomy were prepared by melt pressing nanocomposite granules in a mold at  $180^\circ\text{C}$ . A Reichert-Jung Ultracut E Microtome was used to cut nanocomposite thin films of about 80–100 nm. The films were collected on a 200 mesh copper grids and carbon coated before being examined with a JEOL Fast EM 2010 HR TEM operated at 200 kV. To assure an accurate representation of the nano - clay morphology in the polystyrene matrix numerous (15–20) images were collected for all of the nanocomposites.

### **3.2.3 Thermogravimetric analysis**

Perkin–Elmer Pyris 1 TGA was used to validate that no residual styrene remained in the nanocomposites after drying and to measure the residual mass of clay separated from the processed nanocomposites to verify if polystyrene chains are tethering to the clay surface or not during processing. Also, TGA was used to study the changes in thermal decomposition of polystyrene due to solution blended and supercritical carbon dioxide processing induced dispersion of nano - clay in the corresponding nanocomposites. Temperature ramp measurements

were conducted under inert atmosphere of N<sub>2</sub> from 25 to 650 °C at a rate of 10 °C/min. For the clay-tethering study, samples of each nanocomposite were dissolved in excess toluene to make dilute solutions of clay and polymer in solvent. These samples were then centrifuged at high speed (15000 RPM) and the supernatant removed. The residual material at the bottom was resuspended in solvent and the procedure repeated three times in an attempt to wash any non-bonded organic materials off of the clay.

### **3.2.4 Permeability measurements**

OX-TRAN model 2/10 was used to measure oxygen transmission rates and AQUATRAN model 1 was used to measure the water vapor transmission rates (both from MOCON). For the oxygen permeability testing ASTM F-2622 method was used where the oxygen and nitrogen flow rates were at 10 cm<sup>3</sup>/min and the relative humidity was kept at 25%. In the case of water vapor, 100% the relative humidity on the wet side and 15% relative humidity on the dry side were used for the duration of the test. Both machines were calibrated using films that were in compliance with the National Institute of Standard and Technology. Prior to performing permeability testing samples were prepared by melt pressing films at 180°C between Kapton plates. The polystyrene film thickness varied from sample to sample from 0.1 mm to 0.4 mm. The transmission rates were multiplied by the film thicknesses to find the oxygen or water vapor permeability rates. At least 5 films for each sample were tested to assure statistical viability.

### **3.2.5 Rheology**

The structure characterization of polymer/clay nanocomposites has been typically established using WAXD and TEM. However, another tool used to study nanocomposite is oscillatory shear rheology. It can be used to gain a better insight into the clay structure and nanocomposite morphology due to its sensitivity to the microscale/mesoscale structure of the

nano-clay in the host polymer matrix. More specifically, highly intercalated systems would exhibit a cross frequency shift when compared to the pure matrix polymer. If the crossover frequencies are similar however, it indicates that a high degree of dispersion may exist or a conventional composite may exist. To differentiate between different nanocomposite morphologies, the enhancement of material properties ( $G'$  and  $G''$ ) may further elucidate the structural hierarchy. In highly dispersed systems, the dynamic moduli would show a much higher degree of improvement than would exist in a conventional or intercalated system due to the large available surface area in dispersed systems.

In this study a Rheometric Scientific RSA II rheometer (shear sandwich geometry 15.98 mm x 12.7 mm x 0.55 mm) was used to perform melt rheological measurements under oscillatory shear. The dynamic oscillatory shear measurements were performed by applying a time dependent oscillatory strain,  $\gamma(t) = \gamma_0 \sin(\omega t)$ , and measuring the resulting shear stress  $\sigma(t) = \gamma_0 G' \sin(\omega t) + \gamma_0 G'' \cos(\omega t)$ . The dynamic moduli were then plotted on a log-log plot versus frequency. Many polymer systems obey the William-Landel-Ferry (WLF) equation for time temperature superposition. This relationship allows measurements done at different temperatures to be superposed on a single plot, thereby, expanding the range of information beyond the actual mechanical range employed. In addition, homo-polymers typically display terminal flow behavior (i.e.  $G' \propto \omega^2$  and  $G'' \propto \omega$ ). Such rheological behavior may not be observed in nanocomposite systems where strong interactions between matrix polymer material and clay occur. Prior to performing viscoelastic measurements the 280kPS samples were prepared by melt pressing into a mold at 180°C and 5k PS at 120°C between Teflon plates. The materials were loaded and allowed to equilibrate for 1 h at the desired temperature. Measurements were collected between 140°C - 240°C in 20 °C increments for all 280k PS samples and at 120°C and

150°C for 5k PS. Strain sweeps were performed to ensure that the dynamic moduli are independent of the strains utilized and the linear viscoelastic measurements were made at low strains ( $\gamma_0 < 0.05$ ) to prevent the alignment of the clay platelets and to minimize microstructure destruction. The frequency range used was  $0.01 \leq \omega \leq 100 \text{ rad s}^{-1}$  and the property of time-temperature superposition was used to create master curves with a reference temperature of 140°C for 280k PS and 120°C for 5k PS.

### 3.3 Nanocomposites preparation

Three 5k PS were made to compare the results from four processing techniques. One sample was prepared using the melt blending method under vacuum at 120°C for 24 hours while it was periodically hand-mixed, (5kPS-10A-melt). Another sample was prepared using the scCO<sub>2</sub> method at 120°C, 13.79 MPa for 24 hours under constant stirring (5kPS-10A-scCO<sub>2</sub>) and another sample was prepared using scCO<sub>2</sub> method with a co-solvent (toluene), at 120°C, 13.79 MPa for 24 hours under constant stirring (5kPS-10A-sol-scCO<sub>2</sub>). An additional sample (5kPS-10A-sol) was prepared using the solution blended technique at 120°C for 24hrs under constant stirring as a benchmark to the solvent assisted scCO<sub>2</sub> sample (Table 4). In the case of 280k polystyrene several samples were prepared using the scCO<sub>2</sub> solvent assisted processing method and one where the “as received” 10A was co-extruded with PS (PS-5%10A-extruded) in a lab-scale Haake 3/4-inch extruder with metering pump, temperature-controlled film extrusion head and chilled casting roll. An approximately 30% polystyrene in styrene mixture was first loaded in the reactor and hand mixed until it is homogeneous. Then Xg of clay (X is the mass of clay required for each desired final weight fraction based on polystyrene), was added to the polymer solution and hand-mixed until homogeneous. The mixture was then processed in scCO<sub>2</sub> for a certain amount of time at a specific temperature (below 100°C) and pressure under vigorous stirring.



Styrene was used to lower the viscosity of polystyrene, facilitating better mixing and allowing processing below the glass transition temperature of polystyrene. The low processing temperature minimizes clay modifier degradation, maximizes the rate of CO<sub>2</sub> density change, and improves CO<sub>2</sub>- polystyrene miscibility. Additionally, the reduced temperature and viscosity can allow for longer processing times, giving the polymer chains more time to thoroughly penetrate the clay layers. To investigate the role of clay weight fractions three samples 2, 5 and 10 wt% by clay (PS-2%10A-scCO<sub>2</sub>, PS-5%10A-scCO<sub>2</sub> and PS-10%10A-scCO<sub>2</sub>) were made using “as received” Cloisite 10A in the presence of scCO<sub>2</sub> at 80°C, 13.79 MPa for 24 hours. To compare the effect of the scCO<sub>2</sub> process to solution blending method, three benchmark composites of 2, 5 and 10 wt% clay (PS-2%10A-sol, PS-5%10A-sol and PS-10%10A-sol) were also prepared in the same vessel without the presence of scCO<sub>2</sub> at 80°C for 24 hours. These benchmark samples are also used so the role of thermal annealing and solution blending might play in the results can be eliminated (Tables 5 and 6).

Two 5wt% 10A samples were prepared which were slowly depressurized at a rate of approximately 0.045 MPa/min for PS-5%10A<sub>sd</sub>-scCO<sub>2</sub> and at 0.115 MPa/min for PS-5%10A<sub>5md</sub>-scCO<sub>2</sub> to investigate the role of scCO<sub>2</sub> depressurization on the clay dispersion in the resulting nanocomposite (Table 6). Compared to the later two samples PS-5%10A-scCO<sub>2</sub> was depressurized instantaneously at a rate of approximately 300 MPa/min allowing for the investigation of role that the rate of depressurization has on the morphology of the resulting nanocomposite. The scCO<sub>2</sub> pre-processed clay was utilized to prepare two 5wt% 10A samples: one re-processed again in scCO<sub>2</sub> (PS-5%10A<sub>pe</sub>-scCO<sub>2</sub>) and another in solution (PS-5%10A<sub>pe</sub>-sol) to study the role of clay dispersion on the morphology of the resulting polymer/clay nanocomposite. “As received” Cloisite 93A (PS-5%93A-scCO<sub>2</sub>, PS-5%93A-sol), 15A (PS-

5% 15A-scCO<sub>2</sub>, PS-5% 15A-sol) and Nanocor I30P (PS-5%I30P-scCO<sub>2</sub>, PS-5%I30P-sol) were used to study the effect of nano - clay morphology on the nanocomposite dispersion and properties following scCO<sub>2</sub> and solution blending processing (Table 6).

The effects of processing time (PS-5% 10A-scCO<sub>2</sub> for 24 hours, PS-5% 10A.5-scCO<sub>2</sub> for 0.5 hours, PS-5% 10A4-scCO<sub>2</sub> for 4 hours and PS-5% 10A12-scCO<sub>2</sub> for 12 hours) and pressure (PS-5% 10A-scCO<sub>2</sub> for 13.79MPa, PS-5% 10Ay-scCO<sub>2</sub> for 10.34 MPa and PS-5% 10Az-scCO<sub>2</sub> for 27.58 MPa) were also investigated by preparing 5 wt% samples of Cloisite 10A/PS in scCO<sub>2</sub> (Table 7).

A summary of the nanocomposite compositions, processing conditions and sample names is given in Table 5. After processing, the samples were dried at room temperature for 48 hours followed by 160°C under vacuum for 6 hours. Literature has shown that exceeding temperatures of 105°C or more for long periods of time can cause the degradation of organic modifier bonded to the clay surface, causing gallery collapse comparable to that of montmorillonite. However, this effect is minimal if the temperature does not exceed 200°C or the clay is not kept for long periods of time at a raised temperature.<sup>15, 66</sup>

**Table 4.** 5k Polystyrene/Cloisite 10A nanocomposites sample composition and nomenclature

| <b>Sample Name</b>             | <b>Clay wt%</b> | <b>Processing Variables (120°C, 24 hours and for scCO<sub>2</sub> 13.79 MPa were used for all samples unless specified)</b> |
|--------------------------------|-----------------|---|
| 5kPS                           | 0%              | none  |
| 5kPS-10A-melt                  | 5%              | melt compounded   |
| 5kPS-10A-sol                   | 5%              | solvent   |
| 5kPS-10A- scCO <sub>2</sub>    | 5%              | scCO <sub>2</sub> + fast depressurized  |
| 5kPS-10Asol- scCO <sub>2</sub> | 5%              | solvent + scCO <sub>2</sub> + fast depressurized  |

**Table 5.** Polystyrene/Cloisite 93A, 15A, Nanocor I.30P nanocomposites sample composition and nomenclature

| Sample Name                 | Clay wt% | Processing Variables (80°C and 24 hours were used for all samples, 13.79 MPa for scCO <sub>2</sub> ) |
|-----------------------------|----------|--|
| PS-2%93A-scCO <sub>2</sub>  | 2%       | solvent + scCO <sub>2</sub> + fast depressurized   |
| PS-5%93A-sol                | 5%       | solvent  |
| PS-5%93A-scCO <sub>2</sub>  | 5%       | solvent + scCO <sub>2</sub> + fast depressurized   |
| PS-10%93A-scCO <sub>2</sub> | 10%      | solvent + scCO <sub>2</sub> + fast depressurized   |
| PS-5%15A-sol                | 5%       | solvent  |
| PS-5%15A-scCO <sub>2</sub>  | 5%       | solvent + scCO <sub>2</sub> + fast depressurized   |
| PS-5%I30P-sol               | 5%       | solvent  |
| PS-5%I30P-scCO <sub>2</sub> | 5%       | solvent + scCO <sub>2</sub> + fast depressurized   |

**Table 6.** Polystyrene/Cloisite 10A nanocomposites sample compositions and nomenclature

| <b>Sample Name</b>            | <b>Clay wt%</b> | <b>Processing Variables (80°C and 24 hours were used for all samples, 13.79 MPa for scCO<sub>2</sub>)</b> |
|-------------------------------|-----------------|---|
| PS-5% 10A-extruded            | 5%              | melt compounded (200°C, 15 minutes, 90 rpm)   |
| PS-5% 10A-sol                 | 5%              | solvent   |
| PS-5% 10Ape-sol               | 5%              | solvent + pre-processed clay  |
| PS-5% 10Asd-scCO <sub>2</sub> | 5%              | solvent + scCO <sub>2</sub> + slow depressurized (~0.045MPa/min)  |
| PS-5% 10Amd-scCO <sub>2</sub> | 5%              | solvent + scCO <sub>2</sub> + medium depressurized (~0.115MPa/min)  |
| PS-5% 10A-scCO <sub>2</sub>   | 5%              | solvent + scCO <sub>2</sub> + fast depressurized (~300MPa/min)  |
| PS-5% 10Ape-scCO <sub>2</sub> | 5%              | solvent + scCO <sub>2</sub> + fast depressurized + pre-processed clay                                     |
| PS-2% 10A-sol                 | 2%              | solvent   |
| PS-2% 10A-scCO <sub>2</sub>   | 2%              | solvent + scCO <sub>2</sub> + fast depressurized  |
| PS-10% 10A-sol                | 10%             | solvent   |
| PS-10% 10A-scCO <sub>2</sub>  | 10%             | solvent + scCO <sub>2</sub> + fast depressurized  |

**Table 7.** Polystyrene/Cloisite 10A nanocomposites sample composition and nomenclature

| <b>Sample Name</b>            | <b>Clay wt%</b> | <b>Processing Variables (80°C, 24 hours and 13.79 MPa were used for all samples unless specified)</b> |
|-------------------------------|-----------------|---|
| PS-5% 10A-scCO <sub>2</sub>   | 5%              | solvent + scCO <sub>2</sub> + fast depressurized – polymer/solvent first                              |
| PS-5% 10Aa-scCO <sub>2</sub>  | 5%              | solvent + scCO <sub>2</sub> + fast depressurized – clay/solvent first                                 |
| PS-5% 10A.5-scCO <sub>2</sub> | 5%              | solvent + scCO <sub>2</sub> + fast depressurized – 0.5 hours  |
| PS-5% 10A4-scCO <sub>2</sub>  | 5%              | solvent + scCO <sub>2</sub> + fast depressurized – 4 hours  |
| PS-5% 10A12-scCO <sub>2</sub> | 5%              | solvent + scCO <sub>2</sub> + fast depressurized – 12 hours   |
| PS-5% 10A-scCO <sub>2</sub>   | 5%              | solvent + scCO <sub>2</sub> + fast depressurized – 24 hours   |
| PS-5% 10Ay-scCO <sub>2</sub>  | 5%              | solvent + scCO <sub>2</sub> + fast depressurized – 10.34 MPa  |
| PS-5% 10A-scCO <sub>2</sub>   | 5%              | solvent + scCO <sub>2</sub> + fast depressurized – 13.79 MPa  |
| PS-5% 10Az-scCO <sub>2</sub>  | 5%              | solvent + scCO <sub>2</sub> + fast depressurized – 27.58 MPa  |

To determine if any clay degradation occurs during solvent removal while drying (6 hrs. @ 160°C under vacuum), TGA was performed on Cloisite 10A before and after drying (Figure 18). Notably, after 6 hours of 160°C in a vacuum, the clay shows very little loss in the way of organic content. WAXD was also performed on clay samples before and after annealing with no discernable shift in  $d_{001}$  spacing found (Figure 18). Similar results were obtained for all clays tested here. The “as received” and dried clays samples results from TGA and WAXD are summarized in Table 8. Based on TGA and WAXD data, the relatively short time that the samples spend at a moderate temperature to remove residual volatiles is not enough to cause any appreciable effect on the clay modifier.

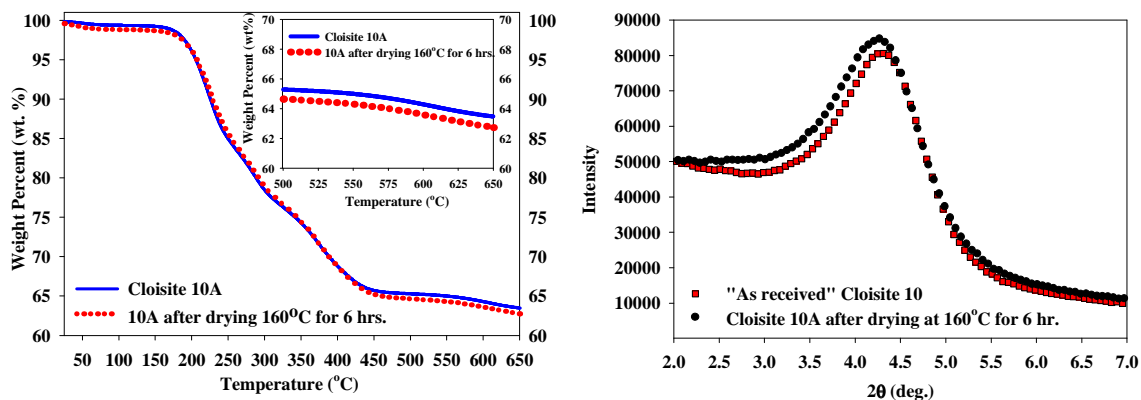


**Figure 18.** TGA (left) and WAXD (right) of “as received” Cloisite 10A and 10A after drying in the vacuum oven at 160°C for 6 hours.

**Table 8.** Summary of TGA and WAXD for “as received” and dried clay at 160°C for 6 hrs. TGA data was taken as weight percent that remained as char at 650°C.

| Clay                 | TGA           |       | WAXD                  |       |
|----------------------|---------------|-------|-----------------------|-------|
|                      | Weight %      |       | d <sub>001</sub> (nm) |       |
|                      | “as received” | Dried | “as received”         | Dried |
| <b>Cloisite 10A</b>  | 63.16         | 63.05 | 1.92                  | 1.91  |
| <b>Cloisite 93A</b>  | 65.94         | 65.31 | 2.36                  | 2.34  |
| <b>Cloisite 15A</b>  | 57.75         | 57.02 | 3.13                  | 3.10  |
| <b>Nanocor I.30P</b> | 68.38         | 67.54 | 2.25                  | 2.24  |

### **3.4 Low molecular weight 5k PS/clay nanocomposites characterization (WAXD and rheology)**

#### **3.4.1 Wide angle X-ray diffraction**

In this section low molecular weight 5k PS/10A nanocomposites were prepared using four different techniques to investigate the effect of PS processing methods on nano - clay dispersion and rheological properties. The aim is to maximize nano - clay dispersion and to compare the scCO<sub>2</sub> processing technique to conventional melt processing and solution blended method. X-ray diffraction and rheology were used as characterization tools to study the morphology of the resulting nanocomposites by probing changes in the level of clay dispersion. We were able to disperse/intercalate Cloisite 10 A in low molecular weight PS no matter what method was employed. Interestingly, all samples regarding of the processing method, displayed the same final  $d_{001}$  of 4.12 nm. Compared to “as received” Cloisite 10A which had a  $d_{001}$  of 1.92 nm, the inner-gallery spacing was increased by 2.20 nm (Figure 19). Moreover, the presence of the  $d_{002}$  peak along with a  $d_{001}$  peak indicates a highly ordered intercalated nanocomposite was present. The second peak was definitely a  $d_{002}$  diffraction peak since it occurs at twice the value of 2 theta of  $d_{001}$  peak. This was surprising at first since a different level of dispersion was expected between the nanocomposites. However, Giannelis and Vaia have previously modeled intercalation behavior of clay in a polymer matrix and determined that there are several factors that contribute to the level of clay dispersion that is attainable in a system. The authors also performed corresponding experiments on several PS/clay hybrids to substantiate the simulation results.<sup>13, 15</sup> Their findings show that there is an entropic balance between the clay modifier that wants to have as much conformational freedom as possible, and the matrix polymer that does not want to be confined between the clay platelets. The entropic gain associated with the organic

modifier from increasing the clay basal spacing only occurs until the modifier chains become fully extended ( $h_{\infty}$ ), after which there is no gain or penalty to increased platelet spacing. However, there is still an entropic penalty to increased spacing that comes from polymer confinement until the clay spacing is greater than the average radius of gyration of the matrix material. In order for the platelet spacing to extend farther than  $h_{\infty}$  would require strong polymer-clay interactions to overcome the entropic barrier. The inter-gallery spacing at full chain extension ( $h_{\infty}$ ) can be expressed in terms of the number of carbon atoms in the aliphatic backbone ( $n'$ ) by:

$$h_{\infty} = (n' - 1)0.127 + A + B \quad (2)$$

where A and B represent the size of a methyl and an ammonium moiety respectively.<sup>67</sup> The fully extended C-18 chains of Cloisite 10A correlate to a calculated spacing of approximately 2.8 nm which compares acceptably with the experimentally measured inter-gallery spacing of 3.32 nm (4.32 nm – 1 nm platelet thickness) keeping in mind the low radius of gyration of 5k PS (1.89 nm) and the positive interactions between the phenol moiety on the clay modifier and PS. The 3.32 nm spacing is bigger than the radius of gyration of 5 k PS and this along with favorable interaction between clay surfactant and PS, the entropic barrier of clay separation can be overcome resulting in further gallery expansion compared to the estimated equilibrium spacing. This can be a possible explanation why all samples regarding of the processing technique displayed the same X-ray diffraction peak. Furthermore, using X-ray diffraction does not probe individual platelets since a significant level of order in any remaining tactoids of even a well dispersed sample will result in a large X-ray peak. It has been previously demonstrated that due to the complex morphologies possible in a clay nanocomposite X-ray diffraction should not be used as a standalone tool for determining dispersion.



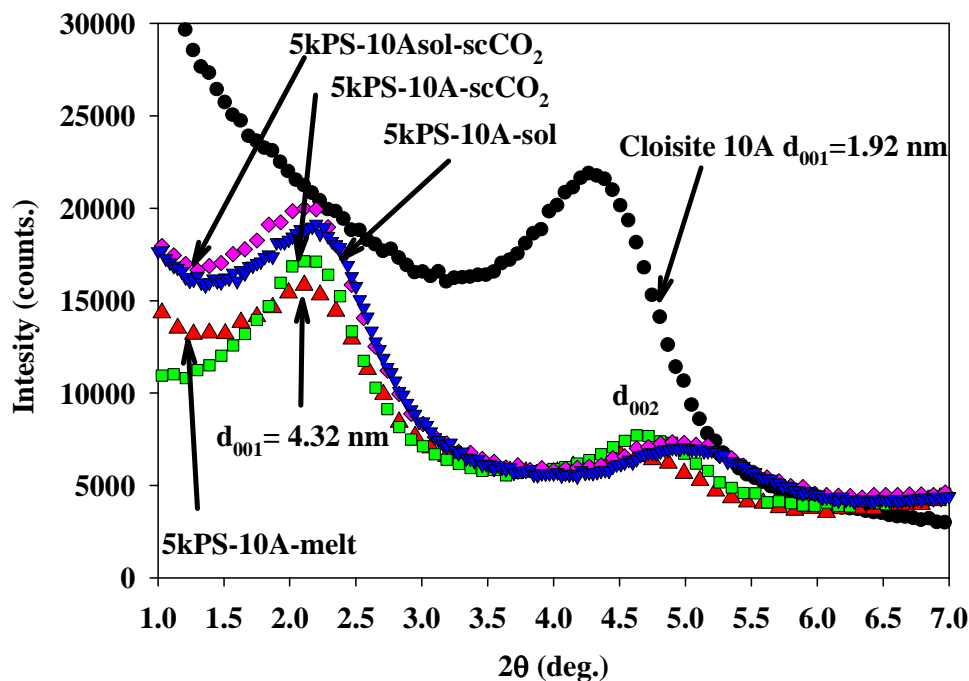


**Figure 19.** X-ray diffractogram of “as received” Cloisite 10A and 5k PS/10A nanocomposite prepared using the melt blending technique. The nanocomposite shows a shift to higher  $d_{001}$  spacing (1.92 to 4.32 nm) due to polymer confinement into the inner gallery spacing of the nano-clay.

### 3.4.2 Rheological measurements

However, X-ray diffraction can be used along with other techniques such as rheology, to get a more complete picture into the nano - clay morphology of the nanocomposite. Clay dispersion along with strong polymer – clay interaction was displayed in rheology due to its extreme sensitivity to dispersion and interactions in filled polymer materials. Therefore, despite all samples showing similar intercalation peak, rheological measurements were telling a different story. The intercalated melt and solution blended nanocomposites showed a modest low frequency enhancement in modulus (less than one order of magnitude) with the evidence of the onset of a low frequency plateau (Figure 20). This was due to good interaction between the polymer and clay due to the good compatibility between polymer and clay surfactant<sup>68</sup>, and the

large amount of polymer confined between platelets. These two nanocomposites prepared using traditional processing methods were expected to be intercalated nanocomposites, because in these methods exfoliation does not occur due to entropic and enthalpic forces holding the platelets together. Therefore the only morphologies that should be present are intercalated or conversely collapsed tactoid structures unless compatibilizers, specifically modified clays or high shear forces, are used that can further increase the enthalpy gain or decrease the entropic penalty. However, the scCO<sub>2</sub> melt processed nanocomposite displayed an order of magnitude higher low frequency plateau in storage modulus compared to melt and solution blended composites indicating solid-like behavior. Moreover, when a little co-solvent (toluene) was used, the rheological behavior was drastically different than the other samples. There was a further increase in storage modulus of more than an order of magnitude compared to the melt scCO<sub>2</sub> processed nanocomposite and an increase in storage moduli at all frequencies and more 3 orders of magnitude enhancement at low frequencies compared to neat PS. This result strongly suggested that the solvent assisted scCO<sub>2</sub> method significantly improved clay dispersion leading to an increase in surface area available for polymer-clay interactions and an increase in the amount of polymer chains that have diffused in-between the clay platelets compared to the other three samples. Furthermore, in the solvent assisted scCO<sub>2</sub> processed sample the improved dispersion caused the formation of a percolated network of clay platelets. It was previously demonstrated that the strengths of polymer - clay interactions play a bigger role in enhancing rheological properties when the percolation network has been fully formed.<sup>69</sup> Therefore, in the case of the solvent assisted scCO<sub>2</sub> processed sample due to the strong interactions present between PS and 10A organic clay modifier, the creation of a percolated network led to superior rheological improvement.

The results from this study demonstrated the flexibility of the scCO<sub>2</sub> processing technique where the PS/clay can be processed with or without a co-solvent present which resulted in nanocomposites with significantly improved viscoelastic properties due to improved nano - clay dispersion compared to traditionally processed composites. This was the first time where a co-solvent was used along with the scCO<sub>2</sub> process in an attempt to maximize nano - clay dispersion leading to an increase in the surface area available for nano - clay interactions. Furthermore, the use of a co-solvent along with scCO<sub>2</sub> led to superior clay dispersion which further led to enhanced rheological properties.

When the results from 5K PS nanocomposites were compared with the results from high molecular weight 280K PS (Chapter 3), the final X-ray diffraction spacing is depended on the polystyrene molecular weight. The nanocomposites prepared with 5k PS and 10A showed a final  $d_{001}$  spacing of 4.32 nm, while the ones prepared with 280k PS and 10A displayed a final spacing of 3.85 nm. It is believed that the reason behind this is the increased amount of PS chains that have penetrated the inner-gallery spacing of the clay in the 5k PS compared to 280k PS nanocomposites, leading to a further increase in the  $d_{001}$  spacing. The smaller radius of gyration of the 5k PS (1.89 nm) compared to 280k PS (14 nm) along with favorable interactions between the polystyrene and clay surfactant may have allowed for more PS chains to diffuse inside the clay gallery spacing causing the platelets to be pushed further apart than their equilibrium spacing. Moreover, the rheological response of the 5k PS/10A sample prepared using the solvent assisted scCO<sub>2</sub> (5kPS-10Asol-scCO<sub>2</sub>) was compared with that from the nanocomposite prepared using 280k PS/10A with the same processing technique (PS-5%10A-scCO<sub>2</sub>). The two nanocomposites displayed the same low frequency plateau in storage modulus at about  $10^5$  dyne/cm<sup>2</sup>. This interesting result further suggested that more 5k PS chains have coated the clay surface or have

interacted with the clay modifier than in the case of 280k PS probably due to their reduced size and higher mobility. The results from X-ray diffraction had already suggested that in 5k PS nanocomposite more chains were confined between the clay inner-gallery spacing due to their smaller size (smaller radius of gyration) and higher mobility compared to 280k PS chains. Therefore, it is believed that the similar rheological results between the two despite the 280k PS higher molecular weight can be explained by the higher amount of polymer chains that are closer to the clay surface or modifier and have reduced mobility compared with the bulk polymer chains in 5k PS nanocomposites.

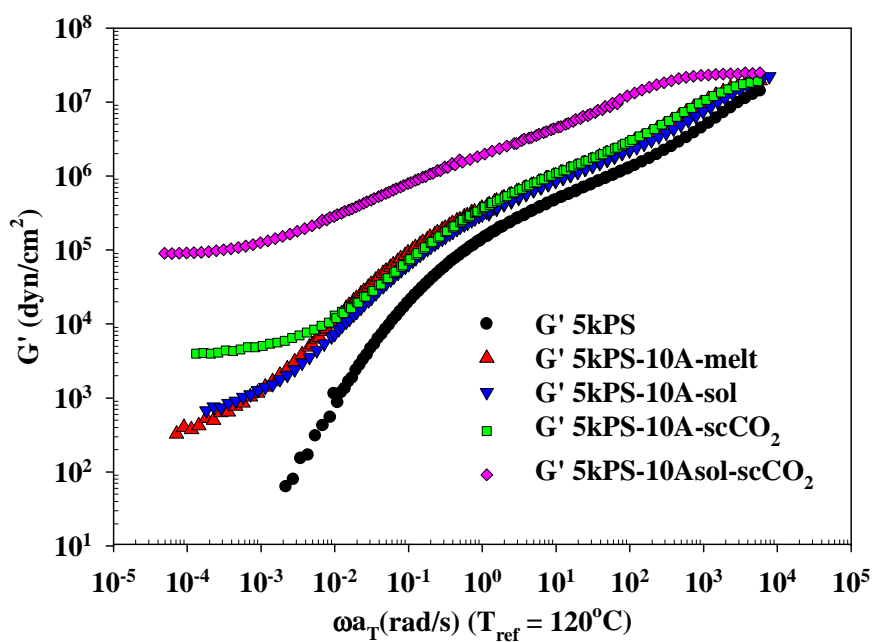


**Figure 20.** Storage modulus of 5k PS and 5k PS/10A nanocomposites.

### **3.5 High molecular weight 280k PS/clay nanocomposites characterization (WAXD, TEM, rheology, permeability and TGA)**

#### **3.5.1 Effect of organic clay modifier on nanocomposites morphology and properties**

In the previous section low molecular weight polystyrene was used in an attempt to maximize nano - clay dispersion and polystyrene properties. However, high molecular weight PS has more industrial applications. In the following section high molecular weight (280,000 g/mol) PS was used along with Cloisite 10A, 15A, 93A and Nanocor I.30P organically modified clays to study the effects of nano - clay organic modifier on the clay structure in the nanocomposites and on the nanocomposites properties. A detailed explanation on the samples processing conditions and nomenclature was given in section 4.2 and Table 4.

In Table 2 the structure of all the “as received” clay in this study can be seen. The presence of short hydrocarbon (C18 tallow) chains in the galleries after modification makes the clay much more organophilic than natural montmorillonite, which is naturally hydrophilic. The clays used in this study were chosen due to their different organic modifier structures which allows for a thorough study of modifier effects on scCO<sub>2</sub> on the final nano - clay morphology in the resulting nanocomposites. Acidic and polar molecules can be better solvated in CO<sub>2</sub> than nonpolar ones, therefore the acid 93A modifier and slightly non-polar 10A modifier should theoretically be more compatible with scCO<sub>2</sub> while the low polarity of 15A and I.30P modifiers should make them less susceptible.<sup>70</sup> It is anticipated that investigating composites of these different clays will allow some insight into interaction effects and their contribution to overall reinforcement and dispersion in scCO<sub>2</sub> processed nanocomposites. The clays were used “as received” and underwent no additional processing, chemical modification, or purification prior to nanocomposite formation.

*Effect of extrusion on polystyrene/clay nanocomposites – wide angle x-ray diffraction and rheology*

In order to process high molecular weight PS a higher temperature than 5 K PS is required to improve polymer mobility and facilitate proper mixing during processing. To accomplish this 280k PS was processed along with “as received” Cloisite 10A in a lab-scale Haake 3/4-inch at 200°C for 20 minutes. There was a shift to higher  $2\Theta$  values of the  $d_{001}$  peak indicating that a collapse of the clay inner-gallery spacing has occurred due to organic modifier degradation (Figure 21). This sample showed only a small improvement in storage modulus compared to pure PS (Figure 22). The same phenomenon was observed by Tanoue and co-workers when they processed different molecular weights of PS and 10A clay in a co-extruder at 200°C.<sup>32, 41</sup> They observed no improvement in rheological properties due to clay modifier degradation that caused the clay platelets to collapse. Processing high molecular weight PS has proven to be a more challenging task than 5k PS since it has a glass transition temperature of 104°C and it requires processing at 200°C or higher even when processed in  $scCO_2$  which has some solvation effect on it. However, as seen in the extruded sample, most of the available organic clay modifier begins to decompose at temperatures between 160°C - 250°C. At 200°C and above the decomposition is accelerated especially when kept there for prolog period of time causing gallery collapse comparable to that of montmorillonite (Figure 6 and Figure 21).<sup>71</sup> The decomposition results in the burning (release) of the organic modifier chains, leading to the collapse of inner-gallery spacing. Furthermore, if enough of the clay organic modifier is decomposed the nano - clay reverts to its' naturally hydrophilic nature (pure Cloisite  $Na^+$ ) making the nano - clay organo-phobic.

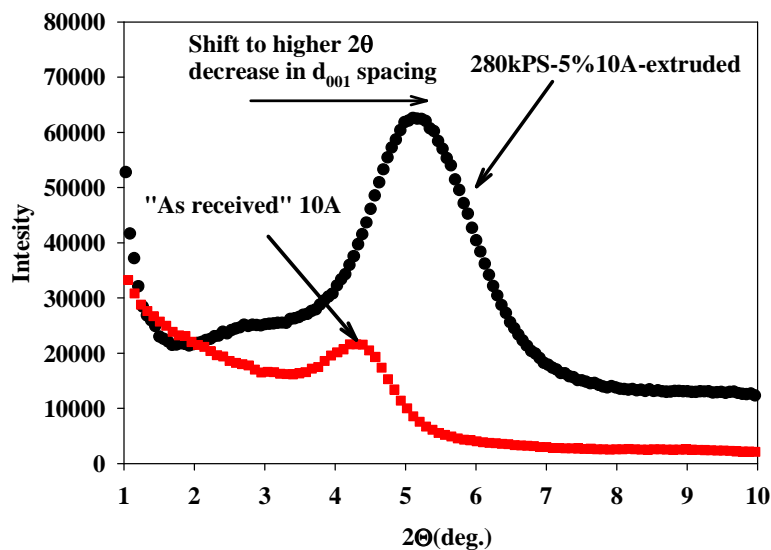


**Figure 21.** X-ray diffractogram of “as received” Cloisite 10A and 280k PS/10A nanocomposite prepared using the melt blending technique.

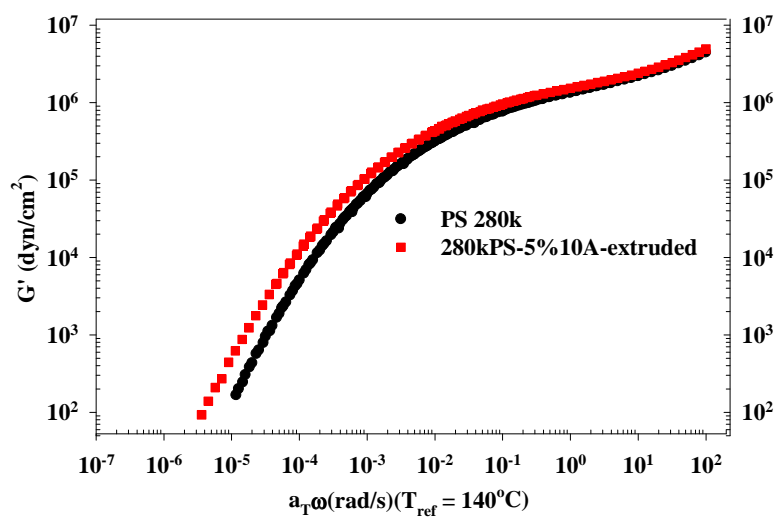


**Figure 22.** Storage modulus of 280k PS and 280k PS/10A nanocomposite prepared using the melt blending technique.

### *Effect of solution blended and scCO<sub>2</sub> processing*

To overcome this problem a little solvent was added to CO<sub>2</sub> which could help here. Adding some solvent to the system allowed us to minimize processing temperatures and

maximize polymer interaction with the clay due to improved mobility. Styrene was used to lower the viscosity of polystyrene, facilitating better mixing and allowing processing below the glass transition temperature of high molecular weight polystyrene (104°C). The low processing temperature had several advantages including minimizing the clay organic modifier degradation, maximizing the rate of CO<sub>2</sub> density change, and improving the CO<sub>2</sub>- polystyrene miscibility. Additionally, the reduced temperature and viscosity allowed for longer processing times without worrying that clay will degrade, giving the polymer chains more time to thoroughly penetrate the clay layers.

In order to benchmark the solvent assisted scCO<sub>2</sub> processing method, solution blending samples of polystyrene with each of the clays (15A, 10A, 93A and I.30P) were created. Table 1 displays the chemical structure of each of the above organic modifiers. As mentioned earlier the presence of short hydrocarbon chains (C18 tallow) in the galleries after modification renders the clay much more organophilic when compared to natural clay. The organically modified clays were chosen for their varied modifier structures which allow for the study of modifier effects on nanocomposite morphology after scCO<sub>2</sub> processing. Carbon dioxide tends to solvate acidic and polar molecules better than nonpolar ones. It is expected that 93A which contains an acidic H<sup>+</sup> as part of the modifier and 10A which contains a slightly polar modifier should be reasonably compatible with scCO<sub>2</sub>, while the compatibility of 15A and I.30P which contain low polarity modifiers should be less.<sup>72</sup> In order to achieve intercalation and/or exfoliation the energy released must compensate the entropy loss during nanocomposite formation. When a polymer is intercalated between the clay platelets there is a loss in conformational entropy that needs to be balanced by the conformational gain of the nano - clay surfactants (organic modifiers) and by the polymer-clay surface and polymer-clay surfactant interactions.<sup>73</sup> Whether or not the organic



modifier is polar or non-polar along with the polymer polarity has an effect on the outcome of the nanocomposite morphology. Also, the number of tallow groups on the organic modifier has been shown to be one of the major determining factors for polymer - clay compatibility. Furthermore, the charge density also plays a key role in influencing the compatibility between the surfactant and the clay. In the case where the interactions are already favorable like in the case of non-polar surfactant with non-polar polymer having a higher surfactant density might facilitate better polymer penetration in between clay layers. Conversely, if there is a polar surfactant and non-polar polymer, a higher surfactant density may prevent and even repel polymer confinement.<sup>73</sup> Giannelis et al. demonstrated both theoretically and experimentally in a series of studies that the entropy gained associated with the surfactant layer separation may not always be able to balance the entropy loss associated with the confinement of a polymer melt and consequently the entropy penalty to the confined polymer inhibit the formation of intercalated and or/exfoliated products.<sup>13, 15</sup> Moreover, the formation of an intercalated system was dominated by the energetic factors which included the pair interactions of silicate surface/polymer, silicate surface/surfactant and surfactant/polymer.<sup>13, 15, 73</sup>

### **3.5.1a Wide angle X-ray diffraction**

“As received” Cloisite 15A and 93A display X-ray diffraction peaks corresponding to 3.13 nm and 2.44 nm spacing respectively (Table 1). The difference in their equilibrium spacing comes from the slight variation in modifier chemistry mentioned. It has been previously theorized that both dimethyl dehydrogenated tallow (2M2HT) and methyl dehydrogenated tallow (M2HT) (15A and 93A respectively) type modifiers arrange in a tilted paraffinic monolayer structure, however due to the higher affinity of M2HT to the clay surface the arrangement may be more compact. This, along with the lower density of modifier chains on the surface of 93A,

results in a reduced interlayer spacing. Based on the number of tallow constituents both clays should show similar compatibility with PS. However 93A contains a more polar surfactant, due to the presence of the acidic hydrogen, compared to 15A and it is expected to interact less with PS compared to 15A.<sup>65, 74</sup> Cloisite 10A and Nanocor I.30P display X-ray diffraction peaks corresponding to 1.92 nm and 2.25 nm  $d_{001}$  spacing respectively (Table 1). The small interlayer distance in Cloisite 10A suggests a lateral bi-layer arrangement of the intercalant while I.30P's basal spacing puts it in a range that is most likely a pseudo bi-layer approaching monolayer-like organization.<sup>75, 76</sup> Both clays contain one tallow tail; however 10A contains one polar moiety while I.30P contains one non-polar tallow part of the organic modifier and a high density making I.30P a good candidate for producing good dispersion in a non-polar polymer like PS. However, Cloisite 10A has a phenyl ring as part of the organic modifier and this type of functional group has previously been shown to be optimal for maximizing miscibility with polystyrene based polymers, therefore it is expected that 10A will show reasonable interaction with the matrix.

X-ray diffraction was used to study the morphology of the resulting nanocomposites by probing changes in the level of clay dispersion. Furthermore, WAXD was also used as a tool to gain some insight on the strength of polymer - clay interactions. The relative amount of polymer that is in contact with the clay surface or interacts with the organic clay modifier can be qualitatively determined by analyzing the location of the clay's characteristic X-ray peaks which represents the average clay platelet spacing. X-ray diffraction at low angles was measured on solution-blended and  $scCO_2$ -processed nanocomposites made with the four different clays (Figure 23). It is pertinent to note at this point that both the  $scCO_2$  and solution-blended samples were processed in solution with styrene and then dried under vacuum, the only difference between the two being the addition of supercritical  $CO_2$  during processing followed by a fast

depressurization (~300 MPa/min) protocol before removing the solvent. Cloisite 10A, Cloisite 15A, Nanocor I.30P and Cloisite 93A solution blended and scCO<sub>2</sub> processed nanocomposites display peak locations at 2 $\Theta$  of 2.29°, 2.32°, 2.54° and 3.07° degrees respectively (Table 9). These values correspond to an average platelet inner-gallery spacing of 3.85, 3.80, 3.47, and 2.87 nm. The final d<sub>001</sub> values correspond to an increase in the inner-gallery spacing of 1.93 nm for 10A, 0.67 nm for 15A, 0.49 nm for 93A and 1.34 nm for I.30P. Cloisite 10A showed the highest shift in the d<sub>001</sub> spacing and the highest final spacing followed by 15A, I.30P and 93A (Table 9 and Figure 23). The X-ray diffractogram showed that whether or not a sample was processed with scCO<sub>2</sub>, the diffraction peak shape and position did not significantly change for all the clays. This behavior is most likely due to the solvent present in both samples that allowed the clay-polymer system to adopt a preferred thermodynamically stable configuration for platelets and tactoids that are in close proximity after their respective processing. A significant level of order in any remaining tactoids of even a well dispersed sample will result in a large X-ray peak. It has been previously demonstrated that due to the complex morphologies possible in a clay nanocomposite X-ray diffraction should not be used as a standalone tool for determining dispersion.<sup>77</sup> However, X-ray diffraction can be used along with other techniques such as TEM, rheology, TGA and permeation testing to get a more complete picture into the nano - clay morphology of the nanocomposite. Furthermore, X-ray diffraction can give some insight into the level of polymer - clay interactions present in the nanocomposite. The larger the final d<sub>001</sub> spacing the more polymer has penetrated in between the clay layers. Moreover, the presence of the d<sub>002</sub> peak along with a tall d<sub>001</sub> peak indicated that highly ordered intercalated nanocomposites are present. The second peak is definitely a d<sub>002</sub> diffraction peak since it occurred at twice the value of 2 times the 2 theta of d<sub>001</sub> peak. Vaia and co-workers have

demonstrated to be thermodynamically feasible to have large inner-gallery spacing if the enthalpic interactions between the polymer and nano - clay are strong enough.<sup>15</sup> As a result, it is anticipated that the strength of polymer - clay interactions is directly correlated to the final gallery spacing at least in the PS/clay prepared with the solution blended and solvent assisted scCO<sub>2</sub> processing methods. Therefore, in the Cloisite 10A nanocomposites, as expected from its phenol moiety as part of the organic modifier, the polymer - clay interactions are the strongest, closely followed by 15A, than by I.30P and 93A.

**Table 9.** X-ray diffraction data summary. The initial and final 2 theta and d<sub>001</sub> spacing are shown for all the “as received” nano-clays and PS/clay nanocomposites.

| x-ray diffraction                 | 10A                 |                       | 15A                 |                       | 93A                 |                       | I30P                |                       |
|-----------------------------------|---------------------|-----------------------|---------------------|-----------------------|---------------------|-----------------------|---------------------|-----------------------|
|                                   | angle (2 $\theta$ ) | d <sub>001</sub> (nm) | angle (2 $\theta$ ) | d <sub>001</sub> (nm) | angle (2 $\theta$ ) | d <sub>001</sub> (nm) | angle (2 $\theta$ ) | d <sub>001</sub> (nm) |
| Pure                              | 4.6                 | 1.92                  | 2.82                | 3.13                  | 3.74                | 2.36                  | 3.92                | 2.25                  |
| PS-scCO <sub>2</sub> and solution | 2.29                | 3.85                  | 2.32                | 3.8                   | 3.16                | 2.85                  | 2.46                | 3.59                  |
| difference                        | -2.31               | 1.93                  | -0.5                | 0.67                  | -0.58               | 0.49                  | -1.46               | 1.34                  |

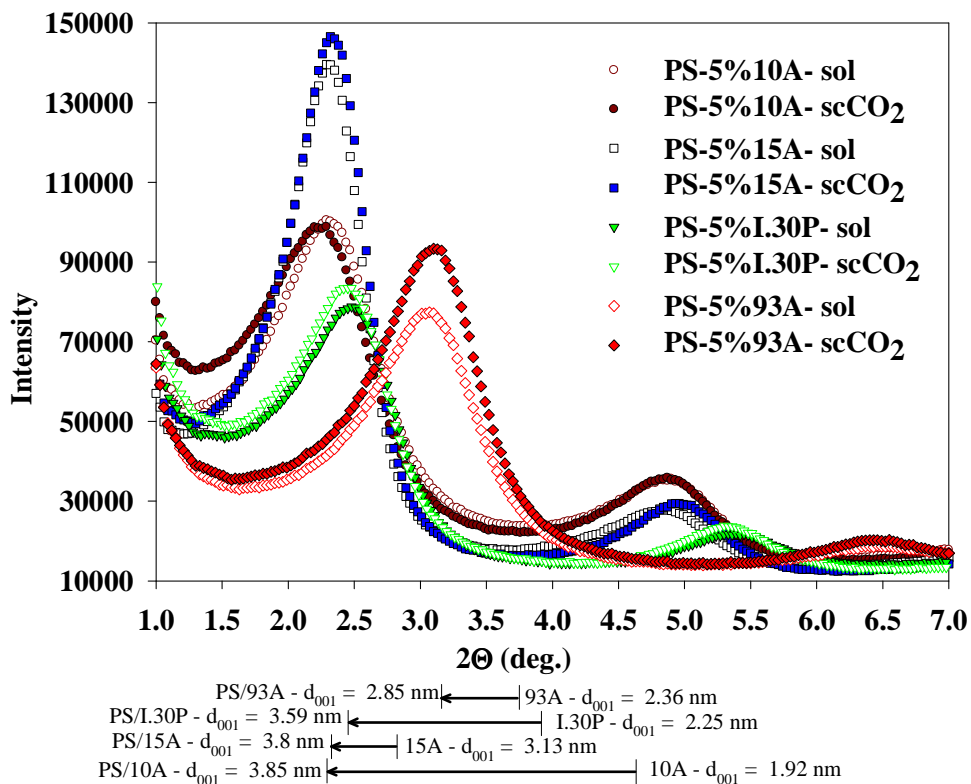


**Figure 23.** X-ray diffractograms of PS/10A, PS/15A, PS/93A and PS/I.30P nanocomposites. Solution blended samples are shown as open symbols while scCO<sub>2</sub> samples are displayed as filled symbols. The change in spacing of each clay from its equilibrium “as received” spacing to the final spacing in the PS/clay nanocomposites is shown below the graph.

### 3.5.1b Transmission electron microscopy

WAXD was inconclusive in elucidating the nanocomposites morphology due to its insensitivity to even large scale dispersion when there are tactoids that still contain a high level of ordered platelets. Transmission electron microscopy, rheology and permeability can be used to provide a better picture into the morphological changes in the polystyrene nanocomposite. Therefore, TEM was used as a technique to complement X-ray diffraction data in order to better visualize the spatial dispersion state of the nano - clay in the nanocomposites. With the sub-nanometer resolution limit of the TEM, individual platelets and platelet stacks can be directly

visualized and a better picture into the nano - clay structure in the nanocomposites can be obtained.

Images of solution-blended and scCO<sub>2</sub> processed Cloisite 10A, 15A and 93A at low and high magnification display a significant reduction in average tactoid size when a sample is processed with scCO<sub>2</sub> versus solution blending (Figure 24 - Figure 29). Additionally, an increase in the number of individual platelets, and double or triple platelet stacks is visible in some of the high magnification images. The size of 50 representative tactoids from each sample over multiple images was studied. The average tactoid thickness in the Cloisite 10A scCO<sub>2</sub> nanocomposites (PS-5%10A-scCO<sub>2</sub>) is 31 nm while the average in solution (PS-5%10A-sol) is 143 nm. Utilizing the d<sub>001</sub> spacing (see Appendix A) the average platelets per tactoids was calculated to be approximately 9 and 37 platelets for the scCO<sub>2</sub> sample and solution blended sample respectively. The average number of platelets per tactoids was calculated to be approximately 6 and 21 platelets for the scCO<sub>2</sub> (PS-5%15A-scCO<sub>2</sub>) and solution blended (PS-5%10A-sol) Cloisite 15A sample respectively. And for the 93 A samples 6 and 16 for the scCO<sub>2</sub> (PS-5%93A-scCO<sub>2</sub>) and solution blended composites (PS-5%93A-sol). Tactoid size measurement for each sample indicates that scCO<sub>2</sub> processing of a nanocomposite produced platelet stacks that were approximately 4 times smaller than when the sample was produced without scCO<sub>2</sub> (Table 10). This significant increase in dispersion has been theorized to be caused by the dramatic expansion of CO<sub>2</sub> between clay platelets during depressurization causing significant dispersion. Care was taken to not include in the tactoid size measurements any individual platelets observed because they were only easily observed at very high magnifications while tactoid sizes were better measured at moderate magnifications. Additionally, imaging of individual platelets was only possible on the thinnest TEM films and best images; therefore it

was not possible to get a representative population measurement for all of the samples. The result was that the average tactoid size reported in the scCO<sub>2</sub> processed samples is actually larger than it would be if individual platelets were also counted. Therefore, irrespective of the WAXD peaks for the solution-blended and scCO<sub>2</sub>-processed samples being similar, the dispersion in the scCO<sub>2</sub>-processed samples is significantly better. The average tactoid size reduction appears to be independent of clay modifier chemistry as well as the clay spacing found in WAXD (Table 10).

**Table 10.** Average tactoid sizes measured from TEM and the number of platelets per tactoid was calculated from the  $d_{001}$  spacing found with WAXD (Appendix A).

| Sample                      | Tactoid size (nm) | Platelets per tactoid | Percent reduction in tactoid size (%) |
|-----------------------------|-------------------|-----------------------|---------------------------------------|
| PS-5% 10A-sol               | 143               | 37                    |                                       |
| PS-5% 10A-scCO <sub>2</sub> | 31                | 9                     | 75.68                                 |
| PS-5% 15A-sol               | 75.5              | 21                    |                                       |
| PS-5% 15A-scCO <sub>2</sub> | 18.81             | 6                     | 71.43                                 |
| PS-5% 93A-sol               | 44.6              | 16                    |                                       |
| PS-5% 93A-scCO <sub>2</sub> | 10.4              | 4                     | 75                                    |

A better level of dispersion was found for both scCO<sub>2</sub> and solution blended Cloisite 93A nanocomposites compared to the rest of nanocomposites when comparing them by their processing method. It has been anticipated and subsequently shown in literature that clays exhibiting strong interaction with the polymer matrix should be more difficult to disperse than similar clays with less preferential interaction.<sup>64, 78</sup> When a polymer matrix has a strong affinity for the organic modifier on the clay surface the tendency is for the clay to form intercalated structures. Intercalation of the polymer into the gallery increases the  $d_{001}$  spacing, however due to favorable interaction with the modifier it is believed that it then may act as a barrier to further platelet separation. This is the case in Cloisite 10A and 15A nanocomposites when there is a

strong affinity of polymer to the clay or organic modifier. Conversely, with poorly interacting matrices the attractive force between polymer and clay or clay modifier is reduced and therefore dispersion in weakly interacting clay like 93A may be more readily attained.

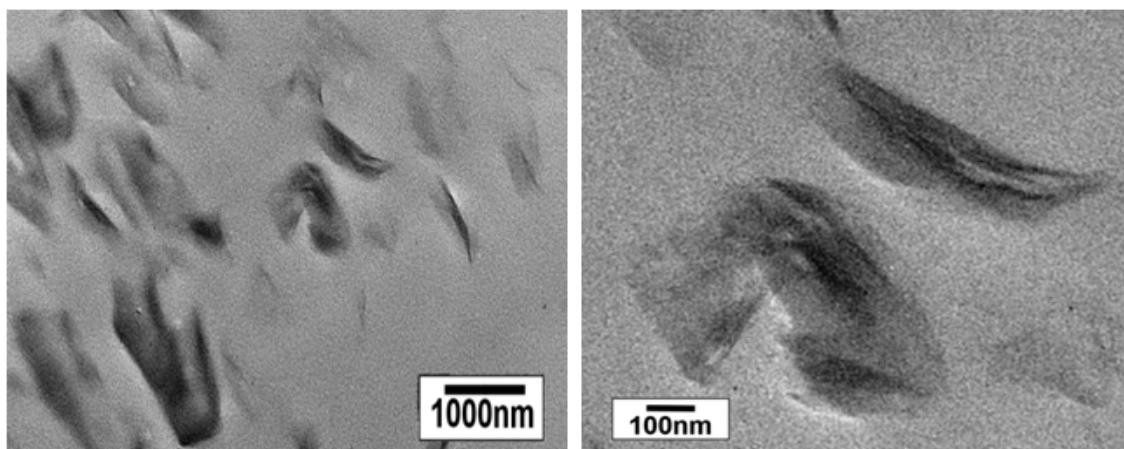


**Figure 24.** TEM micrograph of 5 wt % 10A solution blended with polystyrene at 30K and 200K magnifications.

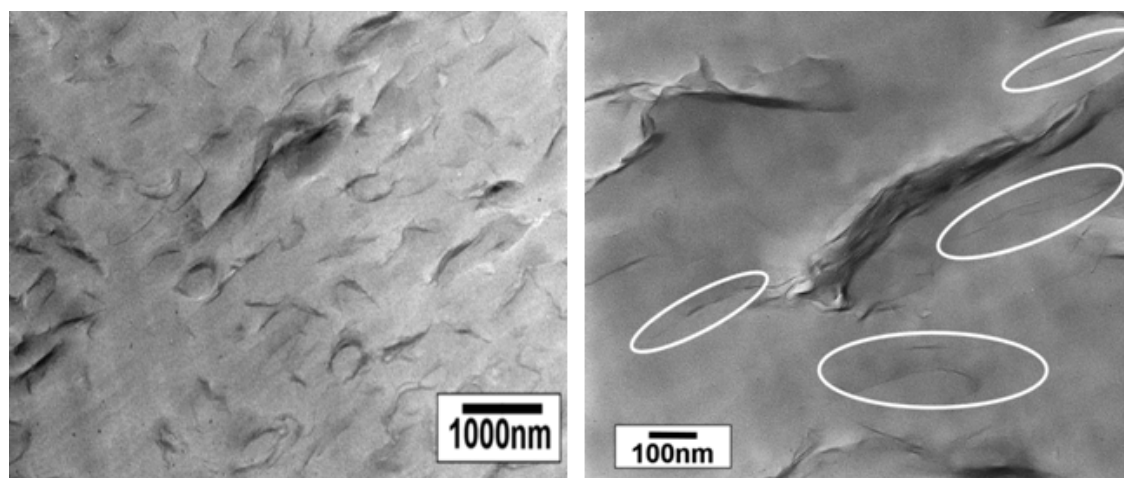


**Figure 25.** TEM micrograph of 5 wt % 10A scCO<sub>2</sub> processed with polystyrene at 30K and 200K magnifications.



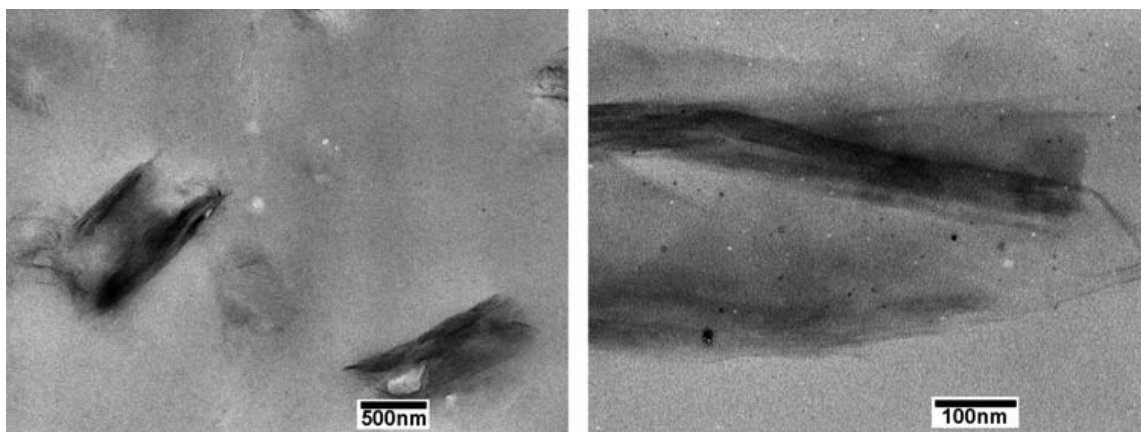


**Figure 26.** TEM micrograph of 5 wt % 15A solution blended with polystyrene at 30K and 200K magnifications.

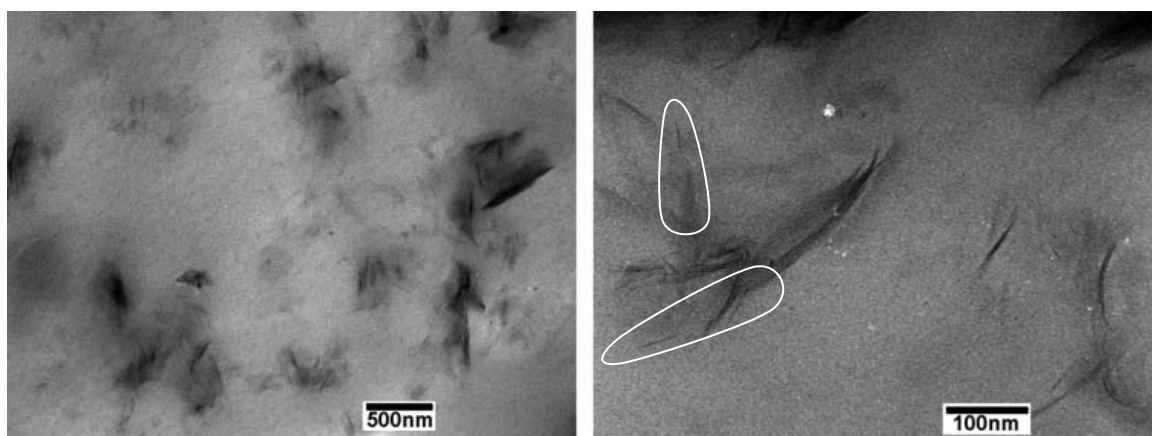


**Figure 27.** TEM micrograph of 5 wt % 15A  $scCO_2$  processed with polystyrene at 30K and 200K magnifications.

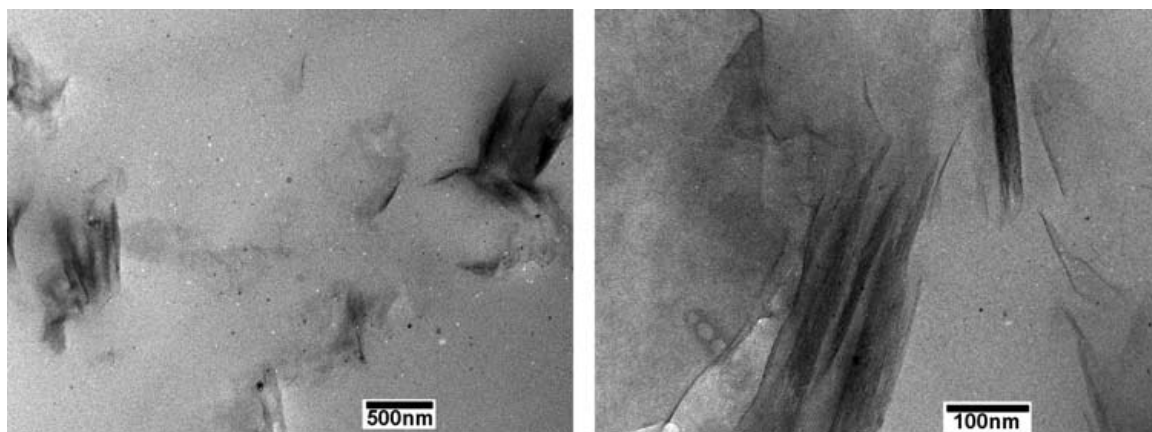


**Figure 28.** TEM micrograph of 5 wt % 93A solution blended with polystyrene at 30K and 200K magnifications.

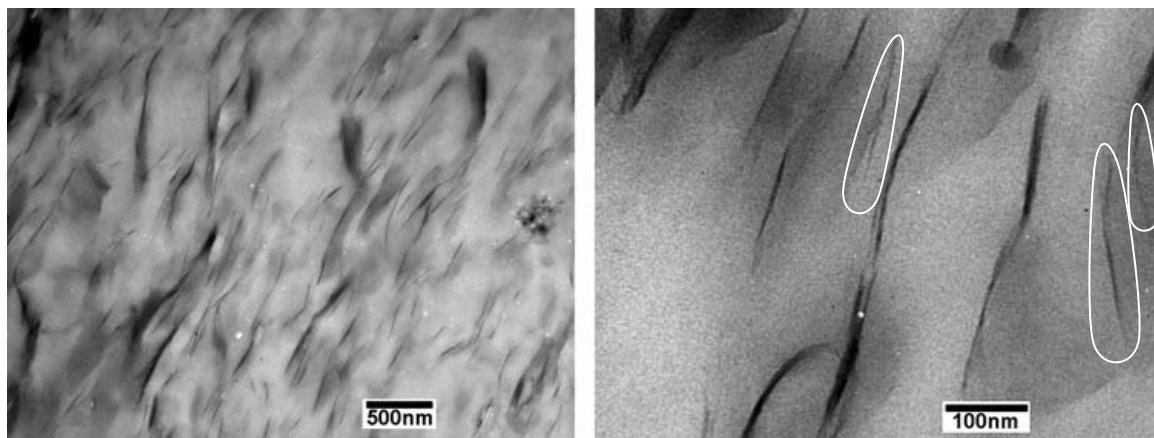


**Figure 29.** TEM micrograph of 5 wt % 93A scCO<sub>2</sub> processed with polystyrene at 30K and 200K magnifications.

### 3.5.1c Rheology

Despite the lack of differentiation between the nanocomposites morphologies in WAXD, TEM gave a deeper insight into the morphological changes that occur upon scCO<sub>2</sub> processing. The scCO<sub>2</sub> processing produces a more complex morphology when compared to solution blending. However, another more sensitive tool needs to be employed to gain a deeper understanding into the nanocomposites morphology and that also helps in differentiating between all the samples employed in this study. Rheology is a very sensitive tool for detecting even small changes in nano - clay dispersion and polymer - clay interactions in nanocomposites. Measuring the viscoelastic response helped in elucidating the effect of organic clay modifiers on polymer - clay interactions and clay dispersion. The frequency dependence at 140°C of the storage modulus ( $G'$ ) for 10A, 15A, 93A and I.30P solution blended and scCO<sub>2</sub> process nanocomposites (Figure 30 and Figure 30 respectively) showed distinct differences between the pure PS and the PS/clay nanocomposites, especially at the low frequencies. The storage modulus and loss moduli for PS-5%10A-scCO<sub>2</sub> (Figure 32A), PS-5%10A-sol (Figure 32B), PS-5%15A-scCO<sub>2</sub> (Figure 32C), PS-5%15A-sol (Figure 32D), PS-5%I.30P-scCO<sub>2</sub> (Figure 32E), PS-

5%I.30P-sol (Figure 32F), PS-5%93A-scCO<sub>2</sub> (Figure 32G), PS-5%93A-sol (Figure 32H) are shown along with 280k PS for easy comparison of results. There was a moderate increase in the low frequency elastic modulus in the solution blended 15A and 10A composites (PS-5%15A-sol and PS-5%10A-sol) with the onset of a low frequency plateau. When samples that have undergone the same solution blending protocol were processed with the scCO<sub>2</sub> process, the resulting nanocomposites (PS-5%15A-scCO<sub>2</sub> and PS-5%10A-scCO<sub>2</sub>) showed significant solid-like behavior evidenced by a well-defined low-frequency plateau. There was more than an order of magnitude increase in the low frequency plateau modulus over the solution blended composites and the scCO<sub>2</sub> composites showed a reduction in frequency dependence of the storage modulus. This significant improvement in modulus is most likely a direct result of the increased dispersion seen in TEM images. The nearly 4-fold reduction in average tactoid size along with the significant increase in dispersed single platelets produced a clay-clay network with more interaction sites and an increase surface area available for polymer-clay and polymer-clay modifier interactions, than in the more poorly dispersed solution composite benchmark.

In stark contrast, nanocomposites formed with 5 wt% 93A showed very little change in rheology after scCO<sub>2</sub> processing despite the similar magnitude of reduction in average tactoid size that was seen in 15A and 10A nanocomposites. The solution blended sample (PS-5%93A-sol) displayed a deviation of the low frequency storage modulus slope from a terminal value of 2 indicating reduced polymer mobility upon the addition of clay. After processing with scCO<sub>2</sub>, the nanocomposite (PS-5%93A-scCO<sub>2</sub>) rheology showed very little change compared to the solution blended benchmark. The only change between the two was the evidence of the onset of a plateau at the lowest frequencies, an effect of the significantly improved dispersion observed in TEM images.

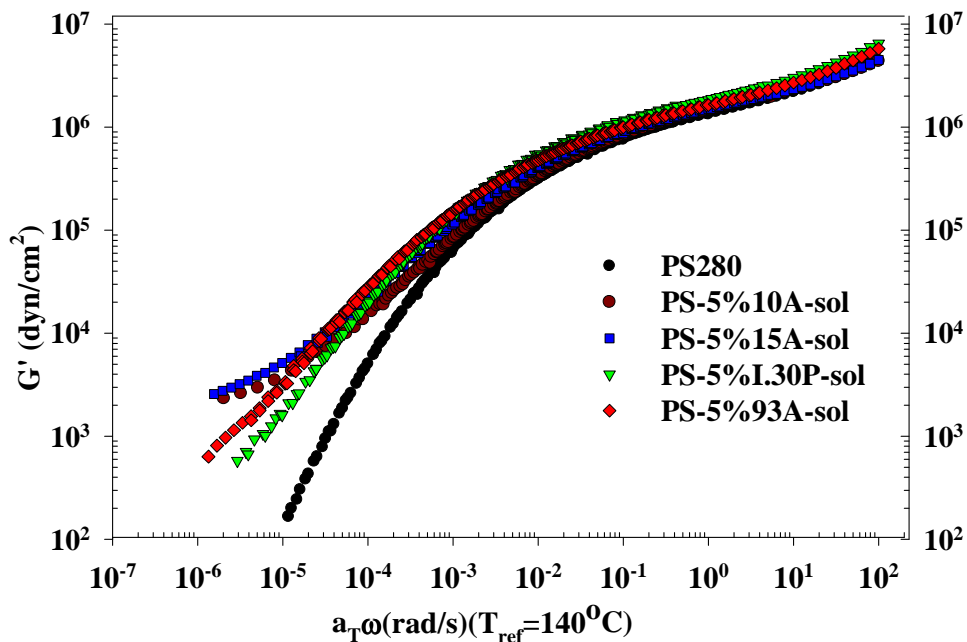


Figure 30. Storage modulus for the 5wt% solution blended nanocomposites.

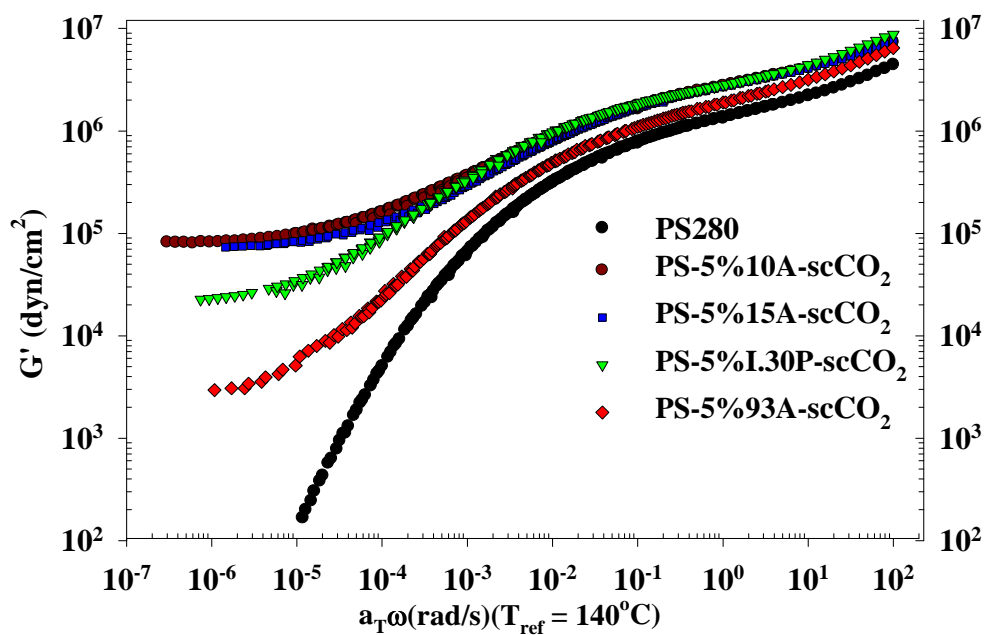
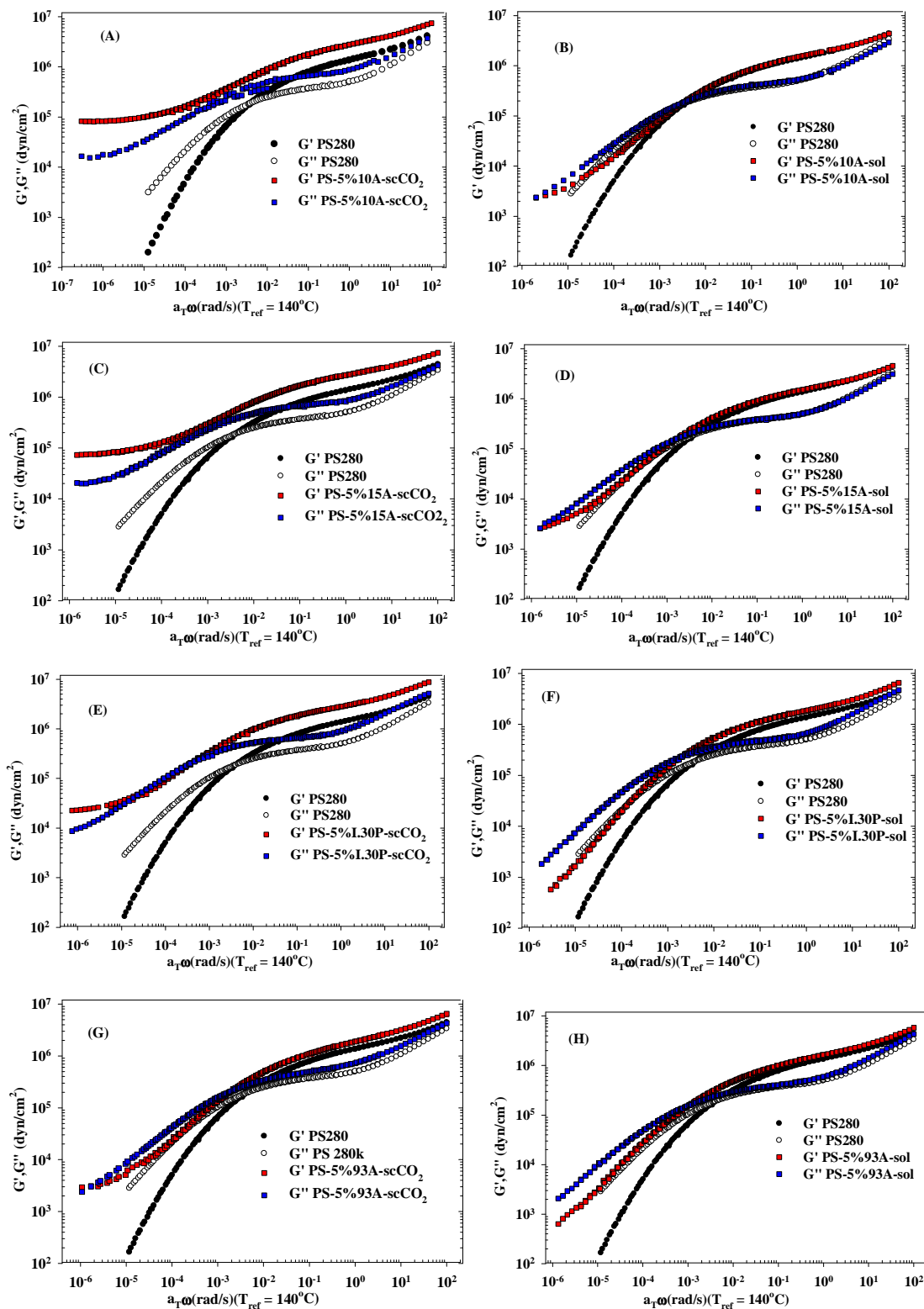


Figure 31. Storage modulus for the 5wt% scCO<sub>2</sub> nanocomposites.



**Figure 32.** Storage and loss moduli for PS-5%10A-scCO<sub>2</sub>(A), PS-5%10A-sol(B), PS-5%15A-scCO<sub>2</sub>(C), PS-5%15A-sol(D), PS-5%L.30P-scCO<sub>2</sub>(E), PS-5%L.30P-sol(F), PS-5%93A-scCO<sub>2</sub>(G), PS-5%93A-sol(H).

When comparing the storage modulus of the all nanocomposites produced in this study the result was somewhat surprising. All of the samples prepared by solution blending have similar tactoid sizes and similar rheology, implying that any differences in polymer - clay interactions were not contributing significantly to the rheological response. Once the samples were processed in scCO<sub>2</sub> the tactoids undergo further (comparable for all clays) reduction in size by a factor of 4. Yet the PS-5%93A-scCO<sub>2</sub> nanocomposite showed almost no improvement in rheology compared to PS-5%93A-sol while the PS-5%15A-scCO<sub>2</sub> nanocomposite improves by as much as 2 orders of magnitude compared to its solution blended counterpart (PS-5%15A-sol). Percolation threshold values shown in Table 11 were calculated based on the equation previously proposed by Ren et. al.<sup>31</sup>

$$\eta_{per} = \frac{4}{3\phi_{per}} \left[ \frac{w_{sil,per} \rho_{org}}{w_{sil,per} \rho_{org} + (1 - w_{sil,per}) \rho_{sil}} \right] \frac{R_h}{h_{sil}} \quad (3)$$

where  $\eta_{per}$  is the average number of platelets per tactoid,  $\Phi_{per} \sim 0.3$  (percolation for spherical domain),  $w_{sil,per}$  is the weight fraction of silicate at the percolation threshold,  $R_h$  is the hydrodynamic radius (radius of platelet),  $\rho_{org}$  is the density of the host polymer,  $\rho_{sil}$  is the density of the silicate and  $h_{sil}$  is the thickness of a platelet.

**Table 11.** Theoretical percolation threshold for all the solution blended and scCO<sub>2</sub> processed PS/5wt% 10A, 15A, 93A and I.30P nanocomposites.

| Sample                      | Theoretical percolation threshold (wt%) |
|-----------------------------|---|
| PS-10A (sol)                | 3.1                                     |
| PS-10A (scCO <sub>2</sub> ) | 12.2                                    |
| PS-15A (sol)                | 2.1                                     |
| PS-15A (scCO <sub>2</sub> ) | 7.1                                     |
| PS-93A (sol)                | 1.4                                     |
| PS-93A (scCO <sub>2</sub> ) | 5.6                                     |

The published average value of 112.5 for the aspect ratio of the clays was used along with the tactoid sizes obtained from TEM in the calculations. It was found that for nanocomposites made with either clay at 5 wt% loading, the pseudo-percolation threshold is reached only after scCO<sub>2</sub> processing (Table 11). Based on these results, it appears that once percolation has occurred, the strength of polymer - clay interaction is the main factor dictating the magnitude of the solid-like response at low frequencies. Of course, when dispersion is improved further, polymer - clay interactions would have even stronger effect.

To explain this phenomenon, the factors affecting the appearance of a low frequency plateau in the storage modulus need to be evaluated. This plateau in G' at low frequencies is indicative of clay - clay or clay - polymer - clay structure formation.<sup>35</sup> When a sufficient fraction of high aspect ratio particles are dispersed in a polymer matrix, their proximity is within a distance that they can "feel" each others' presence through actual particle - particle contact or through transferred stress from particle to polymer to particle. Due to the lack of viscoelastic relaxation of the clay particle, this network or pseudo-network adds a component of stress under shear that does not relax with time (at least in the time frame measured), resulting in reduced time/frequency dependence of viscoelastic properties. Only in an idealized case will the dispersion be perfectly uniform and each clay platelet comes in direct contact with at least one other clay platelet once percolation has occurred. In more realistic cases, the clay - clay interaction will occur equally often through clay - polymer - clay network formation. This will only be true at or near the percolation threshold, i.e. if a large quantity of clay is loaded into a polymer, the rheological effects will largely come from particle - particle contact rather than particle - polymer - particle stress transfer. When a nanocomposite has a fraction of clay that has not yet reached the theoretical percolation threshold, the particles are not in close enough

proximity to interact with each other, leaving their rheological effects to be minimal to moderate. Whether or not there is significant polymer-clay interaction will make some difference, but it will be small compared to that produced by network formation. When the clay gets close enough for a network effect to be produced, the strength of interaction between filler and matrix becomes an important factor in reinforcement. The better the interaction potential is, the more effectively stress will be transferred between clay platelets through the polymer medium.

The rheology of these nanocomposites correlates well with the final basal spacing observed in WAXD. The larger the final equilibrium spacing obtained the higher the resulting  $G'$  is, especially at lower frequencies, reinforcing the earlier observation that clay spacing is a good indicator of interaction strength. The result follows for the solution-blended and  $scCO_2$ -processed composites. This behavior was also observed by Rohlmann and co-workers in polypropylene/clay nanocomposites.<sup>65</sup> Interestingly, there is a significant difference in the rheology between the solution-blended samples and the  $scCO_2$  nanocomposites made with the same clay despite similar WAXD peak location and height. The implication is that X-ray diffraction of nanocomposites of different clays may be a good indicator for polymer - clay interaction strength and potential for reinforcement, but a poor indicator for dispersion state.

A three order of magnitude improvement in low frequency storage modulus in the  $scCO_2$  processed 10A and 15A nanocomposites is significant in polystyrene - clay nanocomposites. Melt processing and solution blending have been shown to give poor improvements many times in the past. Tanoue and co-workers have melt blended high molecular weight PS with organically modified clay and obtained no improvement in dispersion due to modifier degradation at elevated temperatures.<sup>32</sup> However when a clay containing organic modifier with short polystyrene chains was melt blended with PS, Hoffman and co-workers only obtained an



order of magnitude improvement in storage modulus low frequency plateau due to poor clay dispersion.<sup>79</sup> Qi et al. used specially modified clay that was suspended in styrene monomer and polystyrene was polymerized *in-situ* in between the clay galleries. Despite this large level of complexity, the low frequency improvement was not as substantial even when twice the weight fraction of clay was used since they were not able to produced significant dispersion in the nanocomposites.<sup>80</sup>

### 3.5.1d Thermogravimetric analysis

With such significant increases in rheological behavior upon processing nanocomposites in scCO<sub>2</sub>, there was question as to whether the clay modifier was affected during processing or if the matrix polymer could possibly had become attached to the clay surface. To address this possibility, the clay was separated from the polymer by centrifugation of a dilute solution of nanocomposite in toluene. The separated clay was then heated in a thermal gravimetric analyzer where the weight loss that occurs upon degradation of any organics can be measured. If the polymer chains were attached to the clay, we would find that the residual mass of clay after degradation would be significantly less than what was found in the pure clay because the weight fraction of organic material would be much higher. Although, there was a small difference in percent mass loss at 650°C (char content), the difference between the scCO<sub>2</sub> processed and solution blended nanocomposites was even smaller, evidence that no significant amount of material was bonded or removed from the clay surface during scCO<sub>2</sub> processing or solution blending of the nanocomposites (Table 12). This reinforced the explanation that the role of scCO<sub>2</sub> in this system was to be a nano - clay dispersant and that scCO<sub>2</sub> was not stripping the clay modifier, or induced any ionic or covalent interactions between the clay modifier and the polymer. More evidence of the similarities between scCO<sub>2</sub> and solution blended nanocomposites

can be observed in the TGA curves and TGA derivative curves of “as received” clays and the corresponding nanocomposites (Figure 33 for 10A, Figure 34 for 15A Figure 35 for 93A and Figure 36 for I.30P). From the TGA curves it can be seen that the 10A and 15A nanocomposites and to a much lesser extent 93A and I.30P composites showed a loss in weight between 50°C and 150°C. This may be attributed to residual solvent that was left over in the sample. It was not expected that the loss in weight below 150°C to be caused by modifier degradation since the 10A modifier only starts to degrade at 160°C when kept for a prolonged period of time. Furthermore, Xie et. al showed that quaternary ammonium ions only start to degrade after 150°C.<sup>81</sup> Also, the organic modifier in 10A is the least stable of all the clays in this study. In the previous section (Figure 18) it was shown that no loss on clay modifier occurred after drying the clay under vacuum for 6 hours. The sample spends much less time at 160°C to have any effect on the degradation kinetics. Several interesting differences between “as received” clays and nanocomposites were: the disappearance of the peak in derivative weight between 200°C and 350°C in the 93A, 15A and I.30P samples, the shift in the derivative weight peak from 200°C to 275°C and from 375°C to 425°C in the 10A sample and the increase or slight shift in the 400°C peak in the 93A, 15A and I.30P samples. These changes were more evident in 15A and 10A samples which contain excess modifier and less evident in 93A and I.30P samples which do not contain excess modifier. The scCO<sub>2</sub> and styrene might have acted as carriers of excess modifier in the clay inner-gallery and closer to the clay surface where it was shielded from degradation until higher temperatures. A similar phenomenon was demonstrated when the clay was washed with ethanol and the excess modifier was more mobile and moved inside the clay inner-gallery. This in turn increased its thermal stability in a similar fashion to what was observed in this study.<sup>81</sup>

**Table 12.** Residual mass (char %) for “as received” clays and separated clays from solution blended and scCO<sub>2</sub> processed nanocomposites.

| Sample  | % residual mass @ 650°C (%) |
|---|-----------------------------|
| "As received" 10A                                 | 63.16                       |
| separated 10A from PS-5%10A-sol                   | 61.51                       |
| separated 10A from PS-5%10A-scCO <sub>2</sub>     | 62.29                       |
| "As received" 15A                                 | 57.75                       |
| separated 15A from PS-5%15A-sol                   | 59.15                       |
| separated 15A from PS-5%15A-scCO <sub>2</sub>     | 59.42                       |
| "As received" 93A                                 | 64.72                       |
| separated 93A from PS-5%93A-sol                   | 62.06                       |
| separated 93A from PS-5%93A-scCO <sub>2</sub>     | 63.42                       |
| "As received" I.30P                               | 66.38                       |
| separated I.30P from PS-5%I.30P-sol               | 66.23                       |
| separated I.30P from PS-5&I.30P-scCO <sub>2</sub> | 65.76                       |

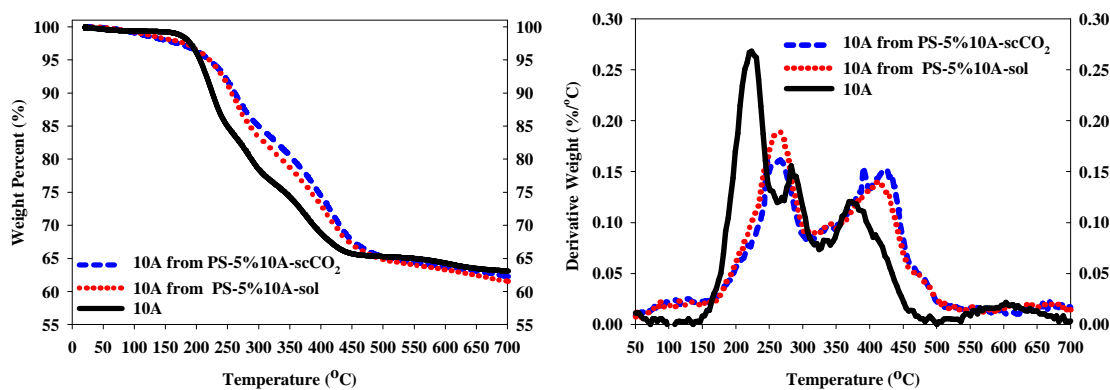


**Figure 33.** TGA curves and Derivative TGA curves for “as received” 10A and separated 10A from PS-5%10A-sol and PS-5%10A-scCO<sub>2</sub>.

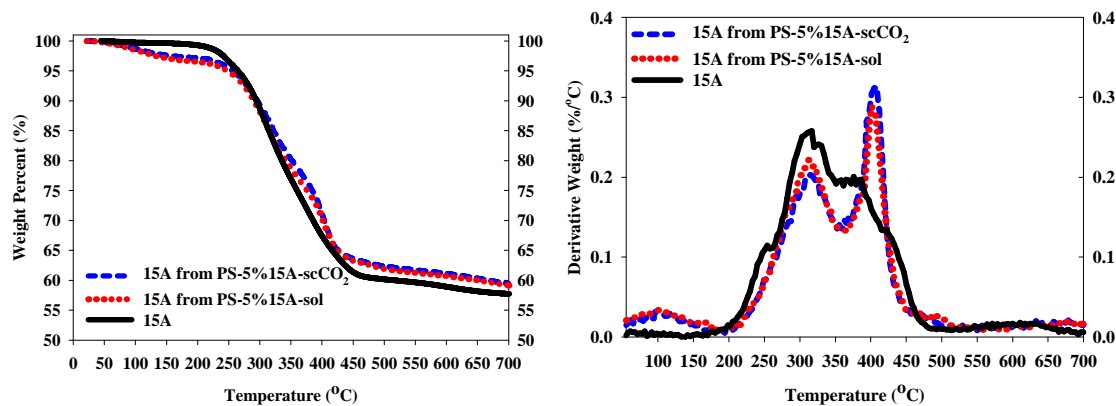


**Figure 34.** TGA curves and Derivative TGA curves for “as received” 15A and separated 15A from PS-5%15A-sol and PS-5%15A-scCO<sub>2</sub>.

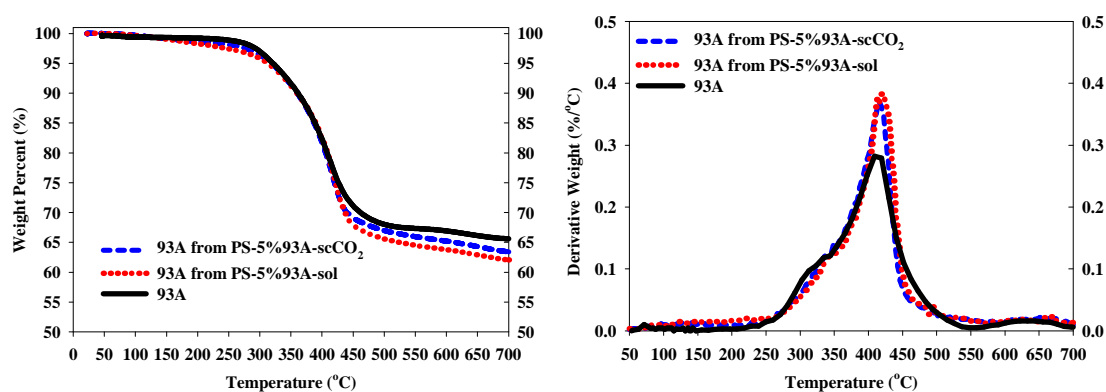


**Figure 35.** TGA curves and Derivative TGA curves for “as received” 10A and separated 93A from PS-5%93A-sol and PS-5%93A-scCO<sub>2</sub>.

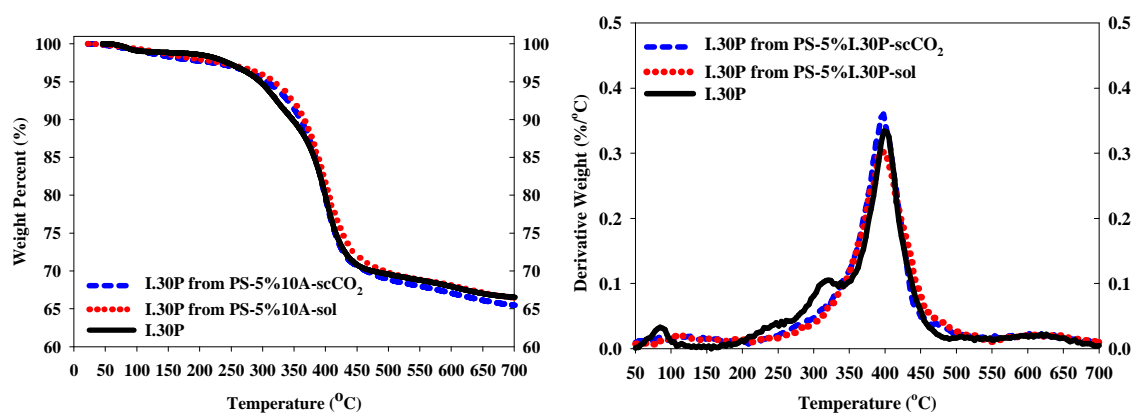


**Figure 36.** TGA curves and Derivative TGA curves for “as received” I.30P and separated I.30P from PS-5% I.30P-sol and PS-5% I.30P-scCO<sub>2</sub>.

TGA was also performed on the scCO<sub>2</sub>-processed and solution-blended 5 wt %

nanocomposites as well as the “as-received” polymer (PS280) to determine any change in the thermal decomposition due to scCO<sub>2</sub> processing. Decomposition effects have been observed in many publications on nanocomposites and have mostly been attributed to polymer confinement between clay platelets which can alter the Hoffman elimination.<sup>68, 82</sup> Table 13 contains the summary of all the TGA results for the 280k PS and the entire nanocomposites prepared in this study. Weight-loss curves of all 5 wt % scCO<sub>2</sub>-processed and solution-blended nanocomposites display a shift in thermal decomposition to a higher temperature compared the pure polymer. However, the 10 A nanocomposites (Figure 37) show the lowest increase despite showing the highest final d<sub>001</sub> WAXD spacing of 3.92 nm (Figure 23) and the largest number of platelets per tactoid compared to the rest of the nanocomposites studied (Table 10). All the other nanocomposites showed similar improvements in thermal decomposition compared to polystyrene despite having different final d<sub>001</sub> spacing and tactoid sizes. This was surprising since it was expected that the 10A nanocomposites will show the highest improvement based on the polymer confinement theory since the higher the d<sub>001</sub> spacing and the higher the tactoid size the more polymer was trapped in-between and shielded from normal degradation. Therefore, it seems that there might be other factors that can also govern the polymer nanocomposites decomposition effects. However, all the scCO<sub>2</sub> nanocomposites performed worse than the solution blended counterparts for all the clay which are expected to be less dispersed. At least if the clays are kept constant the confinement theory holds true, where the less dispersed solution blended composites show 4 to 5°C (2°C for 10A) (Table 13) improvement in the thermal decomposition temperature compared to scCO<sub>2</sub> processed nanocomposites. One possible explanation to the unexpected result is that organic modifier on Cloisite 10A starts to degrade much sooner (~160°C - Figure 33) than the rest of the organic modifiers (~ 200 - 250°C Figure

34 - Figure 36). Although the excess modifier might be shielded following scCO<sub>2</sub> processing as it was shown in the separated clay TGA curves (Figure 33 - Figure 36), this effect was least prevalent in 10A as it was the only one that still showed a degradation peak at 300°C (Figure 33). All the other clays only show a peak at around 400°C or higher. Therefore, it could be possible that the reason we see such a small improvement in 10A nanocomposites is due to the clay organic modifier degrading much sooner than the rest of the clays, opening up room for more polymer to be exposed to degradation at a lower temperature. The TGA of “as received” clays and clays that have been separated from solution blended and scCO<sub>2</sub> samples showed that the residual char was similar, indicating that after scCO<sub>2</sub> processing there was no polymer tethered to the clay surface. The percent residual mass of the nanocomposites reveal a similar conclusion since the scCO<sub>2</sub> and solution blended nanocomposites have similar residual weight percent (Table 13).

**Table 13.** TGA Summary: Temperature at 10 and 50 wt % Weight Loss, Maximum Rate of Decompositions (MRD), Change in MRD Compared to PS (°C) and Percent Char (residual mass fraction at 650°C).

| <b>Sample</b>                 | $T_{10}$ (°C) | $T_{50}$ (°C) | <b>MRD</b><br>(°C) | <b>Change in MRD</b><br><b>Compared to PS (°C)</b> | <b>% residual mass @ 650°C</b><br>(%) |
|-------------------------------|---------------|---------------|--------------------|--|---------------------------------------|
| PS280                         | 395           | 418           | 422                | N/A  | 0.41                                  |
| PS-10A (sol)                  | 396           | 423           | 425                | 3  | 5.53                                  |
| PS-10A (scCO <sub>2</sub> )   | 398           | 424           | 423                | 1  | 5.55                                  |
| PS-15A (sol)                  | 382           | 430           | 432                | 10   | 5.12                                  |
| PS-15A (scCO <sub>2</sub> )   | 397           | 421           | 427                | 5  | 6.04                                  |
| PS-93A (sol)                  | 383           | 428           | 432                | 10   | 4.95                                  |
| PS-93A (scCO <sub>2</sub> )   | 397           | 427           | 428                | 6  | 5.69                                  |
| PS-I.30P (sol)                | 401           | 434           | 436                | 14   | 5.84                                  |
| PS-I.30P (scCO <sub>2</sub> ) | 405           | 428           | 428                | 6  | 6.01                                  |

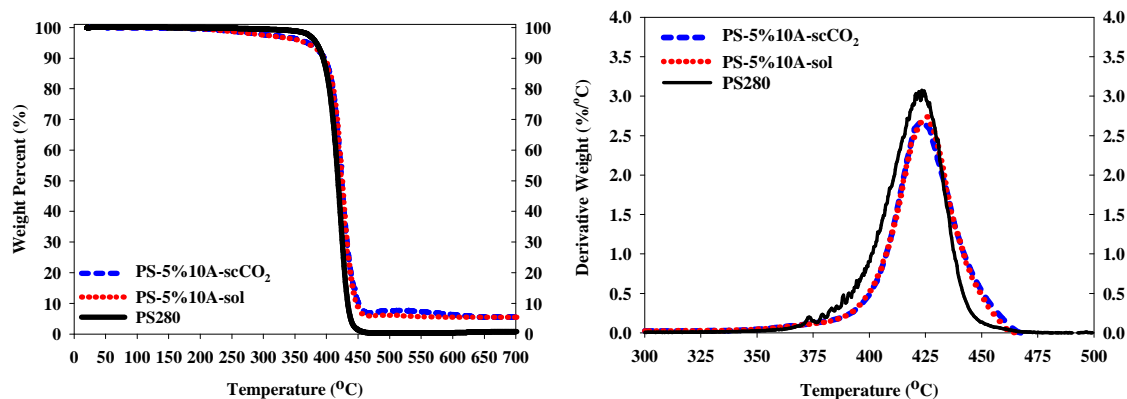


**Figure 37.** TGA curves and Derivative TGA curves for “as received” PS280 and PS-5% 10A-sol and PS-5% 10A-scCO<sub>2</sub>

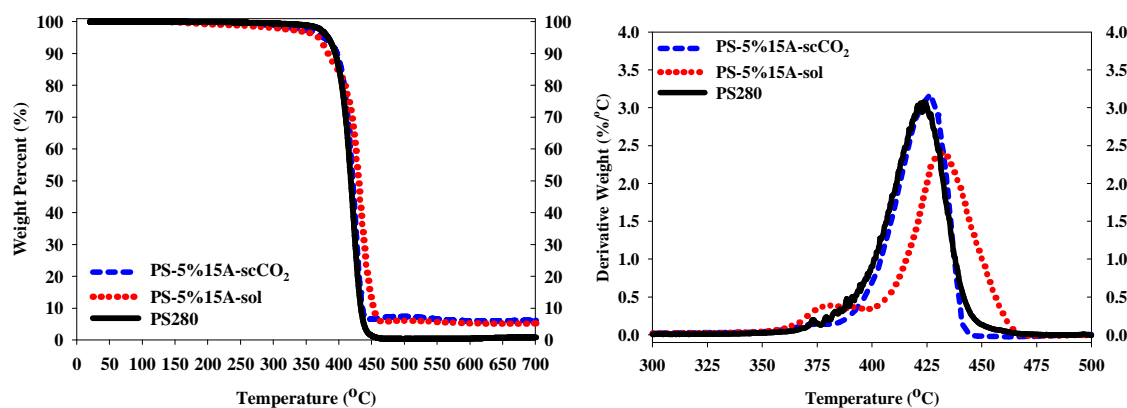


**Figure 38.** TGA curves and Derivative TGA curves for “as received” PS280 and PS-5% 15A-sol and PS-5% 15A-scCO<sub>2</sub>

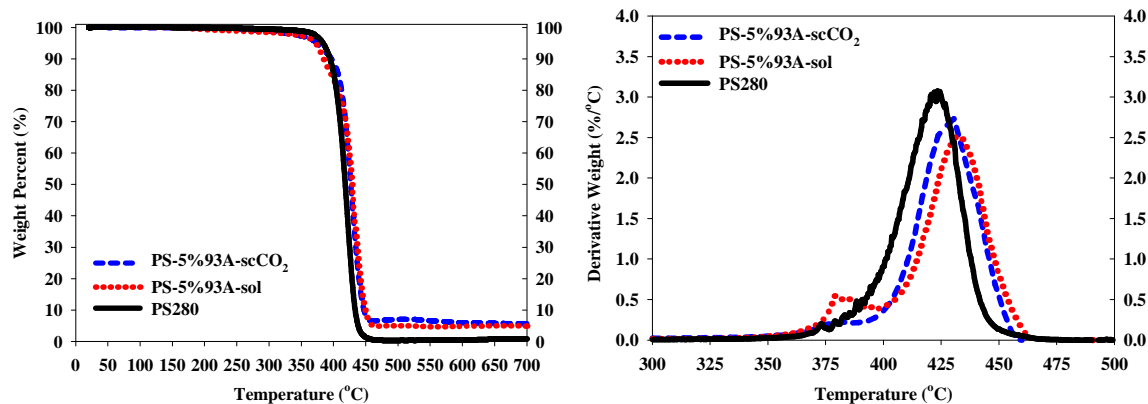


**Figure 39.** TGA curves and Derivative TGA curves for “as received” PS280 and PS-5% 93A-sol and PS-5% 93A-scCO<sub>2</sub>

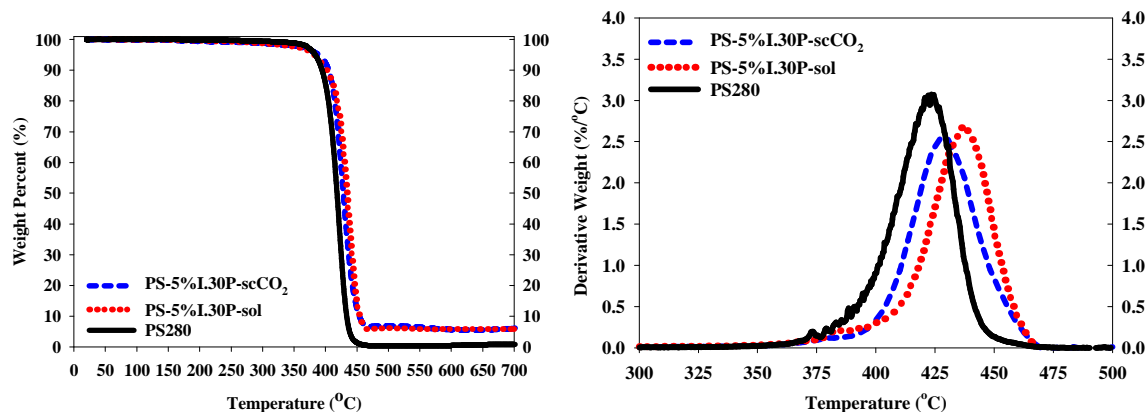


**Figure 40.** TGA curves and Derivative TGA curves for “as received” PS280 and PS-5% I.30P-sol and PS-5% I.30P-scCO<sub>2</sub>

### 3.5.1e Permeability

A major advantage of the polymer/layered nano - clay nanocomposites is their ability to enhance barrier properties. It was reported that gas and water vapor permeability through polymer films can be significantly reduced with small nano - clays loadings (1-5 wt%). Most research on polymer/clay nanocomposite barrier properties is done on oxygen, carbon dioxide and nitrogen barrier films for packaging food industry. Other applications that show increase interests are gas tanks and coatings.<sup>83</sup>



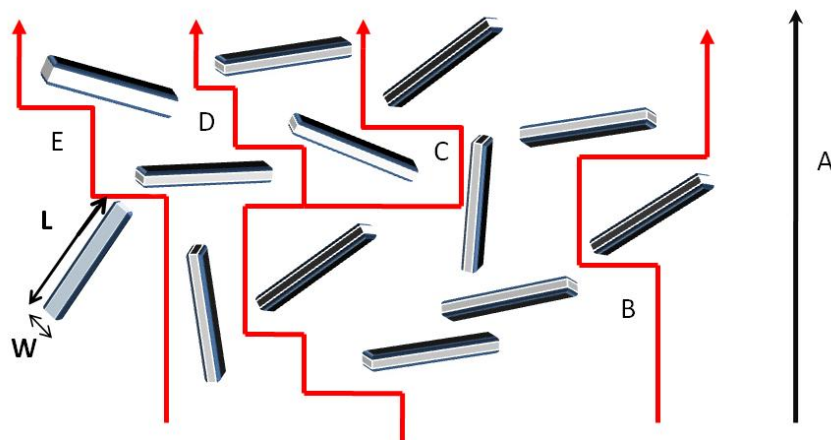


**Figure 41.** Tortuosity path in a polymer/clay nanocomposite. Path A displays the path a gas molecule will take to permeate through a neat polymer. Paths B-E are possible paths that a gas molecule can take in polymer filled with layered clay of different width (W), length (L) and orientation relative to the diffusion direction.

The mechanism behind the mass transport of gasses permeating a polymer/layered clay nanocomposite is similar to that in a semi-crystalline polymer.<sup>83</sup> The nanocomposite is considered to consist of two phases: a permeable phase (polymer matrix) and a second phase consisting of dispersed nano - clay platelets that are non-permeable. The gas-permeability of a polymer/clay nanocomposite is influenced by three main factors: the volume fraction of the nano - platelets, the platelets orientation relative to the diffusion direction and the nano - clay platelet aspect ratio. It is commonly accepted that Frick's law governs the transport mechanism within the polymer matrix. Also, the polymer matrix in a nanocomposite maintains the same properties and characteristics as the neat polymer. The permeability is dependent on solubility and diffusivity of permeate in the nanocomposite. Since the volume that the polymer matrix occupies is reduced due to presence of layered nano - clay, a decrease of the solubility may occur in the nanocomposite, as well as a decrease in diffusion due to a more tortuous path for the diffusing molecules. However, if the volume fraction of nano platelets is low (usually less than 5%) and

the reduction of the matrix volume relatively small and it is expected that the reduction of the diffusion coefficient will be higher than that of the solubility coefficient. Therefore, tortuosity is anticipated to be the major factor in determining the nanocomposite permeability. The tortuosity is determined by the length and width of the filler material and therefore a function of the aspect ratio of the layered clay tactoids (many platelets stacked on top of each other – shown in Figure 41), the degree of dispersion of the nano – clay and the tactoids and platelets orientation. The tortuosity factor can be defined by the following equation:

$$\tau = \frac{d'}{d} = 1 + \frac{L}{2W} \phi_s \frac{2}{3} \left( S + \frac{1}{2} \right) \quad (4)$$

where  $d'$  is the distance that a penetrant must travel to the shortest distance  $d$  that it would travel in the absence of barriers. It is expressed in terms of the length  $L$ , width  $W$ , filler volume fraction  $\phi_s$  and  $S$  represents the order parameter to take in consideration the tactoids and platelets orientation and it's defined as:

$$S = \frac{1}{2} * (3 * \cos^2(\theta) - 1) \quad (5)$$

where  $\theta$  represents the angle between the direction of preferred orientation which is parallel to the direction of permeate and the sheet normal unit vectors. It can range from 1 when the nano - clay platelets and/or tactoids are oriented parallel to direction of the permeate (when  $\theta = 0$ ) to -1/2 when the nano - clay is oriented perpendicular to the permeate direction ( $\theta = \pi/2$ ), and a value of 0, when the nano - clay sheets are randomly oriented.  $S$  would need to be averaged over all the platelets and tactoids. The effect of tortuosity on permeability can be expressed by:

$$\frac{P_n}{P_p} = \frac{(1 - \phi_s)}{\tau} \quad (6)$$

where  $P_n$  and  $P_p$  represent the permeability of the nanocomposite and pure polymer, respectively. Bharadwaj et. al have performed molecular modeling on the polymer/clay nanocomposites based on different parameters. Different nano - platelets orientations relative to the diffusion direction and several tactoids widths used in the molecular modeling by Bharadwaj are shown in Figure 42. As expected the gas permeability in nanocomposites decreased as the tactoids width ( $W$ ) decreases, as the nano-platelet length increased and as the nano - platelets orientation approached perpendicular orientation relative to the diffusion direction (Figure 43).<sup>84</sup> Therefore, to obtain the biggest reduction in permeability, preferably the dispersion should be maximized where the width is minimized and the platelets should be oriented perpendicular to the diffusion direction.

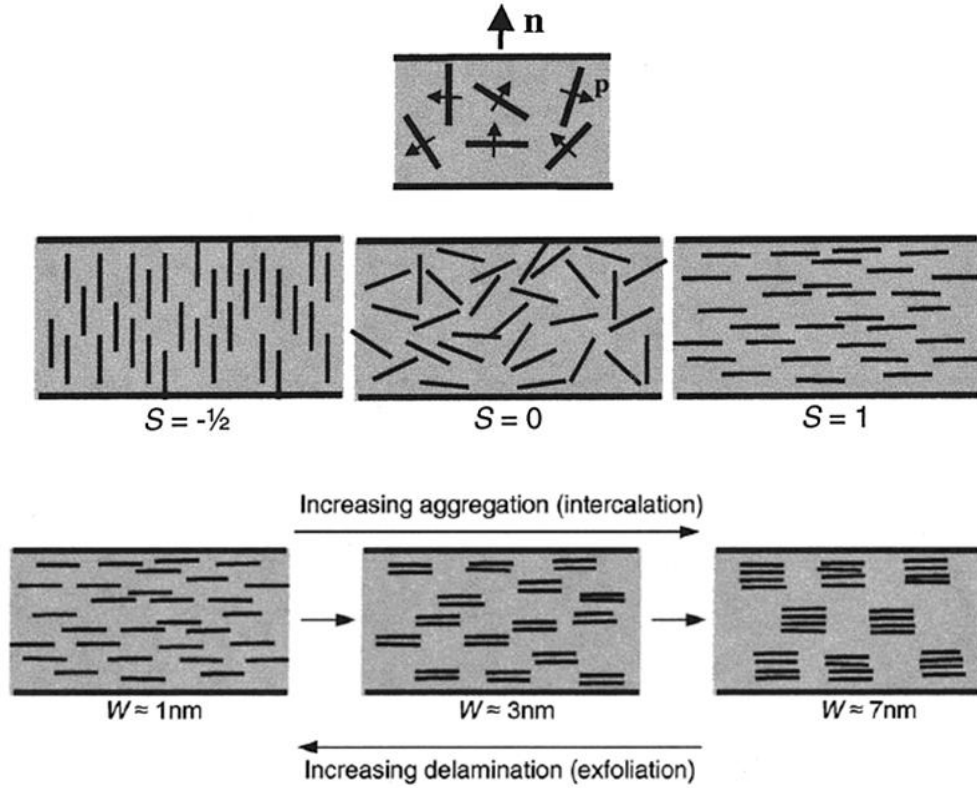


**Figure 42.** Values of the order parameter for three orientations of the platelets (top).<sup>84</sup> Influence of the degree of delamination on the tortuosity factor and the aspect ratio of nano-clay tactoids.  $W$  is the width of the nano-clay tactoid (bottom).<sup>84</sup>

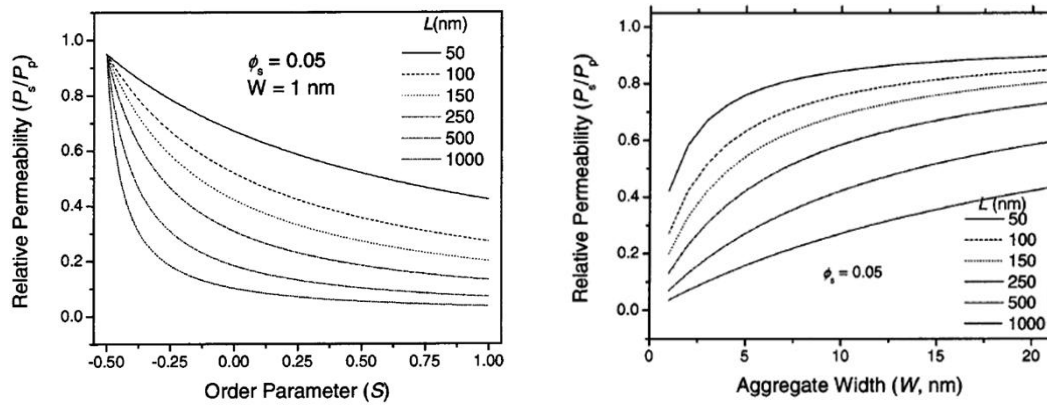


**Figure 43.** Dependence of the relative permeability on the order parameter at different sheet lengths (left).

Dependency of the relative permeability on the average tactoid size ( $W$ ) at several different plate lengths (right).<sup>84</sup>

The transport properties of PS, solution blended and scCO<sub>2</sub> processed 5 wt% nanocomposites were tested in this study to measure the scCO<sub>2</sub> induced dispersion and clay organic modifier effect on oxygen and water vapor permeability. The presence of dispersed nano - clay particles increases the tortuous path that a molecules needs to take to diffuse through the polymer matrix. The permeability was expected to reduce more as the extent of dispersion increased. Therefore, it is anticipated that the scCO<sub>2</sub> processed nanocomposites, having enhanced nano - clay dispersion over to the solution blended benchmarks, should displayed the highest reduction in permeability between the two processing methods. The PS/10A solution blended nanocomposite showed a 9% reduction in oxygen permeability and 33% reduction in water vapor permeability over the neat PS. As anticipated, the scCO<sub>2</sub> processed 10A (PS-5%10A-scCO<sub>2</sub>) nanocomposites displayed a 35% further reduction in oxygen permeability over solution blended benchmark for a total reduction of 45% over neat PS (Figure 44 and Table 14).<sup>85</sup> Also, the scCO<sub>2</sub> processed 10A nanocomposit displayed a further reduction in water vapor permeability over the solution blended benchmark for a total of 39% reduction over neat PS (Figure 45 and Table 15).<sup>85</sup> In contrast, the scCO<sub>2</sub> 10A nanocomposite made with pre - dispersed clay (PS-5%10Ape-scCO<sub>2</sub>) showed no improvement in oxygen permeability over the scCO<sub>2</sub> 10A nanocomposite made with “as received” 10A (PS-5%10A-scCO<sub>2</sub>). However, it did show a modest further reduction of water vapor permeability of 5% (Figure 45). This was unexpected since this sample had enhanced nano - clay dispersion over the scCO<sub>2</sub> nanocomposite made with “as received” 10A. The enhanced dispersion was anticipated to have a similar effect in improving transport properties like it had in improving the rheological properties due the presence of more individual platelets. However, it seems the clay dispersion improvement in this sample did not play a significant role in lowering the permeability or the

improvement was not significant enough to have an effect on transport properties. The nanocomposites made with 5 wt% Cloisite 15A also showed a reduction in both oxygen and water vapor permeability over the pure PS (Figure 46 and Figure 47). Moreover, the 15A nanocomposite prepared using the scCO<sub>2</sub> processing method also displayed a further reduction in both O<sub>2</sub> (by 40%) and water vapor permeability (10%) over the solution blended benchmark for a total of 60% and 29% reduction over PS respectively. In contrast, the nanocomposites made with Cloisite 93A which had the best dispersion compared to the other clays (10A and 15A) only showed a modest 6% reduction in O<sub>2</sub> permeability. However, the solution blended 93A sample (PS-5%93A-sol) displayed an 18% increase in oxygen permeability (Figure 48), although it showed a reduction in water vapor permeability by 29% (Figure 49). The increase in permeability of the solution blended and the modest reduction of the scCO<sub>2</sub> sample in 93A nanocomposites was unexpected since it is known that permeability is dependent on nano - clay dispersion and as dispersion increases the permeability should decrease. This phenomenon was not only shown experimentally<sup>86, 87</sup> but also by modeling.<sup>84, 86, 87</sup> However, sometimes the nanocomposites permeability can be affected by the existence of interfacial regions between the matrix and the inorganic particles. These areas may affect the gas and vapor diffusion coefficient. The interfaces are caused either by the surfactant that is used for the modification of the particles or/and are due to the formation of voids between the different phases.<sup>83, 88, 89</sup> The positive interaction between the clay organic modifier and polymer matrix may cause a region around the clay particles that is denser than the bulk polymer matrix. This higher interphase polymer layer near the inorganic has different properties than the bulk matrix and may cause further reduction in barrier properties.<sup>90</sup> It is also suggested that the strong interfacial interaction may also cause a reduction in free volume like it has been found in styrene-butadiene rubber-

montmorillonite nanocomposites, therefore reducing the gas or vapor permeability.<sup>91</sup> The same effect was observed in poly (ε-caprolactam) clay nanocomposites, where, based on a theoretical model, a reduction of 14% in free volume fraction was reported with the addition of 2 wt% modified clay.<sup>92</sup> Ammala et al. showed in poly(m-xylene adipamide)-montmorillonite nanocomposites that the favorably interacting Cloisite 10A showed a considerable reduction in the oxygen transmission rates of nanocomposites (66% reduction) while Cloisite 93A showed a small increase (4% increase).<sup>93</sup> Since both 93A and 10A nanocomposites showed similar dispersion, the authors were looking for an alternative explanation for the different barrier properties obtained in the two nanocomposites. Therefore, they attributed this increase in oxygen transmission rate in 93A due to the steric effect due to the presence of two long non-polar chains compared to one in 10A, preventing the close approach of the clay particles to the polyamide chains.<sup>93</sup> Although steric hindrance might play a role, it does not seem to be the main cause since both Cloisite 15A solution blended and scCO<sub>2</sub> processed nanocomposites showed much larger permeability reduction compared to 93A and even compared to 10A in the case of oxygen permeability even though 10A only has one C18 non-polar chain. It is more probable that the main cause is the reduced polymer-clay interaction in 93A nanocomposites that are responsible for the poor barrier properties in 93A, similar to what was observed in poor rheological properties in 93A nanocomposites compared to 10A and 15A nanocomposites (see Figure 31). WAXD also showed the same trend where the larger final d<sub>001</sub> spacing can be attributed to increase polymer-clay interactions in 10A and 15A (Figure 23). Therefore, it is probable that the strong interfacial polymer-clay interactions may cause a reduction of free volume in the case of 10A and 15A leading to a decrease in barrier properties. Conversely, the weak polymer clay interaction between the organic modifier in 93A and PS may cause only a

small decrease or even an increase in a free volume in the nanocomposites that can be responsible for the slight increase in O<sub>2</sub> permeability in the 93A solution blended nanocomposite.

<sup>94</sup> However, all nanocomposites including both 93A nanocomposites showed a reduction in the water vapor permeability compared to the neat PS (Table 15). The reduced water vapor permeability was expected even in both 93A nanocomposites due to the hydrophobic nano - clay nature due to the presence of the organic modifiers. Sorrentino and co-workers have found that the permeability of water was reduced whereas the dichloromethane permeability was increases due to due to the specific properties of the interface region, which in turn are determined by the nature of the polymer and of the nano - filler. In the case of dichloromethane, due to these specific properties the formation of preferential pathways in the proximity of the clay surface led to increase in permeability. <sup>88</sup>

Therefore, as expected, all of the scCO<sub>2</sub> nanocomposites containing a higher amount of dispersed nano - clay compared to the solution blended benchmark showed higher reduction in both oxygen and water vapor permeability. Moreover, the results obtained from permeability studies further demonstrate the ability of scCO<sub>2</sub> method to produced highly dispersed nanocomposites with enhanced properties. Furthermore, choosing the right polymer - clay system that can provide both good dispersion and good polymer - clay interactions is imperative in obtaining the desired end property improvements. Two examples of choosing the right system are the 10A and 15A scCO<sub>2</sub> nanocomposites where the oxygen permeability was reduced compared to neat PS by 45% and 60% respectively. The most significant reduction in oxygen permeability in polymer/clay nanocomposites come from those made by using the *in-situ* polymerization method with custom made organic modifiers.<sup>83, 86, 87, 90, 95</sup> Nazarenko et al. used clay that was modified with specialty organic modifiers that are supposed to interact well with



PS to prepare nanocomposites using the *in-situ* polymerization method. They were able to reduce the oxygen permeability between 10 and 30% compared to neat PS depending on what clay they used at 5wt% clay loading.<sup>86</sup>

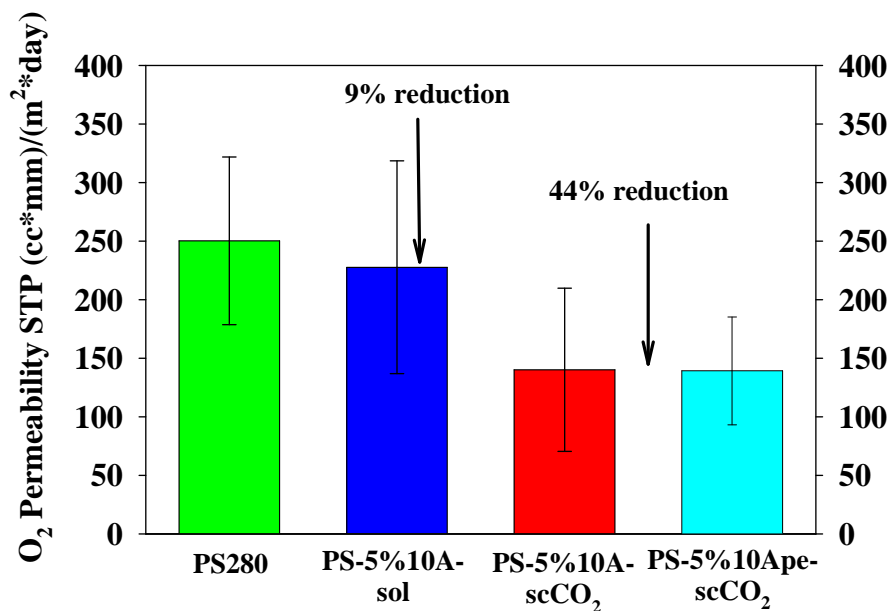


**Figure 44.** Oxygen permeability of 280k PS, solution blended and scCO<sub>2</sub> processed Cloisite 10A nanocomposites.

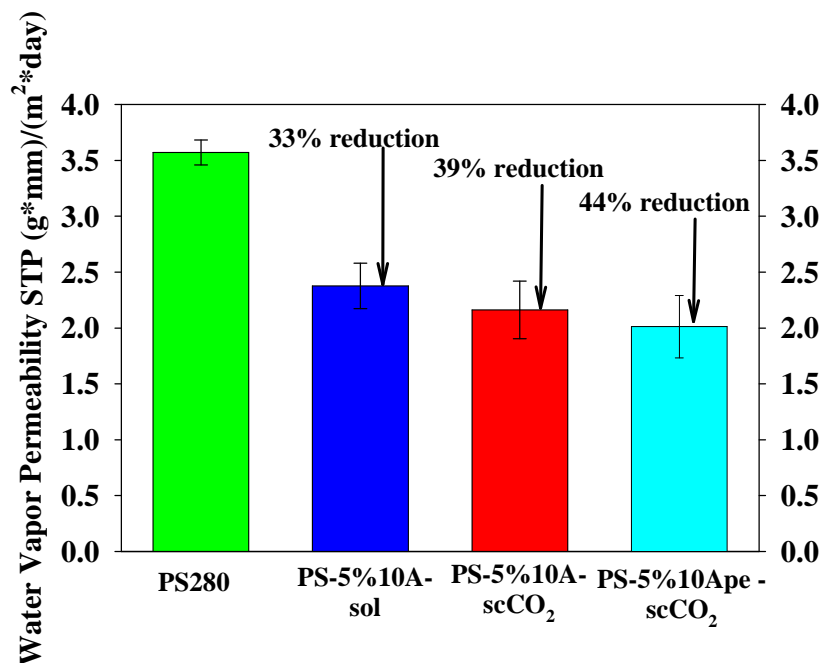


**Figure 45.** Water vapor permeability of 280k PS, solution blended and scCO<sub>2</sub> processed Cloisite 10A nanocomposites.

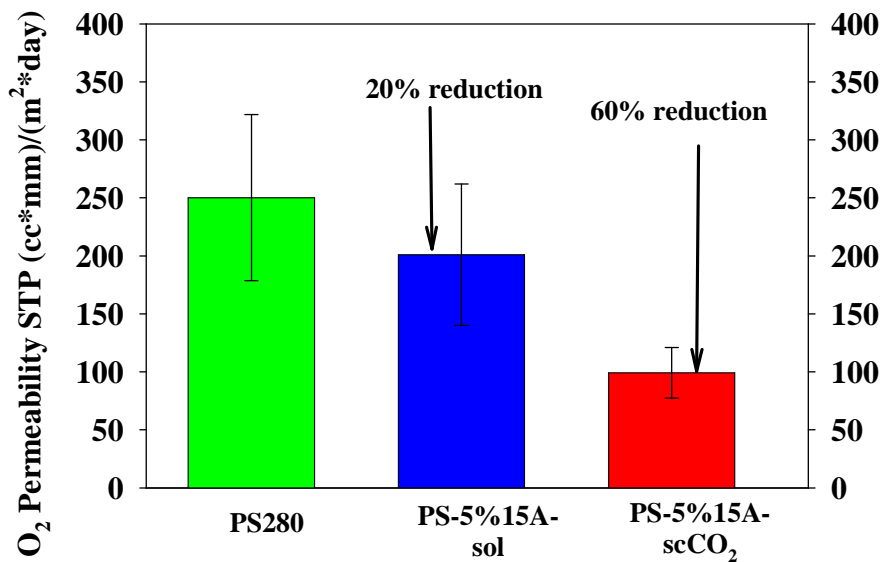


**Figure 46.** Oxygen permeability of 280k PS, solution blended and scCO<sub>2</sub> processed Cloisite 15A nanocomposites.

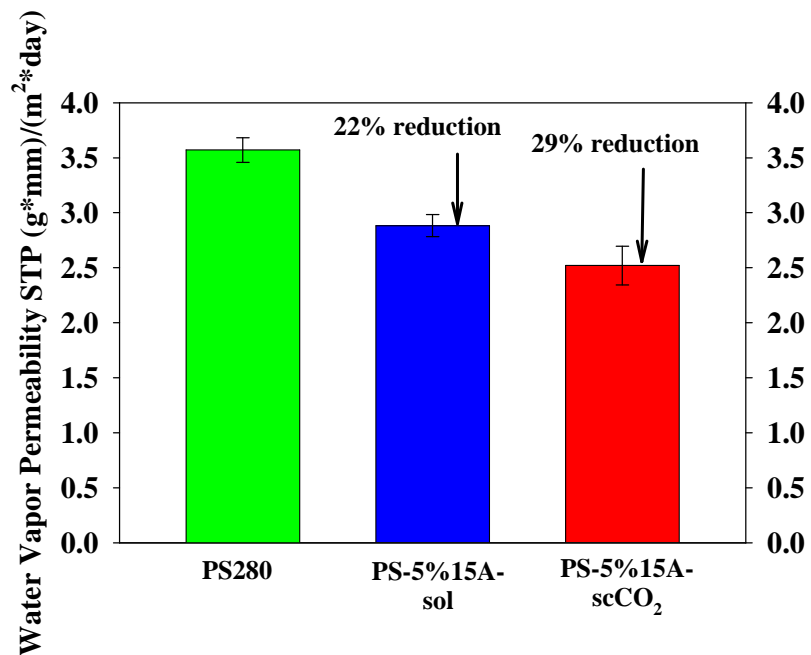


**Figure 47.** Water vapor permeability of 280k PS, solution blended and scCO<sub>2</sub> processed Cloisite 15A nanocomposites.

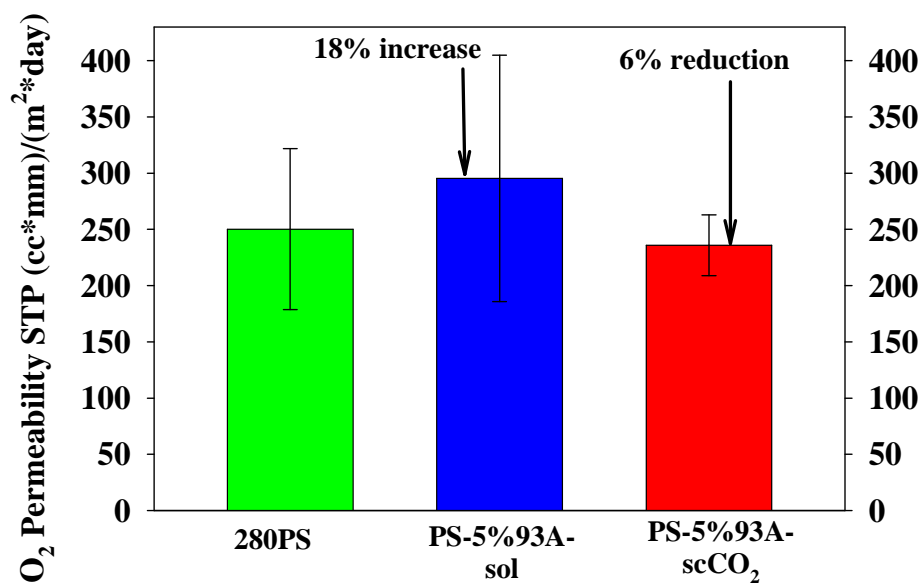


**Figure 48.** Oxygen permeability of 280k PS, solution blended and scCO<sub>2</sub> processed Cloisite 93A nanocomposites.

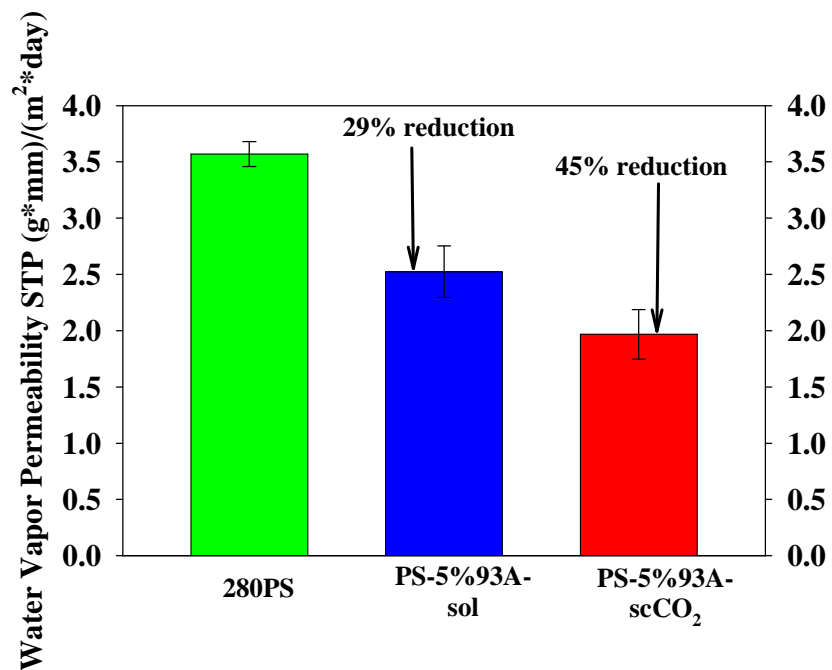


**Figure 49.** Water vapor permeability of 280k PS, solution blended and scCO<sub>2</sub> processed Cloisite 93A nanocomposites.

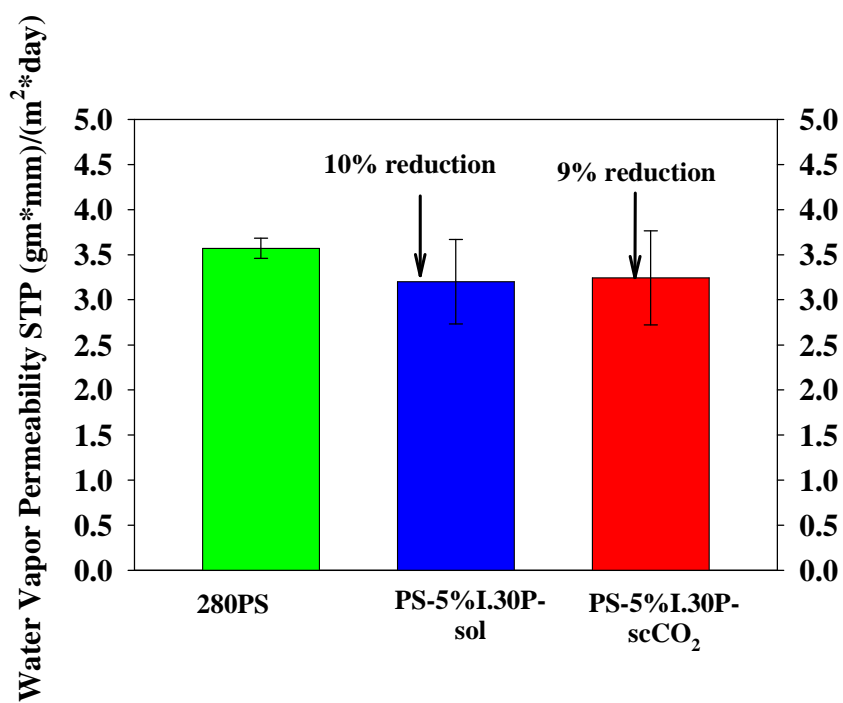


**Figure 50.** Water vapor permeability of 280k PS, solution blended and scCO<sub>2</sub> processed Nanocor I.30P nanocomposites.

**Table 14.** Average and standard deviation data for oxygen permeability of 280k PS, solution blended and scCO<sub>2</sub> processed Cloisite 10A, 93A, 15A and Nanocor I.30P nanocomposites. The table includes percent reduction in O<sub>2</sub> permeability relative to neat 280k PS and to corresponding benchmarks of solution blended nanocomposites.

| Sample                        | O <sub>2</sub> Permeability (cc*mm)/(m <sup>2</sup> *day) |                    |                                 |  |
|-------------------------------|---|--------------------|---------------------------------|--|
|                               | Average   | Standard Deviation | Reduction relative to 280PS (%) | Reduction relative to sol. blended benchmark (%) |
| 280PS                         | 209.66  | 125.17             |                                 |  |
| PS-5t% 10A-sol                | 227.73  | 110.95             | <b>-8.98</b>                    |  |
| PS-5% 10A-scCO <sub>2</sub>   | 140.19  | 69.71              | <b>-43.97</b>                   | <b>-38.44</b>                                    |
| PS-5% 10Ape-scCO <sub>2</sub> | 139.23  | 46.07              | <b>-44.35</b>                   | <b>-38.86</b>                                    |
| PS-5t% 93A-sol                | 295.40  | 136.61             | <b>18.06</b>                    |  |
| PS-5% 93A-scCO <sub>2</sub>   | 236.00  | 7.07               | <b>-5.68</b>                    | <b>-20.11</b>                                    |
| PS-5t% 15A-sol                | 200.93  | 60.89              | <b>-19.69</b>                   |  |
| PS-5% 15A-scCO <sub>2</sub>   | 99.20   | 21.75              | <b>-60.35</b>                   | <b>-50.63</b>                                    |

**Table 15.** Water vapor permeability of 280k PS, solution blended and scCO<sub>2</sub> processed Cloisite 10A, 93A, 15A and Nanocor I.30P nanocomposites. The table includes percent reduction in water vapor permeability relative to neat 280k PS and to corresponding benchmark solution blended nanocomposite.

| Sample                        | Water Vapor Permeability (g * mm) / (m <sup>2</sup> - day ) |                    |                                 |  |
|-------------------------------|---|--------------------|---------------------------------|--|
|                               | Average   | Standard Deviation | Reduction relative to 280PS (%) | Reduction relative to sol. blended benchmark (%) |
| 280PS                         | 3.57  | 0.11               |                                 |  |
| PS-5t% 10A-sol                | 2.38  | 0.20               | <b>-33.42</b>                   |  |
| PS-5% 10A-scCO <sub>2</sub>   | 2.16  | 0.26               | <b>-39.40</b>                   | <b>-8.99</b>                                     |
| PS-5% 10Ape-scCO <sub>2</sub> | 2.01  | 0.28               | <b>-43.63</b>                   | <b>-15.33</b>                                    |
| PS-5t% 93A-sol                | 2.52  | 0.23               | <b>-29.32</b>                   |  |
| PS-5% 93A-scCO <sub>2</sub>   | 1.97  | 0.22               | <b>-44.86</b>                   | <b>-21.99</b>                                    |
| PS-5t% 15A-sol                | 2.78  | 0.11               | <b>-22.04</b>                   |  |
| PS-5% 15A-scCO <sub>2</sub>   | 2.52  | 0.18               | <b>-29.41</b>                   | <b>-9.46</b>                                     |
| PS-5t% I.30P-sol              | 3.20  | 0.47               | <b>-10.36</b>                   |  |
| PS-5% I.30P-scCO <sub>2</sub> | 3.24  | 0.52               | <b>-9.15</b>                    | <b>1.35</b>                                      |

### 3.5.2 Effect of scCO<sub>2</sub> processing parameters on nanocomposite morphology and properties

Gaining a better understanding on the effects that different processing parameters have on the nanocomposite morphology and properties is of great importance. Therefore, a better representation can be developed of the physical representation describing what is occurring during CO<sub>2</sub> processing that can lead to improve nano - clay dispersion. Moreover, once the effects that the parameters have on the resulting nanocomposite morphology and properties are better understood, a better optimization of the scCO<sub>2</sub> process can be performed in order to obtain the desired results. The effect of scCO<sub>2</sub> depressurization rate, scCO<sub>2</sub> soaking, nano - clay pre-dispersion, nano - clay weight fraction, and nanocomposites processing time and pressure were studied.

To study the effect of clay weight fraction on nanocomposites morphology and properties six samples (2, 5 and 10 wt% clay) were made using “as received” Cloisite 10A and 93A using the scCO<sub>2</sub> process (PS-2%10A-scCO<sub>2</sub>, PS-5%10A-scCO<sub>2</sub>, PS-10%10A-scCO<sub>2</sub>, PS-2%93A-scCO<sub>2</sub>, PS-5%93A-scCO<sub>2</sub>, PS-10%93A-scCO<sub>2</sub>). Two 5 wt% 10A sample were also prepared which were depressurized at different rates compared to PS-5%10A-scCO<sub>2</sub> (~300MPa/min) to investigate the role of scCO<sub>2</sub> soaking and depressurization rate on the resulting nanocomposite morphology and properties. The first nanocomposite PS-5%10Amd-scCO<sub>2</sub> was depressurized at ~0.115MPa/min and the second (PS-5%10Asd-scCO<sub>2</sub>) was depressurized even slower at ~0.045MPa/min. Another 5wt% 10A sample was made using clay that was pre-processed in scCO<sub>2</sub>(PS-5%10A-scCO<sub>2</sub>) to investigate the role of clay dispersion on the resulting polymer/clay nanocomposite properties. To eliminate the role of thermal annealing and solution blending, benchmark composites of 2, 5 and 10 wt% by clay (PS-2%10A-sol, PS-5%10A-sol, PS-10%10A-sol, PS-2%93A-sol, PS-5%93A-sol, PS-10%93A-sol) were made in the same vessel without the presence of scCO<sub>2</sub> at 80 °C for 24 hours. WAXD of PS/10A nanocomposites is

displayed in Figure 51, Figure 53 and Figure 55 for PS/93A nanocomposites. Interestingly, all samples showed a large diffraction peak at  $2\theta = 2.29^\circ$  regardless of weight fraction, processing conditions, or rheological enhancement for PS/10A nanocomposites. The shift in the  $d_{001}$  peak from  $4.6^\circ$  for pristine 10A to  $2.29^\circ$  corresponds to a tripling of platelet spacing from 0.92 nm to 2.85 nm, and implies that polymer has been intercalated into the clay galleries. Moreover, the presence of the  $d_{002}$  peak along with a tall  $d_{001}$  peak indicates a highly ordered intercalated nanocomposite is present. Giannelis and Vaia have previously modeled intercalation behavior of clay in a polymer matrix and determined that there are several factors that contribute to the level of clay dispersion that is attainable in system. The authors also performed corresponding experiments on several PS/clay hybrids to substantiate the simulation results.<sup>13, 15</sup> Their findings show that there is an entropic balance between the clay modifier that wants to have as much conformational freedom as possible, and the matrix polymer that does not want to be confined between the clay platelets. The entropic gain associated with the organic modifier from increasing the clay basal spacing only occurs until the modifier chains become fully extended ( $h_\infty$ ), after which there is no gain or penalty to increased platelet spacing. However, there is still an entropic penalty to increased spacing that comes from polymer confinement until the clay spacing is greater than the average radius of gyration of the matrix material. In order for the platelet spacing to extend farther than  $h_\infty$  would require strong polymer-clay interactions to overcome the entropic barrier. The inter-gallery spacing at full chain extension can be expressed in terms of the number of carbon atoms in the aliphatic backbone by equation 2 in Chapter 2.

The polystyrene/styrene/10A system was processed in a good solvent for the clay modifier and it follows that the aliphatic chains will want to be as extended as possible, which would correlate to a spacing of approximately 2.4 nm. This compares favorably with the

experimentally measured inter-gallery spacing of 2.85 nm for 10A. However, since there was also polymer in solution, the barrier to exfoliation of the ordered platelets may be too great to overcome leading to an ordered highly intercalated composite.

### ***3.5.2a Effect of depressurization rate on nanocomposite morphology and properties***

The current understanding about what is happening during depressurization is that when the scCO<sub>2</sub> is leaving the nano - clay inner-gallery spacing during depressurization it pulls the platelets apart due to the sudden expansion (increase in volume). However, no studies have been done in understating the effect of the rate of depressurization on the structure and properties of the resulting nanocomposite. Moreover, is the presence of CO<sub>2</sub> (CO<sub>2</sub> soaking) enough to cause improvements in dispersion and/or properties? In other words, if the sample is depressurized very slowly will the improvements be better than the solution blended and/or will they even be similar to the sample that is suddenly depressurized.

To achieve this task three 5 wt% 10A scCO<sub>2</sub> samples were also prepared which were depressurized at different rates PS-5%10A-scCO<sub>2</sub> at ~300MPa/min, PS-5%10Amd-scCO<sub>2</sub> at ~0.115MPa/min and PS-5%10Asd-scCO<sub>2</sub> at ~0.045MPa/min. All samples that were depressurized at significantly different rates showed similar d<sub>001</sub> spacing (Figure 51).



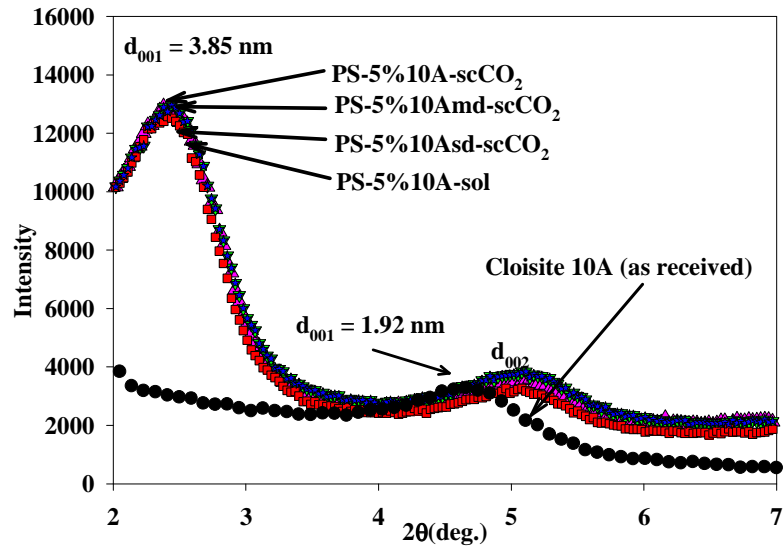


**Figure 51.** X-ray diffractograms of “as received” Cloisite 10A and solution blended, and scCO<sub>2</sub> PS/10A nanocomposites processed and depressurized at various rates prepared.

Despite the lack of differentiation between the nanocomposites morphologies in WAXD, rheological studies revealed significant differences between the samples after scCO<sub>2</sub> processing and depressurizing at different rates. Sample PS-5%10Asd-scCO<sub>2</sub> that was depressurized very slowly over a period of 5 hours at a rate of  $\sim 0.045$ MPa/min showed an improvement in the storage modulus low frequency plateau of almost an order of magnitude compared to the solution blended benchmark sample (Figure 52). This result demonstrates that even if the sample is depressurized slowly, the rate of CO<sub>2</sub> expansion is faster than the CO<sub>2</sub> diffusion out of the inner-galley spacing and the CO<sub>2</sub> is still causing nano - clay dispersion by pushing the platelets apart as it leaves. However, when a similar sample was depressurized 2.5 times as fast at  $\sim 0.115$ MPa/min over a 2 hour period (PS-5%10Amd-scCO<sub>2</sub>) it displayed a further improvement in storage modulus due to improved dispersion. Moreover, when a sample was depressurized nearly instantaneously at  $\sim 300$ MPa/min (PS-5%10A-scCO<sub>2</sub>) it showed an even more significant enhancement in storage modulus at all frequencies. This study demonstrated the need for fast

CO<sub>2</sub> depressurization not just CO<sub>2</sub> soaking in order to maximize nano - clay dispersion during depressurization. Although, CO<sub>2</sub> soaking aids in clay dispersion, it is significantly more important to depressurize as fast as possible in order to push the nano - clay platelets apart and maximize the surface area that can be available for polymer - clay interaction. This reinforces the assertion that the rate at which scCO<sub>2</sub> escapes does in fact have a drastic effect on the resulting nanocomposite structure. When the system was depressurized instantaneously, the scCO<sub>2</sub>, which diffused in between clay layers during processing, underwent a more drastic change in density and effectively pushed the platelets apart. This phenomenon was not observed when the system was slowly depressurized since scCO<sub>2</sub> had a much longer time to diffuse out of the clay galleries without significantly affecting their structure. Although the same d<sub>001</sub> peak was seen for both samples, the viscoelastic results suggest that there is a higher level of dispersed single platelets in PS-5%10A-scCO<sub>2</sub> compared to PS-5%10Asd-scCO<sub>2</sub> and PS-5%10Amf-scCO<sub>2</sub>.

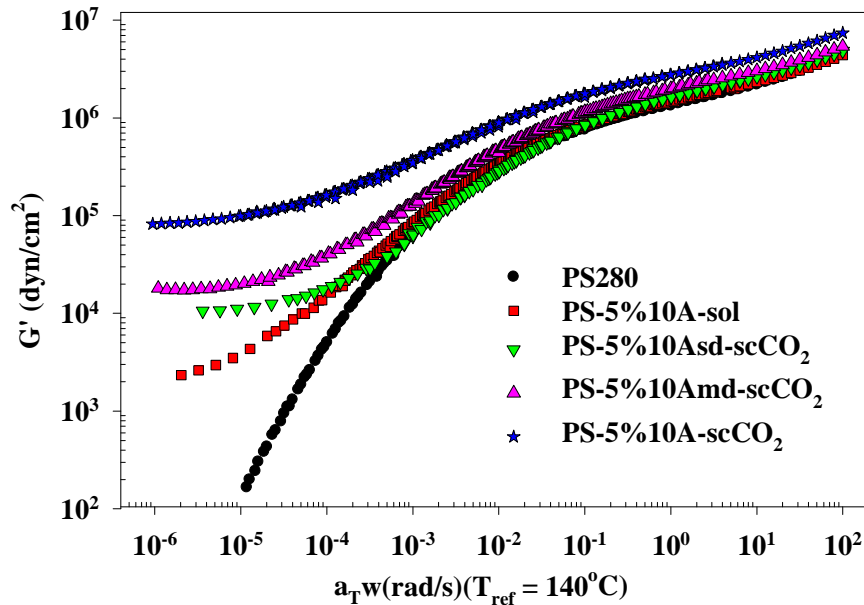


**Figure 52.** Storage modulus of 280k PS and solution blended, and scCO<sub>2</sub> PS/10A nanocomposites processed and depressurized at various rates prepared.

### ***3.5.2b Effect of nano - clay scCO<sub>2</sub> pre - dispersion on nanocomposite morphology and properties***

An interesting phenomenon was the behavior of the pre - dispersed clay when it was reprocessed in a polymer solution using either the scCO<sub>2</sub> processing technique or the traditional solution blending method. Even though the clay itself was scCO<sub>2</sub> processed and determined to have no measurable order as evident by the disappearance of the d<sub>001</sub> peak in WAXD (Figure 8), upon addition to polymer solution it seemed to regain its parallel registry (Figure 53). It has been shown previously that disordered intercalated systems will not give an X-ray peak even if the platelets are still quite close together.<sup>37</sup> If the platelets in the clay have not been exfoliated, and instead have lost their ordered spacing, it is possible that the solvent allows the dynamic reorganization of platelets to a more ordered thermodynamically favorable morphology. The most entropically favorable state in 10A is when the platelets have an inter-gallery spacing of 2.4 nm. It is then expected that if disordered intercalated clay was added into the styrene/polystyrene solution, the platelets will revert to their thermodynamically stable orientations. This would result in a composite that looks like all of the other composites in WAXD, but has a higher level of dispersed platelets and smaller tactoids as it was evident in TEM and rheology.

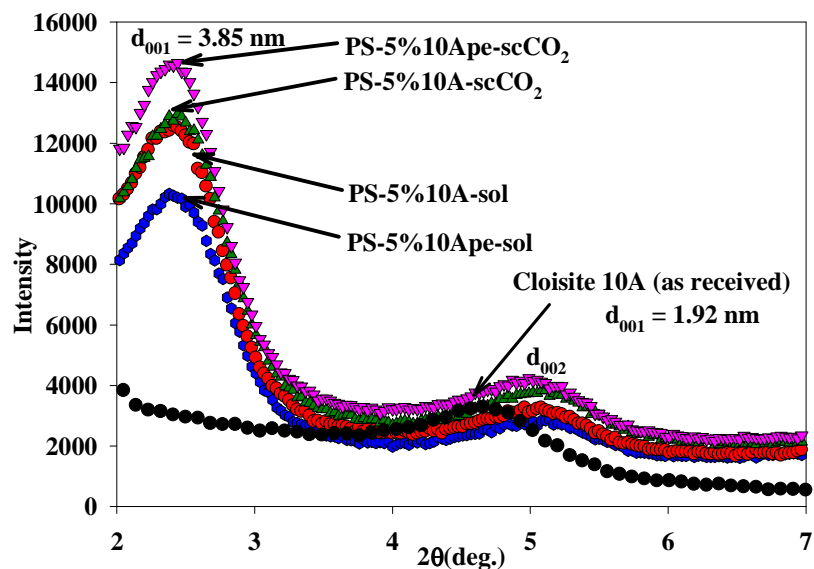


**Figure 53.** X-ray diffractograms of “as received” Cloisite 10A and PS/10A nanocomposites prepared with “as received” and pre-dispersed 10A to determine the effect of nano-clay pre-dispersion of the final nanocomposite morphology and rheological properties.

Again, despite the lack of differentiation between the nanocomposites morphologies in WAXD, TEM gave a deeper insight into the morphological changes that occurred upon  $\text{scCO}_2$  processing. As previously shown, the  $\text{scCO}_2$  processing produced a more complex morphology when compared to solution blending. The storage modulus,  $G'$ , of the 5 wt% 10A nanocomposites ( $\text{scCO}_2$  and solution blended) processed with “as received” and  $\text{scCO}_2$  pre-processed 10A is displayed in Figure 54. The solution blended benchmark sample (PS-5%10A-sol) exhibited similar improvements in the viscoelastic response to previously published data on solution blended hybrids.<sup>35, 47</sup> The morphology of the solution blended sample is believed to be purely intercalated as was supported by WAXD and TEM and in good agreement with recent publications which illustrated that polystyrene/clay nanocomposites made using solution blending alone resulted only in an intercalated morphology.<sup>35, 96</sup> The  $\text{scCO}_2$  pre-dispersed Cloisite 10A was reprocessed in the presence of polystyrene/styrene solution using the solution

blended technique (sample PS-5%10Ape-sol) and in scCO<sub>2</sub> (sample PS-5%10Ape-scCO<sub>2</sub>) in an attempt to improve the clay dispersion in the resulting nanocomposites. The storage modulus of the sample PS-5%10Ape-sol and PS-5%10Ape-scCO<sub>2</sub> sample exhibited a reasonable enhancement (a half an order of magnitude) over the PS-5%10A-sol and PS-5%10A-scCO<sub>2</sub> even though all samples exhibit a similar d<sub>001</sub> peak (Figure 54). Pre - dispersing the clay increases the surface area that is available for interaction with polymer due to the decrease in tactoid size and increase in disorder that clay undergoes during scCO<sub>2</sub> processing and depressurization. The fraction of individual platelets that has been delaminated (as evidenced by SEM - Figure 54) should account for a reasonable increase in available surface area for interaction. The samples prepared with pre - dispersed clay should have richer morphology to account for the improvement observed in the rheological properties. Therefore, in the PS-5%10Ape-sol and PS-5%10Ape-scCO<sub>2</sub> nanocomposites there a larger number of individual platelets present and tactoids contain a smaller amount of platelets compared to the corresponding PS-5%10A-sol and PS-5%10A-scCO<sub>2</sub> samples.

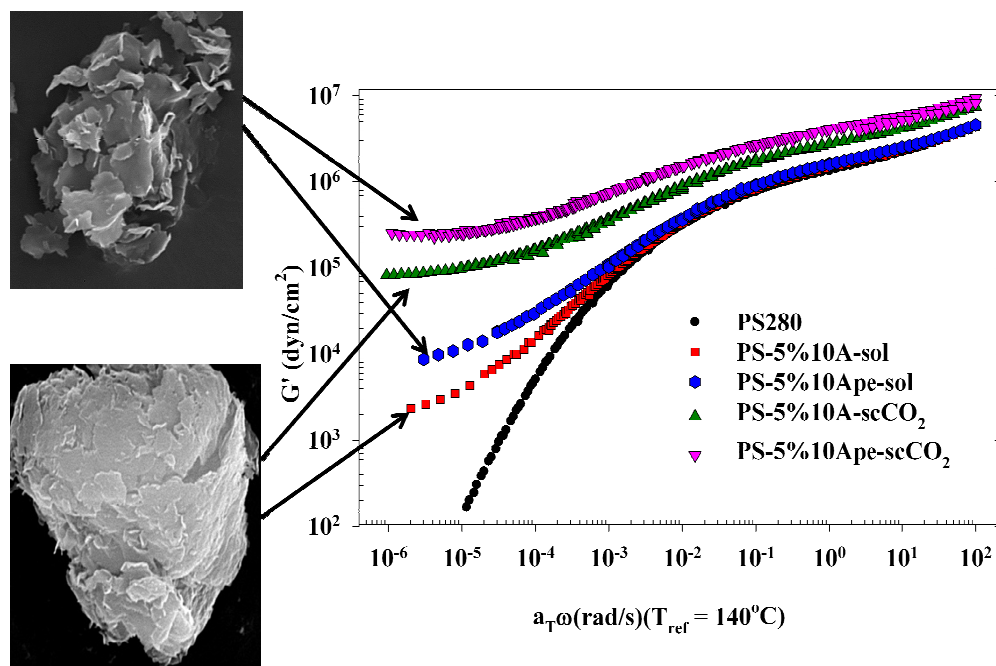


**Figure 54.** Storage moduli of 280k PS and PS/10A nanocomposites prepared with “as received” and pre-dispersed 10A. SEM pictures of “as received” 10A (bottom) and pre-dispersed 10A (top).

### 3.5.2c Effect of nano - clay weight fraction on nanocomposite morphology and properties

The clay weight fraction effect on nanocomposites morphology was also studied by preparing 2, 5 and 10 wt% nano – clay nanocomposites using scCO<sub>2</sub> (10A and 93A) and solution blending methods (only for 10A). As expected, all 10A nanocomposites and 93A nanocomposites (Figure 55) showed the same intercalation peak in WAXD regardless of clay content. The  $d_{001}$  peak for all of the PS/Cloisite 10A samples shifted the same amount from 1.92 nm (Cloisite 10A) to 3.85 nm, which implies that the level of intercalation of 10A in polystyrene was independent of weight fraction. This corresponds to an increase in the equilibrium inter-gallery spacing of 1.93 nm for the Cloisite 10A nanocomposites (Figure 55). The lack of platelet spacing dependence on weight fraction is in good agreement with published data.<sup>35, 97</sup> In contrast, the Cloisite 93A nanocomposites final  $d_{001}$  spacing was only 2.85 nm (Figure 55). The

smaller final spacing in 93A, as previously discussed, was due to poorer interactions between 93As' organic modifier and PS compared to organic modifier in 10A and PS leading to a smaller amount of PS chains to penetrate the inner - gallery spacing of the nano - clay in 93A.

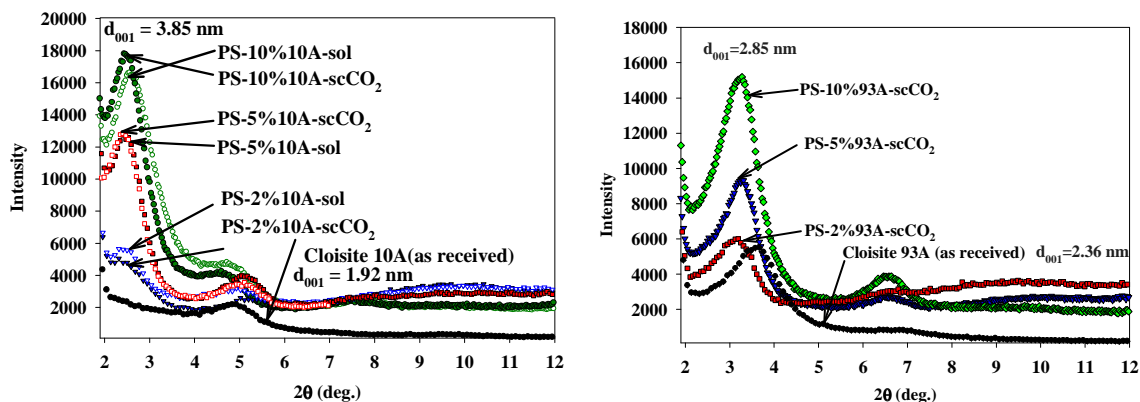


**Figure 55.** X-ray diffractograms of “as received” Cloisite 10A and 93A and PS/10A and PS/93A nanocomposites with varying nano-clay weight fractions.

Even at weight fractions as low as 2 wt% clay, the scCO<sub>2</sub> processed samples, PS-2%10A-scCO<sub>2</sub> (Figure 56) and PS-2%93A-scCO<sub>2</sub> (Figure 57) displayed a low frequency reinforcement in G' which was not observed with the benchmark analog sample (PS-2%10A-sol) (Figure 56) indicating that the scCO<sub>2</sub> processed sample has a higher level of clay dispersion. Though WAXD can only confirm the existence of intercalated clay in the samples, this improvement at such low weight fraction reinforces the belief that there is a fraction of clay platelets present that are well dispersed. As would be expected from the higher level of intercalation and matrix interaction of the PS-2%10A-scCO<sub>2</sub>, the low frequency plateau displays half an order of magnitude increase over the PS-2%93A-scCO<sub>2</sub> composite. The rheology data for all 2% samples overlay for most of the frequency spectrum, implying that though low frequency enhancement may exist, the dynamics of the chains have not been significantly

altered. PS-2%10A-sol showed no change at all over the pure polystyrene even though X-ray diffraction showed that the composite is intercalated. This was also observed by Zhao et al. in a solvent blended nanocomposite with similar clay loadings.<sup>47</sup> In the same paper, it was shown that their sonication technique gave well exfoliated composites, and the results for a 2.5 wt% composite were comparable to our PS-2%10A-scCO<sub>2</sub> composite further substantiating the fact that in the scCO<sub>2</sub> processed sample the level of dispersion is significantly higher than in the solution blended benchmark.

At 5 wt% (PS-5%10A-scCO<sub>2</sub>) G' further increased signifying that a richer morphology is present in the 5 wt% scCO<sub>2</sub> sample where a percolation of clay platelets has occurred. Furthermore, the G' of the 5 wt% scCO<sub>2</sub> sample even becomes larger than the 10 wt% solution blended sample (PS-10%10A-sol) at low frequencies despite having half of the clay content (Figure 56). This further demonstrates that there has to be a higher dispersion level in the scCO<sub>2</sub> processed samples compared to the solution blended samples to obtain such improvements. Also, there is a reasonable 40% increase in both PS-5%10A-scCO<sub>2</sub> and PS-5%93A-scCO<sub>2</sub> over pure polystyrene across the frequency range that continues until  $3 \times 10^{-4}$  rad/s where PS-5%10A-scCO<sub>2</sub> begins to dominate. These reinforce the conclusion that scCO<sub>2</sub> 93A and 10A samples are at least semi-dispersed and that interaction with the PS matrix allows the 10A sample to give superior reinforcement.

The viscoelastic properties of the nanocomposites with 10 wt% clay, PS-10%10A-scCO<sub>2</sub> and PS-10%93A-scCO<sub>2</sub>, both showed significant improvement over the 5 wt% scCO<sub>2</sub> samples and the neat polymer across the entire frequency range demonstrating that the scCO<sub>2</sub> sample must have a high level of clay dispersion in order to achieve this kind of improvements. In the 10 wt% nanocomposites the nano – clay may form a more developed percolated network (not only a



pseudo - network like in the 5 wt% nanocomposites) where there might be clay - clay network not just clay-polymer-clay network where the stress can be more efficiently transferred from clay to clay platelets and/or tactoids. Noteworthy is the difference between the composites prepared with scCO<sub>2</sub> and the solution blended benchmark samples. As discussed earlier, both the scCO<sub>2</sub> processed and the benchmark composites containing 10A showed the same level of intercalation in X-ray diffraction (Figure 23), and all of the 10A composites showed a higher level than the 93A. Though this is true, both of the 10 wt% composites processed in scCO<sub>2</sub> showed an increase of 60% in G' over the benchmark at high frequencies and more than an order of magnitude increase in the low frequency plateau range. The scCO<sub>2</sub> process for dispersing nano - clays has been previously shown to give a high level of delamination in both Cloisite 10A (Chapter 2)<sup>77</sup> and 93A<sup>59</sup> and that some fraction of the clay has been well dispersed and will not register in X-ray diffraction as a shift or a peak. Therefore, the enhancement in viscoelastic response for PS-10%10A-scCO<sub>2</sub> and PS-10%93A-scCO<sub>2</sub> could be attributed to a large fraction of the clay being dispersed during the CO<sub>2</sub> depressurization. The morphology of the non-scCO<sub>2</sub> processed PS-10%10A-sol is assumed to be purely intercalated, and the enhancement of PS-10%10A-sol over the pure PS280 is theorized to result from the good interaction of the clay modifier with polystyrene. This result seems to be in good agreement with recent work by Xu et al.<sup>35</sup> and Han et al.<sup>96</sup> who have shown that solution blending alone in polystyrene composites seems to give only intercalated morphologies, and work by Cho et al. that showed that the 10A modifier should interact well with styrene based polymers.<sup>68</sup>

There is a lack of rheological difference between the 10A and 93A 10wt% scCO<sub>2</sub> processed nanocomposites even though there is a reasonable difference in the clay intercalation between the two according to X-ray and between their 2 and 5 wt% nanocomposites. If both

systems have reached a true percolated network it is possible that we are effectively probing the clay stiffness and the difference in clay-matrix interaction may no longer be resolvable with this measurement method.

Recent works in solution blending show similar results to the benchmark composites at various clay loadings.<sup>96, 98</sup> Sohn and coworkers saw no improvement at low clay loadings but they obtain an order of magnitude increase in an intercalated 10 wt% nanocomposite. The scCO<sub>2</sub> processed 2% composite (PS-5%2A-scCO<sub>2</sub>) displays a viscoelastic improvement comparable to their 10% sample in storage moduli at low frequencies. The clay weight fraction study further substantiates the conclusion that scCO<sub>2</sub> processing of polymer nanocomposites leads to improved clay dispersion.

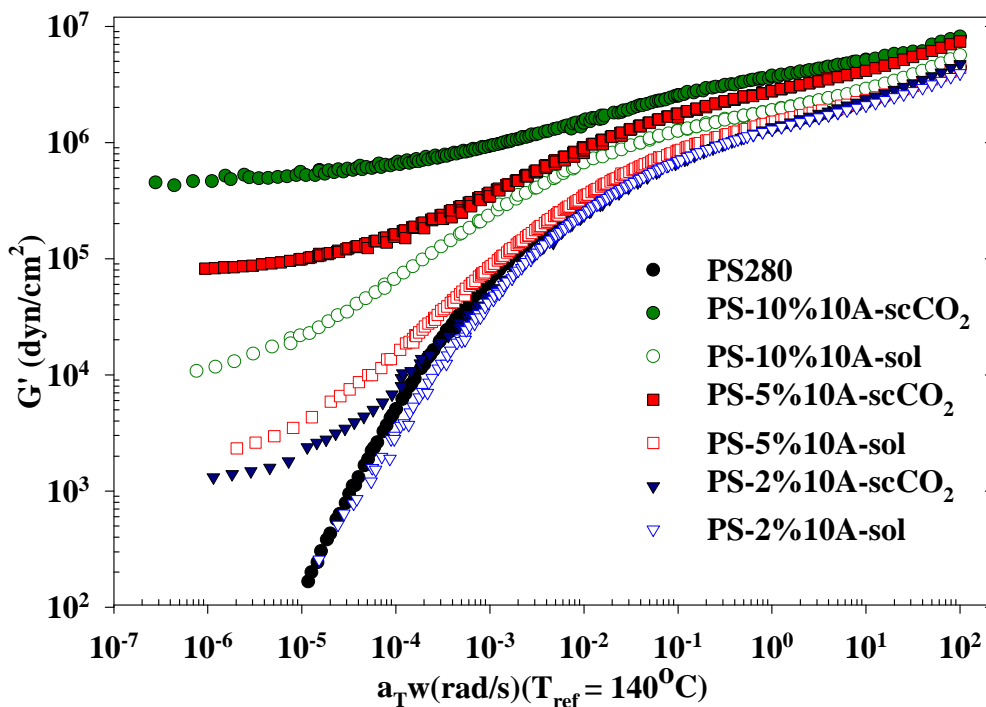


**Figure 56.** Storage modulus of 280k PS, PS/10A scCO<sub>2</sub> and solution blended processed nanocomposites.

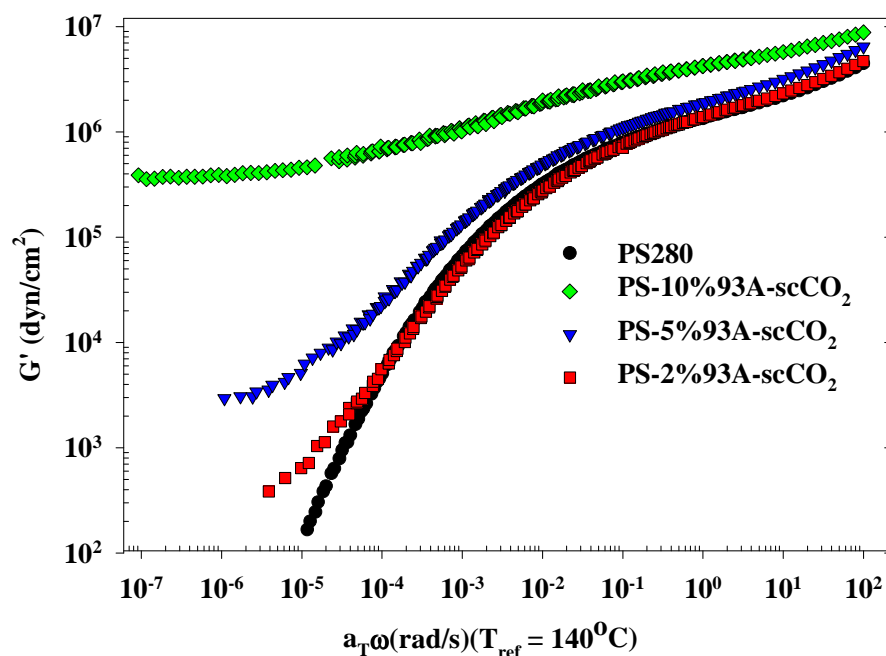


**Figure 57.** Storage modulus of 280k PS and PS/93A scCO<sub>2</sub> processed nanocomposites.

TGA was performed on the 10 wt% scCO<sub>2</sub> and solution blended nanocomposites 10A and scCO<sub>2</sub> 93A nanocomposites to determine the change in the thermal decomposition temperature when the weight percent of clay is doubled compared to the 5 wt% samples (Figure 58). The TGA derivative is useful for determining the temperature at which the maximum rate of decomposition (MRD) occurs (Figure 59). An increase in MRD from 422°C for pure polystyrene to 435°C, 433 °C and 439 °C for PS-10%10A-scCO<sub>2</sub>, PS-10%93A-scCO<sub>2</sub> and PS-10%10A-sol was observed (Table 16). The lower MRD for PS-10%10A-scCO<sub>2</sub> compared to PS-10%10A-sol can be attributed to a higher level of platelet dispersion, and therefore a reduced amount of polymer intercalated between platelets. The PS-10%10A-scCO<sub>2</sub> and PS-10%10A-sol samples displayed a 12 °C and 14 °C respectively improvement in the MRD compared to PS-5%10A-scCO<sub>2</sub> and PS-5%10A-sol. The PS-10%93A-scCO<sub>2</sub> nanocomposites only showed an

improvement of 5 °C over PS-5%93A-scCO<sub>2</sub>. Comparing the 10 wt% results with those from the 5 wt% samples it can be concluded that the higher the amount of polymer confined the higher the higher the decomposition improvement for the same clay. This result is in good agreement with Morgan and co-workers who showed that reducing the amount of polymer intercalated between platelets also reduces the amount of relative decomposition improvement if the clay is kept constant.<sup>82</sup> Moreover, using the TGA it was confirmed that the actual clay loading was in fact 10 wt% and that scCO<sub>2</sub> does not remove any modifier during processing and/or depressurization.

**Table 16.** TGA Summary: Temperature at 10%, 50% Weight Loss, Maximum Rate of Decompositions, and the percent residual mass at 600°C (amount of char left in the nanocomposite).

|                                   | $T_{10}$ (°C) | $T_{50}$ (°C) | MRD (°C) | Change in MRD<br>Compared to PS<br>(°C) | % residual<br>mass @<br>650°C (%) |
|-----------------------------------|---------------|---------------|----------|---|-----------------------------------|
| <b>PS280</b>                      | 395           | 418           | 422      |   | 0.4                               |
| <b>PS-10%10A-scCO<sub>2</sub></b> | 395           | 433           | 435      | 13.0                                    | 9.85                              |
| <b>PS-10%10A-sol</b>              | 394           | 433           | 439      | 17                                      | 9.62                              |
| <b>PS-10%93A-scCO<sub>2</sub></b> | 396           | 435           | 433      | 11                                      | 10.01                             |

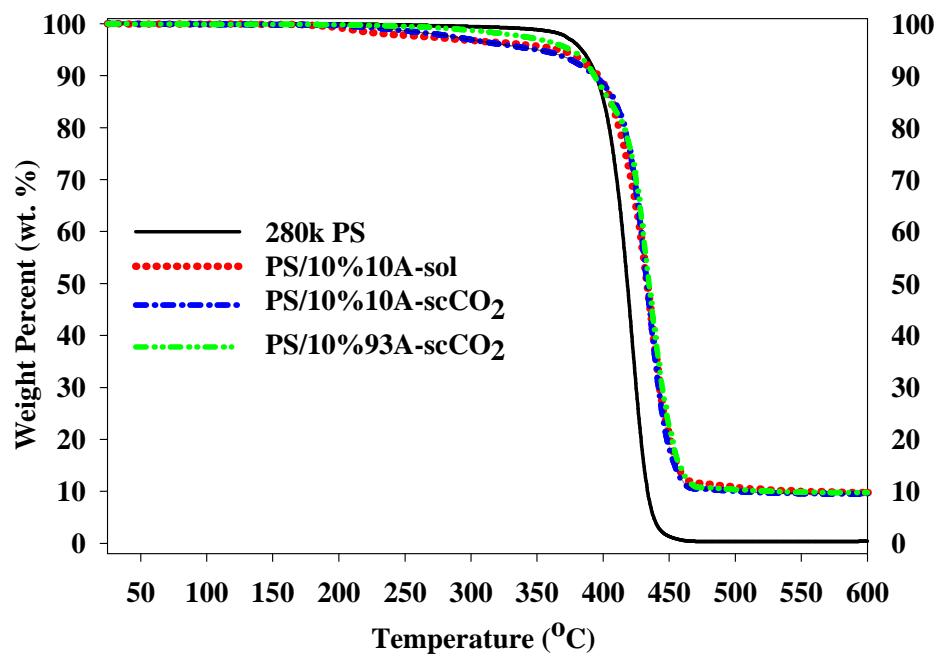


Figure 58. TGA of 10wt% PS/Cloisite 10A and 93A nanocomposites.

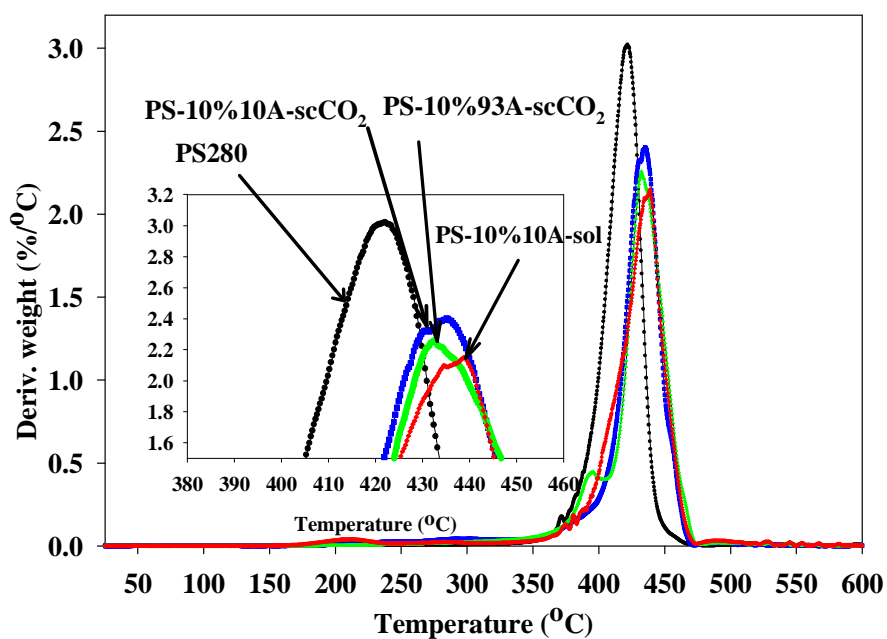


Figure 59. TGA derivative curves for 10wt% PS/Cloisite 10A and 93A nanocomposites detailing the improvement in the maximum rate of decomposition of polymer due to nano-clay addition.

### ***3.5.2d Effect of scCO<sub>2</sub> processing pressure and processing time on the morphology and properties of the resulting nanocomposites***

#### *Effect of processing time*

The effect of scCO<sub>2</sub> processing pressure and processing time was investigated in an attempt to gain a better understanding on the scCO<sub>2</sub> processing method. The aim is to optimize the process in order to maximize nano – clay dispersion and/or nanocomposite properties. The X-ray diffraction again did not show any significant differences between any of the seven samples probed (figure not shown - however Figure 53 shows the final d<sub>001</sub> spacing for the 24 hour and 13.79 MPa nanocomposites which is the same as all the other samples). All samples displayed the same increase in the inner - gallery spacing from 0.92 nm to 2.85 nm. However, there is a 47% improvement in low frequency storage modulus between the sample processed for 0.5 hours (PS-5%10A.5-scCO<sub>2</sub>) to those processed for 4 (PS-5%10A4-scCO<sub>2</sub>) and 12 hours (PS-5%10A12-scCO<sub>2</sub>). Moreover, the sample that was processed for 24 hours (PS-5%10A-scCO<sub>2</sub>) showed a 130% improvement in low frequency storage modulus compared to the sample processed for 0.5 hours (Figure 60). Using WAXD it was not possible to make a conclusion regarding the “true” dispersion state on the nanocomposites since it did not show any differences between samples when the same nano - clay was used. In the previous section the results from the rheological properties were used to investigate the nanocomposites morphology and/or the polymer-clay interactions. The higher the storage modulus was, the higher the level of nano - clay dispersion in that particulate nanocomposite if the same nano - clay was used. Therefore, the sample that was processed for 0.5 hours it is expected to have a lower level of dispersion compared to the other nanocomposites as evident by the lower level of improvement in the storage modulus compared to PS. However, the dispersion in the 4, 12 and 24 hours processed

nanocomposites is expected to be similar since all showed comparable rheological properties. The results from the processing time study illustrated that the processing time does not play a significant role in improving the morphology of the nanocomposites and viscoelastic properties.

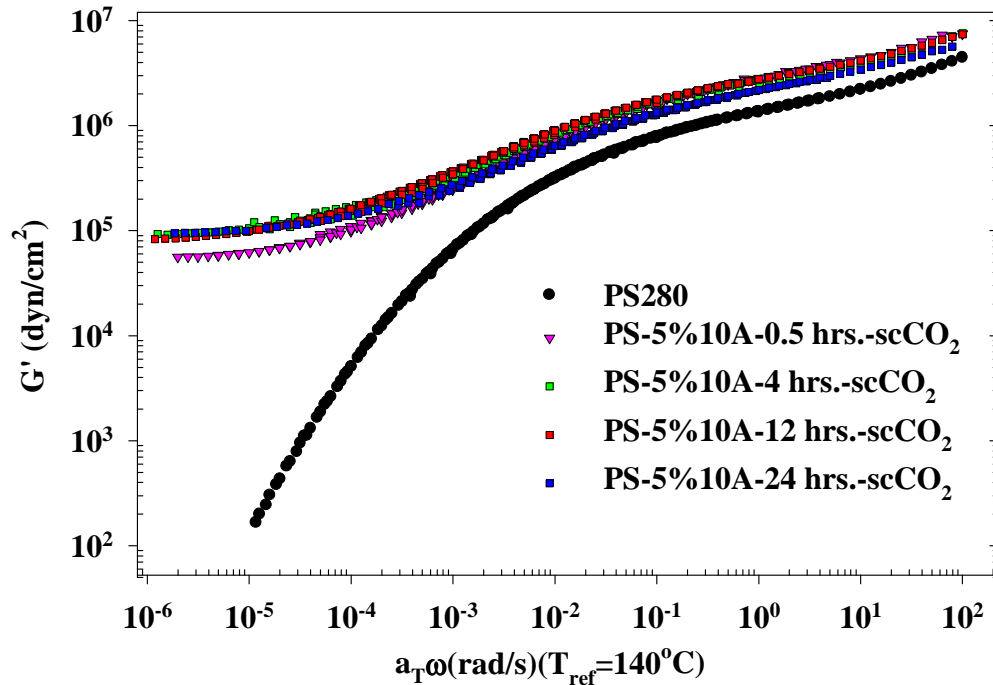


**Figure 60.** Storage modulus of 280k PS and PS/10A scCO<sub>2</sub> nanocomposites processed at various 0.5, 4, 12 and 24 hours.

#### *Effect of processing temperature and pressure*

The effect that the scCO<sub>2</sub> processing pressure has on the resulting nanocomposites morphology has been investigated by processing three nanocomposites at various pressures (10.34MPa (PS-5%10Ay-scCO<sub>2</sub>), 13.79MPa (PS-5%10A-scCO<sub>2</sub>) and 27.58MPa (PS-5%10Az-scCO<sub>2</sub>)) at 80°C for 24 hours. The density of CO<sub>2</sub> as a function of temperature at various pressures (diagram in Figure 61) shows that the CO<sub>2</sub> density can be increased by increasing the processing pressure and lowering the processing temperature. The WAXD did not show any differences between the three scCO<sub>2</sub> processed samples with all displaying a d<sub>001</sub> peak at 3.85

nm. However, rheological measurements did show some differences between the three samples. The nanocomposite that was processed at 10.34 MPa showed a 2.5 order of magnitude improvement in the low frequency storage modulus compared to pure PS (Figure 62) indicating that even when the sample is processed at the lowest pressure significant improvement in dispersion can be achieved. Moreover, when the processing pressure was instead increased to 13.79 MPa the nanocomposites showed a further improvement in the storage modulus at all frequencies indicating that the polymer dynamics have been altered more, possible due to improved nano - clay dispersion in the PS-5%10A-scCO<sub>2</sub> nanocomposite compared to the PS-5%10Ay-scCO<sub>2</sub> nanocomposite. If the processing pressure was doubled to 27.58 MPa, the nanocomposite (PS-5%10Az-scCO<sub>2</sub>) displayed a further improvement in rheological properties compared to the nanocomposites processed at 13.79 MPa (PS-5%10A-scCO<sub>2</sub>). This study revealed that the processing pressure does play a role in the resulting nanocomposite morphology as evident by the differences in the rheological measurements between the three nanocomposites studied. In the 5 wt% the 10A scCO<sub>2</sub> the “pseudo” percolation threshold was attained and that the polymer - clay interaction play a key role in obtaining improved rheological measurements. Horsch et al. showed that as the processing pressure is increased the nano - clay (no polymer matrix present) displayed improved dispersion.<sup>99</sup> As the processing pressure was increased from 10.34 to 27.58 MPa the tactoid size decreased and the number of individual platelets that are present in the nanocomposite increased, creating a larger surface area that can be available for polymer - clay interactions. The increase in the surface are that can be available for polymer - clay interactions led to improvements in the nanocomposite viscoelastic properties.



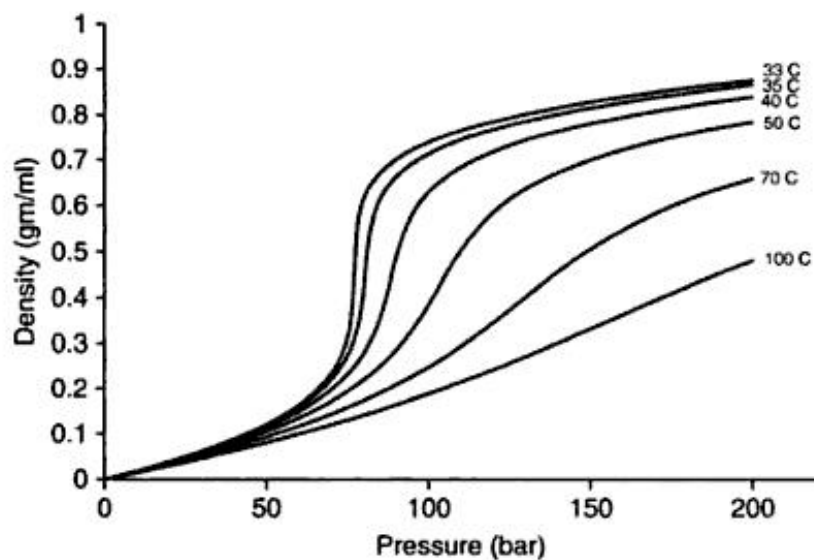


Figure 61. Carbon dioxide density as a function of temperature at various pressures.

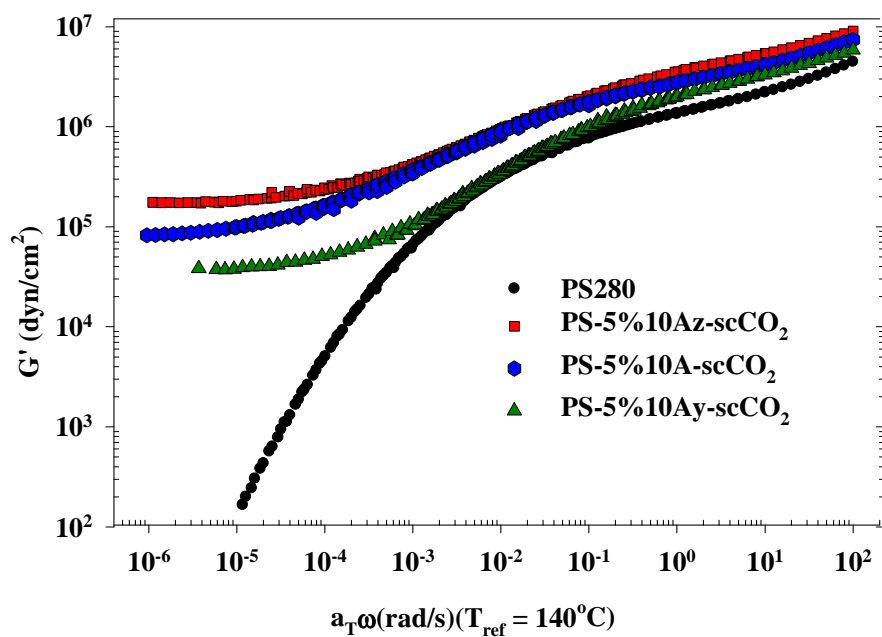


Figure 62. Storage modulus of 280k PS and PS/10A scCO<sub>2</sub> nanocomposites processed for 24 hours at 80°C and 10.34, 13.79 and 27.58 MPa.

Moreover, the processing temperature is supposed to have a bigger effect on CO<sub>2</sub> density change than the pressure since the CO<sub>2</sub> density increases more as the process temperature decreases than when the pressure increases (Figure 61). However, as the temperature decreases so does the polymer solubility in CO<sub>2</sub> and/or solvent. The complete effect that temperature plays on the scCO<sub>2</sub> processing of the PS/clay nanocomposites cannot be entirely predicted. However, the effect of temperature was not studied because at a temperature around 100°C styrene inhibitor becomes less effective and the possibility of polymerization is increased. Furthermore, when a low temperature is used the viscosity of the styrene/polystyrene/clay mixture would be higher than at 80°C (the temperature that was used throughout the study) and in case of styrene polymerization the risk of the stirrer mechanism being damaged due to higher viscosity is increased (the motor that controls the stirring). Therefore, the effect of temperature was not investigated in this study. A different study where the system will be in the melt state should be performed where the effect of temperature on the nanocomposite morphology can be studied more effectively (Chapter 5).

### **3.6 Conclusions**

A series of dispersed polystyrene/clay nanocomposites were successfully created using a novel scCO<sub>2</sub> process. The effects of several processing parameters were investigated (depressurization, scCO<sub>2</sub> contact, filler concentration, nano - clay dispersion, processing pressure and time) on the resulting nanocomposites morphology and properties was investigated by several characterization methods in an attempt to gain a better understanding on the scCO<sub>2</sub> processing technique.

It was shown that scCO<sub>2</sub> processing of polymer - clay nanocomposites in the presence of a solvent significantly improved the dispersion state of the clay in the polymer matrix to a

magnitude that was relatively modifier independent. When this was coupled with favorable clay-polymer interactions, significant property enhancements occurred. As a result of scCO<sub>2</sub> processing, nearly a 4-fold reduction in average tactoid size and a significant increase in dispersed single platelets leading to the formation of clay-clay networks and an increased surface area available for polymer-clay and polymer-clay modifier interactions was obtained. Despite Cloisite 93A's lower interaction strength with the polymer matrix, the scCO<sub>2</sub> process produced similar magnitude reduction in average tactoid size compared to favorably interacting Cloisite 15A and 10A. It was also shown that significant dispersion, without strong polymer-clay interactions (as in the case of PS/93A nanocomposites), was not sufficient for significant property improvement. Conversely, strong interactions without significant dispersion also could not provide high levels of enhancements. To maximize the viscoelastic and transport properties, a polymer-clay system with not only good clay dispersion but also good interactions and a processing technique, that produces high levels of dispersion (*e.g.* scCO<sub>2</sub> processing) needs to be used. Improvements as high as 3 orders of magnitude in the low frequency storage modulus were observed in nanocomposites processed with scCO<sub>2</sub> that had favorable polymer-clay interactions (5wt% 10A and 15A) and only an order of magnitude when poor interaction were present (5wt% 93A). Moreover, a significant reduction in oxygen permeability was observed when good polymer-clay interaction were present 45% (5wt% 10A) and 60% (5wt% 15A) and when poor interaction were present the reduction was only 6% (5wt% 93A). The scCO<sub>2</sub> processed 5 wt% nanocomposites showed a reduction in oxygen properties of 20 to 50% compared to solution blended benchmark due to enhanced dispersion present in the scCO<sub>2</sub> processed nanocomposites.

Replacing “as received” clay with pre – dispersed clay led to a different, more richer morphology. Although, there were still platelets in tactoids form the amount of individual platelets has increased leading to an increase in the surface area for polymer - clay interaction. This in turn led to a further improvement in rheological properties and once again emphasized the positive effect clay dispersion has on the material properties of polystyrene.

The presence of scCO<sub>2</sub> alone during processing improved the polymer transport to the clay surface as evident in the enhancement in rheological measurements. However, when the polystyrene/10A system was rapidly depressurized, it led to an improved clay dispersion and further reinforcement of the matrix compared to slow depressurization, implying that clay platelets are effectively being dispersed by the dramatic CO<sub>2</sub> expansion. The scCO<sub>2</sub> processing time did play a small role in enhancing nanocomposite morphology and rheological properties. However, there was only a small improvement from processing for 0.5 hours to 24 hours. As the processing pressure was increased from 10.34 to 27.58 MPa, nano - clay dispersion was also increased. The increased surface area available for polymer - clay interactions led to improvements in the nanocomposite viscoelastic properties.

## CHAPTER 4

### **Role of Polymer-Clay Interactions and Nano-clay Dispersion on the Viscoelastic Response of Supercritical CO<sub>2</sub> Dispersed Polyvinylmethylether (PVME)-Clay Nanocomposites**

Over the past decade, considerable effort has been put forth to understand the structure-property relationships of polymer/clay nanocomposites. In particular, the linear viscoelastic response of polymer-clay nanocomposites has been extensively studied in order to understand the mechanical and rheological properties of these systems and elucidate how these properties relate to the type of microstructure/mesostructure formed.<sup>63, 79, 100-102</sup> In general, these investigations revealed that the principle of time-temperature superposition is obeyed with the temperature dependence of the frequency shift factor ( $a_T$ ) being independent of silicate loading and dispersion. Moreover, the mesoscale dispersion strongly impacts the low frequency viscoelastic behavior of the dynamic moduli and the low shear rate viscosity. Good dispersion typically results in a low frequency plateau in the storage modulus ( $G'$ ) and diverging complex viscosity at low shear rates. The pseudo solid-like behavior has been attributed to a “so-called” percolated structure.<sup>31</sup> However, as Krishnamoorti and Giannelis demonstrated for example, a sufficient active interactions between the polymer (soft phase) and the clay (hard phase) is a necessary component for pseudo solid-like rheological behavior to be prevalent.<sup>102</sup> In some of their nanocomposites, the matrix polymers utilized were only lightly entangled yet a low frequency plateau was observed in  $G'$  suggesting that entanglement is not a necessity for pseudo solid-like behavior to exist. We have recently reported the rheological response of dispersed PDMS/clay and PS/clay nanocomposites prepared by a novel supercritical CO<sub>2</sub> (scCO<sub>2</sub>) processing method. In these nanocomposites the pseudo solid-like low frequency response appeared dependent on the “effective” molecular weight of the polymer<sup>59, 77</sup>. Our results suggest

that low molecular weight polymer chains may preferentially transport to the nano-clay surface because of their increased solubility in  $scCO_2$ . As a result, the polymer chains interacting with the nano-clay surface are too short to form a network with the bulk polymer or other clay structures and liquid-like behavior is observed even when the nano-clay is highly dispersed. We have also seen pseudo solid-like behavior in PS based nanocomposites that have good interactions between the PS matrix and the nano-clay surface.<sup>77, 103</sup> In the case of the PS based nanocomposites the molecular weight of the polymer was 5000 g/mol, well below the entanglement molecular weight of PS, and as such the chains were not capable of forming a network between chains on the clay surface and the host matrix. Therefore, it appears that in the absence of good interactions, high molecular weight polymers may still be able to help sustain the mesoscale structure. In cases where good polymer-clay interactions exist, entanglement between chains on the clay surface and in the bulk may not be a necessary component to sustain the structure.

In this chapter, the role of polymer-clay interactions and filler dispersion on the linear viscoelastic response of  $scCO_2$  processed polymer clay nanocomposites is investigated. Polyvinylmethylether (PVME) was chosen as the host matrix for natural montmorillonite and three organophilic nano-clays. PVME appears to be highly swellable in  $scCO_2$  even at a molecular weight of 90,000 g/mol. In contrast to other  $scCO_2$ -swellable polymers, such as PDMS and PS, PVME is hydrophilic, and may enable processing of even natural clay. Natural montmorillonite was chosen as a reference for the strength of the polymer-filler interactions because it has weak interactions with PVME. Poly(ethylene oxide) (PEO) was also used as the host matrix for natural montmorillonite to compare the extent of PEO-filler interactions with that of PVME-filler interactions. In contrast, the organophilic clays used in this study may have

varying degrees of interactions with the host matrix, in addition to having different clay dispersions upon  $scCO_2$  processing. Specifically, Cloisite 30B (methyl tallow bis-2-hydroxyethyl ammonium salt) may form a hydrogen bond between the host matrix and the surfactant, and Nanomer I.30P (trimethyl hydrogenated tallow ammonium salt) has a moderate loading of alkyl groups, thereby altering the extent of the polymer-clay interactions in each system. The  $scCO_2$  processed nanocomposites were contrasted with a highly dispersed (disordered) Cloisite  $Na^+$ /PVME nanocomposite produced from a solution cast/freeze drying method, with water as a solvent. As a result of the selected processing conditions, the nanocomposites produced via the  $scCO_2$  method had intercalated or disordered intercalated morphologies.

The rheological response of the partially exfoliated Cloisite  $Na^+$ /PVME nanocomposite is compared with the response of the intercalated Cloisite  $Na^+$ /PVME nanocomposite to understand the role of clay structure on the linear viscoelasticity of “weakly-interacting” polymer/clay nanocomposites. The rheological response of Cloisite  $Na^+$ /PEO was compared to that of Cloisite  $Na^+$ /PVME to understand the role of polymer – clay interactions in the two nanocomposites and demonstrate that in the case of PVME/ $Na^+$  system there are weak interactions present. And, the viscoelastic response of intercalated organophilic clay-PVME nanocomposites is compared to the intercalated “weakly-interacting system” to determine the impact of specific polymer-clay interactions. The molecular weight of the polydispersed PVME used in this study is 90,000 g/mol, which has ~ 13 entanglements per chain and should be of sufficient chain length to create a network between polymer chains near the clay surface, the bulk polymer, and the mesoscale structure (PVME has an entanglement molecular weight of 6450 g/mol<sup>104</sup>). In addition, all the nanocomposites had a nano-clay loading of 15 wt% to ensure that a percolated structure could form even if the nanocomposites were intercalated. The existence of a "so-called" percolated

structure allows probing the role of polymer-clay interactions on the ability to sustain this nano-clay network under deformation.

#### **4.1 Materials**

In this study Cloisite 30B and Na<sup>+</sup> and Nanocor I.30P nano-clays were used. The composition and physical properties of the clays are summarized in Table 17. The PVME used in this research was purchased from Scientific Polymer Product Inc. The polydispersed PVME used had a weight average molecular weight of 90,000 g/mol (density of 1.05 g/ml at 20°C) and was shipped in water. Before nanocomposite preparation, the PVME was cooled to -25°C and placed in a freeze dryer for 4 days to remove the water. The polymer was then dissolved in toluene and filtered to remove any impurities. The toluene was removed in a vacuum oven operated at 80°C for 2 weeks. The PEO used in this study had a molecular weight of 100,000 g/mol and was purchased from Scientific Polymer Product Inc.



**Table 17.** Nano-clay surfactant composition, basal spacing, and platelet density, as reported by supplier. T is Tallow (~65% C18; ~30% C16; ~5% C14) and HT-Hydrogenated Tallow (~65wt% C18; ~30wt% C16; ~5wt% C14).

| Nanoclay Name            | Organic Modifier   | $d_{001}$ Spacing (nm) | Density (g/ml) |
|--------------------------|--|------------------------|----------------|
| Cloisite Na <sup>+</sup> | None   | 1.2                    | 2.86           |
| Cloisite 30B             | $\begin{array}{c} \text{CH}_2\text{CH}_2\text{OH} \\   \\ \text{T} - \text{N}^+ - \text{CH}_3 \\   \\ \text{CH}_2\text{CH}_2\text{OH} \end{array}$ | 1.85                   | 1.98           |
| I.30P                    | $\begin{array}{c} \text{CH}_3 \\   \\ \text{HT} - \text{N}^+ - \text{CH}_3 \\   \\ \text{CH}_3 \end{array}$  | 2.25                   | 1.71           |

## 4.2 Methods of characterization

### 4.2.1 Wide-angle X-ray diffraction

WAXD was used to determine the inter-gallery spacing of the neat clay and the clay in the polymer-clay nanocomposites. The  $d_{001}$  spacing was determined using the JADE software accompanying the diffractometer. The inter-gallery spacing was calculated by subtracting 1 nm (platelet thickness) from the  $d_{001}$  spacing. All data were collected using a Rigaku Rotaflex Powder Diffractometer with a CuK $\alpha$  X-ray source ( $\lambda=1.54 \text{ \AA}$ ) and an accelerating voltage of 40 kV at a current of 150 mA. To perform scans, samples were placed in a custom made zero background quartz sample-holder that is 0.9 mm in depth. Diffraction data was collected from 1 to 10 degrees 2 theta at a step size of 0.03 degrees and at a rate of 0.3 degrees/minute. XRD was collected before and after performing melt rheological measurements to assure that that no changes are taking place during rheological measurements.

### 4.2.2 Rheology

Melt rheological measurements were performed under oscillatory shear using an RSA II rheometer (shear sandwich geometry  $15.98 \times 12.7 \times 0.55 \text{ mm}^3$ ). Measurements were carried out at temperatures of 30, 55, and  $80^\circ\text{C}$  for PVME and  $80^\circ\text{C}$  and  $100^\circ\text{C}$  for PEO; and the data were time-temperature superimposed by using a frequency shift factor ( $a_T$ ). The experimental shear frequency range was  $0.01 \leq \omega \leq 100 \text{ rad s}^{-1}$  for all samples. The samples were loaded, compressed and allowed to equilibrate for 1 hr at the desired temperature. Linear viscoelastic measurements were made at low strains ( $\gamma_0 < 0.07$ ) and strain sweeps were performed to ensure the dynamic moduli were independent of the strains utilized. Each set of rheological measurements took about 10 hours and after the first set was completed a second set of measurements were carried out the following day to check results reproducibility.

### 4.2.3 Thermogravimetric analysis

TGA of the nanocomposites was performed on a Perkin-Elmer Pyris 1 instrument. Measurements were done in a nitrogen atmosphere and at a heating rate of  $10^\circ\text{C min}^{-1}$  over a temperature range of  $50^\circ\text{C}$  to  $550^\circ\text{C}$ . The sample was loaded at  $20^\circ\text{C}$  and raised to  $50^\circ\text{C}$  over a period of 10 minutes. The sample was allowed to equilibrate for an additional 10 minutes at  $50^\circ\text{C}$  prior to starting the temperature ramp test.

### 4.3 Nanocomposite formation

The scCO<sub>2</sub> processing method exposes the polymer nano-clay mixtures to CO<sub>2</sub> in a high pressure vessel; the system is then raised above the critical point for CO<sub>2</sub> and the material is allowed to soak for an appropriate time; the system is then rapidly depressurized to atmospheric pressure. A preliminary hypothesis for the mechanism is: during the soak step, under the selected processing conditions, the mixture of the CO<sub>2</sub> and polymer diffuses between the clay layers. The

high diffusivity and low viscosity of the CO<sub>2</sub>-philic polymer in the mixture enable clay layer penetration. During depressurization, expansion of the scCO<sub>2</sub> between the layers pushes them apart resulting in delaminated or intercalated nanocomposites. When the CO<sub>2</sub> is completely removed the organic material remains between the layers, coating the surfaces of the layers, exposing the host matrix to the large available surface area of the nano-clays.<sup>59, 77, 105</sup>

#### **4.3.1 Nanocomposite formation using the scCO<sub>2</sub> processing technique**

Three PVME/clay nanocomposites were formed via scCO<sub>2</sub> processing: 15 wt% Cloisite Na<sup>+</sup> (15-NA), 15 wt% Cloisite 30B (15-30B), and 15 wt% I.30P (15-I.30P). Also, a 15 wt% Cloisite Na<sup>+</sup>/PEO nanocomposite was processed via scCO<sub>2</sub> processing. The nanocomposites were formed by mechanically mixing the nano-clay with PVME or PEO and then processing the mixture in scCO<sub>2</sub>, under quiescent conditions, for 24 hrs at a temperature of 75°C and a pressure of 13.78 MPa. The system was then rapidly depressurized to atmospheric pressure. The high loadings of nano-clay were to insure a percolated structure was possible even if the nanocomposite was intercalated rather than exfoliated.

#### **4.3.2 Nanocomposite Formation using the solution cast freeze drying method**

A natural montmorillonite/PVME nanocomposite (15NA-S) was formed by mixing 1 g of Cloisite Na<sup>+</sup> with 500 ml of distilled water in a sealed container. The mixture of clay and *water* were vigorously mixed for 96 hrs at which time 5.7 g of PVME was added. The mixture was stirred for an additional 48 hrs, rapidly frozen with liquid nitrogen and kept in a freezer at -30°C for 12 hrs. The frozen mixture was placed in a freeze dryer for 14 days to remove the water. Immobilizing the exfoliated nano-clay platelets in a polymer matrix via freezing the mixture prevented the nano-clay platelets from re-organizing into tactoids during the removal of the solvent.

#### 4.4. Nanocomposite characterization

##### 4.4.1 Determination of clay mass fraction in organophilic nano-clays

The organophilic nano-clays consist of platelets and organically modified ammonium salts. In determining the percolation threshold for the nano-clay it is necessary to know the mass fraction of clay because only the clay plays a role in the creating the percolated network. In order to determine the mass fraction for a particular nano-clay, TGA analysis was performed. Analysis was performed on all the organophilic nano-clays and sodium montmorillonite. The natural clay was tested to ensure that the clay itself did not decompose and skew the results of the TGA analysis. Further, the testing was performed in the absence of polymer to guarantee that the weight loss was only due to the ammonium salt modifier on the clay surface. Cloisite Na<sup>+</sup>, 30B, and Nanocor I.30P retained 94%, 76% and 68% of their total mass respectively (Figure 63). The actual loading of clay in 15-30B, and 15-I.30P samples is 11.4 wt%, 10.35 wt% respectively, and the loading for samples 15-NA and 15NA-S is 14.1 wt%. The 6% reduction in weight of the Cloisite Na<sup>+</sup> was attributed to evaporation of water and the weight losses in the organophilic clays was attributed entirely to loss of organic modifier. The actual weight fraction of clay ranged from 10.35 – 14.1 wt%, which is still well above the theoretical reported value of 4 – 7 wt% (1.4 – 2.7 vol% - depending on the clay used and its density) needed for percolation to occur.<sup>31</sup> Assuming that the inorganic clay layers have the density of the unmodified nano-clay matter (2.86 g/cm<sup>3</sup> for Cloisite series and 2.6 g/cm<sup>3</sup> for) both Cloisite 30B and Nanocor I.30P nanocomposites contain 4vol% of inorganic matter. Cloisite Na<sup>+</sup> nanocomposites contain 5 vol% of inorganic matter. The percolation threshold depends on the morphology of the clay (aggregates, self-assembly, interlaced, exfoliated, or any combination of these) and it can occur above or below the theoretical value. However, in this study the samples are well above the

theoretical threshold and it is reasonable to assume that the nano-clays have formed a “so-called” percolated network.

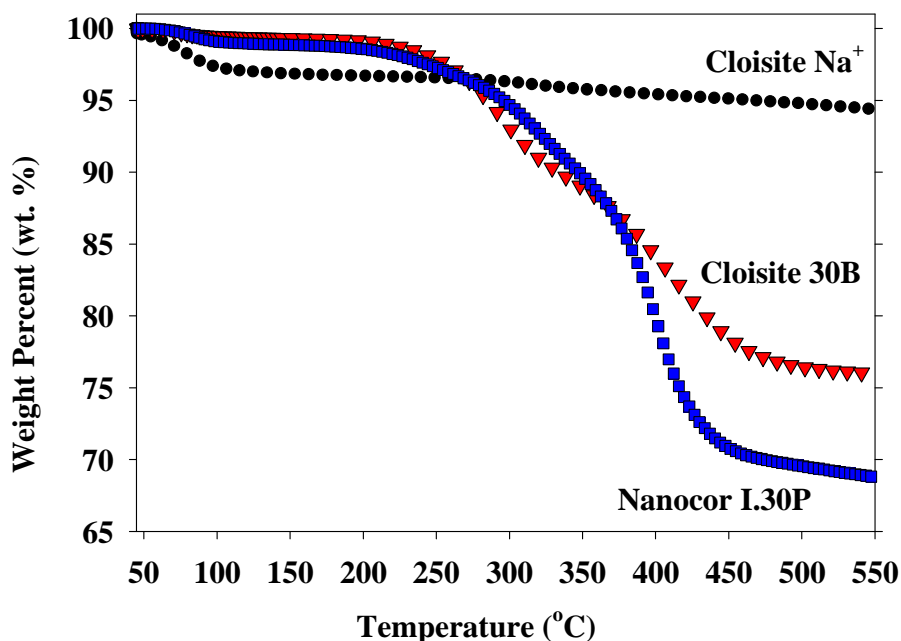


**Figure 63.** TGA analysis of pure nano-clays, Cloisite Na<sup>+</sup>, Cloisite 30B and Nanocor I.30P, The 6% reduction in weight of Cloisite Na<sup>+</sup> is attributed to the evaporation of water.

#### 4.4.2 Role of substantial nano-clay dispersion with ‘weak’ polymer-clay interactions

In this section, the role of *substantial* nano-clay dispersion on the linear viscoelastic response in systems where only “weak polymer-clay interactions” are present was investigated. In order to achieve this goal we have prepared two PVME/Cloisite Na<sup>+</sup> nanocomposites. In one of the samples Cloisite Na<sup>+</sup> was *intercalated* with PVME via *scCO<sub>2</sub> processing* (sample 15-NA) and the other was highly dispersed in PVME via a solution cast freeze drying method using water as a solvent (sample 15NA-S). The nano-clay, Cloisite Na<sup>+</sup>, was chosen for two reasons:

(1) it swells and disperses in water (the use of a high concentration water-PVME-clay solution, and the subsequent freeze drying is expected to largely prevent clay-reaggregation), and (2) there are no oligomeric modifiers to form solvent/solute interactions, hydrogen bonds, or any other specific interactions with the host PVME. Therefore, these two samples are used to clarify the role of dispersion on the linear viscoelasticity of “*weakly interacting*” polymer clay systems as well as providing a reference point for the polymer-filler interactions. Also, we have prepared an *intercalated* Cloisite Na<sup>+</sup>/PEO nanocomposite using scCO<sub>2</sub> technique to attempt to compare the extent of polymer/clay interactions in the scCO<sub>2</sub> processed Cloisite Na<sup>+</sup>/PVME.

**PVME versus PEO:**

WAXD was used to determine the nano-clay morphology in the host PVME and PEO polymer (Figure 20 and Figure 65). In contrast to the organophilic clays (to be discussed later in section 3.1) the Cloisite Na<sup>+</sup>/PVME sample (15-NA) displayed a low intensity, poorly-defined  $d_{001}$  diffraction peak and an absence of higher order peaks. Tactoid size could not be determined for this sample using the Scherrer equation because the diffraction peak did not resemble a Gaussian distribution and the intensity was too low. The diffraction patterned for this nanocomposite was collected again with at a slower rate 0.1 degrees/ min in an attempt to obtain a better peak, but no significant changes in the diffraction pattern were observed. One possible explanation for the low intensity peak is that the inter-gallery spacing of the Cloisite Na<sup>+</sup> in sample 15-NA achieved a similar equilibrium spacing as the organo-philic nano-clays resulting in weak parallel registry of the clay platelets. If the platelets are not parallel and one side/end is more open than the opposite, the inter-gallery spacing ( $d_{001}$ ) couldn't be determined since the spacing varies from one end to the other and WAXD is not sensitive to this morphology. This expansion correlates to more than an order of magnitude increase in the inter-gallery spacing of

Cloisite Na<sup>+</sup> (~ 0.2 nm to ~ 2.6 nm). Since the clay platelets are held together by van der Waals forces, Lennard - Jones potential is often used to model such forces and the attractive force scales inversely with the distance between attractive particles to the 6<sup>th</sup> power.<sup>25</sup> Therefore, the attractive forces decrease exponentially as the platelet distance increases. Further, in the case of Cloisite Na<sup>+</sup>, there are no oligomeric modifiers on the surface that can assist in stabilizing the parallel registry of the platelets at large distances.

A distinctive difference between the scCO<sub>2</sub> processed Na<sup>+</sup>/PEO nanocomposite and the scCO<sub>2</sub> processed Na<sup>+</sup>/PVME nanocomposite is the smaller final inter-gallery spacing of 1.9 nm for the PEO sample compared to 2.6 nm for the PVME sample (15-NA). Although, both scCO<sub>2</sub> nanocomposites are intercalated, the smaller final spacing may indicate that a smaller amount of polymer may have penetrated the inter-gallery spacing of the Cloisite Na<sup>+</sup>/PEO nanocomposite. There might be some polymer that has been intercalated in interstitial spacing of the clay layers; however this could be the possibility in all the nanocomposites and it's believed that it does not play a big role in the final results.

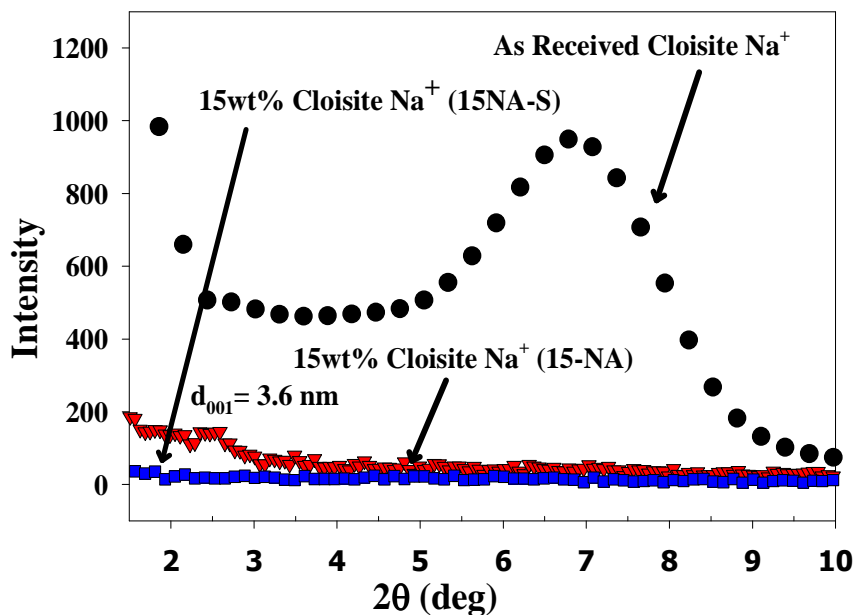


**Figure 64.** WAXD of PVME/Na<sup>+</sup> samples 15-NA, 15NA-S, and as received Cloisite Na<sup>+</sup>.

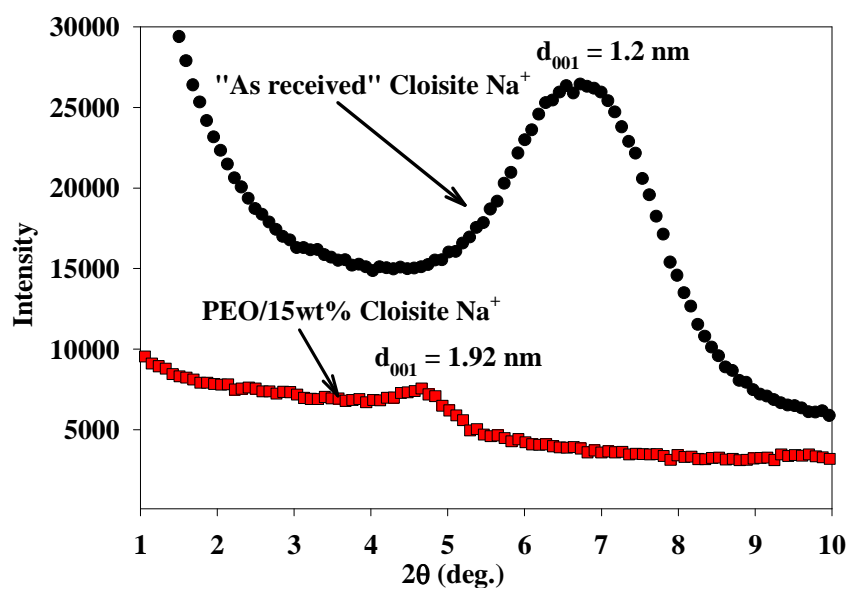


**Figure 65.** WAXD of sample Cloisite Na<sup>+</sup>/PEO reveals the sample is intercalated as evident by the significant shifting of the  $d_{001}$  diffraction peak and the presence of higher order peaks ( $d_{002}$ ).



Despite showing a much smaller final inter-gallery spacing compared to 15wt% Cloisite Na<sup>+</sup>/PVME nanocomposite, the 15wt% Cloisite Na<sup>+</sup>/PEO nanocomposite shows an approximately 2500% improvement in G' at low frequencies over pure PEO along with a low frequency plateau (Figure 67). In contrast, the Cloisite Na<sup>+</sup>/PVME only shows a 100% improvement in G' at low frequencies and does not display a low frequency plateau in the frequency range tested. Since the extent of dispersion is higher in the Cloisite Na<sup>+</sup>/PVME nanocomposite (based on WAXD), the lack of a substantial improvement in the low-frequency moduli (compared to PEO system), suggests that the extent of interactions between Cloisite Na<sup>+</sup> and PVME is 'weak', at least relative to that of PEO. Furthermore, the intercalated Cloisite Na<sup>+</sup>/PEO nanocomposite shows 'comparable' improvements in G' at low frequencies compared with the "highly dispersed" 15-NA-S sample, further supporting the claim that the level of interactions between PEO and Cloisite Na<sup>+</sup> are stronger than in the case of PVME and Na<sup>+</sup>. Pandey and Farmer showed that in the presence of repulsive polymer matrix clay layers exfoliate and in the presence of attractive polymer matrix, clay platelets intercalate <sup>78</sup>. Their findings further support our WAXD and rheological observations. Strawhecker and Manias indicated that there are strong specific interactions between the ether oxygens and the sodium interlayer cations between PEO and Cloisite Na<sup>+</sup>.<sup>106</sup> PVME is a water-soluble polymer, with a sub-ambient glass transitions temperatures and very similar solubility parameters like PEO with one ether linkage per repeating unit. While PVME is unable to crystallize as PEO can, these polymers are otherwise quite similar. Therefore, it is expected that PVME will have some interactions with the sodium ions present in-between the layers of Cloisite Na<sup>+</sup>. However, in Na<sup>+</sup>/PVME sample these interactions are very weak compared to Na<sup>+</sup>/PEO sample as evident from the significant differences in the rheological behavior between the two nanocomposites (Figure 66 and Figure

67), despite a larger inter-gallery spacing in the PVME nanocomposite compared to the PEO sample (Figure 64 and Figure 65). Therefore, we will refer to the Cloisite Na<sup>+</sup>/PVME samples as “weakly interacting” as a basis of comparing them to other organically modified clay/PVME samples which can exhibit other more favorable interactions.

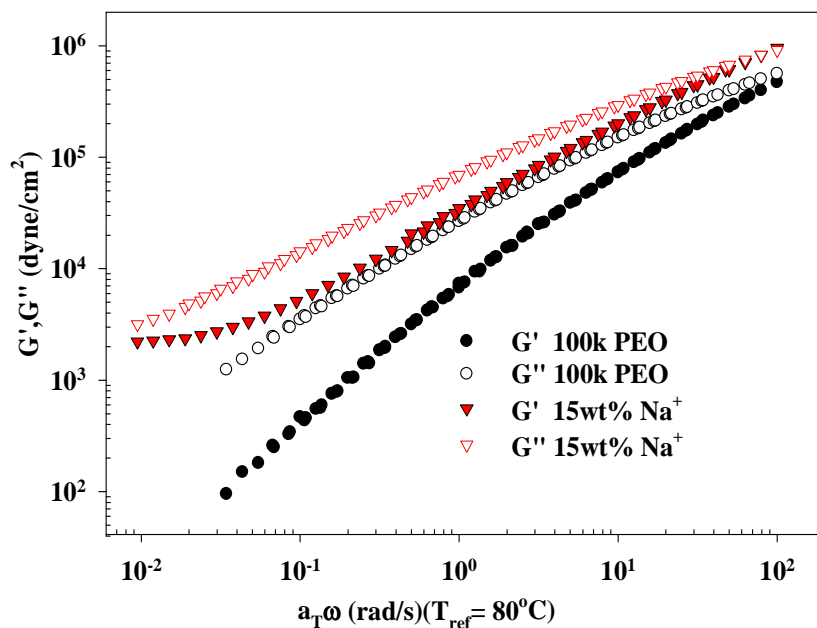


**Figure 66.** Storage and loss moduli for PEO and PEO/15wt% Cloisite Na<sup>+</sup> nanocomposite with a reference temperature of 80°C.

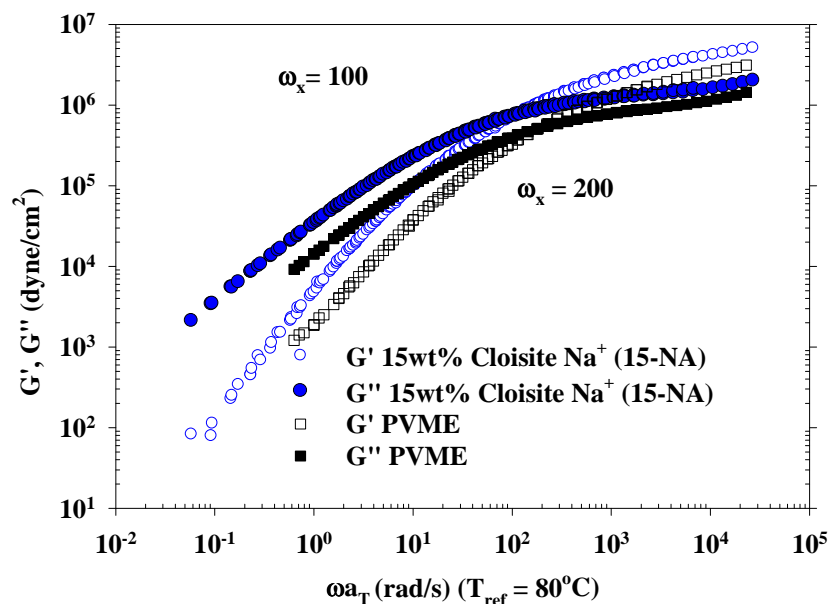


**Figure 67.** Storage and loss moduli for PVME and PVME 15wt% Cloisite Na<sup>+</sup> nanocomposite with a reference temperature of 80°C for comparison with the PEO nanocomposites.

### **PVME – highly dispersed versus scCO<sub>2</sub>-processed**

A key difference between the *scCO<sub>2</sub>* processed samples and the freeze dried sample is the absence of a coherent diffraction peak for freeze-dried sample 15NA-S (Figure 64). The lack of a  $d_{001}$  diffraction peak in this sample is indicative of a “highly dispersed” nanocomposite. This is expected because Cloisite Na<sup>+</sup> swells and dissociates in water. The presence of the polymer in a viscous water solution, and the subsequent lyophilization would be expected to reduce the re-aggregation of some of the clay platelets that is usually seen in solution blending. Although a disappearance of the peak in XRD does not alone indicate exfoliation, the clay loading in the sample is high enough (3 times higher than that needed to produce a coherent diffraction peak) to ensure that WAXD provides an adequate representation of the clay morphology. Morgan *et. al* showed at silicate loadings of less than 5 wt%, coherent diffraction patterns were not always present.<sup>107</sup> The absence of a diffraction peak was further corroborated by additional

measurements on different regions of the sample which readily superposed onto the reported diffraction data. Therefore, we fully expect that sample 15NA-S is a highly dispersed nanocomposite. It is worth noting that WAXD data collected from different regions of the intercalated Cloisite Na<sup>+</sup> based nanocomposite (15-NA) and other similar samples, not otherwise discussed in this paper, always resulted in a small but perceivable diffraction peak. This suggests that at these filler loadings it is unlikely that a significant decrease in parallel registry alone could account for the lack of a diffraction peak from sample 15NA-S but rather the platelets are separated beyond the small angle limit of WAXD.

Linear viscoelastic measurements of the *intercalated* “weakly-interacting” scCO<sub>2</sub>-processed nanocomposite (sample 15-NA) show a 100% increase in G' near the plateau region and the terminal region (Figure 68). The frequency dependence of the dynamic moduli is similar to that of pure PVME. The crossover frequency (Figure 70) of the intercalated scCO<sub>2</sub>-processed sample is factor of 2 lower than that of pure PVME. Even though this is a filled system, with a spectrum of relaxation times, the small change in the matrix chain crossover frequency suggests that the chain relaxation may not have been significantly altered by the clay. This could be a consequence of weaker polymer-clay interactions and relatively poor dispersion.

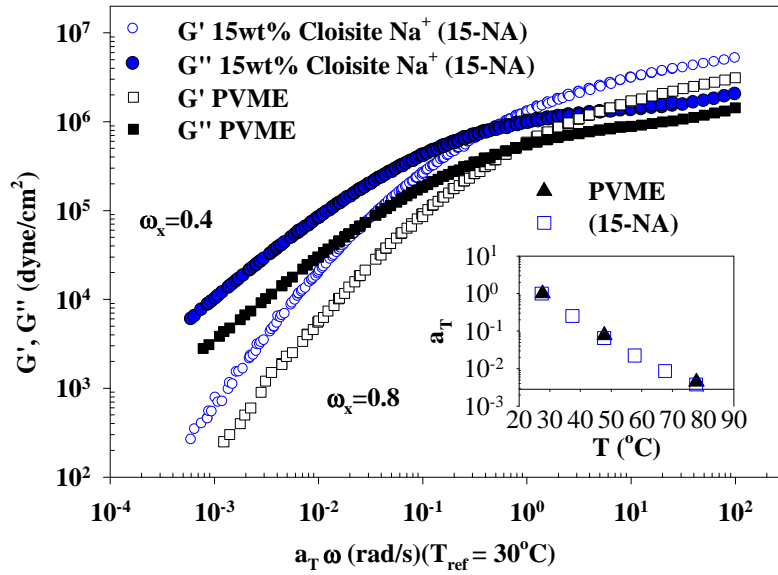


**Figure 68.** Storage and loss moduli for PVME and 15-NA nanocomposite (frequency shift factors shown as inlays).

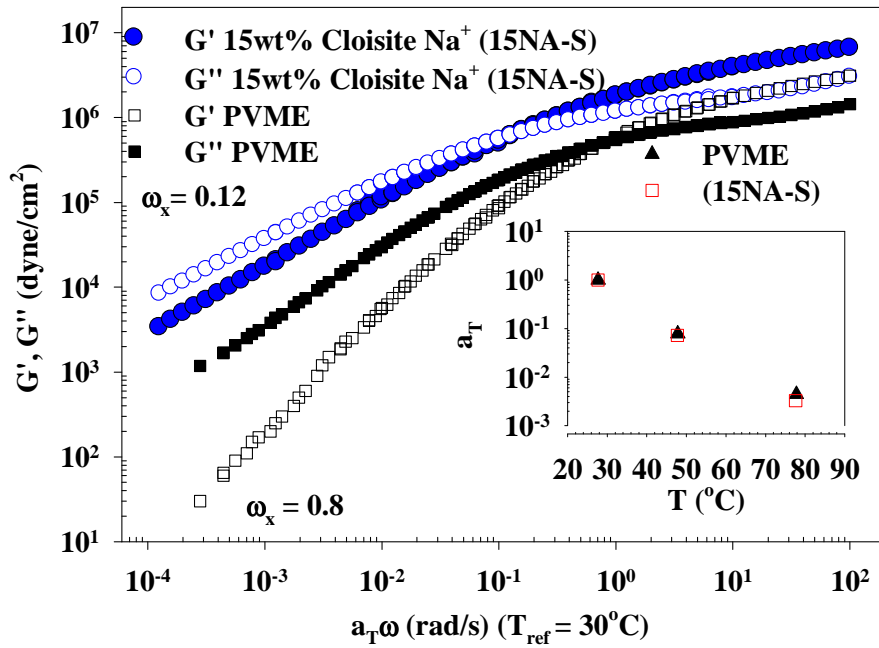


**Figure 69.** Storage and loss moduli for PVME and 15NA-S nanocomposite (frequency shift factors shown as an inlay).

Conversely, the frequency dependence of the highly dispersed “weakly interacting” nanocomposite (sample 15NA-S) is distinctly different from that of the host matrix (Figure 69). The dynamic moduli for the highly dispersed nanocomposite do not exhibit terminal relaxation behavior like the host matrix or the intercalated nanocomposite.  $G'$  and  $G''$  are more than an order of magnitude higher, at low frequencies, than the neat matrix. The 15NA-S nanocomposites exhibits non-terminal behavior with  $G' \propto \omega^{0.8}$  and  $G'' \propto \omega^{0.7}$  rather than  $G' \propto \omega^2$  and  $G'' \propto \omega$  which may be due to the pseudo-solid network form by the presence of the dispersed nano-clay. The cross-over frequency for the highly dispersed nanocomposite is also significantly decreased relative to the host matrix ( $\sim$  factor of 7). When looking at a log-log plot of the dynamic moduli vs. frequency, the  $G'$  and  $G''$  curves of the partially exfoliated “weakly-interacting” hybrid display an extended region where their values are very close, which makes it difficult to see the cross-over frequency. In order to clarify the cross-over frequency shifts, the dynamic moduli for the neat polymer and the hybrids are plotted on a log-linear graph, which clearly reveals the cross-over points of the two nanocomposites relative to the neat PVME. The temperature dependence of the frequency shift factors ( $a_T$ ) for intercalated “weakly-interacting” and partially exfoliated “weakly-interacting” hybrids appear unaltered by the silicate loading and the degree of dispersion suggesting that the temperature dependent segmental relaxation dynamics are unaffected by the presence of the silicate (shift factor plots can be seen as inlays in the plots of dynamic moduli). This behavior has been well documented for many nanocomposites and is attributed to the small percentage of polymer chains that are constrained by the silicate surface<sup>31</sup>. Interestingly, the global relaxation dynamics of the polymer chains appear to be sensitive to the degree of silicate dispersion as noted by the significant change in characteristic relaxation time ( $\sim 2\pi/\omega_x$ ) of the nanocomposites relative to the polymer. The

characteristic relaxation time of the intercalated nanocomposite is  $\sim 16$  sec compared with  $\sim 8$  sec for the neat polymer matrix. The partially exfoliated nanocomposite has a characteristic relaxation time of  $\sim 52$  sec. Chain dynamics of polymer confined by dispersed nano-clay platelets may deviate significantly from that in their one-component melt. Polymer-clay and clay-clay interactions add further complexity by introducing multi-scale relaxation processes. For example, when clay dispersion is significant, there can be appreciable interactions between the clay and the polymer, thereby contributing slower relaxation modes, which lower the 'overall' terminal relaxation times. In contrast, when there is poor dispersion, the polymer-clay contacts are diminished, with the matrix polymer relaxation mainly unaltered. In our system, the differences in the cross-over frequency may provide insights into the degree of silicate dispersion. The cross-over frequency of the partially exfoliated nanocomposite is much lower than that of the intercalated nanocomposite, most likely the result of higher exposed surface area in the case of the partially exfoliated sample, slowing down the 'mean terminal relaxation' of the polymer chains.

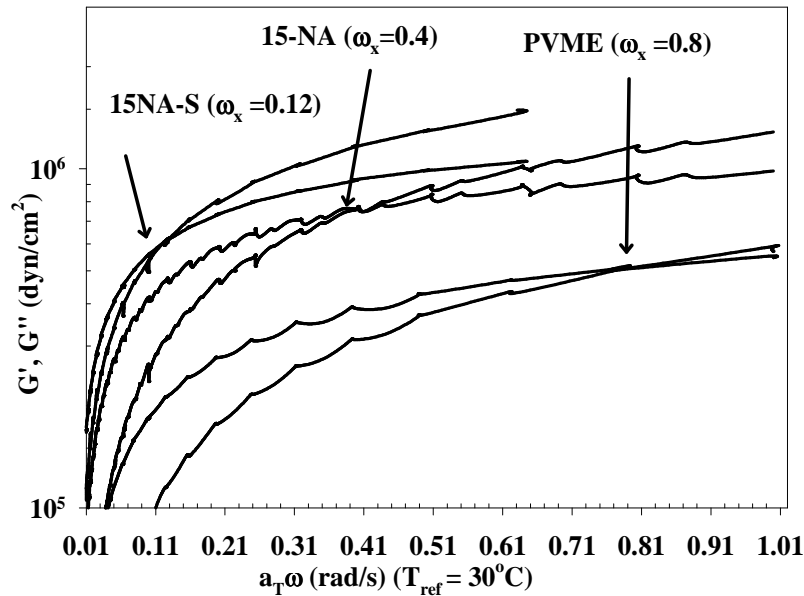


**Figure 70.** Log-linear plot of dynamic moduli vs. reduced frequency to more clearly show the cross-over frequency of the neat PVME, 15NA and 15NA-S.

In addition to changes in  $G'$  and  $G''$ , the complex viscosity also exhibits significantly different behavior as a function of dispersion (Figure 71). The intercalated sample (15-NA) has ~ 150% increase in “complex” zero-shear viscosity and displays Newtonian-like behavior at low frequencies like the neat polymer. At the lowest frequencies measured, the highly dispersed sample (15NA-S) has ~ 1000% increase in viscosity relative to the host matrix and exhibits shear thinning behavior at all shear rates measured. Although,  $G'$  and  $G''$  of the highly dispersed sample never becomes independent of frequency, and the zero-shear viscosity does not diverge, it is clear that dispersion still plays a key role in the viscoelastic response of “weakly-interacting” polymer silicate nanocomposites.



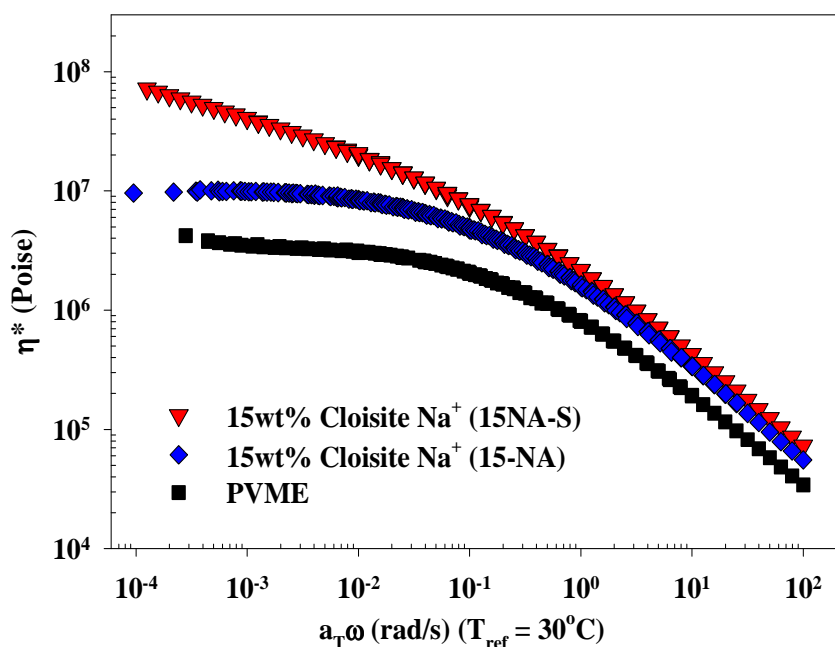


**Figure 71.** Complex viscosity of the neat PVME, 15NA and 15NA-S.

#### 4.4.3 Role of polymer-clay interactions with comparable levels of intercalation

In the previous section the impact of nano - clay dispersion on the melt rheological properties of nanocomposites when “weakly-interacting” PVME-clay nanocomposites are either ‘highly dispersed’ or ‘intercalated’ was described. In this section the role of polymer-clay interactions on the viscoelastic response of a series of PVME organo-clay nanocomposites using three intercalated organophilic clay/PVME nanocomposites prepared via  $scCO_2$  processing [Cloisite 30B (sample 15-30B), and I.30P (sample 15-I.30P)], is investigated. The extent of polymer-clay interactions could vary with each of the organically modified clays. Cloisite 30B is expected to form hydrogen bonds with PVME. All the nanocomposites discussed in this section were made via the  $scCO_2$  process and as a result of the selected processing conditions are intercalated.

The presence of hydrogen bonds in sample 15-30B was studied using FTIR spectroscopy (Figure 72). IR spectroscopy of Cloisite 30B shows a small OH stretching peak at  $3650\text{ cm}^{-1}$ . No OH stretching peak is present in the pure PVME or clay). The nanocomposite displays two distinct peaks in the region for OH stretching, the one at  $3650\text{ cm}^{-1}$  are free hydroxyl groups and the peak at  $3350\text{ cm}^{-1}$  are hydroxyl groups which have formed weak hydrogen bonds with the PVME (Figure 72c). The proposed hydrogen bond may be between the surfactant and the PVME (Figure 72d) not directly with the surface of the nano-clay as is the case with polyamide-6 nanocomposites. The hydrogen bonds are considered weak because the shift in wave number relative to the wave number of the free hydroxyl group is less than  $500\text{ cm}^{-1}$ . The FTIR spectra of the other polymer-clay systems did not show the presence of any additional peaks other than these from PVME and clay. It is difficult to quantify hydrogen bonding interactions in these complex systems. The detailed characterization is beyond the scope of the manuscript. The difference in the FTIR spectral signatures between the different clays, may be indicative of hydrogen bonding, as used before by others.<sup>108, 109</sup>

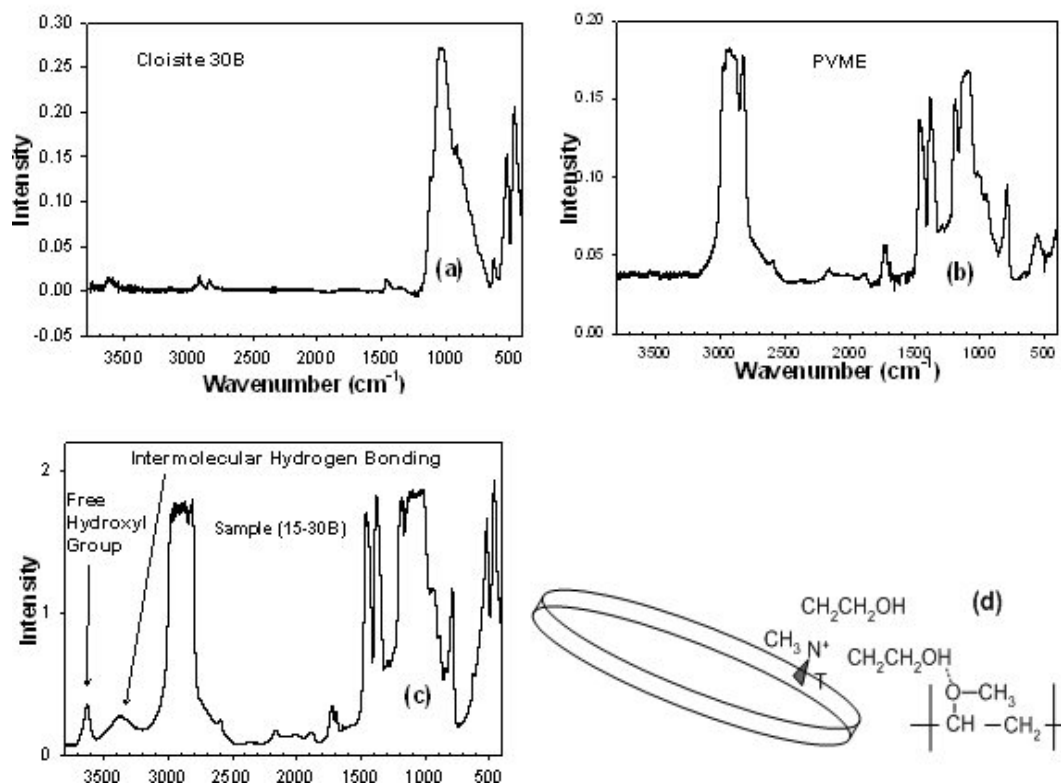


**Figure 72** (a) FTIR spectroscopy of Cloisite 30B shows free hydroxyl group stretch (peak  $3650\text{ cm}^{-1}$ ). (b) FTIR spectroscopy of PVME shows the absence of an intermolecular hydrogen bond peak ( $3350\text{ cm}^{-1}$ ). (c) FTIR spectroscopy of sample 15-30B has an intermolecular hydrogen bond peak ( $3350\text{ cm}^{-1}$ ). (d) Proposed hydrogen bond between surfactant and PVME.

The inter-gallery spacing of I.30P (sample 15-I.30P) and Cloisite 30B (sample 15-30B) in PVME was determined to be 2.7 and 2.4 nm respectively (Figure 73 and Figure 74). These inter-gallery spaces represent an increase of 1.2 nm for I.30P and 1.55 nm for Cloisite 30B. This increasing in spacing may be a strong indication that polymer has penetrated the space between the clay platelets. In addition to a decrease in the Bragg angle, indicated by the increase in the basal spacing, diffraction patterns from the nanocomposites formed from the organically modified clays (samples 15-30B, and 15-I.30P) exhibited changes in peak profile compared with the “as-received” clay. Specifically, the peak breadth at full-width half maximum “B” decreased

in the nanocomposites relative to their corresponding as-received nano-clay. The decrease in peak breadth is expected with intercalated nano-clays because the clay galleries expand, resulting in an increase in the overall tactoid size (height). Previous research shows that small crystal sizes give broad diffraction patterns and larger crystals have narrower patterns.<sup>110</sup> The shape and width of the diffraction patterns were analyzed to provide a rough approximation of the tactoid size. Because the diffraction patterns produced by the organo-philic nanocomposites were Gaussian in nature we employed the Scherrer Equation to determine the average tactoid thickness.

**Table 18** The first entry in each column refers to the nanocomposite and the second, in parenthesis, refers to the as-received nano-clay corresponding to a particular nanocomposite. n/a appears where no diffraction pattern was observed or the pattern did not resemble a Gaussian distribution.

| Name                          | B (rad)       | d <sub>001</sub> (nm) | # platelets /tactoid | 2θ <sub>B</sub> (deg) |
|-------------------------------|---------------|-----------------------|----------------------|-----------------------|
| 15-30B (30B)                  | 0.022 (0.025) | 3.4 (1.85)            | 3 (4)                | 2.59 (4.78)           |
| 15-NA (Na <sup>+</sup> )      | n/a           | 3.6 (1.2)             | n/a                  | 2.45 (7.1)            |
| 15-I.30P (I.30P)              | 0.011 (0.034) | 3.7 (2.5)             | 5 (3)                | 2.5 (3.5)             |
| 15NA-S (Na <sup>+</sup> )     | n/a           | n/a (1.2)             | n/a                  | n/a (7.1)             |
| Cloisite Na <sup>+</sup> /PEO | 0.024 (0.035) | 1.9 (1.2)             | 3 (3)                | 4.69 (7.1)            |

$$t := \frac{\lambda}{B \cdot \cos\theta_B}$$

From the average tactoid thickness we determined the average number of platelets per tactoid using the following equation:

$$\eta := \frac{t - 10}{d_{001}} + 1$$

Where  $t$  is the tactoid thickness determined from the Scherrer equation, 10 is the thickness of a platelet in angstroms,  $d_{001}$  is the basal spacing of the nano-clay, and  $\eta$  is the number of platelets rounded to the next integer (see justification in appendix A). The Scherrer equation predicted the minimum average number of platelets per tactoid as 3-5 for the  $\text{Na}^+$  nanocomposites (Table 18). The values obtained from the Scherrer equation are underestimated since the correction for equipment broadening is not used in the calculations. Also, the shape of the clay particles is not truly spherical and the Scherrer equation can only provide a rough estimate of the tactoid size. The presence of 3 diffraction peaks in some of the samples further supports the existence of larger structures because tens of plates are needed to obtain well defined higher order diffraction patterns.<sup>111</sup> The values calculated via the Scherrer equation agree well with literature.<sup>31</sup>

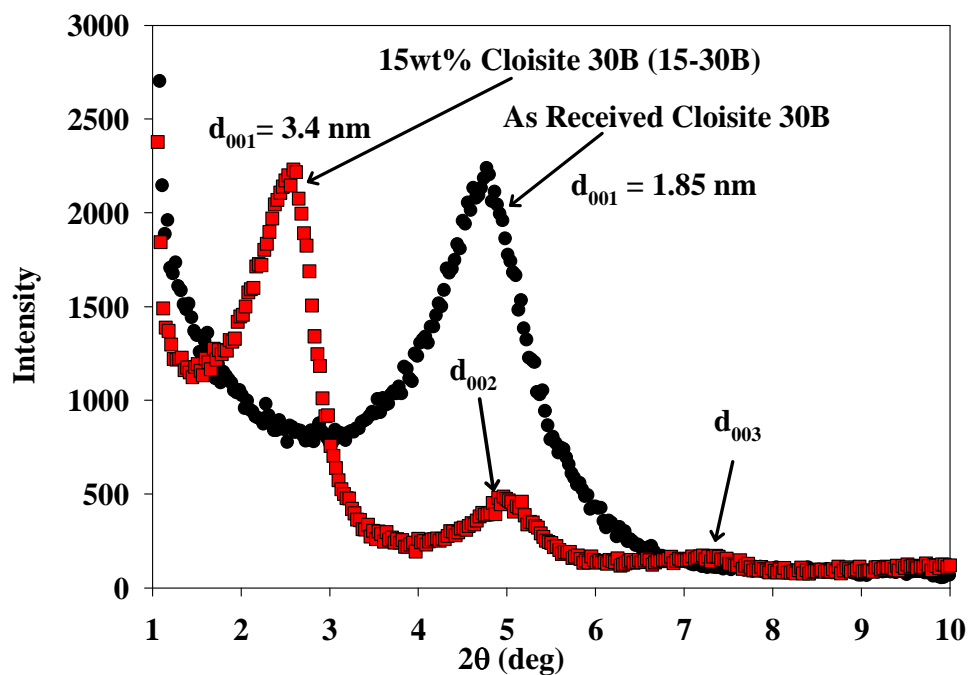


Figure 73. WAXD of “as received” 30B and sample 15-30B.

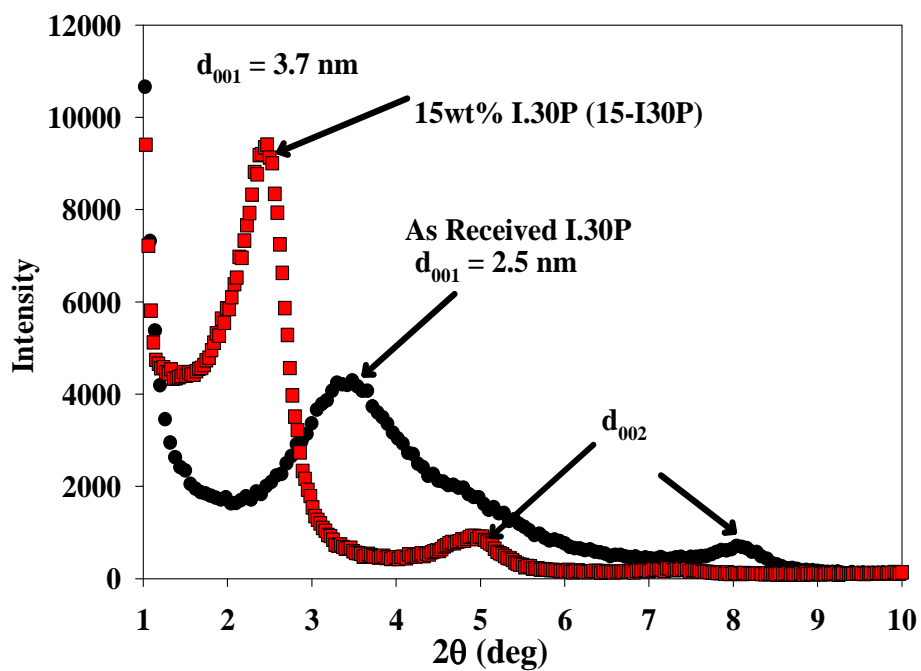
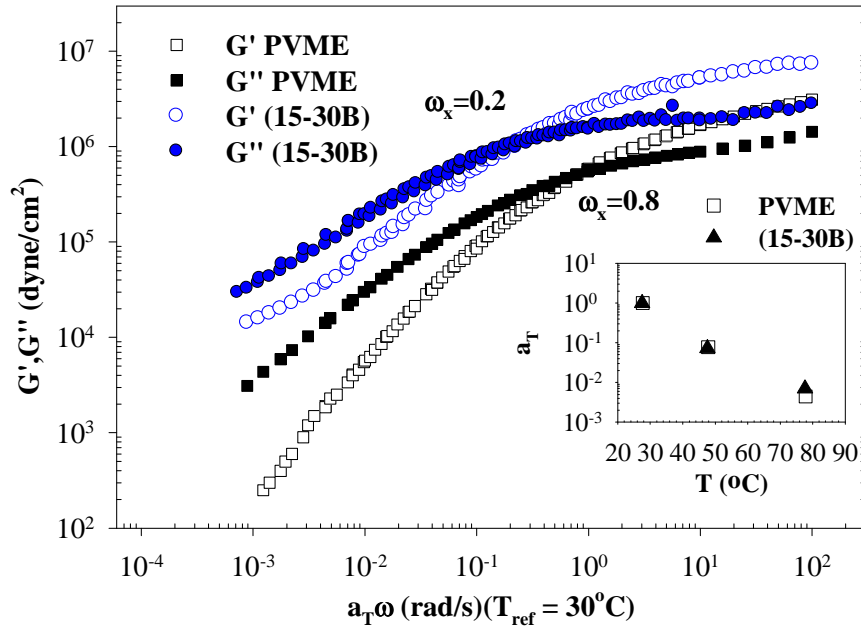


Figure 74. WAXD of “as received” I.30P and sample 15-I.30P.

Even though the WAXD measured d-spacing in I.30P and 30B intercalated nanocomposites are somewhat similar they have the same volume fraction of inorganic nano-clay (4vol%) which is important when comparing the viscoelastic properties of nanocomposites, rheology shows significant difference. The dynamic moduli for the samples are compared in three regions: below the cross-over frequency (terminal region), above the cross-over frequency (plateau region), and at the cross-over frequency.

### **PVME-30B nanocomposite**

$G'$  of the hydrogen bonded nanocomposite (sample 15-30B) was increased by 150% in the plateau region and more than an order of magnitude in the terminal region (Figure 75). At low frequencies, sample 15-30B displays distinctly non-terminal behavior with  $G' \propto \omega^{0.5}$  and  $G'' \propto \omega^{0.7}$ . This non-terminal behavior is also apparent in the complex viscosity, which exhibits shear thinning behavior over the entire frequency range with a trend toward diverging viscosity at the lowest shear rates measured (Figure 76). The cross-over frequency of sample 15-30B is reduced by  $\sim$  a factor of 4 relative to the host matrix. To verify that the change in cross-over frequency was indeed the result of changes in relaxation time and not a manifestation of time temperature superposition, the frequency shift factors of the nanocomposite and the neat matrix were compared. The frequency shift factors for the nanocomposite are nearly identical to that of pure PVME. This suggests that local (segmental) chain dynamics of the intercalated nanocomposite are unaltered, at least within the sensitivity of the measurement and that the polymer chains do not form hydrogen bonds directly with the silicate surface as is the case in many polyamide-6 nanocomposites.<sup>36</sup> Furthermore, it shows that the global chain dynamics have been impacted by the presences of the nano-clay in the PVME.



**Figure 75.** Log Storage and loss moduli for PVME and 15-30Bnanocomposite (frequency shift factors shown as an inlay).

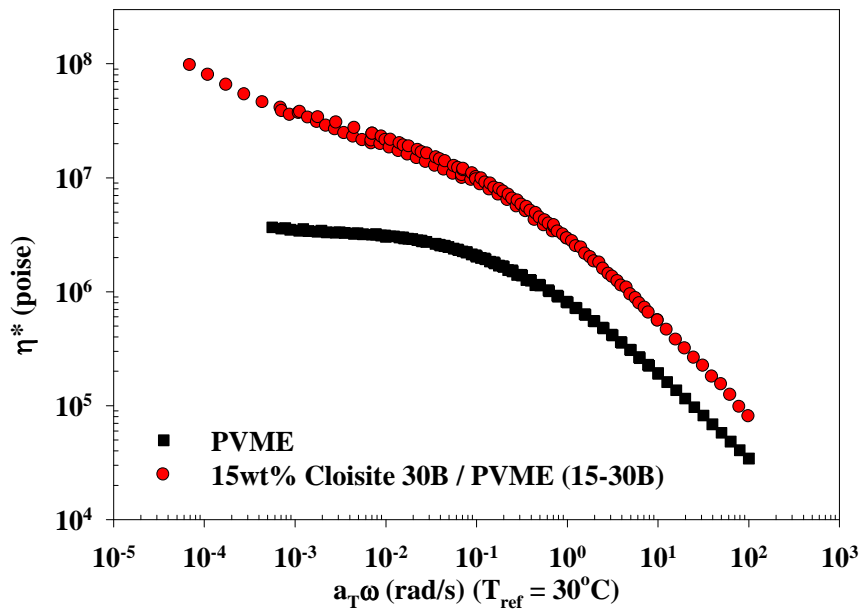


**Figure 76.** Complex viscosity vs. reduced frequency for sample 15-30B diverges at low frequencies.



**PVME-I.30P nanocomposite**

The storage modulus of scCO<sub>2</sub> processed 15-I.30P sample increases by ~ 100% in the plateau region. Furthermore, 15-I.30P exhibits no terminal behavior ( $G' \propto \omega^{0.5}$  and  $G'' \propto \omega^{0.6}$ ) and is nearly 2 orders of magnitude larger than the neat PVME in the terminal region (Figure 77). The cross-over frequency shifts by an order of magnitude relative to the neat PVME and the characteristic relaxation time increases from ~ 8 s to ~ 78 s. The frequency shift factors for sample 15-I.30P are nearly identical to the neat polymer suggesting that the change in cross-over frequency was indeed the result of changes in relaxation time. The pseudo solid-like behavior seen in  $G'$  of sample 15-I.30P is also observed in the complex viscosity at low shear rates where the viscosity diverges with shear thinning behavior prevalent throughout the whole frequency spectrum (Figure 78). The cross-over frequency shift of sample 15-I.30P is much greater than that of sample 15-NA, suggesting that the relaxation dynamics of the polymer chain may be significantly impacted by the strength of the polymer-clay interactions. In addition, longer relaxation events are also affected by the strength of the polymer-clay interactions as evident by the non-terminal behavior in sample 15-I.30P and the terminal behavior seen in sample 15-NA.

Samples 15-30B and 15-I.30P displayed qualitatively similar rheological behavior with 15-I.30P nanocomposite showing more low-frequency enhancement than that of sample 15-30B. The viscosity of sample 15-I.30P increases by ~ 2 orders of magnitude and that of sample 15-30B increases by ~ 1.5 orders of magnitude. The extent of intercalation is expected to be similar between these samples because the inter-gallery spacing is similar in each of the nano-clays with both reaching a new equilibrium spacing within 20% of each other. Therefore, both samples are expected to be highly intercalated. The reason for the large disparity in cross-over frequencies of the two samples is not clear. This may be the result of a slightly higher degree of intercalation in

sample 15-I.30P but is more likely the result of how the polymer interacts with the clay. Nanocor I.30P has an average higher aspect ratio of 350 (Nanocor) while Cloisite 30B has an average aspect ratio of 110 (Southern Clay Products). With 4vol% and 350 average aspect ratio, Nanocor I.30P nanocomposite there are  $\sim 416$  platelets/ $\mu\text{m}^3$  which leads to a maximum nano-clay surface area of  $\sim 81$   $\text{m}^2/\text{cm}^3$  of nanocomposite. In the case of Cloisite 30B the 4vol% and 110 average aspect ratio there are  $\sim 4346$  platelets/ $\mu\text{m}^3$  which leads to a maximum nano-clay surface area of  $\sim 84$   $\text{m}^2/\text{cm}^3$  of nanocomposite. The viscoelastic response depends strongly on the volume fraction of inorganic platelets, the dispersion state, and the level of interactions between polymer and clay and also between the clay platelets themselves. The clay platelets interaction is in the form of clay platelet edge-to-face interactions and it results in the formation of a so-called “house of cards” structure, which is generally recognized to be the primarily culprit for the increase in  $G'$  at low shear rates (the structure breaks up at higher shear rates). However since both samples contains the same volume fraction of inorganic matte, we believe that the clay-clay interactions should play a big role in the rheological differences between the two nanocomposites. Both samples have the same volume fraction of inorganic nano-clay and similar maximum surface areas available for polymer-clay interactions; however the Nanocor I.30P nanocomposite shows improved rheological properties compared to Cloisite 30B nanocomposites. This suggests that PVME can interact with and coat Nanocor I30P to a greater extent compared to Cloisite 30B, which we believe may be responsible for the differences in the viscoelastic properties between 15-I.30P and 15-30B. Also, since the I.30P average aspect ratio is higher than 30B could be another explanation of why 15-I.30P nanocomposite shows improvements in viscoelastic properties over 15-30B nanocomposite. Higher aspect ratio platelet results in a more effective load transfer and is observed to give greater increases in  $G'$ . This

phenomenon was also observed in fiber composites if the critical fiber length is short<sup>112</sup>. Sample 15-30B still displays significant improvement in viscoelastic properties over the polymer matrix which suggests that hydrogen bonding between the ammonium salt and the PVME (Figure 72d) may play a role in the overall viscoelastic response of sample 15-30B. Comparison of samples 15-I.30P and 15-30B with sample 15-NA, strongly suggests that the extent of interactions between the clay and the polymer plays a key role in the linear viscoelastic response of these nanocomposites. Another plausible explanation for the differences in the viscoelastic response between these systems is that 15-NA contains a slightly higher volume of inorganic matter (5vol%) compared to 15-30B and 15-I.30P (4vol%) which can increase the parallel stacking of the layers and / or agglomerate formation. The increase in the parallel stacking disfavors edge-to-face interactions because there is physically no room for such interactions to occur and more faces become inaccessible to the layer edges. This, in turn, would be expected to suppress the formation of a strongly interacting filler network, which can be a plausible explanation for the less improvement in  $G'$  in the (higher inorganic content)  $\text{Na}^+$  system vs. the (lower inorganic content) 30B and I.30P systems. However, the differences in volume loading of inorganic matter are small and we believe that it doesn't impact the rheological response to a great extent. Furthermore, Cloisite  $\text{Na}^+$  contains no organic modifier while 30B and I.30B both do and the interactions between PVME and the organically modified clay are expected to be stronger than PVME- $\text{Na}^+$  interactions. Previously, Shi *et. al* demonstrated that interactions between the alkyl chains of the ammonium salt and the polymer matrix were weak and had a small impact on the reinforcement properties (tensile strength) of the nanocomposite relative to the host matrix. They concluded that polymer chains binding (adsorbed) directly to the clay surface were responsible for the majority of the enhancements<sup>113</sup>.

Therefore, it appears that the adsorption of PVME onto the clay surface is at least partially governed by the type of organic modifier present and that the modifier may significantly improve the adsorption.

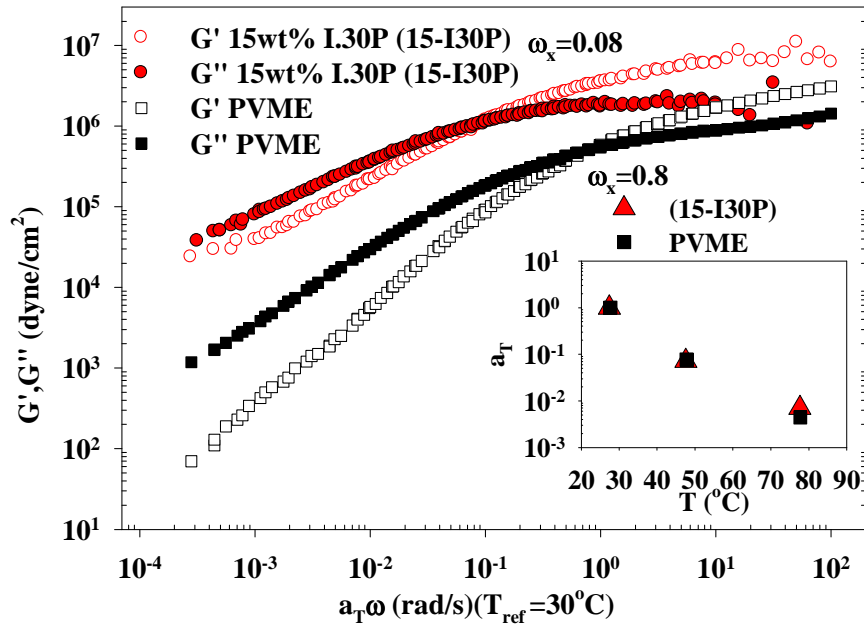


**Figure 77.** Storage and loss moduli for PVME and 15-I30P nanocomposite (frequency shift factors shown as an inlay).

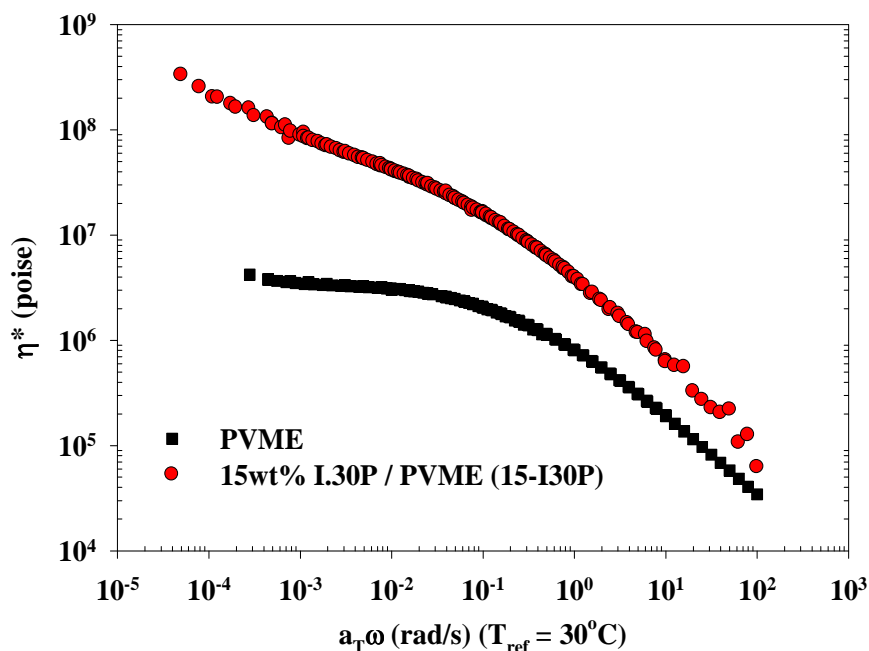


**Figure 78.** Complex viscosity vs. reduced frequency for sample 15-I.30P displays a diverging viscosity at low frequencies.

#### 4.5 Conclusions

In this chapter the impact of nano - clay dispersion and polymer - clay interactions on the viscoelastic response of PVME/clay and PEO/clay nanocomposites with varying degrees of dispersion and polymer-clay interactions was investigated. The use of water-soluble PVME and water-soluble natural clay provided a benchmark for a highly dispersed sample. The use of  $\text{scCO}_2$  processing produced intercalated nanocomposites with somewhat similar final WAXD patterns, yet the rheological properties were significantly different. Even though the extent and the nature of dispersion and interactions in these complex systems are tough to quantify, rheology offers valuable insights into the mesoscale structure and interactions. The viscoelastic response of polymer-clay nanocomposites is sensitive to the extent of dispersion and the degree of interaction. Comparison of  $\text{scCO}_2$ -processed (intercalated) and water-processed (highly

dispersed) Cloisite Na<sup>+</sup> /PVME nanocomposites with “weak polymer-filler interactions” (suggested that high level clay dispersion resulted in non-terminal behavior ( $G' \propto \omega^{0.8}$  and  $G'' \propto \omega^{0.7}$ ) and a factor of 8 decrease in the cross-over frequency, and an order of magnitude increase in the low-frequency storage moduli; while intercalation resulted in a filler effect with the relaxation behavior of the bulk polymer virtually unaltered by the presence of the nano-clay. In contrast, for intercalated systems with "stronger" polymer-clay interactions (PVME/I.30P), there was a low-frequency plateau, an order of magnitude decrease in the crossover frequency, and more than two orders of magnitude increase in low-frequency storage moduli. Furthermore, PVME/I.30P sample displayed enhanced rheological properties compared to PVME/30B sample despite having similar dispersion, same inorganic volume fraction and same maximum surface area indicated the presence of stronger polymer-clay interactions. These results suggested that rheology can offer valuable insights into these complex systems. When ‘strong’ polymer-clay interactions were present, even an intercalated structure can produce significant property improvements (even more than highly dispersed systems). Hence, the combination of WAXD and rheology can provide insights into the extent of dispersion and compatibility of the nano-clay with the chosen polymer matrix.

## CHAPTER 5

### Future Work

#### 5.1 Surface modification of “as received” Cloisite Na<sup>+</sup>

The commonly used organo-modification agents are long carbon-chain alkyl ammonium salts. Although these modification agents have been gaining significant success in the preparation of polymer/MMT nanocomposites, their common shortcoming is the poor thermal stability. Xie et al. have studied the thermal stability of MMT modified by long carbon-chain alkyl quaternary ammonium ions and found that the on-set decomposition temperature was approximately 180°C.<sup>81</sup> Vaia and co-workers have shown that at temperatures exceeding 200°C after 2 hours degradation of organic modifier bonded to the clay surface occurs which causes gallery collapse comparable to that of montmorillonite<sup>71</sup>. Unfortunately, the preparation and processing of most of the polymer/clay nanocomposites require a temperature much higher than this value, and the thermal decomposition of the long carbon-chain alkyl quaternary ammonium salts is inevitable. Tanoue et al. saw that the decomposition of the organic modifier led to a collapse of the clay inter-gallery layer which resulted in poor rheological enhancements for the PS/Cloisite 10A nanocomposites prepared at 200°C.<sup>41</sup> Delozier et al. also observed that during the preparation of polyimide/clay nanocomposites, the decomposition of the organic modifier led to the collapse of the clay particles into larger agglomerates.<sup>114</sup> The degradation of organic modifier may pose significant effect on the morphological structure, the preparation, performance, application and service life of nanocomposites.

Introducing a solvent can lower the processing conditions but the solvent needs to be removed following processing which poses as a hazard to the environment. Furthermore, some polymers require very potent solvents which are also a health hazard on top of being

environmentally benign. To mediate this problem researchers have started to modify their own clays by using organic modifiers that are more stable at higher temperatures. Also, the modifiers can be tailored toward a certain polymer and polymer - clay interactions can be improved.<sup>12, 33, 34, 63</sup> Montmorillonite will be modified with a surface modifier that has the potential of interacting with polystyrene. Following the modification of MMT, the resulting clay will be processed in scCO<sub>2</sub> and WAXD and SEM will be used to investigate the dispersion level. Also, polystyrene/clay nanocomposites will be made in the presence of scCO<sub>2</sub> as well as melt intercalation benchmark samples. The ultimate goal of this research is to understand how clay modification impacts the properties of the resulting nanocomposites and to develop clays that can be exfoliated/dispersed in an industrially important polymer matrix and have the potential of being processed at high temperatures without degrading the clay surface modifier.

### **5.1.1 Preliminary results**

As a preliminary results “as received” montmorillonite was modified with two surface modifier in an attempt to make a more stable clay that is favorable to interact with polystyrene. Before the ion-exchange reaction, one of the organic modifiers needed to be synthesized. The first organic modifier was 1-hexadecyl amine and was purchased from Sigma Aldrich (modifier A) and the second one N-[4-(40-aminophenoxy)] phenyl phthalimide (modifier B) (Figure 79) was synthesized following the synthesis similar to that previously reported by Liang et al.<sup>115</sup>



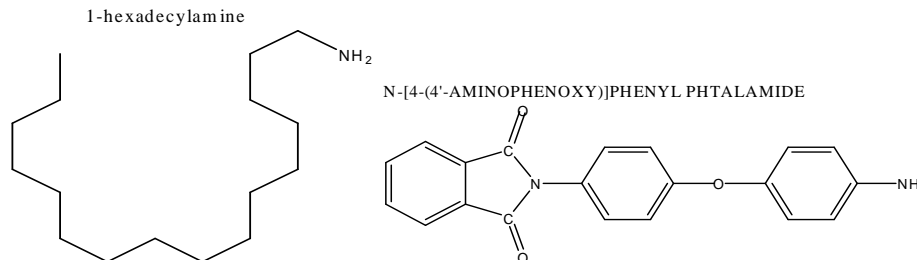


**Figure 79:** 1-hexadecyl amine (left) and N-[4-(4-aminophenoxy)] phenyl phthalimide (right).

The two organically modified MMTs, MMT-A and MMT-B, were prepared via ion exchange reaction in water using modifiers A and B following the reaction similar to that previously reported by Liang et al.<sup>115</sup> The compatibility between N-[4-(4-aminophenoxy)] phenyl phthalimide MMT (MMT-B) and PS may be very high due to the presence of three phenol in the organic modifier (B). Cloisite 10A which contained only one phenol ring as part of its organic modifier resulted in enhanced dispersion, rheology and permeability compared to neat PS and other nano-clays. If this is the case the positive interaction between PS and MMT-B may lead to even higher improvements in dispersion and properties compared to 10A.

Fourier transform infrared spectroscopy (FTIR) and WAXD were used to verify the organic modifiers and the corresponding modified-MMT clays that were prepared. Na-MMT showed the characteristic absorption band at  $1100\text{ cm}^{-1}$  (Figure 80 - a). MMT-A showed the characteristic bands of C-H stretching between  $3000$  and  $2800\text{ cm}^{-1}$  (Figure 80 - b) while MMT-B displayed the characteristic absorption bands of aromatic imide between  $1800$  -  $1700$  and  $1385\text{ cm}^{-1}$  and of C-O-C unsymmetrical stretching at  $1246\text{ cm}^{-1}$  (Figure 80 - b). The FTIR of MMT-A (Figure 80 - c) and MMT-B (Figure 80 - e) shows that the clays contained modifiers A and B respectively. However, using FTIR you cannot tell whether or not the organic modifier entered the inner-gallery spacing.

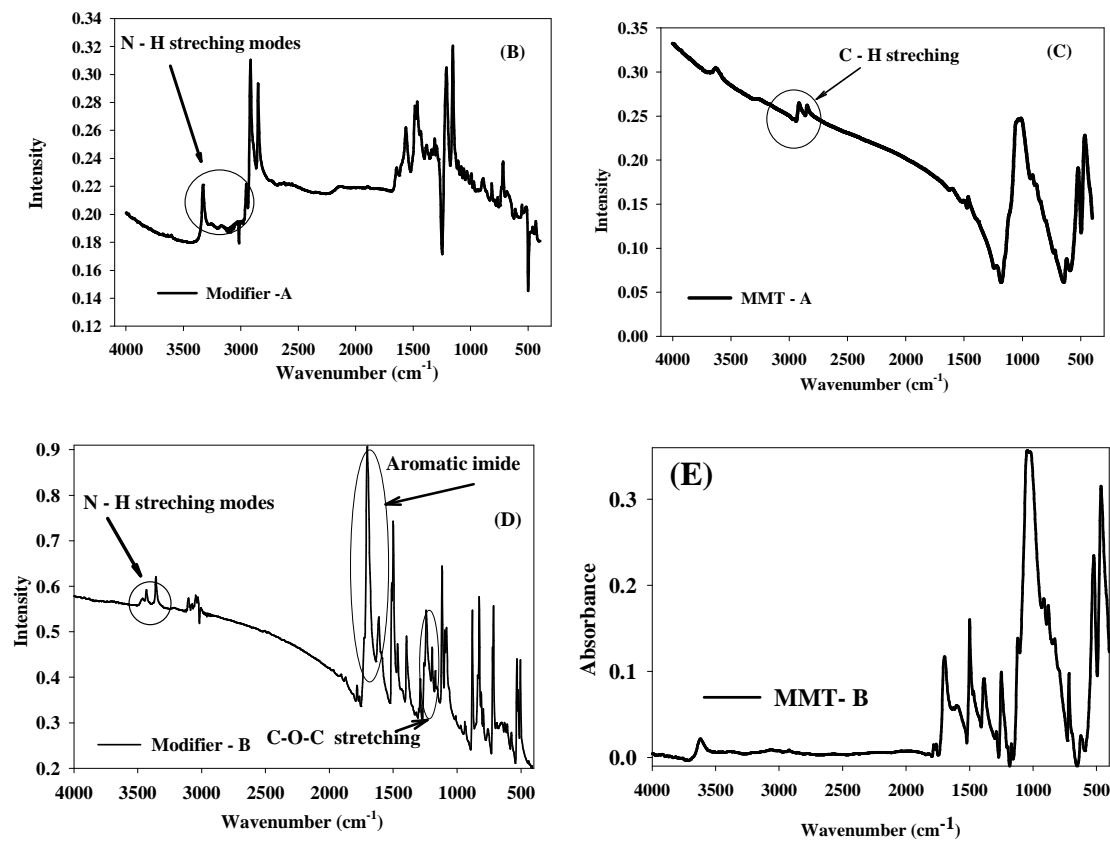


**Figure 80.** FTIR of Na<sup>+</sup> (A), the organic modifiers 1-hexadecyl amine (B) and N-[4-(40-aminophenoxy)] phenyl phthalimide (D) and of the organically modified Na<sup>+</sup>, MMT-1-hexadecyl amine (MMT-A) (C) and (and N-[4-(40-aminophenoxy)] phenyl phthalimide (MMT-B) (E).

Therefore, WAXD was used to determine if the modifier actually entered the clay layers. Pure MMT-Na<sup>+</sup> showed a  $d_{001} = 1.2$  nm corresponding to an inner-gallery spacing of 0.2 nm (Figure 81). MMT-A displayed a  $d_{001} = 1.92$  nm which corresponds to a spacing of 0.92 nm similar to Cloisite 10A. In contrast MMT-B showed two peaks one equal to 1.58 nm and the other 2.45 nm, corresponding to an inner-gallery spacing 0.58 nm and 1.45 nm respectively. In MMT-B one smaller diffraction peak is shifted even more to the left (smaller 2 theta) indicating a higher inner-gallery spacing. However, the bigger diffraction peak in MMT-B is at a higher 2 theta indicating a smaller inner-gallery spacing compared to MMT-A (Figure 81). The presence

of two peaks in MMT-B may be due to the reaction where a byproduct could have been formed and essentially there are two different modifiers that have different thermodynamically stable equilibrium spacing. The reaction needs to be optimized where the product is only modifier-B where no other by-products are present. Despite the two different clay spacing populations, MMT-B clay was very thermally stable. When kept at 200°C for 24 hours, it only lost about 2% of its modifiers after 24 hours. In contrast, MMT-A lost 9% of its modifier after 10 hours and 11% after 24 hours. Also, Cloisite 93A and 30B which are two of the most stable commercially available clays from Southern Clay lost 4.5% and 8% respectively after 10 hours and 6% and 9% respectively after 24 hours. MMT-B is stable at 200°C for a long period of time only losing 2% of its modifier after 24 hours (Figure 82). It could offer a possible offer a solution for melt compounding with the polymer of choice at 200°C without worrying about clay degradation (like it was previously shown where 10A showed platelet collapse even when it was compounded at 180°C for 15 minutes in the presence of PS – Chapter 3).

However, in the reaction where N-[4-(40-aminophenoxy)] phenyl phthalimide (modifier-B) was made needs to be optimized to produce only the desired product in order to maximize the inner-gallery spacing. Once the reaction scheme is optimized, the modified nano-clay (MMT-B) can be processed using the scCO<sub>2</sub> technique with and without a polymer present, to test whether or not it can be dispersed. Moreover, this scCO<sub>2</sub> processed modified nano-clay should be compounded with PS and other industrially important polymers like high density polyethylene and polypropylene which typically need higher processing temperatures. Due to its high thermal stability it should allow for processing of these nanocomposites using melt extrusion and the resulting nanocomposites it's anticipated to have improved dispersion and properties.

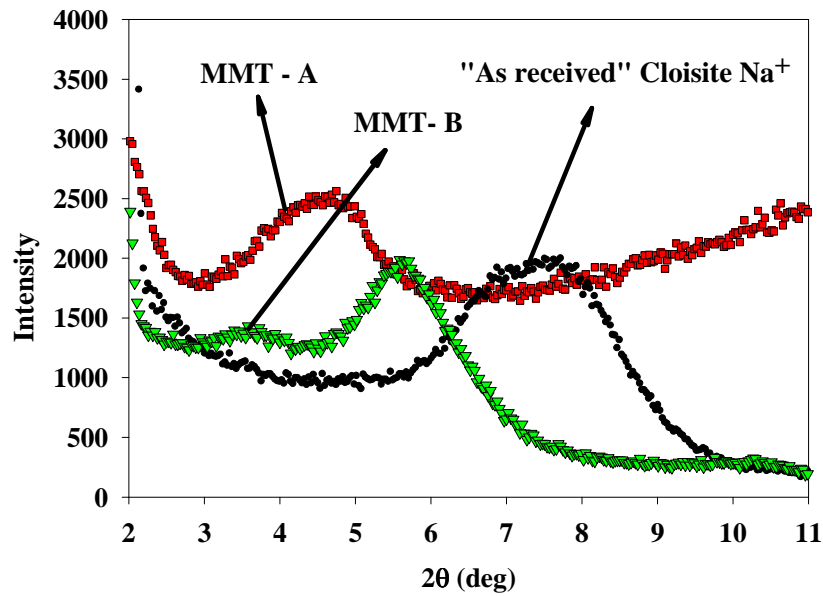


Figure 81. WAXD of MMT – Na<sup>+</sup>, MMT- A and MMT- B.

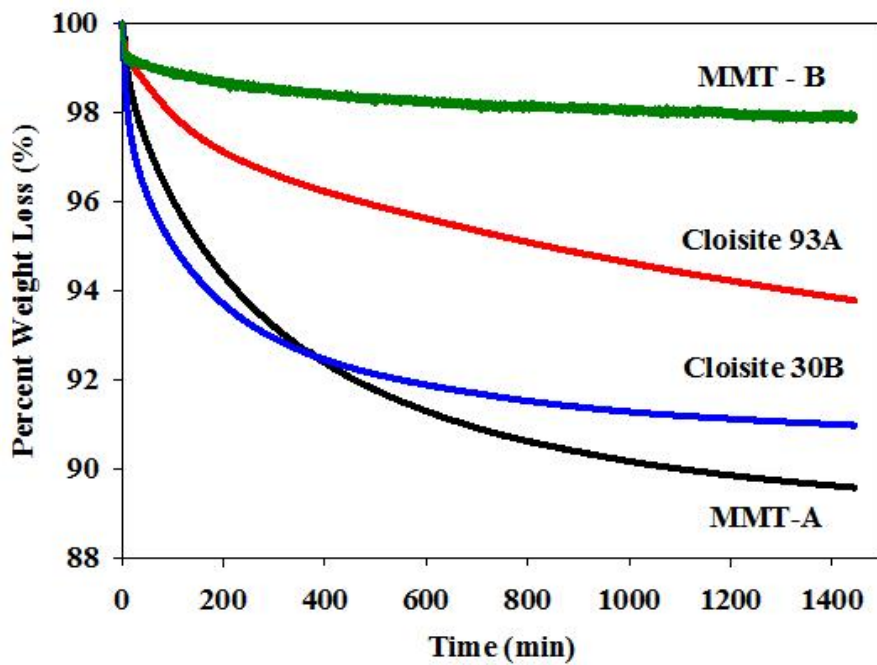


Figure 82. TGA at 200°C for 24 hours for MMT-A, MMT-B, Cloisite 93A and 30B.

## 5.2 Styrene-butadiene-styrene (SBS)/clay nanocomposites

The styrene-butadiene-styrene triblock copolymer (SBS) is of the most commercially used thermoplastic elastomers (TPE) which exhibits the characteristics of plastic (polystyrene)

and rubber (butadiene) with rubber like properties while still retaining significant stiffness without the need of chemical crosslinking.<sup>116</sup> Researchers have been preparing SBS/clay nanocomposites using solution blended<sup>117-119</sup>, melt compounding<sup>116, 120</sup> and *in-situ* polymerization<sup>121</sup> methods using various clays with various success in dispersing the clay and obtaining enhancements in rheological, mechanical, transport and thermal properties. Due to the immiscibility of PS and PB in SBS the two organize in different microdomains. SBS also exhibits an Order-Disorder Transition (ODT) temperature below which due to the microdomains organization researchers have found that it is a challenge to obtain rheological improvements in SBS/clay nanocomposites.<sup>122, 123</sup> Using rheological measurements whether or not SBS is above or below the ODT at the temperature tested can be determined. If SBS is below the ODT at the temperature tested there should be a slope lower than 2 in the storage modulus terminal regime.<sup>122</sup> Moreover, before TEM the SBS/clay nanocomposites films can be stained with osmium tetroxide (OsO<sub>4</sub>) which stains the PB chains and the TEM images can reveal the microphase type.

However, the applicability of the scCO<sub>2</sub> process on the SBS/clay nanocomposites has not yet been studied. To study the scCO<sub>2</sub> processing effects several nanocomposites should be prepared using several nano - clays including Cloisite 10A, 15A and 20A at different weight fractions. Cloisite 10A and 15A has already been shown to produce highly dispersed PS/clay nanocomposites with enhanced rheological and thermal properties and reduced permeability (Chapter 3).<sup>69, 77, 94</sup> Cloisite 10A, 20A and 15A have been used by other researchers to produce SBS/clay nanocomposites with various results.<sup>116, 118-121</sup> In SBS, clays tend to interact with PS more than polybutadiene (PB) which is already the stiffer of the two, therefore the resulting nanocomposites exhibit only small improvements in properties. In an attempt to address this

issue, SBS nanocomposites using two clays should be used, one that likes polystyrene more and another that likes PB more in an attempt to test the likelihood that some of the clay will go into PB and the resulting properties may be enhanced. Benchmark nanocomposites should also be prepared using the solution blended technique in toluene and using the melt compounding method to compare the results with those obtained using the scCO<sub>2</sub> processing technique. WAXD, rheology, TEM, permeability measurements, mechanical properties and thermal properties should be measured on the resulting nanocomposites to determine the ability of scCO<sub>2</sub> to produce dispersed SBS/clay nanocomposites with enhanced properties.

### **5.2.1 Preliminary results**

As preliminary results, four SBS/5wt% clay nanocomposites were prepared with Cloisite 10A and 20A (which is the same as 15A but has a CEC of 95 meq) using solution blended and scCO<sub>2</sub> processing techniques. The SBS used in this study has a molecular weight of 100,000g/mol and contains 30% PS content. The solution blended samples were prepared in toluene at 80°C for 24 hours. The scCO<sub>2</sub> processed samples were made using the same protocol as the solution blended; the only difference was the presence of scCO<sub>2</sub> at 13.79 MPa. WAXD was collected using the same procedure as in Chapter 3. X-ray diffraction revealed that the polymer were successfully intercalated in-between the nano - clay particles as evident by the shift of the d<sub>001</sub> peak to lower 2 theta values for the nanocomposites compared to “as received” clay. Cloisite 20A nanocomposites prepared using solution blended and the scCO<sub>2</sub> processed method both displayed the same final d<sub>001</sub> spacing of 3.84 nm corresponding to an inner-galley spacing increase of 1.42 nm (Figure 83). The two nanocomposites having the same final is due processing in a solvent and the modifier having a thermodynamically stable state. This phenomenon was also observed in PS/clay nanocomposites in Chapter 3 that were also processed

in a solvent. Furthermore, the presence of  $d_{002}$ ,  $d_{003}$  and even  $d_{004}$  diffraction peaks indicate the presence of highly ordered nanocomposites.

However, in the nanocomposites prepared using Cloisite 10A there was a small difference in the final  $d_{001}$  spacing between the solution blended ( $d_{001} = 4.2$  nm) and  $scCO_2$  processed nanocomposites ( $d_{001} = 4.4$  nm). However, TEM does not show any difference between the  $scCO_2$  process and solution blended nanocomposites. This is somewhat surprising since  $scCO_2$  nanocomposite is supposed to have improved dispersion. However, prior to collecting TEM images thin film needed to be cut using an cryo-ultramicrotome at  $-80^\circ C$  and obtaining thin films was a great challenge. Therefore, since the films were not thin enough, TEM images did not have good enough quality to observe if the tactoid size has been reduced or whether or not there are some individual platelets present in the  $scCO_2$  process nanocomposite. Therefore, TEM images are only used to give a broad view of the dispersion state (Figure 85). The 0.2 nm increase in the  $scCO_2$  nanocomposites compared to the solution blended might be due to the presence of  $CO_2$  during processing which may further expand the inner - gallery spacing allowing for more polymer chains to penetrate the clay spacing and get closer to the clay. If this is true the  $scCO_2$  sample should display improved rheological properties compared to solution blended due to improved polymer - clay interactions similar to what was observed in the PS/clay nanocomposites (Chapter 3).

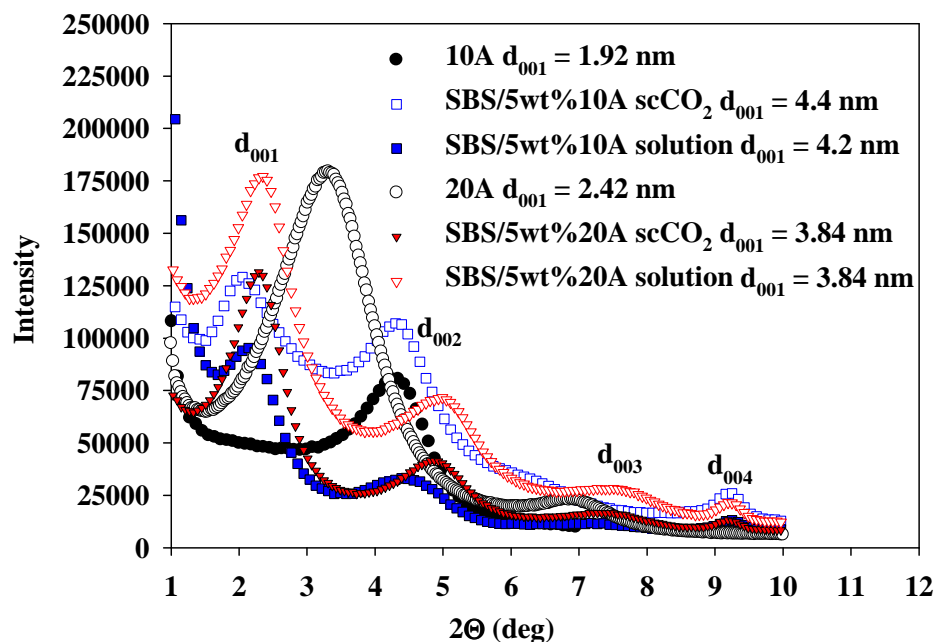


**Figure 83.** WAXD of 10A and SBS/10A nanocomposites prepared using solution blended and  $\text{scCO}_2$  processing methods.

The SBS/20A nanocomposites displayed similar rheological properties between the solution blended and  $\text{scCO}_2$  processed nanocomposites (Figure 84) (rheology was collected using the same procedure as in Chapter 3 at 80 and 100°C and a reference temperature of 100°C was used to construct the TTS curve). However, the  $\text{scCO}_2$  processed SBS/10A nanocomposite shows an additional 100% improvement in low frequency storage modulus over the solution blended benchmark suggesting that there must be improved dispersion in the  $\text{scCO}_2$  nanocomposite to account for the improvement in storage modulus (Figure 84). The reason that 10A/SBS  $\text{scCO}_2$  nanocomposite showed an improvement over the solution blended benchmark sample and the 20A/SBS did not may be due to the higher polymer - clay interactions present between the 10A-SBS than between 20A-SBS as shown by the higher final  $d_{001}$  spacing in the 10A nanocomposites. This was also observed in PS nanocomposites where the higher clay - polymer interactions resulted in higher  $d_{001}$  spacing and higher rheological and barrier properties.



Rheology of the pure SBS confirmed that the sample is below the ODT since the slope in the storage modulus low frequency regime is about 0.3.<sup>122</sup>

The tensile properties were collected on SBS films at a rate of 500% per minute until break. Young's Modulus was calculated from the slope of the linear portion of the stress strain curve at low strains using an Instron 3366 in extension mode. Prior to performing mechanical measurements SBS 1" by 6" films were made by pressing them between Teflon sheets at 125°C in a Carver hydraulic press. Both scCO<sub>2</sub> and solution blended 5wt% 10A nanocomposites showed an increase in Young's modulus of 270% and 310% and a modest increase in strain at break of 2% and 8% compared to SBS respectively (Figure 86). However, both nanocomposites showed a similar decrease in tensile strength. Moreover, despite showing a 100% increase in low frequency storage modulus and higher final d<sub>001</sub> spacing, the scCO<sub>2</sub> processed 5wt% 10A/SBS sample only showed a small increase in tensile modulus over the solution blended benchmark. This small increase was unexpected as scCO<sub>2</sub> process nanocomposites was expected to have improved dispersion over the solution blended benchmark which results in increased surface area available for polymer - clay interactions. This increase should have lead to improved mechanical properties. The reason for this small increase is not well understood and TEM could not provide a good dispersion picture to be able to conclude on the difference in clay dispersion between the two samples. Also, the two nanocomposites showed a decrease in tensile strength of about 45% compared to SBS. This result was also unexpected as researches usually report no change or slight increase (about 10%) in tensile strength following clay addition.<sup>124, 125</sup> A more detailed study is proposed to gain a better understanding on the effects of scCO<sub>2</sub> procession of SBS/clay on mechanical properties.

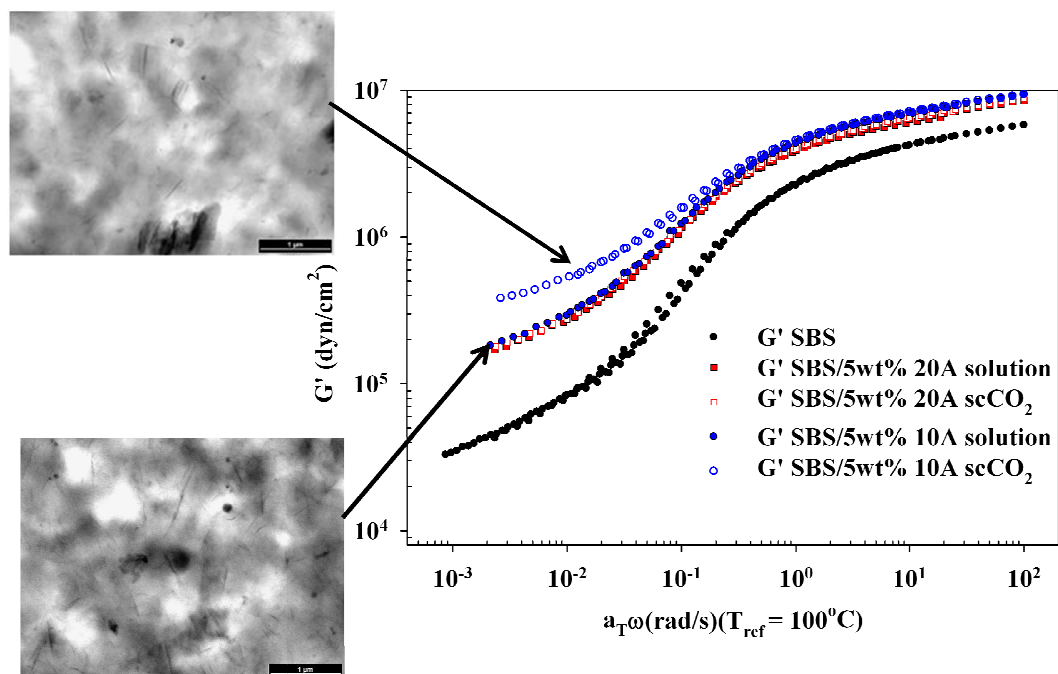


**Figure 84.** Storage modulus of SBS and 5 wt% 10A and 20A/SBS nanocomposites prepared using solution blended and scCO<sub>2</sub> processing methods. At the right are TEM images of 5 wt% 10A nanocomposites 30,000 magnification (scCO<sub>2</sub> – top and solution blended – bottom).

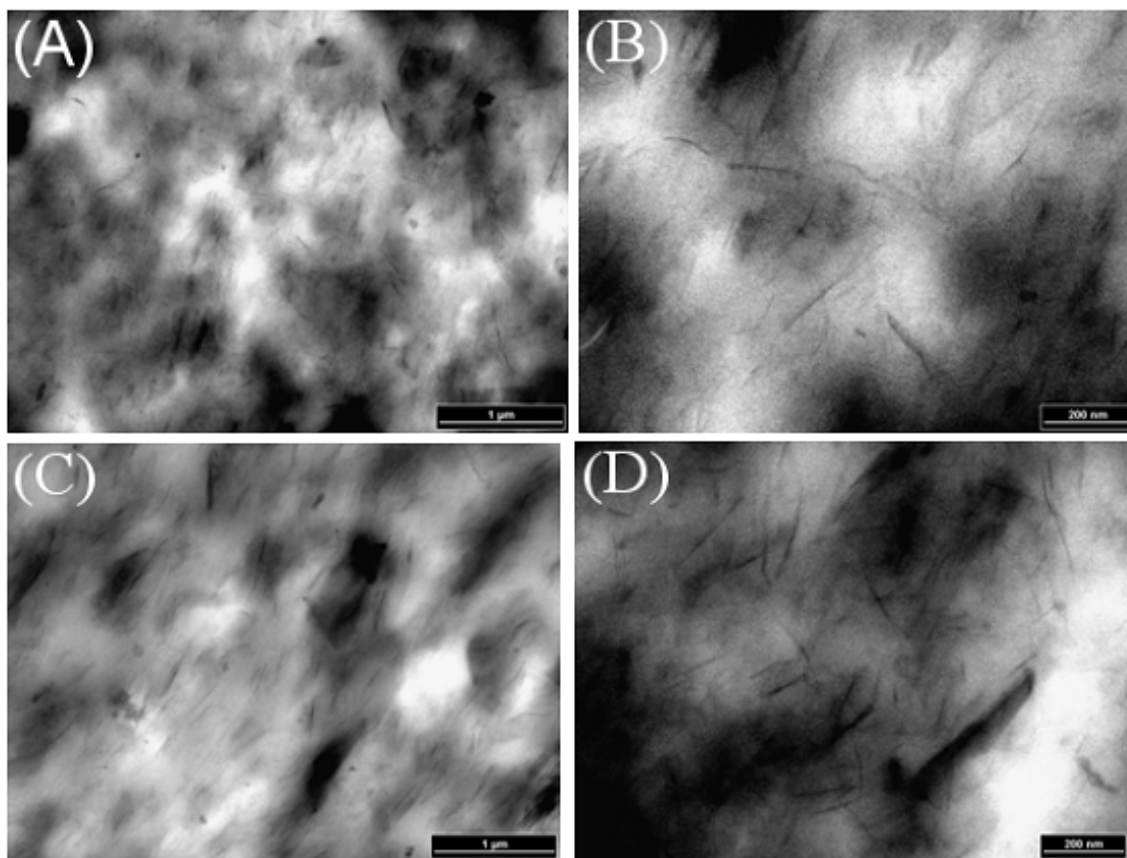


**Figure 85.** TEM images of SBS/5wt% 10A scCO<sub>2</sub> processed nanocomposite (30k magnification (A), 100k magnification (B)) and images of SBS/5wt% 10A solution blended sample (30k magnification (C), 100k magnification (D)).

To gain a better understanding on effects that scCO<sub>2</sub> processing of SBS/clay nanocomposite has on dispersion, rheological, mechanical and transport properties a more detailed study needs to be performed as described in the proposed research for SBS. Moreover, a better TEM analysis needs to be performed where the SBS should be stained with OsO<sub>4</sub> where the placement/orientation of PB chains can be better observed. This along with better image quality may allow for a better picture on the nano - clay dispersion. Moreover, if several clay weight fractions are used a better understanding on the affect of nano - clay dispersion on the tensile properties can be obtained. Also, barrier properties should also be collected as they are

more sensitive to nano - clay dispersion and the effect of scCO<sub>2</sub> on nano - clay dispersion in SBS can be better evaluated. Furthermore, the use of more than one clay a time, as proposed in the beginning of this section may also allow for the understanding of the effect of dispersion on mechanical properties as one clay may prefer PS or PB more and create a more effective dispersion. Performing this study may allow for optimizing the property improvements by using the optimum clay combination which may also allow for maximizing clay dispersion in both polymers leading to improved surface area for polymer - clay interactions.

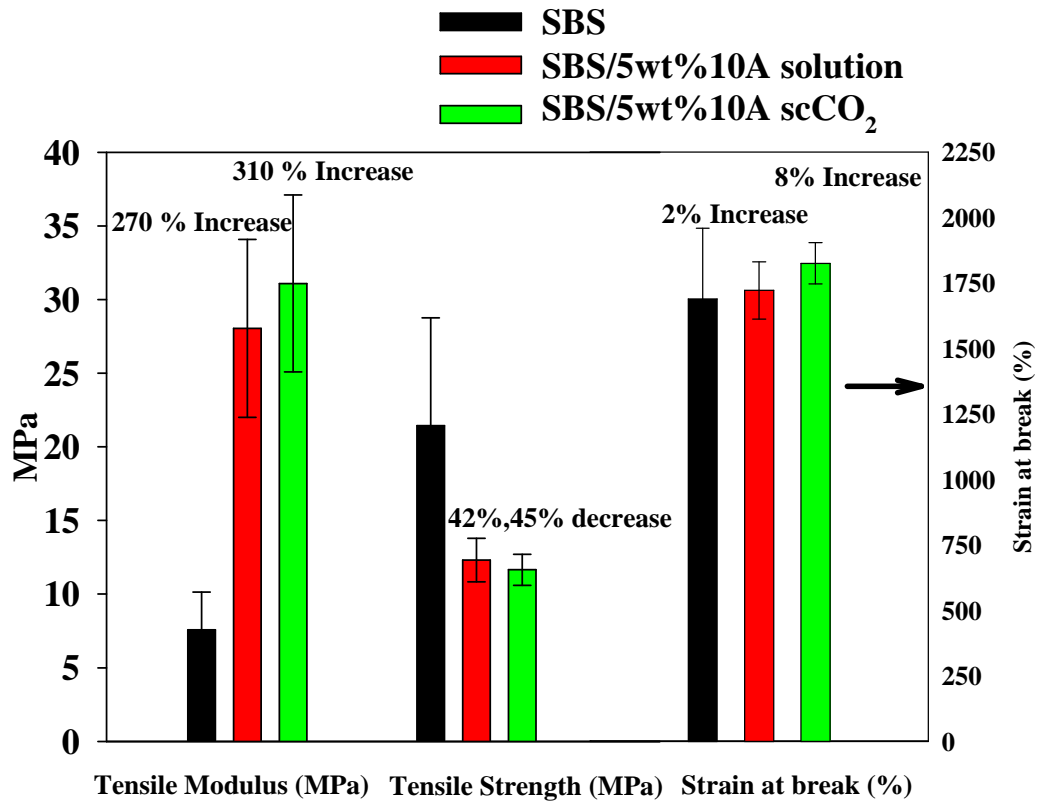


**Figure 86.** Tensile modulus, tensile strengths and stain at break for the SBS and SBS/10A scCO<sub>2</sub> and solution blended nanocomposites.

### 5.3 High density polyethylene (HDPE)/clay nanocomposites

The polyethylene is of the most widely used polymer in the world and it is primarily used in the packaging industry.<sup>126</sup> Researchers have been preparing HDPE/clay nanocomposites main using melt compounding processing technique using various clays.<sup>127-129</sup> However, the applicability of the scCO<sub>2</sub> process on the HDPE/clay nanocomposites has not yet been studied. To study the scCO<sub>2</sub> processing effects several nanocomposites should be prepared using several nano - clays including Cloisite 10A, 15A and 20A at different weight fractions. Cloisite 10A, 20A and 15A have been used by other researchers to produce HDPE/clay nanocomposites with various results.<sup>128, 129</sup> Prior to processing the polymer can clay together, the nano - clay should be pre-dispersed using the scCO<sub>2</sub> method. Pre-dispersing the clay opens up the clay galleries and it may minimize the time that clay and polymer needs to spend in the extruded in order to prevent any clay modifier degradation. The scCO<sub>2</sub> pre-processed clay can be co-extruded with HDPE with and without the presence of HDPE-MA (maleic anhydride). Benchmark nanocomposites should also be prepared using “as received” clay. WAXD, rheology, TEM, permeability measurements, mechanical properties and thermal properties should be measured on the resulting nanocomposites.

#### 5.3.1 Preliminary results

As preliminary results two HDPE/5wt% Cloisite 15A clay nanocomposites (one with “as received” 15A and another with scCO<sub>2</sub> pre-processed 15A) were prepared using a lab-scale Haake 3/4-inch at 180°C for 10 minutes. The HDPE used in this study has a melt flow index of 2.2. The scCO<sub>2</sub> processed nano - clay was prepared using the same protocol as discussed in Chapter 2. WAXD was collected using the same procedure as in Chapter 3. X-ray diffraction revealed that the polymer were successfully intercalated in-between the nano - clay particles as evident by the shift of the d<sub>001</sub> peak to lower 2 theta values for the nanocomposites compared to

neat HDPE. Nanocomposites prepared using “as received” and  $\text{scCO}_2$  pre-processed clay both displayed the same final  $d_{001}$  spacing of 3.80 nm corresponding to an inner-galley spacing increase of 3.13 nm (Figure 87). The similar  $d_{001}$  spacing in the two nanocomposites is due to the organic modifier having a thermodynamically stable state that is close to the final  $d_{001}$  spacing obtained in the nanocomposites. This phenomenon was also observed in SBS/clay and PS/clay nanocomposites in Section 5.2 and Chapter 3 respectively.

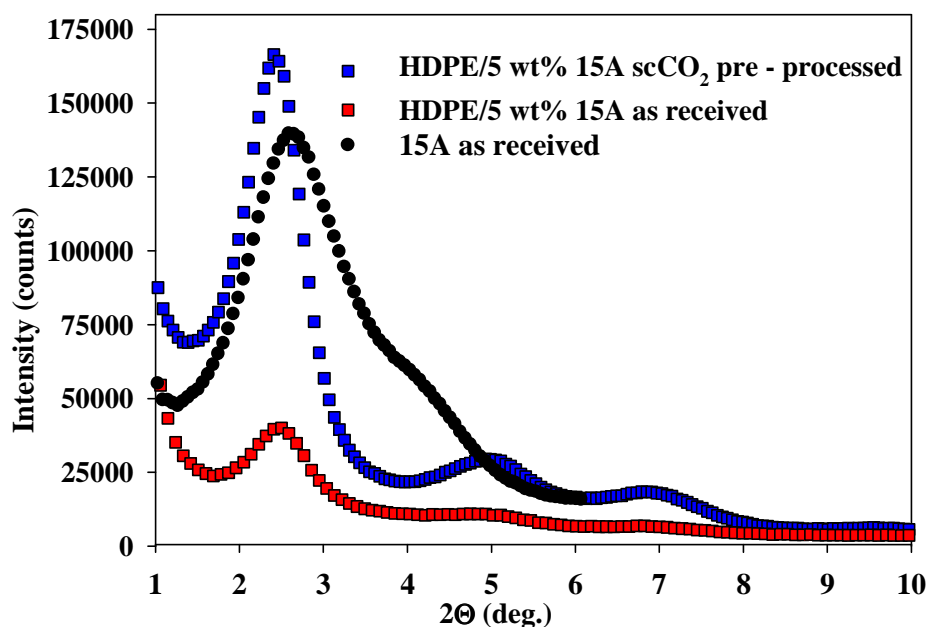


**Figure 87.** WAXD of “as received” 15A and HDPE/5 wt% 15A nanocomposites.

Rheology was collected using the same procedure as in Chapter 3 at 150°C. The nanocomposite prepared using “as received” 15A showed no improvement in rheological properties over pure HDPE. However, the nanocomposite prepared using  $\text{scCO}_2$  pre-processed 15A shows an order of magnitude improvement in low frequency storage modulus over the HDPE suggesting the presence of higher dispersion in the  $\text{scCO}_2$  pre-dispersed clay nanocomposite compared to the one made using “as received” clay (Figure 88). The

improvement in the storage modulus obtained from the nanocomposite prepared with pre-dispersed clay is more than what Joshi et. al obtained when using 10% specifically modified clay.<sup>130</sup> However, Swain et. al obtained more than 2 orders of magnitude improvement in storage modulus when ultrasonication was used at 10 wt% clay.<sup>131</sup> The permeability testing was done in the same manner as in Chapter 3. The nanocomposite prepared using pre-dispersed 15A reduced the oxygen permeability by 44% while the sample made with “as received” clay reduced it by 34% (Table 19). In contrast, Swain et. al obtained even a smaller reduction on O<sub>2</sub> permeability even at 10 wt% clay loading.<sup>131</sup>

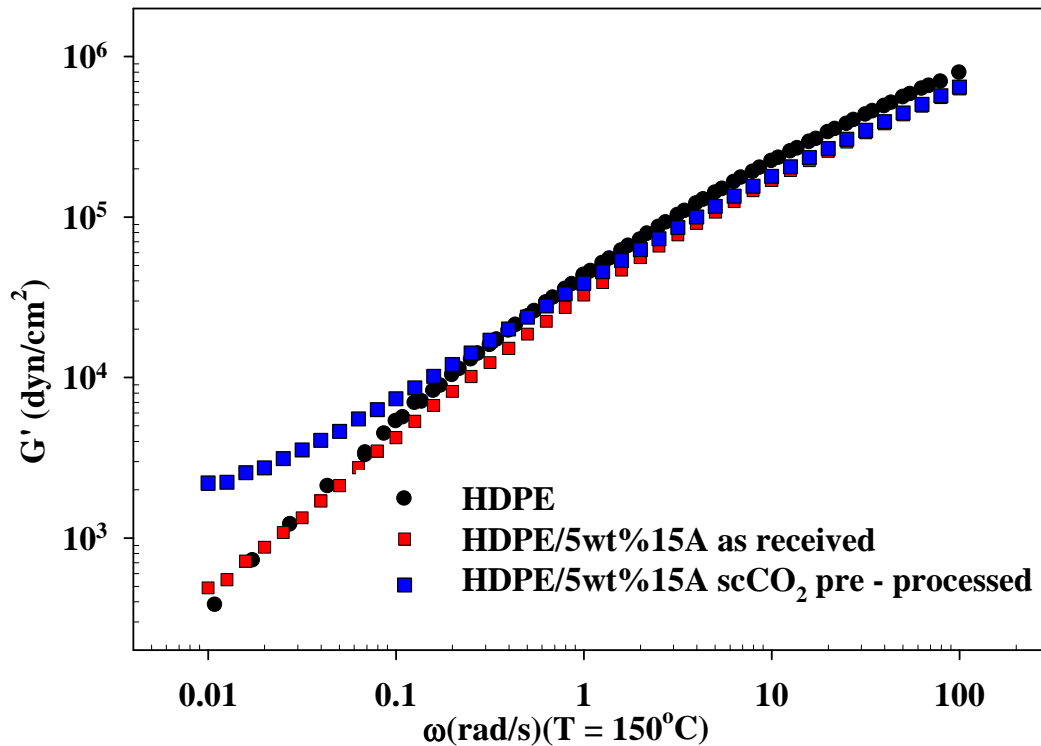


**Figure 88.** Storage modulus of HDPE and HDPE/5 wt% 15A nanocomposites.

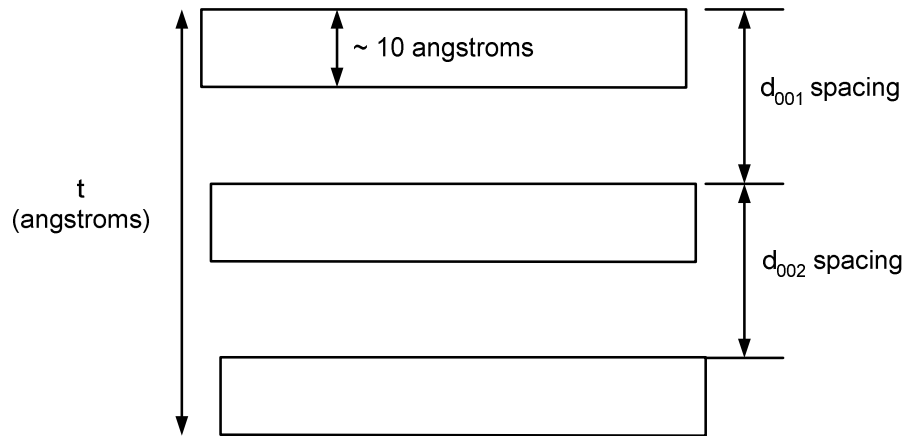
**Table 19.** Oxygen permeability of HDPE and HDPE/5 wt% 15A nanocomposites.

|   | <b>O<sub>2</sub> Permeability</b>  | <b>Reduction</b> |
|---|------------------------------------|------------------|
|   | <b>cc * mm/m<sup>2</sup> - day</b> | <b>%</b>         |
| HDPE  | 64.00                              |                  |
| HDPE/5wt% 15A as received                       | 42.52                              | - 34.2           |
| HDPE/5wt% 15A scCO <sub>2</sub> pre - processed | 36.14                              | - 44.4           |

Although the improvements in rheological properties and reduction in permeability are close to what other researchers have obtained, optimization of the processing conditions is necessary in order to attempt to further improve the properties of HDPE. Many researchers have shown that the polar clay and non - polar HDPE do not mix well unless compatibilizers like maleic anhydride, is introduced to promote better compatibility between them. Moreover, it has been shown that with careful optimization of the extrusion condition (screw speed, temperature and extrusion time) as well as with an optimum weight fraction of compatibilizer is used property improvement can also be maximized <sup>129, 131, 132</sup>. A more careful study should be performed where the extruder parameters can be tuned to obtained better dispersion and mixing. Moreover, several HDPE maleic anhydride weight fractions and different clays (Cloisite 10A, 15A and 93A) should be used to study their effect on the nanocomposites end properties. Permeability, tensile and rheological measurements along with WAXD and TEM should be performed to gain a better understanding on the ability of scCO<sub>2</sub> pre-dispersed clay to enhance HDPE mechanical, transport and rheological properties.



## Appendix A



$$t = d_{001} \times (n-1) + 10$$

**Figure 89.** Tactoid thickness calculation diagram.

From the drawing it can be seen that the thickness of a tactoid can be represented by the equation above where  $(n-1)$  is the number of clay platelets in the tactoid minus 1 and is equal to the number of inter-gallery spacing that needs to be accounted for. Multiplying  $(n-1)$  with the  $d_{001}$  spacing gives the height of the stack shy the thickness of one plate. The 10 on the right hand side of the equation, at the end, represents that plate thickness and has units of angstroms. The Scherrer equation can be used to determine the thickness “ $t$ ” from the FWHM value of the  $d_{001}$  diffraction peak. From there, the equation above is solved for  $n$ .

## REFERENCES

1. Rubinstein, M., *Polymer Physics*. Oxford University Press Inc.: 2003.
2. Schwartz, M., *Composite Materials*. Prentice Hall PTR: Upper Saddle River, N.J., USA,, 1997; Vol. 1.
3. Moropoulou, A.; Bakolas, A.; Anagnostopoulou, S. *Cement and Concrete Composites* **2005**, 27, 295 - 300.
4. Theng, B., *Formation and properties of clay-polymer complexes*. Elsevier: Amsterdam, 1979.
5. Vaia, R. A.; Price, G.; Ruth, P. N.; Nguyen, H. T.; Lichtenhan, J. *Applied Clay Science* **1999**, 15, (1-2), 67-92.
6. Kojima, Y.; Usuki, A.; Kawasumi, M.; Okada, A.; Kurauchi, T.; Kamigaito, O. *Journal of Materials Research* **1993**, 8, 1185 - 1189.
7. Hussain, F.; Hojjati, M.; Okamoto, M.; Gorga, R. E. *Journal of Composite Materials* **2006**, 40, 1511-1575.
8. Okamoto, M.; Morita, S.; Taguchi, H.; Kim, Y. H.; Kotaka, T.; Tateyama, H. *Polymer* **2000**, 41, (10), 3887-3890.
9. A.B. Morgan, L. C., J. D. Harris. *Fire Materials* **2005**, 29, 213-229.
10. Gilman, W. J. *Applied Clay Science* **1999**, 15, (1-2), 31-49.
11. Zhu, J.; Wilkie, C. A. *Polymer International* **2000**, 49, 1158 - 1163.
12. Zhang, J.; Jiang, D. D.; Wilkie, C. A. *Polymer Degradation and Stability* **2006**, 91, 298e304.
13. Vaia, R. A.; Giannelis, E. P. *Macromolecules* **1997**, 30, (25), 7990 - 7999.
14. Balazs, A. C.; Singh, C.; Zhulina, E. *Macromolecules* **1998**, 31, 8370 - 8381.

15. Vaia, R. A.; Giannelis, E. P. *Macromolecules* **1997**, 30, (25), 8000-8009.
16. Lee, J. Y.; Baljon, A. R. C.; Loring, R. F.; Panagiopoulos, A. Z. *Journal of Chemical Physics* **1998**, 109, 10321 - 10330.
17. Blumstein, A. *Bull. Soc. Chim. Fr.* **1961**, 899.
18. Blumstein, A. *Journal of Polymer Science, Part A: General Papers* **1965**, 3, (7), 2653-64.
19. BKG, T., *Formation and properties of clay-polymer complexes*. Elsevier: Amsterdam, 1979.
20. Okada, A.; Kawasumi, M.; Usuki, A.; Kojima, Y.; Kurauchi, T.; Kamigaito, O. In *Synthesis and properties of nylon-6/clay hybrids*, MRS Symposium Proceedings, Pittsburgh, 1990; DW, S.; JE, m., Eds. Pittsburgh, 1990; pp 45-50.
21. Vaia, R. A.; Ishii, H.; Giannelis, E. P. *Chemistry of Materials* **1993**, 5, (12), 1694-6.
22. Bailey, S. W., *The status of clay mineral structures, Clay and Clay Minerals Proc. 14th Nat. Conf.*. 1966.
23. Theng, B. K. G., *Formation and Properties of Clay-Polymer Complexes*. Elsevier: New York, 1979.
24. Manke, C. W.; Gulari, E.; Mielewski, D. F.; Lee, E. C. System and method of delaminating a layered silicate material by supercritical fluid treatment. US Patent 6,469,073, October 2002.
25. Ray, S. S.; Okamoto, M. *Progress in Polymer Science* **2003**, 28, (11), 1539-1641.
26. Fischer, H. *Materials Science and Engineering: C* **2003**, 23, (6-8), 763-772
27. Yu, M.; Zhang, Q.; Fu, Q. *Chinese Journal of Polymer Science* **2003**, 22, (1), 43 - 47.
28. Chow, W. S.; Ishak, Z. A. *Polymer Letters* **2007**, 1, (2), 77 - 83.

29. Maarouf, B. T.; Bagher, R. *Iranian Journal of Polymer Science & Technology (Persian Edition)* **2007**, 20, (1), 59 - 64.
30. Messersmith, P. B.; Giannelis, E. P. *Chemistry of Materials* **1994**, 6, (10), 1719–1725.
31. Ren, J.; Silva, A. S.; Krishnamoorti, R. *Macromolecules* **2000**, 33, 3739 - 3746.
32. Tanoue, S.; Utracki, L. A.; Garcia-Rejon, A.; Tatibouët, J.; Cole, K. C.; Kamal, M. R. *Polymer Engineering and Science* **2004**, 44, (6), 1046 - 1060.
33. Joshi, M.; Butola, B. S.; Simon, G.; Kukaleva, N. *Macromolecules* **2006**, 39, 1839-1849.
34. Solomon, M. J.; Almusallam, A. S.; Seefeldt, K. F.; Somwangthanaroj, A.; Varadan, a. P. *Macromolecules* **2001**, 34, 1864 - 1872.
35. Liang Xu, S. R., Mahesh Thopasridharan, Jiexiang Ren, Devon A Shipp, Ramanan Krishnamoorti. *Nanotechnology* **2005**, 16, (7), S514-S521
36. Kojima, Y.; Usuki, A.; Kawasumi, M.; Okada, A.; Kurauchi, T.; Kamigaito, O. *Journal of Polymer Science Part A: Polymer Chemistry* **1993**, 31, (7), 1755.
37. A.B. Morgan, J. W. G. *Journal of Applied Polymer Science* **2003**, 87, (8), 1329-1338.
38. Vaia, A., R.; Jandt, D., K.; Kramer, J., E.; Giannelis, P., E. *Macromolecules* **1995**, 28, (24), 8080-5.
39. O. Meincke, B. H., C. Dietrich, C. Friedrich. *Macromolecular Chemistry and Physics* **1003**, 204, (5-6), 823 - 830.
40. Lim, Y. T.; Park, O. O. *Rheologica Acta* **2001**, 40, (3), 220-229.
41. Tanoue, S.; Utracki, L. A.; Garcia-Rejon, A.; Sammut, P.; Ton-That, M.-T.; Pesneau, I.; Kamal, M. R.; Lyngaae-Jørgensen, J. *Polymer Engineering & Science* **2004**, 44, (6), 1061 - 1076.
42. Weon, J.-I.; Sue, H.-J. *Polymer* **2005**, 46, 6325-6334.

43. Suprakas Sinha Ray, M. O. *Progress in Polymer Science* **2003**, 28, (11), 1539-1641.
44. Kuznetsov, D. V.; Balazs, A. C. *Journal of Chemical Physics* **2000**, 112, (9), 4365.
45. Kawasumi, M.; Hasegawa, N.; Kato, M.; Usuki, A.; Okada, a. A. *Macromolecules* **1997**, 30, (20), 6333 -6338.
46. Zhong, Y.; Zhu, Z.; Wang, S.-Q. *Polymer* **2005**, 46, (9), 3006-3013.
47. Zhao, J.; Morgan, A. B.; Harris, J. D. *Polymer* **2005**, 46, 8641–8660.
48. Kirby, C. F.; McHugh, M. A. *Chemical Reviews (Washington, D. C.)* **1999**, 99, (2), 565-602.
49. JL, P.; EJ, B., *Supercritical Fluid Technology in Materials Science and Engineering*. Marcel Dekker: 2002.
50. Tomasko, D. L.; Li, H.; Liu, D.; Han, X.; Wingert, M. J.; Lee, L. J.; Koelling, K. W. *Industrial & Engineering Chemistry Research* **2003**, 42, (25), 6431-6456.
51. Daneshvar, M.; Gulari, E., Partition Coefficients of Poly(ethylene glycol)s in Supercritical Carbon Dioxide. In *Supercritical Fluid Science and Technology*, American Chemical Society: Washington, DC, 1989; pp 72-85.
52. Tang, H.; Gulari, E.; Rothe, E. W. *The Journal of Supercritical Fluids* **2000**, 18, (3), 193-200.
53. Serhatkulu, G. K.; Dilek, C.; Gulari, E. *The Journal of Supercritical Fluids* **2006**, 39, (2), 264-270.
54. Kwag, C.; W.Manke, C.; Gulari, E. *Industrial & Engineering Chemistry Research* **2001**, 40, (14), 3048-3052.
55. Hoefling, T. A. *Journal of Supercritical Fluids* **1993**, 6, (3), 165 - 171.
56. Consani, K. A.; Smith, R. D. *Journal of Supercritical Fluids* **1990**, 3, (2), 51

57. Zhao, Q.; Samulsk, E. T. *Macromolecules* **2003**, 36, (19), 6967-6969.
58. Garg, A.; Gulari, E.; Manke, C. W. *Macromolecules* **1994**, 27, (20), 5643-5653.
59. Horsch, S.; Serhatkulu, G.; Gulari, E.; Kannan, R. M. *Polymer* **2006**, 47, (21), 7485-7496.
60. Gerhardt, L. J.; Manke, C. W.; Gulari, E. *Journal of polymer Science Part B: Polymer Physics* **1997**, 35, (3), 523-534.
61. Li, J.; Xu, Q.; Peng, Q.; Pang, M.; He, S.; Zhu, C. *Journal of Applied Polymer Science* **2006**, 100, (1), 671-676.
62. Lim, Y. T.; Park, O. O. *Macromolecular Rapid Communications* **2000**, 21, (5), 231 - 235.
63. Xu, L.; Reeder, S.; Thopasridharan, M.; Ren, J.; Shipp, D. A.; Krishnamoorti, R. *Nanotechnology* **2005**, 16, (7), 514-521.
64. Pandey, R. B.; Anderson, K. L.; Farmer, B. L. *Journal of polymer Science Part B: Polymer Physics* **2006**, 44, (24), 3580-3589.
65. Rohlmann, C. O.; Horst, M. F.; Quinzani, L. M.; Failla, M. D. *European Polymer Journal* **2008**, 44, (2749-2760).
66. W, X.; Z, G.; WP, P.; D, H.; A, S.; R, V. *Chem Mater* **2001**, 13, 2979.
67. S. W. Brindley, G. B., *Eds. Crystal Structure of Clay Minerals and their X-ray Diffraction*. Mineralogical Society: London,, 1980.
68. Doh, J. G.; Cho, I. *Polymer Bulletin* **1998**, 41, 511-518.
69. Bellair, R. J.; Manitiu, M.; Gulari, E.; Kannan, R. M. *Polymer Science Part B: Polymer Physics* **2010**, 48, (8), 823 - 831.
70. Kurnik, R.; Holla, S.; Reid, R. *Journal of Chemical Engineering Data* **1981**, 26, 45 - 51.
71. R.A. Vaia, E. P. G. *Macromolecules* **1997**, 30, (25), 8000-8009.

72. R. Kurnik, S. H., R. Reid. *Journal of Chemical Engineering Data* **1981**, 26, 47-51.
73. Yang, I. K.; Tsai, P.-H. *Polymer* **2006**, 47, (14), 5131-5140.
74. Toth, R.; Coslanicha, A.; Ferronea, M.; Fermeagliaa, M.; Pricl, S.; Miertu, S.; Chiellini, E. *Polymer* **2004**, 45, 8075-8083.
75. E. Hackett, E. M., E.P. Giannelis *JOURNAL OF CHEMICAL PHYSICS* **1998**, 108, 7410 - 7415.
76. JT Yoon , W. J., MS Lee , MB Ko *Polymer* **2001**, 42, 329-336.
77. Manitiu, M.; Bellair, R. J.; Horsch, S.; Gulari, E.; Kannan, R. M. *Macromolecules* **2008**, 41, 8038-8046.
78. Pandey, R. B.; Farmer, B. L. *Journal of Polymer Science: Part B: Polymer Physics* **2008**, 46, 2696.
79. Hoffmann, B.; Dietrich, C.; Thomann, R.; Friedrich, C.; Mülhaupt, R. *Macromolecular Rapid Communications* **2000**, 21, 57-61.
80. Qi, R.; Jin, X.; Huang, S. *Journal of Applied Polymer Science* 115, (5), 2723-2727.
81. Xie, W.; Gao, Z.; Pan, W.-P.; Hunter, D.; Singh, A.; Vaia, R. *Chemistry of Materials* **2001**, 13, (9), 2979-2990.
82. Morgan, A. B.; Chu, L.; Harris, J. D. *Fire Materials* **2005**, 29, 213-229.
83. Choudalakis, G.; Gotsis, A. D. *European Polymer Journal* **2009**, 45, (4), 967-984.
84. Bharadwaj, R. K. *Macromolecules* **2001**, 34, (26), 9189-9192.
85. Lan, T.; Kaviratna, P. D.; Pinnavaia, T. J. *Chem. Mater* **1994**, 6, 573 - 575.
86. Nazarenko, S.; Meneghetti, P.; Julmon, P.; Olson, B. G.; Qutubuddin, S. *Journal of polymer Science Part B: Polymer Physics* **2007**, 45, (13), 1733-1753.

87. Ku, B.-C.; Blumstein, A.; Kumar, J.; Samuelson, L. A.; Kim, D. W., Barrier Properties of Ordered Polymer Nanocomposites. In *Dekker Encyclopedia of Nanoscience and Nanotechnology*, 2nd ed.; Vol. 1, p 267 — 277.
88. Sorrentino, A.; Tortora, M.; Vittoria, V. *Journal of polymer Science Part B: Polymer Physics* **2006**, 44, (2), 265-274.
89. Hiltner, A.; Liu, R. Y. F.; Hu, Y. S.; Baer, E. *Journal of polymer Science Part B: Polymer Physics* **2005**, 43, (9), 1047-1063.
90. Vaia, R. A.; Giannelis, E. P. *MRS buletin* **2001**.
91. Wang, Y.; Wu, Y.; Zhang, H.; Zhang, L.; Wang, B. W. a. *Z. Macromol. Rapid Commun* **2004**, 25, 1973.
92. Utracki, L. A.; Garcia-Rejon, R. S. a. A. *Macromolecules* **2003**, 36, 2114.
93. Ammala, A.; Pas, S. J.; Lawrence, K. A.; Stark, R.; Webb, R. I.; Hill, A. J. *Journal of Materials Chemistry* **2008**, 18, 911-916.
94. Manitiu, M.; Bellair, R. J.; Gulari, E.; Kannan, R. M. *In preparation* **2010**.
95. Gorrasi, G.; Tortora, M.; Vittoria, V.; Pollet, E.; Lepoittevin, B.; Alexandre, M.; Dubois, P. *Polymer* **2003**, 44, (8), 2271-2279.
96. Han, S. S.; Kim, Y. S.; Lee, S. G.; Lee, J. H.; Zhang, K.; Choi, H. J. *Macromolecular Symposia* **2006**, 245 - 246, (1), 199-207.
97. Alexander B. Morgan, J. D. H. *Polymer* **2004**, 45, 8695 - 8703.
98. Sohn, J. I.; Lee, C. H.; Lim, S. T.; Kim, T. H.; Choi, H. J.; Jhon, M. S. *Journal of Materials Science* **2003**, 38, (9), 1849-1852.
99. Horsch, S. Dissertation Thesis.



100. Krishnamoorti, R.; Ren, J.; Silva, A. S. *Journal of Chemical Physics* **2001**, 114, (11), 4968-4973.
101. Krishnamoorti, R.; Yurekli, K. *Current Opinion in Colloid & Interface Science* **2001**, 6, (5,6), 464-470.
102. Krishnamoorti, R.; Giannelis, E. P. *Macromolecules* **1997**, 30, (14), 4097-4102.
103. Horsch, S.; Serhatkulu, G.; Gulari, E.; Kannan, R. M. *Unpublished Data*.
104. Fetters, L. J.; Colby, D. J. L. a. R. H., Chain Dimensions and Entanglement Spacings In *Physical Properties of Polymers Handbook*, Springer New York: 2007; pp 447-454.
105. Manitiu, M.; Horsch, S.; Gulari, E.; Kannan, R. M. *Polymer* **2009**, 50, 3786 - 3796.
106. Strawhecker, K. E.; Manias, E. *Chem. Mater.* **2003**, 15, 844-849.
107. Morgan, A. B.; Gilman, J. W. *Journal of Applied Polymer Science* **2003**, 87, (8), 1329-1338.
108. B.D Cullity , S. R. S., *Elements of X-ray Diffraction*. 3 ed.; Pearson Education: 2001.
109. RM Silverstein , F. W., *Spectrometric Identification of Organic Compounds*. 6 ed.; John Wiley & Sons, Inc.: 1998.
110. Cullity, B. D.; Stock, S. R., *Elements of X-ray Diffraction*. 3 ed.; Pearson Education: 2001.
111. Brindley, S. W.; Brown, G., *Crystal Structures of Clay Minerals and Their X-ray Identification*. Mineralogical Society: London: 1980.
112. Kardos, J. L. *Pure & App. Chem.* **1985**, 57, (11), 1651 - 1657.
113. Shi, H.; Lan, T.; Pinnavaia, T. J. *Chemistry of Materials* **1996**, 8, (8), 1584-1587.
114. DM, D.; RA, O.; JF, C.; NJ, J.; JG, S. J.; JW, C. *Polymer* **2002**, 43, 813.
115. Liang, Z.-M.; Yin, J.; Xu, H.-J. *Polymer* **2003**, 44, 1391-1399.

116. Xu, H.; Li, Y.; Yu, D. *Journal of Applied Polymer Science* **2005**, 98, 146 -152.
117. Laus, M.; Francescangeli, O.; Sandrolini, F. *J Mater Res* **1997**, 12.
118. Zhang, Q.; Tsui, O. K. C.; Du, B.; Zhang, F.; Tang, T.; He, T. *Macromolecules* **2000**, 33, 9561-9567.
119. Liao, M.; Zhu, J.; Xu, H.; Li, Y.; Shan, W. *Journal of Applied Polymer Science* **2005**, 92, 3430 – 3434.
120. Lira, Y. T.; Park, O. O. *Korean J. Chem. Eng.*, **2001**, 18, 21 - 25.
121. Zhang, Z.; Zhang, L.; Li, Y.; Xu, H. *Journal of Applied Polymer Science* **2006**, 99, (2273–2278).
122. Carastan, D. J.; Demarquette, N. R.; Vermogen, A.; Masenelli-Varlot, K. E. *Rheologica Acta* **2008**, 47, 521 - 536.
123. Ha; Kwon, Y.-H.; Breiner, Y.; Chan, T.; Tzianetopoulou, E. P.; Cohen, T.; Boyce, R. E.; Thomas, M. C.; L., E. *Macromolecules* **2005**, 38, (5170 - 5179).
124. Zhang, L.; Wang, Y.; Wang, Y.; Sui, Y.; Yu, D. S. *Journal of Applied Polymer Science* **2000**, 78, 1873 - 1878.
125. Lai, S. M.; M.Chen, C. *Journal of Polymer Science: Part B: Polymer Physics* **2008**, 2696 - 2706.
126. Piringer, O. G.; Baner, A. L., *Plastic packaging: interactions with food and pharmaceuticals*. 2008.
127. Liang, G.; Xu, J.; Bao, S.; Xu, W. *Journal of Applied Polymer Science* **2004**, 91, 3974–3980.
128. Jacquelot, E.; Espuche, E.; Ge´rard, J.-F.; Duchet, J.; Mazabraud, P. *Journal of Polymer Science: Part B: Polymer Physics* **2006**, 44, 431-440.

129. Lee, S.-Y.; Park, S.-Y.; Song, H.-S. *Journal of Applied Polymer Science* **2007**, 103, 3326–3333.
130. Joshi, M.; Butola, B. S.; Simon, G.; Kukaleva, N. *39* **2006**, 1839-1849.
131. Swain, S. K.; Isayev, A. I. *Polymer* **2007**, 48.
132. Wang, K. H.; Xu, M.; Choi, Y. S.; Chung, I. J. *Polymer Bulletin* **2001**, 46, 499-505.

**ABSTRACT****SUPERCRITICAL CARBON DIOXIDE PROCESSING OF NANO - CLAYS AND  
POLYMER/CLAY NANOCOMPOSITES**

by

**MIHAI MANITIU****August 2010****Advisor:** Rangaramanujam Kannan**Co-Advisor:** Esin Gulari**Major:** Chemical Engineering**Degree:** Doctor of Philosophy

Effective dispersion of the fillers in a polymer matrix and improvement of polymer - clay interactions are two key challenges in the field of nanocomposites. A novel processing method that utilizes the unique properties of supercritical carbon dioxide (scCO<sub>2</sub>) to disperse nano - clay and prepare a series of polymer/clay nanocomposites with enhanced properties was explored.

Significant dispersion was achieved using the scCO<sub>2</sub> process with Cloisite 10A without the presence of an organic phase as evident by the absence of the diffraction peak in WAXD and the presence of individual tactoids that lost their parallel registry. The expanded flexible structure of the scCO<sub>2</sub> processed clay exposes more of the available surface area allowing for more contact between the polymer and clay surface, and the platelets should be easier to disperse into a polymer matrix than the “as received” clay.

Enhanced nano - clay dispersion and improved properties were achieved in the scCO<sub>2</sub> processed polystyrene/clay nanocomposites compared to melt compounding and solution blended benchmarks. There was a three-fold reduction in the number of tactoids in the scCO<sub>2</sub>

samples compared to solution blended benchmark that was independent of the clay modifier used leading to an increase in the surface area available for polymer-clay interactions. Significant dispersion, without strong polymer-clay interactions, was not sufficient for significant nanocomposites property improvement. Also, favorable polymer-clay interaction without clay dispersion was also not enough to obtain the maximum property enhancement. Improvements as high as 3 orders of magnitude in the low frequency storage modulus were observed in nanocomposites processed with 5wt% 10A and 15A scCO<sub>2</sub> that had favorable polymer-clay interactions. Supercritical carbon dioxide processed nanocomposite showed a reduction of 45% (5wt% 10A) and 60% (5wt% 15A) in oxygen permeability compared to PS. Moreover, the scCO<sub>2</sub> processed nanocomposites reduced the oxygen permeability by 20 to 50% compared to solution blended benchmark samples depending on the clay used. Replacing “as received” clay with pre-dispersed clay increased the surface area available for polymer-clay interactions, resulting in a significant doubling of G' at low frequencies over the standard scCO<sub>2</sub> processed sample. The scCO<sub>2</sub> samples showed solid-like behavior at loadings as low as 2 wt%, and elastic modulus improvements as high as 3.5 orders of magnitude in the 10 wt% nanocomposites over the pure polymer.

Comparison of scCO<sub>2</sub>-processed and water-processed Cloisite Na<sup>+</sup> /PVME nanocomposites with “weak polymer-filler interactions” suggested that high level clay dispersion resulted in non-terminal while intercalation resulted in a filler effect with the relaxation behavior of the bulk polymer virtually unaltered by the presence of the nano-clay. In contrast, for intercalated systems with "stronger" polymer-clay interactions (PVME/I.30P), there was more than two orders of magnitude increase in low-frequency storage moduli. Similarly to what was

observed in PS, in PVME systems, when 'strong' polymer - clay interactions were present coupled with significant nano - clay dispersion produced significant property improvements.

## AUTOBIOGRAPHICAL STATEMENT

**Name:** Mihai Manitiu

**Date of Birth:** March 31, 1982

**Education:**

2007 - M.S. Chemical Engineering, Wayne State University, Detroit, MI 48202

2005 - B.S. Chemical Engineering – “Summa Cum Laude” Wayne State University, Detroit, MI 48202

**Publications:**

1. *Investigating Clay Modifier Effects in Supercritical Carbon Dioxide Processed Nanocomposites*. Bellair, Robert J.; **Manitiu, Mihai**; Gulari, Esin; Kannan, Rangaramanujam M., *Journal of Polymer Science Part B: Polymer Physics*, 48(8), 823-831 (2010)

2. *Permeability of supercritical carbon dioxide processed dispersed polystyrene/nano-clay nanocomposites*. **Manitiu, Mihai**; Bellair, Robert J.; Gulari, Esin; Kannan, Rangaramanujam M., In Preparation, 2010.

3. *Structure, Mechanical Properties and Biocompatibility of Supercritical Carbon-Dioxide Processed Resorbable Polymer Nanocomposites*. K.C. Baker, **M. Manitiu**, R. Bellair, H.N. Herkowitz, R.M. Kannan, In Preparation, 2010.

4. *Role of Polymer-Clay Interactions and Nanoclay Dispersion on the Viscoelastic Response of Supercritical CO<sub>2</sub> Dispersed PVME-Clay Nanocomposites*, **Manitiu, Mihai**; Horsch, Steven; Gulari, Esin; Kannan, Rangaramanujam M., *Polymer* (2009), 50, 3786-3796 .

5. *Structure and mechanical properties of supercritical carbon dioxide processed porous resorbable polymer constructs*. Baker, KC, R. Bellair, **M. Manitiu**, HN Herkowitz, RM Kannan, *Journal of Mechanical Behavior of Biomedical Materials* (2009), 2(6) 620-626.

6. *Supercritical Carbon Dioxide-Processed Dispersed Polystyrene-Clay Nanocomposites*. **Manitiu, Mihai**; Bellair, Robert J.; Horsch, Steven; Gulari, Esin; Kannan, Rangaramanujam M. *Macromolecules* (2008), 41 (21), 8038-8046.

**Patents:**

*Supercritical carbon dioxide processed PLA/PLGA nanocomposites for use in packaging, structural tissue engineering, and drug delivery constructs*. Baker, K. C.; Kannan, R. M.; Bellair, R. J.; **Manitiu, M.**; Herkowitz, H. M. **Application in process**, 2010.